Dynamical Studies of Some Ecological and Eco-epidemiological Models with Various Factors

THESIS

Submitted in partial fulfilment of the requirements for the degree of

DOCTOR OF PHILOSOPHY

by

ASHVINI GUPTA
(2019PHXF0423P)

Under the Supervision of

PROF. BALRAM DUBEY

BIRLA INSTITUTE OF TECHNOLOGY AND SCIENCE, PILANI

2024

BIRLA INSTITUTE OF TECHNOLOGY & SCIENCE, PILANI

CERTIFICATE

This is to certify that the thesis titled **"Dynamical Studies of Some Ecological and Eco-epidemiological Models with Various Factors"** submitted by **Ms. Ashvini Gupta**, ID No. **2019PHXF0423P** for the award of Ph.D. of the institute embodies original work done by her under my supervision.

_____

Signature of the Supervisor
Name: **PROF. BALRAM DUBEY**
Designation: **Professor**

Date: **March 28, 2024**

Acknowledgments

First and foremost, I sincerely thank my Ph.D. supervisor, Prof. Balram Dubey, for his invaluable guidance, support, and encouragement throughout my Ph.D. journey. His passion for research always motivates me to become a better researcher everyday. It has been a great experience learning so much from him.

I am grateful to the Vice-Chancellor, Director, Dean Academic (AGSRD), and Registrar of BITS Pilani for providing me with an opportunity to get a challenging position and use my skills to demonstrate my worth. I am also grateful to them for the research facilities and a healthy environment. I am thankful to BITS Pilani, and University Grants Commission (UGC), New Delhi, for the financial support, without which my research would not have been possible. Furthermore, I want to acknowledge the Springer Nature team and the Ministry of Education, Government of India for awarding me under the theme "Her Research, Our Future Empowering Women in Research"- A G20 Initiative to promote women researchers. I express my heartfelt gratitude to the Science and Engineering Research Board (SERB) for providing me the International Travel Grant to participate in The 15th Conference on Dynamical Systems Applied to Biology and Natural Sciences, DSABNS 2024, held at NOVA SCHOOL OF SCIENCE AND TECHNOLOGY | NOVA FCT, Portugal.

I would like to express my sincere thanks to Prof. Devendra Kumar, Head of the Mathematics Department, and Prof. B. K. Sharma, the former HoD, for giving me the wonderful chance to work in the Department and for their help in bringing this work to completion on schedule. I also want to thank the mathematics department's faculties and staff for their unwavering support and sincere interest in student's learning.

I am also thankful to Prof. Ashish Tiwari and Prof. B. K. Sharma, members of the doctoral advisory committee (DAC), for their insightful feedback and helpful suggestions throughout my doctoral research.

I would like to express my gratitude towards my collaborators, Prof. A.K. Misra and his student Soumitra Pal, Department of Mathematics, Institute of Science, Banaras Hindu University, for valuable discussions, Prof. Uma S. Dubey, Department of Biological Sciences, BITS Pilani, Pilani Campus, for her constructive suggestions, which improved the overall quality of the work.

I deeply appreciate and owe a lot to my senior colleagues Dr. Ankit Kumar, Dr. Sajan (who are also my collaborators) for helping me to understand the concepts and teaching me the process of research. Moreover, I want to thank Dr. Sourav Kumar Sasmal, IIT Roorkee for

helping me with the conceptual doubts. I would also like to thank Anshu, Masoom, and Arjun (my collaborator) for some really productive talks in the field of Mathematical Biology.

I feel fortunate to be surrounded by my friends Shipra, Anshu, Suman, Umesh, Gourav, and Amit. I want to thank them for making my Ph.D. journey enjoyable and simpler. I also want to thank my long-distance friend Neha for always being there for me.

The note of thanks is incomplete without paying earnest and heartfelt gratitude to my family. First, my parents, Mr. Mohan Lal Gupta and Mrs. Santosh Gupta, for encouraging me to commence this journey. Their love and blessings are an incredible source of energy to me. I would also like to thank my parents-in-law, Mr. Sitaram Gupta and Mrs. Indra Devi, and brothers-in-law, Suchit Gupta and Rohit Gupta, sister-in-law Priti Gupta, and my aunt, Archana Goyal, for their endless love and support they have constantly provided. I am lucky to have them as well-wishers throughout this journey.

Last but not least, I am very much grateful to my beloved husband, Rachit Kumar Gupta, for always believing in me and motivating me to work towards my career goals freely. From being a listening ear in challenging times to celebrating my achievements, he made my Ph.D. life easier and happier.

Place: BITS Pilani
Date: March 28, 2024

Ashvini Gupta
(Department of Mathematics)

Abstract

Population models in ecology are mathematical depictions of biological populations in natural ecosystems that are used to understand and forecast their behavior. Ecologists can use these models to gain insight into the factors that drive population growth, decline, and stability. It serves as a foundation for ecological research, allowing scientists to test hypotheses, make predictions, and create natural resource and biodiversity management strategies. Relationships between prey and predator are an essential component of Mathematical Ecology. Examining prey-predator interactions in the presence of an infectious disease has become vital in recent years. The spread of infectious diseases is one of the epidemiological factors that can influence population size, structure, and dynamics. Differential equation is a standard tool used to model prey-predator interactions mathematically. Every model becomes different when the predation rate is represented by a particular functional response. Several factors affect the predation rate and the population density tremendously, such as fear of predation and its carry-over effects, group defense, hunting cooperation, prey refuge, additional food for predators, prey herd shape, counter-attacking by strong prey, migration, time delay, seasonality, etc. Including these factors make the model more realistic and challenging to study.

This thesis investigates various ecological and eco-epidemiological models that depict interactions between prey and predators in the presence of diverse environmental factors, which can significantly impact the system dynamics. The variations in population traits offer valuable insights into ecosystem management. The thesis comprises seven chapters, the first of which is an introduction to the research. Subsequent chapters present the formulation and analysis of unique models represented as ordinary differential equations or delay differential equations. All proposed models are demonstrated to be well-posed, and their feasible steady-state solutions are determined. Numerous results are established regarding the existence and stability of equilibrium points. We examine the system dynamics by applying stability theory to both non-delayed and delayed models, exploring bifurcation theory, chaos theory, and the theory for seasonal models. To validate our theoretical findings, we conducted extensive numerical simulations. The mathematical results obtained are interpreted in the context of ecology. The abstract of every chapter is given as follows.

Chapter 1 presents the basic introduction to the forthcoming chapters. It contains the background and motivation of the research work carried out in this thesis. A brief overview of the key concepts frequently employed throughout this thesis is included. This chapter also contains the thesis objectives and most used mathematical tools in subsequent chapters.

In Chapter 2, we examined the dynamical features of a Leslie-Gower prey-predator model incorporating the effect of fear and group defense among prey and the mechanism of cooperative hunting by predators. A temporal delay in the prey species' specific growth rate to examine the impact of the fear reaction has been considered. The existence and uniqueness of the interior equilibrium are explained, and sufficient conditions for the local and global stability behavior are obtained. Regarding the fear parameter and cooperation strength parameter, the system undergoes Hopf-bifurcation, transcritical bifurcation, and saddle-node bifurcation. Additionally, we noticed how stability dynamics change when fear and delay are simultaneously varied. Moreover, the system exhibits bi-stability between two interior equilibrium points. The basin of attraction of these attractors is also plotted. We examined system dynamics for the fear-response delay and observed that the stability of positive equilibrium changes multiple times via supercritical Hopf bifurcation. Furthermore, we obtained two Hopf-point critical values of the fear parameter in the presence of delay.

In Chapter 3, we analyzed a system of delay differential equations incorporating prey's refuge, fear, fear-response delay, extra food for predators and their gestation lag. We assumed that the predator can choose between additional food and its favorite food (prey). We examined the system with or without delay. The persistence, stability (local and global) and various bifurcations are discussed. We performed detailed analysis for transcritical and Hopf-bifurcation. The existence of positive equilibria and the stability of prey-free equilibrium are interrelated. It is shown that (i) fear can stabilize or destabilize the system, (ii) prey refuge in a specific limit can be advantageous for both species, (iii) at a lower energy level (gained from extra food), the system undergoes a supercritical Hopf-bifurcation and (iv) when the predator gains high energy from extra food, it can survive through a homoclinic bifurcation, and prey may become extinct. The possible occurrence of bi-stability with or without delay is discussed. We observed switching of stability thrice via subcritical Hopf-bifurcation for fear-response delay. On changing some parametric values, the system undergoes a supercritical Hopf-bifurcation for both delay parameters. The delayed system undergoes Hopf-bifurcation, so we can say that both delay parameters play a vital role in regulating the system's dynamics.

In Chapter 4, we discussed the impact of additional food on prey-predator system in the presence of an infectious disease among prey. We formulated a three-dimensional system in which, along with additional food, the predator consumes susceptible (S) and infected (I) prey using a modified Leslie-Gower scheme. The predator can switch between prey and the provided extra food (similar to Chapter 3). Our study aims to control the existing disease in the system with the provision of alternative food. To achieve the goal, we investigated the suggested model and its disease-free subsystem theoretically and numerically. The scope of our analysis is broadened to encompass both local and global bifurcations. Hopf-bifurcation, transcritical bifurcation, saddle-node bifurcation, homoclinic bifurcation, heteroclinic bifurcation,

all occur due to stability transitioning between steady states or cycles. Numerical results indicated that the additional food parameter α_A contributes to the complex dynamics of the system. A slight modification in α_A can significantly change the characteristics of the entire system. In a specific range of α_A, all of these unanticipated changes render the system bi-stable and multi-stable. In such cases, we plotted their basins of attraction. Consequently, a set of starting values for which the system is disease-free is obtained. We also illustrated the phenomenon of global stability toward the positive equilibrium. Furthermore, the infection rate is capable of altering the dynamics of the system. Through a subcritical Hopf-bifurcation, it can control the oscillations in species around their positive steady state. However, ample energy from the alternative food may lead to disease eradication even for higher infection rates.

Chapter 5 also discusses an eco-epidemic model where prey exhibits herd behavior. The shape of the herd can alter the system dynamics significantly. When strong (susceptible) prey forms a herd to defend against the predator, it can reverse their role. This chapter focused on spotlighting the impact of disease, generalized herd shape, predator mortality due to prey group, the attack rate for healthy prey, and time delay. These factors crucially govern the system's dynamics like Hopf-bifurcation, transcritical bifurcation, and chaos. The sketch of the maximum Lyapunov exponent confirmed the chaotic nature. Extensive theoretical and numerical analysis revealed the existence and stability of steady-states in the presence or absence of delay. We found that disease spread in prey can enhance the chances of predator survival. Furthermore, sensitivity analysis demonstrates the influence of some epidemic and ecological parameters on the reproduction numbers of the proposed eco-epidemic system.

Chapter 6 highlights the reverse side of the same ecological coin by considering the counter-attack of prey on immature predators. We assumed that the birth rate of prey is affected by the fear of adult predators and its carry-over effects (COEs). Next, we introduced two discrete delays to show time lag due to COEs and fear-response. We observed that the existence of a positive equilibrium point and the stability of the prey-only equilibrium is independent of fear and COEs. Furthermore, the necessary condition for the co-existence of all three species is determined. Our system experiences several local and global bifurcations, like, Hopf, saddle-node, transcritical, and homoclinic bifurcation. The simultaneous variation in the attack rate of prey and predator results in the Bogdanov–Takens bifurcation. Our numerical results explained the paradox of enrichment, chaos, and bi-stability of node-focus and node-cycle types. The system, with and without delay, is analyzed theoretically and numerically. Using the normal form method and center manifold theorem, the conditions for stability and direction of Hopf-bifurcation are also derived. The cascade of predator attacks, prey counter-attacks, and predator defense exhibit intricate dynamics, which sheds light on ecological harmony.

The carrying capacity's functional dependence illustrates the reality that any species' activities can enhance or diminish its carrying capacity. Migration is the need of many species to

achieve better opportunities for survival. Chapter 7 deals with a tri-trophic system with variable carrying capacity, where the middle predator often immigrates to consume its prey and often emigrates to secure themselves from predators. We performed a detailed analysis to prove the boundedness of the solutions. Further, we examined the existence and stability of equilibrium points, followed by the bifurcation analysis. We explored various local and global bifurcations like Hopf, saddle-node, transcritical, and homoclinic for the critical parameters β (measuring the impact of prey activities on the carrying capacity) and k_1 (measuring the migration rate of a predator). Higher values of β generate unpredictability, which helps explain the enrichment paradox. The presence of a chaotic attractor and bi-stability of node-node type is demonstrated via numerical simulation. The migratory behavior of middle predators can control chaos in the system. Furthermore, we studied the proposed model in the presence of seasonal fluctuations. Persistence of the non-autonomous system, existence, and global stability of periodic solutions are proved. The seasonality in β brings the bi-stability of a chaotic and periodic attractor. Moreover, the bi-stability in the autonomous system shifts to the global stability of an equilibrium in the seasonal model. When birth and death rates are seasonal along with β, the extinction of one or more populations is possible. Our findings revealed that the population's intense constructive and destructive actions can allow the basal prey to thrive while eradicating both predators.

Contents

List of Figures

List of Tables

Dedicated To

My Parents and Husband,

The Pillars of My Strength

Chapter 1

Introduction

1.1 Basic introduction and literature survey

Mathematical biology is one of the most captivating and growing modern applications of mathematics. In recent years, this interdisciplinary field of study has brought together an enormous number of biologists, physicists, engineers, and mathematicians. Mathematical biologists develop models to depict biological processes such as population interaction, metabolic reactions, disease propagation, and evolutionary dynamics. These models assist scientists in simulating and analyzing real-world natural events in a regulated, theoretical context. Population biology involves various natural elements influencing populations, such as birth rates, mortality rates, migration, predation, competition, and environmental changes. The study of population dynamics examines how the population's density, structure, and distribution vary over time. In 1798, Thomas Robert Malthus [1] established the fundamental mathematical model to illustrate the exponential growth of any population. The renowned Malthus model is given by

$$\frac{dx}{dt} = rx,$$

with $x(0) = x_0$ is the initial population density, and r is the population growth rate.
Although this model served as the cornerstone for population dynamics, it fails to represent reality accurately. Due to the limited resources, every habitat has a limited capacity to sustain its inhabitants. This presumption became the primary basis of contention for the Malthusian hypothesis. Later on, in 1838, Pierre F Verhulst [2] worked on the shortcomings of Malthus model, and proposed the following logistic growth population model.

$$\frac{dx}{dt} = rx\left(1 - \frac{x}{K}\right),$$

where r is the intrinsic growth rate, and K is the environmental carrying capacity. The nonlinearity in the logistic growth function explains the overcrowding effect limiting the population

growth.

Although the logistic growth model discusses only a single species, one can rely on other species for food, habitat, or other resources. For conservation efforts, it is essential to comprehend these dependencies. A species' disruption can have a massive impact on the whole ecosystem. The interaction between species can drastically alter the system's dynamics. In ecological research, it is vital to investigate the interactions between organisms to sustain balanced growth. These interactions are represented as mathematical models, which aid in understanding the system's ongoing dynamics.

Predator-prey interactions are a major evolutionary driving force, mediating the behavior of both predator and prey. Initially, Lotka and Volterra (LV) [3, 4] expressed the relationship of prey and predator in terms of two-dimensional ordinary differential equations, given by

$$\begin{aligned}\frac{dx}{dt} &= ax - bxy,\\ \frac{dy}{dt} &= cxy - dy,\end{aligned}$$

where $x(t)$ and $y(t)$ are the prey and predator population density at any time t, respectively, a is the natural growth rate of prey and d is the natural mortality rate of predator. The predator attacks on prey with rate b, and $\frac{c}{b}$ is the conversion efficiency. This is the basic model developed to describe oscillations in several populations. Nevertheless, it does not relate to many realistic scenarios. One of which is that the prey population grows unbounded without predation. The other shortcoming of the LV model is that the feeding rate of the predator increases with the number of prey linearly without saturation. This model also considers that the predator is a specialist, i.e., they consume only a specific type of prey. However, when the predator consumes more than one type of food resource (generalist predator), it can not be represented through the LV model. Notwithstanding its limitations, the model has influenced population biology and ecology by offering a framework for comprehending interactions between predators and prey.

Leslie [5] introduced a predator-prey model where the carrying capacity of the predator is directly proportional to the prey density. The Leslie-Gower formulation [6] posits that a predator population's decline is proportional to the per capita availability of its favorite food. They expressed predator's growth as a logistic growth function. Therefore, the Leslie-Gower (LG) model is given by

$$\begin{aligned}\frac{dx}{dt} &= (r_1 - b_1 x - a_1 y)x,\\ \frac{dy}{dt} &= \left(r_2 - a_2\frac{y}{x}\right)y,\end{aligned}$$

where r_1 and r_2 are the growth rates of prey and predator, respectively, b_1 measures the strength

of competition among individuals of species x, a_1 (respectively, a_2) is the maximum value at per capita reduction rate of x (respectively, to y) can attain. When there is extreme scarcity, y can switch to other populations, but its development will be constrained by the lack of its most preferred food x. This issue can be resolved by increasing the denominator by a positive constant d, it measures the extent to which environment provides protection to predator. Thus, the predator's equation of the modified Leslie-Gower model becomes

$$\frac{dy}{dt} = \left(r_2 - a_2\frac{y}{x+d}\right)y,$$

where $\frac{y}{x+d}$ is the modified LG term showing that the predator y can survive even in the absence of its favorite food x [7].

Ideally, to maximize the fitness of a prey-predator relationship, we analyze the impact of various factors affecting their interaction, like hunting rate, handling time, search efficiency, feeding rate, predator interference, and several environmental factors. Studying these concepts is crucial and challenging, making the system more consistent with the real world. A predator's per capita feeding rate on prey is called its functional response [8]. Using distinct functional responses allows ecologists to accurately formulate a wide range of ecosystems and investigate complex dynamics. The famous LV and LG models showed that the predator's feeding rate linearly increases with prey abundance using Holling type I functional response. However, the predator's limited capacity to process food and the time required for handling the prey cannot be ignored. This led to the proposal of Holling type II, a non-linear functional response. Another functional response, Holling type III, was developed considering additional factors such as prey switching and the learning time of the predator. When the prey density is abundant, they can form groups to defend themselves against predators. This ecological aspect is represented through the Holling type IV functional response. All these responses are merely prey-dependent functions, which are widely used by researchers to present a specific ecological scenario [9, 10, 11, 12].

Functional responses implemented in the system represent direct killing only. However, a predator's mere presence might have an impact on the prey's physical and mental health [13]. While looking for food, there is often a risk of predators, which might lead to starvation [14]. The fearful prey may not get an appropriate environment to breed young ones. And the indirect effect of dread can be more lethal than the direct effect of killing [15, 16, 17]. Many experimental studies suggest that fear can significantly affect the reproduction rate of prey [18, 19]. Wang *et al.* [17] proposed the basic prey-predator model incorporating fear effect on the reproduction rate. According to their study, a high level of fear can control oscillations and stabilize the system, and it can also reverse the direction of Hopf-bifurcation from supercritical to subcritical. Following this, numerous authors focused on understanding predator fear using

mathematical models [20, 21, 22]. However, several clinical trials in recent years have revealed that such non-lethal effects are not restricted to a single species generation but have a long-term impact lasting many generations [23]. This explains the term "carry-over effect (COE)," which refers to how past conditions affect the current state of prey survival, behavior, and reproductive success. The conditions may influence breeding success in one season encountered the previous season [24]. Therefore, studying ecological COEs has become a growing trend in mathematical modeling. Several researchers [21, 23, 25, 26] investigating fear and its COEs found that increased COE enhances prey growth because of lessons learned from previous incidents.

It is critical to secure the safety of the prey in order to preserve biodiversity and maintain ecological balance. Nature can provide some shelter to prey to help them avoid predators through prey refuge. It regulates population densities and reduces the over-exploitation of prey. However, prey refuge up to a large extent can cause difficulty for predators to capture them, and consequently, their population starts to decline [27]. Therefore, there is a need to balance the prey refuge and hunting capability. In nature, many predators hunt in groups for a common target, which improves their communal attack rate. For example, spotted hyenas succeeded in 15% of solo hunts of wildebeest Connochaetes taurinus calves, whereas 74% of team hunts [28]. Group hunting offers several advantages, such as decreasing searching time, chasing distance, and increasing the hunting probability of large prey. The mathematical implementation of this factor modifies the functional response, precisely the attack rate. Pal *et al.* [20] investigated the integrated impact of fear and cooperative hunting in their model, detecting various bifurcations and multi-stability.

Apart from predators forming groups, prey can also gather in groups for foraging and self-defense. Group defense is an effective anti-predator behavior exhibited by many prey species. It enhances their chances of survival, strengthens their social bond, and reduces the predation risk. According to an experimental investigation, minnows' shoaling behavior reduces the risk of predation. Ajraldi *et al.* [29] gave the fundamental mathematical model describing the prey herd behavior so that the predator cannot reach the herd's interior. Only the prey on the boundaries can be the victims. They represented the prey herd by using a square root term $(\sqrt{X})$ instead of the simple prey term (X). Nevertheless, it could explain only two-dimensional herd shapes. Venturino and Petrovskii [30] came up with further advancements and gave the concept of a generalized herd shape by introducing X^{α}, where $\alpha \in (0,1)$ signifies the type of herd shape. Subsequently, many researchers used this concept to describe prey-predator inter-relationships [31, 32]. Sometimes, when strong prey exhibit herd behavior, they can not only protect themselves but also kill the predator [33]. This shows the role reversal of prey and predator due to herd behavior. The phenomenon of role reversal can also be witnessed in the stage-structured prey-predator system. When an adult predator kills prey, then prey takes revenge by counter-attacking predator juveniles [34]. This provokes parent predators to hunt

more, and the tug-of-war goes on offering rich dynamics to understand the mathematical and ecological perspective.

The dominance of prey defense can lead to predator extinction [35]. The provision of additional food to the predator increases their chances of survival. Kumar and Dubey [36] found that without additional food, both populations oscillate, and these oscillations can be completely controlled by increasing the predator's need for extra food. Indeed, supplying additional food is advantageous for weak and suffering predators. For example, lionesses at AENP were given culled warthog carcasses while they were struggling to keep newborn cubs alive [37]. Some articles suggest that additional food for the predator regulates the effect of fear and prey refuge by promoting persistence [38, 39]. Furthermore, supplying alternative food to the predator is proven to be a non-chemical method of disease control among prey [40].

The first mathematical description of contagious diseases in populations was formulated by Kermack and McKendric [41]. They classified the whole population into three primary compartments: susceptible-infected-recovered (SIR), which inspired a lot of researchers to study the spread of infectious diseases through mathematical modeling. Depending upon the nature of the disease, different incidence rates, such as bilinear, saturation, etc., are used [42, 43]. It is a fundamental metric for understanding the risk and impact of a disease within a community. Nowadays, illness in ecosystems has evolved into an exciting field of study known as eco-epidemiology. This field examines how different species interact in the presence of an infectious disease and how their dynamics are affected. Anderson and May [44] introduced the basic concept of mathematical modeling in eco-epidemiology. They found that the pathogen invasion in a prey-predator system could alter the stability behavior. In an eco-epidemic model with alternative food for the predator, Haque and Greenhalgh [45] pointed out that alternative food may play an essential role in promoting the persistence of predator-prey systems. Banerjee *et al.* [46] conducted a thorough analysis of local and global bifurcations for an eco-epidemic model with healthy prey showing herd behavior.

Many researchers in the past have seen that very complex dynamics can arise in a system with three or more species. One necessary approach to studying an ecological community begins with an important object: its food web. In literature, the dynamics of a tri-trophic system are found to be of greater interest than a simple two-dimensional system. Initially, Hastings and Powell [47] detected chaos in a tri-trophic food chain model with Holling type II functional response for biologically reasonable parameter values. Later on, a multitude of research articles were published comprising food-chain models and their complex dynamics [48, 49]. In a phytoplankton-zooplankton-fish system, zooplankton shows anti-predator behavior by migrating from the system. It moves down into the sea's deepest depths to evade being noticed by fish, the top predators [50]. Hossain *et al.* [51] remarked that immigration and emigration of middle predators can be crucial in controlling chaos in a food-chain system.

Another aspect that can bring more realism in population dynamics is considering the carrying capacity as non-constant. Carrying capacity is the maximum sustainable population strength an environment can support with the available resources. However, it is significantly depleted or enriched by the impact of population activities [52]. Recently, the concept of the variable carrying capacity of any species, formulated as the combination of the natural carrying capacity and its density, has been highlighted [53, 54]. Constructive activities such as establishing wildlife reserve zones for animals can increase their carrying capacity. In contrast, destructive activities like overgrazing by animals can degrade the land, resulting in a decrement in their carrying capacity. Therefore, it is crucial to investigate the impact of population activities on the system dynamics.

Time delay plays a fundamental role in most natural and man-made processes. This indicates that any event that occurred at a past time influences the current state, represented mathematically by delay differential equations [55]. Delay differential equations show biological events more realistically and elicit intricate dynamics [56]. Natural processes usually demonstrate a temporal lag between the occurrence of an event and the visualization of its consequences. For example, it takes time to process gestation, maturation, anti-predator response, defense mechanism, behavioral change, etc. Therefore, there is a large body of literature on ecological systems incorporating time delays [11, 21, 22, 33, 36]. Considering time delays in mathematical modeling is essential for capturing the real-world dynamics of systems and developing more accurate predictions.

Most ecological phenomena are examined under a constant environment, which is odd. The seasonally varied parameters produce periodic oscillations in the system [57]. This aspect is generally modeled using time-dependent parameters. The resulting non-autonomous system is quite challenging to analyze compared to the non-seasonal autonomous system. Mondal *et al.* [58] compared the seasonal and non-seasonal pre-predator models with fear, cooperation, and refuge. Their numerical results reveal the presence of higher periodic and chaotic attractors. Zeng [59] employed Mawhin's coincidence degree theory to show the existence of periodic solutions in a non-autonomous food-chain model.

1.2 Objectives of the thesis

This thesis aims to examine various factors that significantly affect the harmony of an ecosystem and to address some biological population-related challenges that can alter ecological stability. We found some gaps based on the abovementioned literature review, which we state as our thesis objectives.

1. To analyze the impact of fear, hunting cooperation, and time delay in a Leslie-Gower prey-predator model.
2. To study the complex dynamics of a Leslie-Gower prey-predator model with fear, refuge, and additional food effects under multiple delays.
3. To understand the correlation between disease and alternative food in an eco-epidemic model.
4. To explore the occurrence of bifurcations and chaos: consequences of prey configuration in an eco-epidemic system.
5. To investigate the role-reversal phenomenon in a delayed stage-structured prey-predator model with fear and its carry-over effects.
6. To study the chaotic dynamics in a seasonal food-chain model with migration and variable carrying capacity.

1.3 Some useful definitions and key concepts

Most dynamical systems in ecology can be adequately expressed as differential equations. The general form of the system of ordinary differential equations is given by

$$\frac{du}{dt} = f(u),\ u(t_0) = u_0, \tag{1.1}$$

where $u(t) = (u_1(t), u_2(t), ..., u_n(t))^T$, $f(u(t)) = (f_1, f_2, ..., f_n)^T$ and t_0 is the initial time of the solution. The sufficient smoothness of f guarantees the existence and uniqueness of the solution for (1.1).

Definition 1.3.1. *The solution $u(t)$ of (1.1) is said to be **stable** if, for each $\varepsilon > 0$, there exists a $\delta = \delta(\varepsilon) > 0$ such that, for any solution $\bar{u}(t) = u(t, t_0, \bar{u_0})$ of (1.1), the inequality $\|\bar{u_0} - u_0\| < \delta$ implies $\|\bar{u}(t) - u(t)\| < \varepsilon\ \forall t \geq t_0$.*

Definition 1.3.2. *The solution $u(t)$ of (1.1) is called **locally asymptotically stable** if it is stable and there exists a $\delta_0 > 0$ such that $\|\bar{u_0} - u_0\| < \delta_0$ implies $\|\bar{u}(t) - u(t)\| \to 0$ as $t \to \infty$.*

Definition 1.3.3. *The solution $u(t)$ of (1.1) is called **unstable** if it is not stable.*

Definition 1.3.4. *A point $u^* \in R^n$ is called an **equilibrium point** or steady-state solution of (1.1) if $f(u^*) = 0$. This equilibrium point is said to hyperbolic if no eigenvalue of $Df(u^*)$ (Jacobian of f calculated at u^*) have zero real part.*

Definition 1.3.5. *An equilibrium point u^* of system (1.1) is called* ***source*** *(unstable) or* ***sink*** *(stable) if all the corresponding eigenvalues of $Df(u^*)$ have positive or negative real parts, respectively. u^* is called a* ***saddle point*** *if at least one eigenvalue has a real part of the opposite sign from other eigenvalues.*

Definition 1.3.6. *An equilibrium point u^* of (1.1) is called* ***globally asymptotically stable*** *if every solution initiated from a bounded domain converges to u^*.*

Definition 1.3.7. *A closed solution trajectory of (1.1) is said to be* ***periodic orbit or cycle*** *if it is not a steady-state. The stability of this periodic orbit or cycle can be defined similar to the stability of an equilibrium point.*

Definition 1.3.8. *The* ***trajectory or orbit*** *$\phi(t_0)$ of (1.1) is defined as*

$$\phi(t_0) = \{u \in R^n : \ u = u(t, t_0, u_0), t \in R\},$$

where $u(t, u_0)$ is any solution of (1.1) defined $\forall t \in R$.

Definition 1.3.9. *[60] A point $q \in E$ (subset of R^n such that $f \in C^1(E)$) is called a* ***ω-limit point*** *of ϕ if $\exists$ a sequence $\{t_n\}$, $t_n \to \infty$ as $n \to \infty$ such that*

$$\lim_{n\to\infty} \phi(t_n, y_0) = q.$$

In a similar manner, a point $p \in E$ is called an ***α-limit point*** *of ϕ if $\exists$ a sequence $\{t_n\}$, $t_n \to -\infty$ as $n \to \infty$ such that*

$$\lim_{n\to\infty} \phi(t_n, y_0) = p.$$

Definition 1.3.10. *[60] A periodic solution Γ of (1.1) is called* ***limit cycle*** *if it is either ω or α-limit set of some another orbit. If a periodic orbit Γ is ω-limit set (or α- limit set) of every orbit in its neighbourhood then it is called a stable limit cycle (or unstable limit cycle). If Γ is α-limit set of one orbit other than itself and ω-limit set of another orbit than itself then is known as semi-stable limit cycle.*

Definition 1.3.11. *A set $\Omega \in R^n$ is called an* ***invariant set*** *if for every solution u, $u(t_0) \in \Omega$ implies $u(t) \in \Omega \ \forall t > t_0$.*

Definition 1.3.12. *The collection of initial points $u_0 \in R^n$ is called the* ***basin of attraction*** *for an attractor $\tilde{a}$ of (1.1) if*

$$\lim_{t\to\infty} u(t, u_0) = \tilde{a}.$$

Definition 1.3.13. *In a dynamical system,* ***multi-stability*** *occurs when more than one attractors are present at the same time. The curve separating their basin of attraction is known as* ***separatrix***.

Definition 1.3.14. *An individual who is healthy and can get disease under certain conditions is said to be **susceptible** (S). The ones who have contracted the disease are called **infected** (I) and can transmit the illness to the susceptible population.*

Definition 1.3.15. *The **Basic reproduction number** (R_0) is defined as the average number of secondary infections caused by an infected individual, in a fully susceptible population. In commonly used infection models, when $R_0 > 1$ the infection will be able to start spreading in a population, but not if $R_0 < 1$.*

Definition 1.3.16. *In dynamical systems theory, a **bifurcation** is a qualitative change in the behavior of a system as one or more parameters are varied. Qualitative change can occur by the variation in the number of steady-states or stability behavior.*

Definition 1.3.17. *With variation in a parameter, when one saddle and one stable equilibrium points approach each other and annihilate at a critical point, it is called **saddle-node bifurcation**.*

Definition 1.3.18. *The **transcritical bifurcation** occurs when two equilibrium points exchange their stability with the variation of a single parameter.*

Definition 1.3.19. *The transition from a steady-state to periodic oscillations arises due to **Hopf-bifurcation**. At the bifurcation point, the real part of the complex eigenvalues becomes zero.*

Definition 1.3.20. *In **supercritical Hopf-bifurcation**, a stable equilibrium loses its stability, and a stable limit cycle occurs when a parameter crosses a threshold.*

Definition 1.3.21. *In **subcritical Hopf-bifurcation**, an unstable equilibrium gains stability by generating an unstable limit cycle on crossing a parameter critical point.*

Definition 1.3.22. *When a limit cycle expands and connects a saddle point, it is called **homoclinic bifurcation**, and the formed structure is a homoclinic orbit.*

Definition 1.3.23. *In **heteroclinic bifurcation**, a limit cycle collides with two or more saddle points. The resultant periodic orbit is called heteroclinic orbit.*

Definition 1.3.24. *The **Bogdanov-Takens bifurcation** involves the interaction of different bifurcations like saddle-node, homoclinic, and Hopf bifurcations when two parameters are simultaneously varied. It is a well-known example of co-dimension two bifurcation.*

Definition 1.3.25. *A **chaotic** solution is defined as behavior that is extremely sensitive to initial conditions and appears unpredictable even when the system is deterministic and governed by certain equations.*

Definition 1.3.26. *A **delay differential equation** (DDE) is a differential equation using delays as the dependent variable. In other words, the rate of change of dependent variables at a given time is determined by their current and previous states. The general form of DDE is given by*

$$\frac{du(t)}{dt} = f(t, u(t), u_\tau),$$

where $u_\tau = \{u(\tau) : 0 \leq \tau \leq t\}$ represents the solution trajectory in the past.

Definition 1.3.27. *A **functional response** in mathematical ecology refers to the link between the density of a prey population and the consumption rate or feeding rate of its predators. It illustrates how the pace at which predators consume prey fluctuates with changes in prey abundance. Some frequently used functional responses in the literature with their mathematical forms are enlisted in Table 1.1.*

Table 1.1: Some of the most common functional responses used in the literature.

Functional response	Mathematical expression	Reference(s)
Holling type I	αx	[61, 62]
Holling type II	$\frac{\alpha x}{1+\alpha h x}$	[61, 62]
Holling type III	$\frac{\alpha x^2}{1+\alpha h x^2}$	[61, 62]
Holling type IV	$\frac{\alpha x}{\frac{x^2}{i}+x+b}$	[63]
Beddington DeAngelis	$\frac{\alpha x}{1+\alpha h x+by}$	[64]
Crowley Martin	$\frac{\alpha x}{(1+\alpha h x)(1+by)}$	[65]

Definition 1.3.28. *A system of differential equations is referred to as **non-autonomous** when (1.1) explicitly depends on time; otherwise, it is an autonomous system.*

Definition 1.3.29. *[66] Let $D \subset R^N$ be a bounded open set and $T : \bar{D} \to R^N$ be a continuously differentiable map. Let $T'(u)$ be its Jacobian, and det $T'(u)$ be the Jacobian's determinant. If $z \notin T(\partial D)$, then the **Brouwer degree** can be given as*

$$deg(T, D, z) := \sum_{u \in T^{-1}(z)} sign\ det\ T'(u).$$

Definition 1.3.30. *[67] Let X and Y be two Banach spaces and an operator $T : X \to Y$ is named as **Fredholm operator** if dimension of its kernel and codimension of its image are finite. The index of the Fredholm operator is given by*

$$indexT = dimKerT - codimImT.$$

1.4 Methodology

To analyze the properties like stability, chaos, basic reproduction number, bifurcation associated with our proposed models defined by ordinary differential equations and delay differential equations, we adopt the following different approaches:

1. **Linearization of differential equations:** Assume that our model can be represented in the following form
$$\frac{dX(t)}{dt} = F(X(t)), \tag{1.2}$$
where $X(t) = (x_1(t), x_2(t), ..., x_n(t))^T$ and $F(X(t)) = (f_1, f_2, ..., f_n)^T$.
Let $Z(t) = (z_1(t), z_2(t), ..., z_n(t))^T$ such that $z_i(t) = x_i(t) - x_i^*,\ i = 1, 2, ..., n$ and $E^* = (x_1^*, x_2^*, ..., x_n^*)^T$ be the equilibrium point corresponding to the given system (1.2). Linearizing (1.2) about E^*, we get
$$\frac{dZ(t)}{dt} = DZ(t), \tag{1.3}$$
where $D = \frac{\partial F}{\partial X}\Big|_{E^*}$ is the Jacobian matrix evaluated at E^*.

2. **Local stability:** To determine stability of an equilibrium point in its neighbourhood, we first evaluate the characteristic equation corresponding to Jacobian matrix at the equilibrium point, and then we check the sign of real part of the eigenvalues of this equation. For this we use following theorem:

Theorem 1.4.1. *(Hurwitz's Theorem)[68] A necessary and sufficient condition for the negativity of the real parts of all the roots of the equation*
$$\lambda^n + a_1\lambda^{n-1} + ... + a_n = 0, \tag{1.4}$$
with real coefficients is the positivity of all principle diagonals minors of the Hurwitz matrix
$$H_n = \begin{bmatrix} a_1 & 1 & 0 & 0 & 0 & 0 & 0 & \dots & 0 \\ a_3 & a_2 & a_1 & 1 & 0 & 0 & 0 & \dots & 0 \\ a_5 & a_4 & a_3 & a_2 & a_1 & 1 & 0 & \dots & 0 \\ \vdots & \vdots & \vdots & \vdots & \vdots & \vdots & \vdots & \vdots & \vdots \\ 0 & 0 & 0 & 0 & 0 & 0 & 0 & 0 & a_n \end{bmatrix}.$$

Remark: The characteristic equation (1.4) is said to be stable if all its roots have negative real part.

3. **Global stability:** If a trajectory initiating from anywhere in its domain approaches to the same equilibrium point, then that equilibrium is said to be globally stable. In this method, we choose a positive definite Lyapunov function to establish the sufficient conditions for the global stability of the system around the critical point.
   Let us consider an autonomous system of ODEs:

$$\frac{dx}{dt} = f(x), \tag{1.5}$$

   where $f \in C^1(R^n)$ and $S_\rho = \{x \in R^n : ||x|| < \rho\}$ such that f is smooth enough to ensure the existence and uniqueness of (1.5) and x^* is the equilibrium point for it.
   We have some important results to ample the conditions ensuring the global stability of the system. Thus, we can state the following theorems.

Theorem 1.4.2. *If there exists a scalar function $V(x)$ which is positive definite about x^* such that $V'(x) < 0$ (derivative of $V(x)$ along (1.5) is negative definite) on S_ρ, then x^* is asymptotically stable.*

Theorem 1.4.3. *If there exists a scalar function $V(x)$ which is positive definite about x^* such that $V'(x) \leq 0$ on S_ρ, then x^* is stable.*

Theorem 1.4.4. *If there exists a scalar function $V(x); V(0) = 0$ such that $\frac{dV}{dt} > 0$ on S_ρ and if in every neighbourhood N of the x^*, $N \subset S_\rho$, there is a point x_0 where $V(x_0) > 0$ then then x^* is unstable.*

Theorem 1.4.5. *Consider system (1.2) with $n = 2$ and B is a continuously differentiable function on a simple connected domain D. Now, we define*

$$\nabla = \frac{\partial}{\partial x_1}(f_1 B) + \frac{\partial}{\partial x_2}(f_2 B).$$

If the sign of ∇ remains same throughout D, then according to the Bendixson-Dulac criteria, system (1.2) (for $n = 2$) will not have a periodic solution in D.

4. **Bifurcation theory:** If varying a parameter changes the qualitative behavior of steady state(s) of a dynamical system then we say that the system undergoes bifurcation.

   For an illustration of the Sotomayor theorem's conditions [60] to show the occurrence of saddle-node and transcritical bifurcation, we consider the following system.

$$\frac{dx}{dt} = f(x, \alpha), \tag{1.6}$$

where α as the bifurcation parameter. Let $x = x_0$ be the hyperbolic equilibrium of system (1.6) at the critical point $\alpha = \alpha_0$. Now, we determine the eigenvectors p and q for the zero eigenvalue of $A = Df(x_0, \alpha_0)$ and A^T, respectively. Further, we proceed with Theorems 1.4.6 and 1.4.7.

Theorem 1.4.6. *System (1.6) experiences saddle-node bifurcation about $x = x_0$, a hyperbolic equilibrium, at $\alpha = \alpha_0$ if the following conditions of the Sotomayor's theorem [60] are fulfilled.*

(i) $q^T f_\alpha(x_0, \alpha_0) \neq 0$, *and*

(ii) $q^T [D^2 f(x_0, \alpha_0)(p, p)] \neq 0$.

Theorem 1.4.7. *System (1.6) experiences transcritical bifurcation about $x = x_0$, a hyperbolic equilibrium, at $\alpha = \alpha_0$ if the following conditions of the Sotomayor's theorem [60] are fulfilled.*

(i) $q^T f_\alpha(x_0, \alpha_0) = 0$,

(ii) $q^T [Df_\alpha(x_0, \alpha_0)p] \neq 0$, *and*

(ii) $q^T [D^2 f(x_0, \alpha_0)(p, p)] \neq 0$.

In Hopf-bifurcation, $Df(x_0, \alpha_0)$ has a pair of complex eigenvalues. The supercritical or subcritical Hopf-bifurcation occurs when the complex eigenvalue crosses the imaginary axis from left to right (negative to positive) or right to left (positive to negative).
Let us consider a planar system

$$\frac{dx_1}{dt} = f_1(x_1, x_2, \alpha), \ \frac{dx_2}{dt} = f_2(x_1, x_2, \alpha). \tag{1.7}$$

Now, we suppose that the jacobian matrix about $E^* = (x_1^*, x_2^*)$ has eigenvalues $\lambda_{1,2}(\alpha) = \xi(\alpha) \pm i\omega(\alpha)$. Further, we assume that the following conditions hold at $\alpha = \alpha_0$:

(i) non-hyperbolicity condition:

$$\xi(\alpha_0) = 0, \ \omega(\alpha_0) = \omega > 0,$$

(ii) transversality condition:

$$\left.\frac{d\xi(\alpha)}{d\alpha}\right|_{\alpha=\alpha_0} = d \neq 0,$$

then system (1.7) experiences Hopf-bifurcation about E^* at $\alpha = \alpha_0$ [69]. Furthermore, to determine the direction of Hopf-bifurcation, using [17], we calculate

$$\sigma = \frac{1}{16}(f_{1x_1x_1x_1} + f_{1x_1x_2x_2} + f_{2x_1x_1x_2} + f_{2x_2x_2x_2}) + \frac{1}{16\omega}(f_{1x_1x_2}(f_{1x_1x_1} + f_{1x_2x_2}) - f_{2x_1x_2}(f_{2x_1x_1} + f_{2x_2x_2}) - f_{1x_1x_1}f_{2x_2x_2} + f_{1x_2x_2}f_{2x_2x_2}),$$

where $f_{x_1x_2} = \left.\frac{\partial^2 f}{\partial x_1 \partial x_2}\right|_{E^*,\alpha=\alpha_0}$, and other derivatives can be written in a similar manner. Therefore, the obtained Hopf-bifurcation is supercritical (or subcritical) if σ is negative (or positive).

5. **Chaos detection:** Some dynamical systems exhibit chaos. In this case, the system is extremely sensitive to initial conditions. A minor change in the initial condition generates a large change in the system's behavior, making it unpredictable in the future. However, not all systems are chaotic. For chaos confirmation, we determine the maximum Lyapunov exponent, defined as

$$\lambda = \lim_{t\to\infty} \lim_{\delta Z_0 \to 0} \frac{1}{t} ln \frac{\delta Z(t)}{\delta Z_0},$$

where δZ_0 is the perturbation in the initial condition, and $\delta Z(t)$ is the resulting change in the solution.
Remark: For a system to be chaotic, the corresponding maximum Lyapunov exponent must be positive.

6. **Basic reproduction number (R_0):** To calculate this number we shall use a standard method i.e., next generation matrix method [70]. The dominant eigenvalue of this matrix is equal to the basic reproduction number. We use this method for the analysis of an eco-epidemic model.

7. **Sensitivity analysis:** Sensitivity indices help us to quantify the relative change in a state variable when a parameter is changed. The normalized forward sensitivity index of differentiable R_0 dependent on any of its parameters p is defined as follows.

$$\gamma_p^{R_0} = \frac{\partial R_0}{\partial p} \frac{p}{R_0},$$

where $\gamma_p^{R_0}$ represent the sensitivity level with regard to any parameter p for R_0. A positive sensitivity index implies that an increase (or decrease) in the value of a parameter corresponds to an increase (or decrease) in the reproduction number. In contrast, negative

index parameters indicate that a rise (or reduction) in the value of the parameter results in a drop (or increase) in the reproduction number [71].

8. **Existence and global stability of a periodic solution in non-autonomous system:** In a non-autonomous system, the time-dependent parameters can cause the system to have a periodic solution. The illustration of the periodic solution's existence and global stability is a complex task and requires advanced mathematical techniques. We use the following theory to understand the same.

   Lemma 1.4.8. *[56] If function g is non-negative, uniformly continuous and integrable on* $[0,\infty)$*, then* $\lim_{t\to\infty} g(t) = 0$.

   For the existence of periodic solutions of a non-autonomous model, we use continuation theorem from coincidence degree theory by Gains and Mawhin [72]. Let P and Q be two normed vector spaces, $F: DomU \subset P \to Q$ is a linear map, and $W: P \to Q$ is a continuous map. If F is a Fredholm operator of index zero i.e., dim Ker$F$ =codim Im $F < \infty$ and there exists a non-continuous projection $S: P \to Q$ and $R: V \to V$ such that Im S =Ker F, Im F =Ker R =Im$(I-R)$ then $F|DomF \cap KerS : (I-S)X \to ImF$ is invertible. Let F_S^{-1} be the inverse of F. Let ϕ be an open bounded subset of P such that $RW(\bar{\phi})$ is bounded and $F_S^{-1}(I-R)W : \bar{\phi} \to P$ is compact then W is said to be F-compact on $\bar{\phi}$. Let Im R is isomorphic to Ker F, so there exists an isomorphism $K: ImR \to KerF$.

   Lemma 1.4.9. *[72] Let F be a Fredholm operator with index zero and W be a F-compact on* $\bar{\phi}$*. If*

   (a) for each $\rho \in (0,1)$*, each solution u of* $Fu = \rho Wu$ *is such that* $u \notin \partial\phi$*,*

   (b) $RWu \neq 0$ *for every* $u \in \partial\phi \cap KerF$*,*

   (c) the Brouwer degree $deg(KRW, \phi \cap KerF, 0) \neq 0$*,*

   then the equation $Fu = Wu$ *has atleast one solution in* $DomF \cap \bar{\phi}$*.*

9. **Numerical Simulation:** In every forthcoming chapter of this thesis, we perform extensive numerical simulations with the help of Mathematica/MATLAB to validate the theoretical findings. We mainly use standard MATLAB solvers *ode*45 and *dde*23 to solve system of ODEs and DDEs, respectively. The obtained plots help us to visualize population dynamics with respect to the crucial ecological factors.

Chapter 2

Bifurcation Analysis of a Leslie-Gower Prey-Predator Model with Fear, Cooperative Hunting and Time Delay[1]

2.1 Introduction

A classic use of mathematics in ecology is the study of prey-predator interactions using differential equations. The dynamics of such systems are often altered due to various ecological factors. Employing these factors makes the system more consistent with the real world. Many field experiments conducted by ecologists show that the growth rate of prey is affected not only by direct killing by its predator but also by the non-consumptive action of the predator [19, 73, 74]. According to naturalists, it comes from predation-induced fear in the prey species. Due to this, prey exhibits various anti-predation behaviors, such as changes in habitat, foraging behavior, and other physiological changes. In the long run, these actions decrease the fecundity and survival of prey species. Wang *et al.* [17] proposed and analyzed the basic mathematical model that takes into account the cost of fear, which lowers the birth rate of prey. From thereon, many researchers studied the complex dynamics with respect to fear in various predator-prey models [22, 75, 76]. Introducing fear may cause the interacting populations to oscillate or stabilitate about their steady-state [20]. These oscillations are most commonly due to the occurrence of Hopf-bifurcation [77].

In population dynamics, group defense is a common concept that describes an instance in which prey form groups to defend against the predator, which can cut off the predation rate. According to an experimental investigation, minnows' shoaling behaviour reduces the risk of predation [78]. Considering Holling type IV or Monod-Haldane type functional response is the most frequent and accessible technique to implement group defense [79, 80]. Mishra *et al.*

[1] A considerable part of this chapter is published in *Nonlinear Dynamics and Applications: Proceedings of the ICNDA 2022*, 1069-1080, 2022.

[81] explored a Leslie-Gower prey-predator model with group defence and found that increased prey defensive ability results in model destabilization, which can result in periodic and chaotic variations. It is evident from the research that dominance of defense could lead to predator's extinction [82]. The cooperation among predators to hunt down the target significantly increase the chances of their survival [83]. Saha and Samanta [84] extensively studied a 3-D prey-predator model involving cooperative hunting strategy and group defense mechanism. They observed transcritical bifurcation, saddle-node bifurcation, Hopf- bifurcation, and many other type of bifurcations. Pal *et al.* [20] studied the combined effect of fear and cooperative hunting and they observed various bifurcations and bi-stability in their model. The predator often switches to a different food to prevent extinction and becomes a generalist. The standard way to incorporate this feature is to use the modified Leslie-Gower scheme. Many authors [7, 85, 86] remarked the persistence of species in the modified Leslie-Gower prey-predator model.

The presence of time lag is common in most natural and man-made events. This indicates that the impact of an event occurring at a former period is perceived at the present moment, which is mathematically represented by delay differential equations. Biological events represented by delay differential equations appear more lifelike and induce complicated dynamics [55, 56]. In general, natural processes like gestation, maturation, incubation, etc., have a temporal lag between the occurrence of an event and the visualization of its impact. Tiwari *et al.* [75] investigated a non-autonomous predator-prey system implementing fear, hunting cooperation, and prey refuge with multiple time delays, including fear response delay. They found that while fear, hunting cooperation, and fear response delay destabilize the system, a larger time lag in the fear response pushes the system back to a stable state. Based on the aforementioned facts, ecological systems with time delays have been extensively studied [22, 87, 88, 89].

As per our knowledge, there is no work done comprising fear, fear-response delay, group hunting, and group defense in a Leslie-Gower prey-predator model. Hence our main purpose is to study the effects of group defense in prey, group hunting in predator and fear induced by predator in prey on the dynamical behavior of prey-predator system.

2.2 The mathematical model

The survival of species is one of the most fundamental and significant issues in ecology. In this section, we formulate a system of differential equations explaining the interaction of prey $x(t)$ and predator $y(t)$ at any instant of time t in the presence of several ecological factors.

1. The modified Leslie-Gower prey-predator model formulation is an interesting approach in species conservation. According to this scheme, the predator acts as a generalist, which increases their chances of survival [90]. Therefore, we assume that the predator

can consume prey as well as other food provided, and their relationship is represented using modified Leslie-Gower scheme.

2. The fear of predation can cause a significant reduction in the growth rate of prey [17]. So, we multiply the growth rate r with the term $\frac{1}{1+Ky}$, a decreasing function of predator population, where K denotes the level of fear. As the impact of the anti-predation traits adopted by prey species on its demography is not instantaneously observed; therefore, we consider its effect on growth rate with a fear response delay τ.

3. Since many small size predators prefer to hunt in packs to boost their success rate. We incorporate the effect of group hunting in the attack rate by introducing a function $h(y) = \alpha + \lambda y$ [91], where α is the attack rate of lone predator, and λ denotes the cooperation strength.

Inspiring from aforementioned facts and pioneering literature as cited in the introduction, we propose the following model.

$$\begin{aligned}
\frac{dx}{dt} &= \frac{rx}{1+Ky(t-\tau)} - r_0 x - r_1 x^2 - \frac{(\alpha+\lambda y)xy}{a+x^2}, \\
\frac{dy}{dt} &= sy - \frac{\omega y^2}{b+x}, \\
x(s) = \phi_1(s) > 0,\ & y(s) = \phi_2(s) > 0, \text{ where } s \in [-\tau, 0] \text{ and } \phi_1, \phi_2 \in C([-\tau, 0], R).
\end{aligned} \tag{2.1}$$

In the absence of time delay, model (2.1) reduces to the following system of ordinary differential equations.

$$\begin{aligned}
\frac{dx}{dt} &= \frac{rx}{1+Ky} - r_0 x - r_1 x^2 - \frac{(\alpha+\lambda y)xy}{a+x^2} := f(x,y), \\
\frac{dy}{dt} &= sy - \frac{\omega y^2}{b+x} := g(x,y), \\
x(0) \geq 0,\ & y(0) \geq 0.
\end{aligned} \tag{2.2}$$

The variables and parameters involved in the model are listed in Table 2.1 with their biological meaning and dimensions.

Table 2.1: Biological explanation and dimension of variables/parameters employed in model (2.2).

Variables/Parameters	Biological explanation	Dimensions
x	Prey density	Biomass
y	Predator density	Biomass
r	Birth rate of prey	Time^{-1}
K	Cost of fear	Biomass^{-1}
r_0	Prey mortality rate	Time^{-1}
r_1	Death rate of prey due to competition among them	Biomass^{-1}Time^{-1}
α	Predation rate	Biomass Time^{-1}
λ	Cooperation strength of predators	Time^{-1}
a	Half saturation constant of prey	Biomass^2
b	Half saturation constant of predator	Biomass
s	Intrinsic growth rate of predator	Time^{-1}
ω	The highest rate of predator eradication per capita	Time^{-1}

2.3 Dynamics of the non-delayed system

The model (2.2) can be re-written as

$$\frac{dx}{dt} = x\phi_1(x,y), \quad \frac{dy}{dt} = y\phi_2(x,y),$$

where

$$\phi_1(x,y) = \frac{r}{1+Ky} - r_0 - r_1 x - \frac{(\alpha+\lambda y)y}{a+x^2}, \ \phi_2(x,y) = s - \frac{\omega y}{b+x}.$$

It follows that

$$x(t) = x(0)e^{\int_0^t \phi_1(x(\theta),y(\theta))d\theta} \geq 0, \quad y(t) = y(0)e^{\int_0^t \phi_2(x(\theta),y(\theta))d\theta} \geq 0.$$

Hence, in R^2_+, all $(x(t),y(t))$ solutions with the positive starting point stay positive.

Nature does not enable any species to spread rapidly due to a lack of resources. As a result, it is critical to ensure that the solutions of the proposed model are bounded.

Theorem 2.3.1. *All solutions initiating in R^2_+ are contained in the domain $\Omega = \{(x,y) \in R^2_+ : 0 \leq x \leq K_1, \ 0 \leq y \leq \frac{s(b+K_1)}{\omega}\}$, where $K_1 = \frac{r-r_0}{r_1} > 0$.*

Proof. We may write the first equation of the model as

$$\dot{x} \leq rx - r_0 x - r_1 x^2.$$

This implies

$$\limsup_{t\to\infty} x(t) \leq \frac{r-r_0}{r_1} := K_1.$$

To show the boundedness of $y(t)$, we can write

$$\dot{y} \leq sy - \frac{\omega y^2}{b+K_1}.$$

This entails

$$\limsup_{t\to\infty} y(t) \leq \frac{(b+K_1)s}{\omega} := K_2,$$

which completes the proof. □

2.3.1 Equilibrium points

The proposed system has four feasible equilibrium points: extinction equilibrium; $E_0(0,0)$, predator-free equilibrium; $E_1(K_1,0)$, prey-free equilibrium; $E_2(0,\frac{bs}{\omega})$ and interior equilibrium; $E^*(x^*,y^*)$. Here x^* is a positive root of the following quartic equation:

$$A_1x^4 + A_2x^3 + A_3x^2 + A_4x + A_5 = 0, \tag{2.3}$$

where

$$A_1 = r_1\omega^2 sK,$$

$$A_2 = \omega^2(r_0Ks + r_1\omega + r_1Ksb) + s^3\lambda K,$$

$$A_3 = \omega^2Ks(r_0b + r_1a) + 3b\lambda Ks^3 + s^2\omega(\lambda + \alpha K) - (r-r_0)\omega^3,$$

$$A_4 = (r_0Ksa + r_1a(\omega + Ksb))\omega^2 + 3\lambda Kb^2s^3 + s\alpha\omega^2 + 2bs^2\omega(\lambda + \alpha K),$$

$$A_5 = \lambda Kb^3s^3 + b^2s^2\omega(\lambda + \alpha K) + b\omega^2 s(\alpha + r_0aK) - (r-r_0)a\omega^3.$$

Since A_1, A_2 and A_4 are positive. Therefore, according to the Descartes' rule of signs, Eq. (2.3) will have unique, two, three or no positive root based on the sign of A_3 and A_5 (refer to Table 2.2 and Fig. 2.1). It is worthy to note here that when $A_3 > 0$ and $A_5 < 0$, Eq. (2.3) has a unique positive solution x^*. On obtaining x^* from Eq. (2.3), we can easily determine y^* from the relation

$$y^* = \frac{s(b+\omega)}{x^*}.$$

Table 2.2: Existence of positive root of (2.3)

A_3	A_5	Number of positive roots	Color
$-$	$+$	2 or 0	yellow
$-$	$-$	3 or 1	red
$+$	$-$	1	green
$+$	$+$	0	blue

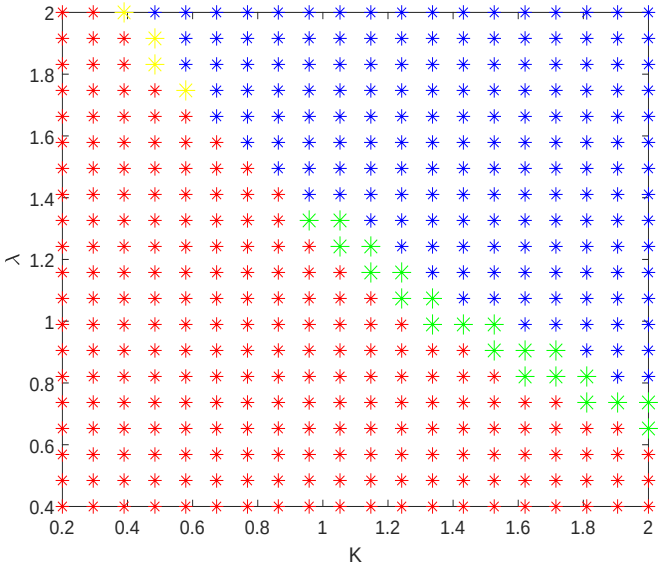

Fig. 2.1: Different colors showing all cases of Table 2.2 in $K\lambda$-plane, where $r = 0.6,\ a = 1,\ \alpha = 0.4,\ \omega = 1,\ b = 1,\ s = 0.4,\ r_0 = 0.05,\ r_1 = 0.05$.

2.3.2 Stability analysis

The local stability feature of any equilibrium can be established using eigenvalue theory. The boundary equilibria with their local stability feature are described in Table 2.3.

Table 2.3: The local stability characteristics of system (2.2)'s boundary equilibria

Equilibrium points	Stability characteristics
$E_0(0,0)$	Unconditionally unstable
$E_1(K_1,0)$	Always saddle point
$E_2(0,\frac{bs}{\omega})$	Asymptotically stable if $r < (1+\frac{bKs}{\omega})(r_0+\frac{(\alpha\omega+\lambda bs)bs}{a\omega^2})$; saddle if $r > (1+\frac{bKs}{\omega})(r_0+\frac{(\alpha\omega+\lambda bs)bs}{a\omega^2})$

Biological significance: As per the concept of the modified Leslie-Gower prey-predator model, the predator can switch to other food when prey is absent. Moreover, predator performs cooperative hunting and induce fear in prey. Due to all these factors, predators may not become

extinct. Therefore, when the prey's birth rate is less than a critical value, they might become extinct, nevertheless, predator always persists due to their generalist nature. Hence the prey-free equilibrium $E_2(0,\frac{bs}{\omega})$ can be stable, but the extinction state $E_0(0,0)$ and predator-free state $E_1(K_1,0)$ can never be stable.

Theorem 2.3.2. *$E^*(x^*,y^*)$ is locally asymptotically stable if and only if $B_1>0$ and $B_2>0$, where B_1 and B_2 are stated in the proof.*

Proof. The Jacobian matrix, computed at positive equilibrium $E^*(x^*,y^*)$) is given by

$$J|_{E^*}=\begin{pmatrix} -r_1x^*+\frac{2(\alpha+\lambda y^*)x^{*2}y^*}{(a+x^{*2})^2} & -\frac{rKx^*}{(1+Ky^*)^2}-\frac{(\alpha+2\lambda y^*)x^*}{a+x^{*2}} \\ \frac{\omega y^{*2}}{(b+x^*)^2} & -\frac{\omega y^*}{b+x^*} \end{pmatrix}.$$

The characteristic equation for the aforementioned matrix is as follows:

$$\xi^2+B_1\xi+B_2=0, \tag{2.4}$$

where

$$B_1=r_1x^*-\frac{2(\alpha+\lambda y^*)x^{*2}y^*}{(a+x^{*2})^2}+\frac{\omega y^*}{b+x^*},$$

$$B_2=\frac{\omega x^*y^*}{b+x^*}\left[r_1-\frac{2(\alpha+\lambda y^*)x^*y^*}{(a+x^{*2})^2}+\frac{y^*}{(b+x^*)}\left(\frac{rK}{(1+Ky^*)^2}+\frac{(\alpha+2\lambda y^*)}{a+x^{*2}}\right)\right].$$

As per the Routh-Hurwitz criterion, the interior equilibrium $E^*(x^*,y^*)$ is locally asymptotically stable if and only if $B_1>0$ and $B_2>0$. □

Remark. If $r_1>\frac{2(\alpha+\lambda y^*)x^*y^*}{(a+x^{*2})^2}$, then $E^*(x^*,y^*)$ is locally asymptotically stable.

In a two-dimensional system, the possible attractors inside the positive invariant set could be equilibrium points and periodic solutions. If we are able to show that no periodic solution exists, and all boundary equilibrium points are unstable, then, in that case, all trajectories starting in the positive invariant region will eventually converge to the interior equilibrium E^* if it exists uniquely.

Theorem 2.3.3. *Let the positive equilibrium E^* exists uniquely. Then it is globally asymptotically stable under the following conditions:*

(i) $r>(1+\frac{bKs}{\omega})(r_0+\frac{(\alpha\omega+\lambda bs)bs}{a\omega^2})$,

(ii) $\frac{3\sqrt{3}(\alpha+\lambda K_2)}{8a\sqrt{a}}<\frac{r_1}{K_2}+\frac{\omega}{K_1(b+K_1)}$.

Proof. If (i) holds, it directly implies $E_2(0,\frac{bs}{\omega})$ is a saddle point. Now, to show the non-existence of periodic solution, consider a function that is continuously differentiable in R^2_+,

$H = \frac{1}{xy}$ and we define

$$\nabla = \frac{\partial}{\partial x}(fH) + \frac{\partial}{\partial y}(gH).$$

Simple calculation yields

$$\nabla = -\frac{r_1}{y} + \frac{2x(\alpha+\lambda y)}{(a+x^2)^2} - \frac{\omega}{x(b+x)}.$$

∇ remains negative if $\frac{3\sqrt{3}(\alpha+\lambda K_2)}{8a\sqrt{a}} < \frac{r_1}{K_2} + \frac{\omega}{K_1(b+K_1)}$.
Hence, system (2.2) cannot have a closed trajectory in the interior of the positive xy-plane, according to the Bendixson-Dulac criteria. In such a case, all solutions starting in Ω will converge to the interior equilibrium E^*, if it exists uniquely. □

2.3.3 Bifurcation analysis

Theorem 2.3.4. *System (2.2) experiences a transcritical bifurcation between the axial equilibrium $E_2(0, \frac{bs}{\omega})$ and interior equilibrium $E^*(x^*, y^*)$ with respect to the fear parameter at $K = K^{[tc]} = \frac{\omega}{bs}\left(\frac{(r-r_0)a\omega^2-(\alpha\omega+\lambda bs)bs}{r_0a\omega^2+(\alpha\omega+\lambda bs)bs}\right)$ if $(r-r_0)a\omega^2 > (\alpha\omega+\lambda bs)bs$ and $\delta_3 \neq 0$, where δ_3 is defined in the proof.*

Proof. At $K = K^{[tc]}$,

$$A = J|_{E_2} = \begin{pmatrix} 0 & 0 \\ \frac{s^2}{\omega} & -s \end{pmatrix}.$$

$v = (1, \frac{s}{\omega})$ and $w = (1,0)$ are the eigenvectors of matrix A and A^T for the zero eigenvalue, respectively. Let $F = (f,g)^T$, where f and g are the RHS functions of model (2.2). Now, we define
$\delta_1 = w^T F_K(E_2, K^{[tc]})$, $\delta_2 = w^T[DF_K(E_2, K^{[tc]})v]$, and $\delta_3 = w^T[D^2F(E_2, K^{[tc]})(v,v)]$.
Simple computation yields

$$\delta_1 = 0,\ \delta_2 = -\frac{rbs\omega}{(\omega+bKs)^2} < 0$$

and

$$\delta_3 = -2r_1 - \frac{2}{ra^2\omega^4 b}(r_0a\omega^2 + (\alpha\omega+\lambda bs)bs)((r-r_0)a\omega^2 - (\alpha\omega+\lambda bs)bs).$$

If $\delta_3 \neq 0$, then all the conditions of the Sotomayor's Theorem [60] are satisfied. Hence, the system experiences a transcritical bifurcation at $K = K^{[tc]} = \frac{\omega}{bs}\left(\frac{(r-r_0)a\omega^2-(\alpha\omega+\lambda bs)bs}{r_0a\omega^2+(\alpha\omega+\lambda bs)bs}\right)$ between prey-free equilibrium E_2 and coexistence equilibrium E^*. □

Theorem 2.3.5. *Let us assume that B_2 is positive. Then system (2.2) experiences a Hopf-bifurcation with respect to the cooperation strength λ at $\lambda = \lambda^{[hf]}$ around the coexistence equilibrium E^*.*

Proof. It can be noted that

(i) When $B_1 > 0$ and $B_2 > 0$, E^* is locally asymptotically stable for $\lambda < \lambda^{[hf]}$.

(ii) When $B_1 < 0$ and $B_2 > 0$, E^* is unstable for $\lambda > \lambda^{[hf]}$.

Here B_1 and B_2 are defined in Eq. (2.4). This indicates that there is a switching of stability when cooperative strength λ crosses the critical value $\lambda = \lambda^{[hf]}$. At this point, $B_1 = 0$ and $B_2 > 0$, which implies that the eigenvalues are purely imaginary. Furthermore, we check the transversality condition *viz.*,

$$\left.\frac{dB_1}{d\lambda}\right|_{\lambda=\lambda^{[hf]}} = -\frac{2x^{*2}y^{*2}}{(a+x^{*2})^2} < 0.$$

Therefore, by the Andronov-Hopf bifurcation theorem, the system undergoes Hopf-bifurcation at $\lambda = \lambda^{[hf]}$ near the equilibrium point E^*. □

2.4 Analysis of the delayed system

In this section, we discuss the effect of fear-response delay on the stability dynamics of the proposed system. For this, we linearize system (2.1) about E^*, which is given by the following matrix.

$$J = P + Qe^{-\lambda\tau},$$

where

$$P = \begin{pmatrix} -r_1x^* + \frac{2(\alpha+\lambda y^*)x^{*2}y^*}{a+x^{*2}} & -\frac{(\alpha+2\lambda y^*)x^*}{a+x^{*2}} \\ \frac{\omega {y^*}^2}{(b+x^*)^2} & -\frac{\omega y^*}{b+x^*} \end{pmatrix} \text{ and } Q = \begin{pmatrix} 0 & -\frac{rKx^*}{(1+Ky^*)^2} \\ 0 & 0 \end{pmatrix}$$

are the jacobian matrices about E^* in the direction of t and $(t-\tau)$.
The characteristic equation of matrix J can be written as

$$\xi^2 + \Theta_1\xi + \Theta_2 + \Theta_3 e^{-\xi\tau} = 0, \tag{2.5}$$

where $\Theta_1 = r_1x^* - \frac{2(\alpha+\lambda y^*)x^{*2}y^*}{a+x^{*2}} + \frac{\omega y^*}{b+x^*}$, $\Theta_2 = \frac{\omega x^*y^*}{b+x^*}\left(r_1 - \frac{2(\alpha+\lambda y^*)x^*y^*}{a+x^{*2}}\right) + \frac{(\alpha+2\lambda y^*)\omega x^*y^{*2}}{(a+x^{*2})(b+x^*)^2}$, $\Theta_3 = \frac{rK\omega x^*y^{*2}}{(b+x^*)^2(1+Ky^*)^2}$.
If every characteristic root of Eq. (2.5) has a negative real component, then system (2.1) is stable

around the positive equilibrium point E^*. The characteristic root must cross the imaginary axis to demonstrate stability switching via Hopf-bifurcation. This leads us to assume that the root of Eq. (2.5) is $i\eta_2(\eta_2 > 0)$. Substituting $\xi = i\eta_2$ in Eq. (2.5), the real and imaginary components are given by

$$\Theta_3 cos(\eta_2\tau) = {\eta_2}^2 - \Theta_2, \tag{2.6}$$

$$\Theta_3 sin(\eta_2\tau) = \Theta_1\eta_2. \tag{2.7}$$

On solving (2.6) and (2.7), we obtain the following expression to determine the critical value of τ for the occurrence of Hopf-bifurcation.

$$tan(\eta_2\tau) = \frac{\Theta_1\eta_2}{{\eta_2}^2 - \Theta_2}, \tag{2.8}$$

where η_2 is the positive root of the following bi-quadratic equation obtained by squaring and adding Eqs. (2.6) and (2.7).

$${\eta_2}^4 + (\Theta_1^2 - 2\Theta_2){\eta_2}^2 + ({\Theta_2}^2 - {\Theta_3}^2) = 0. \tag{2.9}$$

To derive the transversality condition for Hopf-bifurcation, we substitute $\xi = \eta_1 + i\eta_2$ in Eq. (2.5). Separating real and imaginary parts, we obtain

$$\eta_1^2 - \eta_2^2 + \Theta_1\eta_1 + \Theta_2 + \Theta_3 e^{-\eta_1\tau} cos(\eta_2\tau) = 0, \tag{2.10}$$

$$2\eta_1\eta_2 + \Theta_1\eta_2 - \Theta_3 e^{-\eta_1\tau} sin(\eta_2\tau) = 0. \tag{2.11}$$

Now we differentiate Eqs. (2.10) and (2.11) with respect to τ and set $\eta_1 = 0$, $\tau = \tau_0$ (conditions for the Hopf-bifurcation point) to get

$$M_1\eta_{1\tau} + M_2\eta_{2\tau} = N_1, \tag{2.12}$$

$$-M_2\eta_{1\tau} + M_1\eta_{2\tau} = N_2, \tag{2.13}$$

where

$$M_1 = \Theta_1 - \Theta_3\tau_0 cos(\eta_2\tau_0),$$

$$M_2 = -2\eta_2 - \Theta_3\tau_0 sin(\eta_2\tau_0),$$

$$N_1 = \Theta_3\eta_2 sin(\eta_2\tau_0),$$

$$N_2 = \Theta_3\eta_2 cos(\eta_2\tau_0).$$

Solving Eqs. (2.12) and (2.13), we get

$$\frac{d(Re(\xi))}{d\tau}\bigg|_{\tau=\tau_0} = \eta_{1\tau}\bigg|_{\tau=\tau_0} = \frac{N_1M_1 - N_2M_2}{M_1^2 + M_2^2}.$$

Therefore, the transversality condition for Hopf-bifurcation given by

$$\frac{d(Re(\xi))}{d\tau}\bigg|_{\tau=\tau_0} \neq 0$$

holds if

$$N_1M_1 \neq N_2M_2.$$

2.5 Numerical simulation

We use MATLAB R2021a to run numerical simulations to validate our analytical results of both models (2.1) and (2.2). The dataset we have picked is as follows:

$$r = 0.6,\ \lambda = 0.7,\ K = 0.1,\ a = 1,\ \alpha = 0.0005,\ \omega = 1,\ b = 1,\ s = 0.4,\ r_0 = 0.05,\ r_1 = 0.05 \tag{2.14}$$

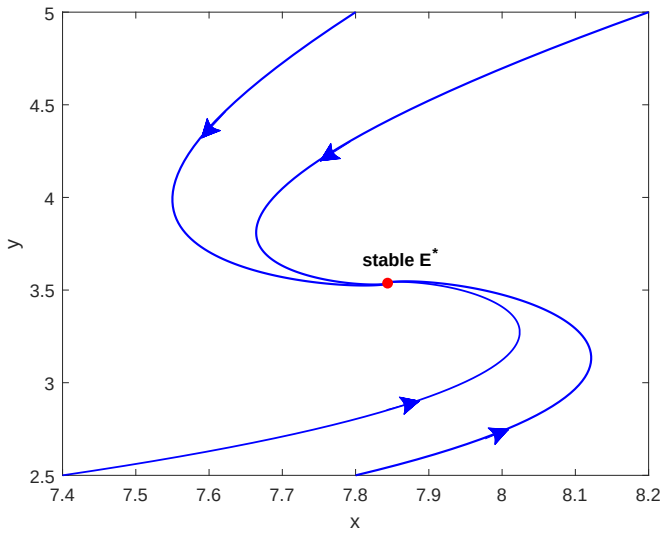

Fig. 2.2: Trajectories of system (2.2) started from different initial conditions are converging towards globally stable node E^*.

In the non-delayed system (2.2), for $\lambda = 0.005$ and other parameters from (2.14), the predator-only state $(0, 0.4)$ is a saddle-point. As per Theorem 2.3.3, we obtain $\frac{3\sqrt{3}(\alpha+\lambda K_2)}{8a\sqrt{a}} -$

$\frac{r_1}{K_2} + \frac{\omega}{K_1(b+K_1)} = -0.002$, implying that the system cannot have a closed trajectory in R^2_+. The interior equilibrium $E^*(7.8437, 3.5374)$ exists uniquely, and is a globally stable focus with eigenvalues $-0.395 \pm 0.2044i$. This phenomenon can be seen in Fig. 2.2.

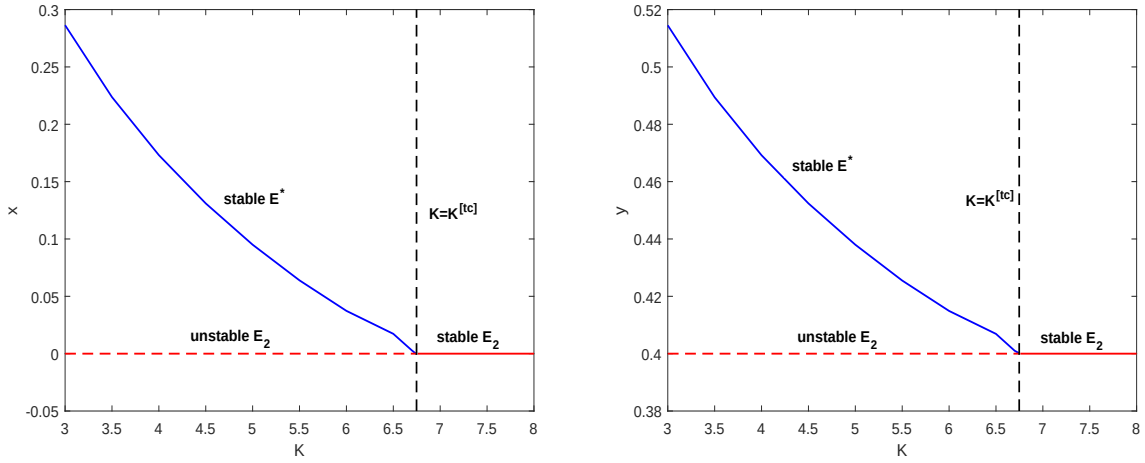

Fig. 2.3: System (2.2) experiences transcritical bifurcation with respect to the fear parameter K between interior and prey-free steady-states. The other parameters are from (2.14).

As large literature demonstrates intriguing dynamics with respect to the fear parameter [88, 76, 20], we investigate model (2.2) against the fear parameter K. As per Theorem 2.3.4, we obtained $K^{[tc]} = 6.7478$ and $\delta_3 = -0.3367 \neq 0$. All conditions of the theorem are satisfied, hence the system undergoes a transcritical bifurcation at $K = K^{[tc]}$. The phenomenon of transcritical bifurcation is easy to understand with the help of a bifurcation diagram. It can be depicted from Fig. 2.3, E^* is stable and E_2 is unstable when $K < K^{[tc]}$. In this range, the value of ∇ remains negative. Therefore, E^* is globally stable. After crossing the threshold value of the fear parameter, the stability of E^* is transferred to E_2 via a transcritical bifurcation.

The traits of the system (2.2) are not limited to transcritical bifurcation. It has been observed that there are three positive equilibrium points, out of which two are stable, and the other is a saddle-point for the parameters given in (2.14) with $\alpha = 0.7$. The stable point $E^{*(1)}$ and saddle-point $E^{*(2)}$ approach towards each other with the decrease in cooperation strength. At $\lambda = \lambda^{[sn]}$, they annihilate one another by means of a saddle-node bifurcation (see Fig. 2.4).

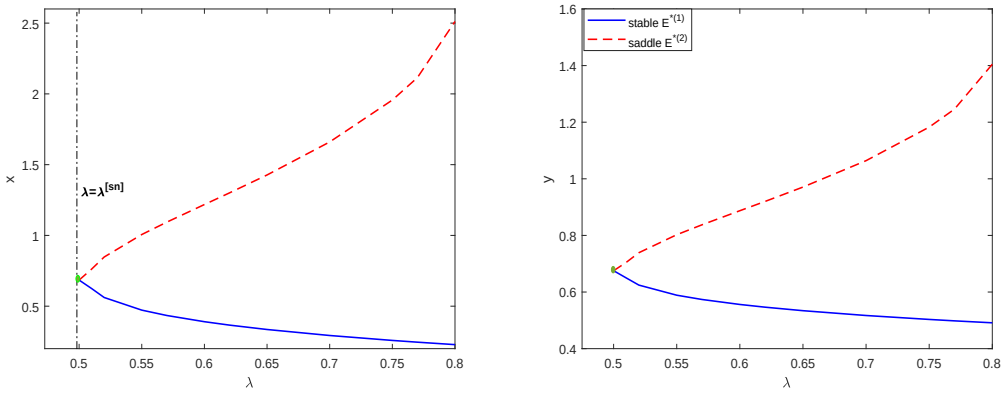

(a) (b)

Fig. 2.4: System exhibits saddle-node bifurcation for two interior equilibrium points (one stable and one saddle) with respect to the cooperation strength λ, where $\alpha = 0.7$ and other parameters are same as in (2.14).

The phase portrait diagram illustrating focus-node bi-stability between two interior equilibrium points ($E^{*(1)}$, $E^{*(3)}$) along with one saddle interior equilibrium $E^{*(2)}$ and saddle prey-free equilibrium E_2 is shown in Fig. 2.5 (a). In such a case, the initial condition of the solution decides its convergence. Here, the solutions from red color $*$ will eventually go to the attractor $E^{*(1)}(0.2929, 0.5171)$. On the other hand, if the solution begins from blue color $*$, it will approach $E^{*(3)}(4.088, 2.0352)$ in the future (refer to Fig. 2.5(b)).

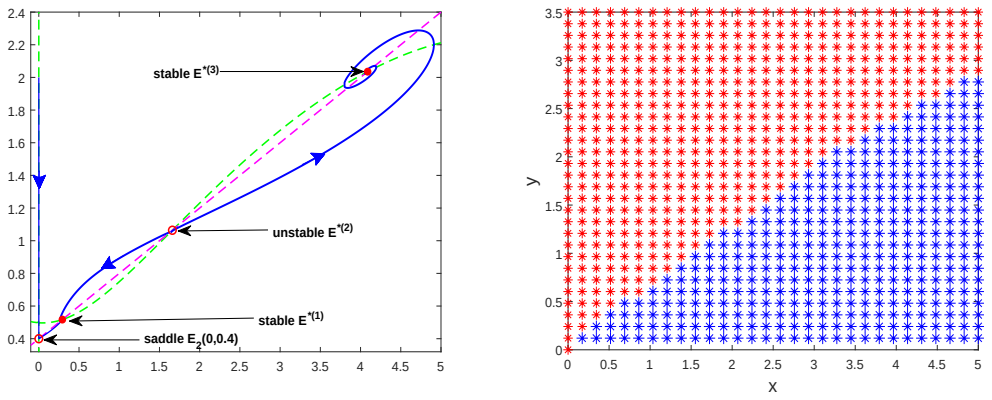

(a) (b)

Fig. 2.5: (a) Bi-stability between two interior equilibrium points at $\alpha = 0.7$ and other parameters are from (2.14). Here green and magenta color dashed curves represent the prey and predator nullclines, respectively. (b) The basin of attraction for two stable points is shown by blue color for $E^{*(3)}(4.088, 2.0352)$ and red color for $E^{*(1)}(0.2929, 0.5171)$.

For $s = 0.2$, $\alpha = 0.7$ and keeping other parameters same as in (2.14), we compute the value of Hopf-bifurcation point $\lambda^{[hf]}$ by equating B_1 to zero, and we obtained $\lambda^{[hf]} = 3.6567$. At this value, $B_2 = 0.0424 > 0$, and $\left.\frac{dB_1}{d\lambda}\right|_{\lambda=\lambda^{[hf]}} = -0.1064 < 0$. Hence, according to Theorem 2.3.5, the system experiences Hopf-bifurcation at $\lambda^{[hf]} = 3.6567$ around $E^*(5.0208, 1.2041)$.

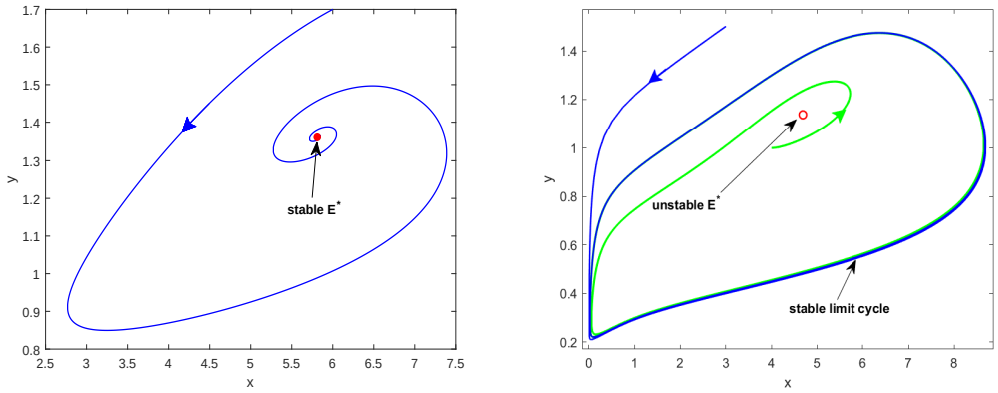

(a) (b)

Fig. 2.6: (a) Phase portrait showing E^* as stable focus at $\lambda = 3$. (b) After $\lambda > \lambda^{[hf]}$, stable limit cycle surrounding unstable E^* at $\lambda = 3.9$.

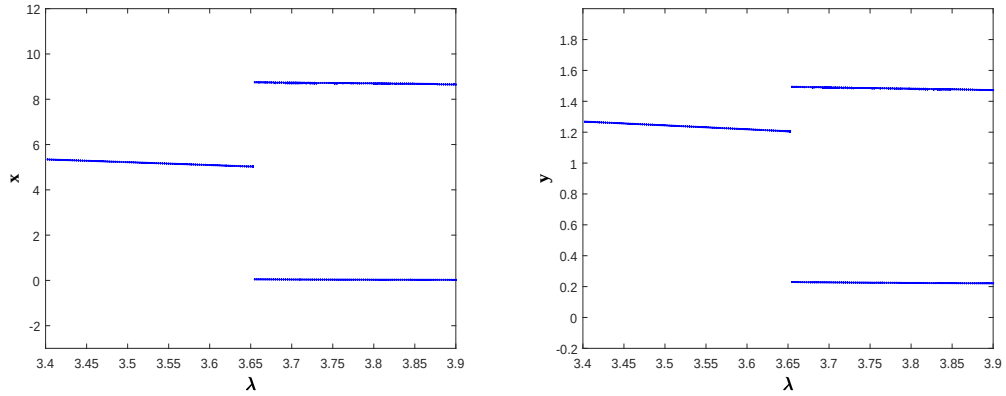

(a) (b)

Fig. 2.7: Stability change of system (2.2) about positive equilibrium through Hopf-bifurcation with respect to λ.

For the lower value of cooperation strength λ, both species fluctuate for a finite time around their steady-state. They eventually reach the positive equilibrium E^* (see the phase portrait in Fig 2.6 (a) at $\lambda = 3 < \lambda^{[hf]}$). When the value of λ is increased, E^* loses its stability with the formation of a stable limit cycle through Hopf-bifurcation at $\lambda = \lambda^{[hf]} = 3.6567$. The phase

portrait after Hopf-bifurcation is depicted in Fig. 2.6 (b) at $\lambda = 3.9 > \lambda^{[hf]}$. Furthermore, for better visualization of the stability switching via Hopf-bifurcation, we sketch the Hopf-bifurcation diagram in Fig. 2.7. In this figure, we plot the maximum and minimum values of the population density in the non-transient period. For $\lambda < \lambda^{[hf]}$, the maximum and minimum coincides, illustrating the stability of E^*. However, both population densities oscillate between one maximum and one minimum, showing the existence of limit cycle for $\lambda > \lambda^{[hf]}$. This sudden change in the dynamics is due to the supercritical Hopf-bifurcation at $\lambda = \lambda^{[hf]}$.

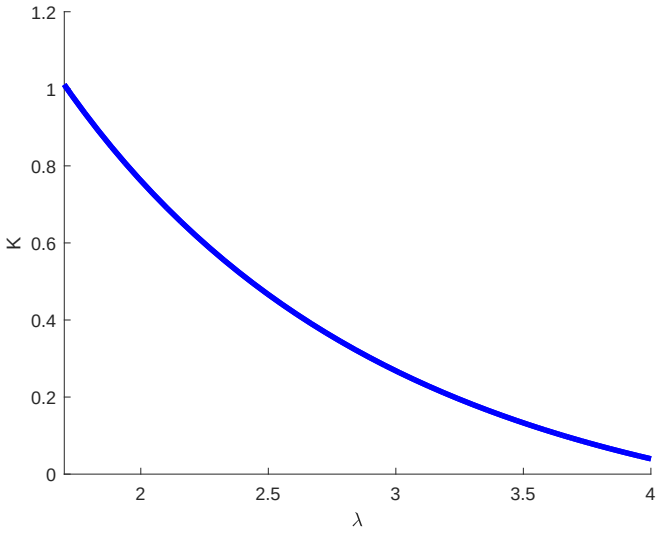

Fig. 2.8: Hopf-bifurcation curve in λK-plane for system (2.2). The interior equilibrium is stable below the curve, and above the curve it becomes unstable through Hopf-bifurcation.

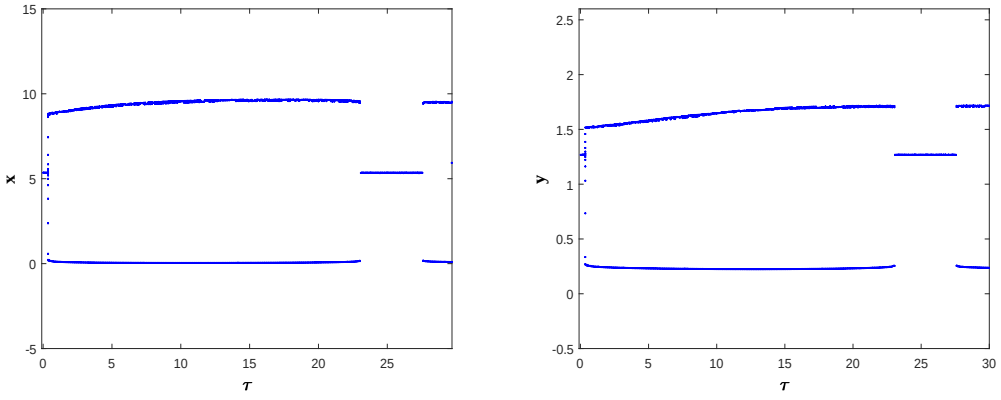

(a) (b)

Fig. 2.9: System (2.2)'s stability change about positive equilibrium through Hopf-bifurcation with respect to τ.

Since our model has complex dynamics with respect to the fear and cooperation strength, this motivates us to perform bi-parametric analysis for λ and K, simultaneously. In Fig. 2.8, for each λ, we obtain a critical value of K at which the Hopf-bifurcation occurs. Joining all these bifurcation points, we obtain a Hopf-bifurcation curve in λK-plane.

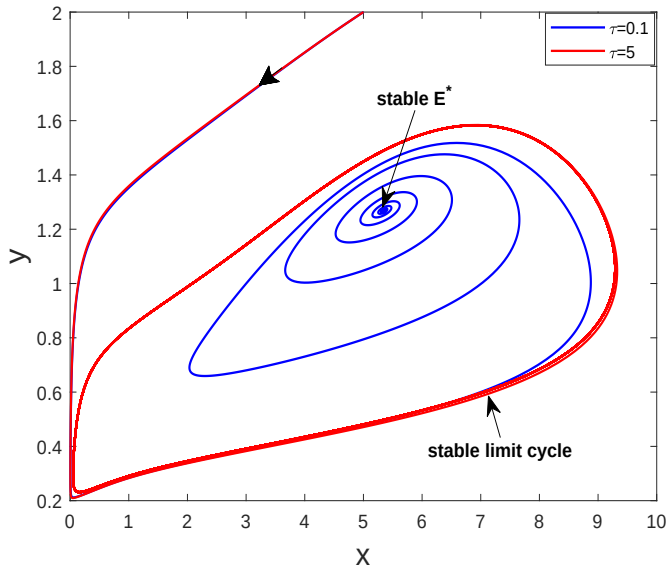

Fig. 2.10: Phase portrait showing the solution behavior before and after the Hopf-bifurcation with respect to τ. The blue colored solution trajectory is going to the interior equilibrium point at $\tau = 0.1$, and the red colored trajectory is converging towards the stable limit cycle at $\tau = 5$.

Moving forward to the delayed system, we explore the stability traits of system (2.1) with respect to the fear-response delay τ. For the chosen set of parameters from (2.14) with $\alpha = 0.7$, $s = 0.2$ and $\lambda = 3.4$, the interior equilibrium $E^*(5.344, 1.2688)$ is locally asymptotically stable in the absence of time delay. With a slight increase in τ, population starts to oscillate periodically about E^* at $\tau = \tau_{01} = 0.2518$ via a supercritical Hopf-bifurcation. These oscillations occur for a wide range of τ, and then gets controlled at $\tau = \tau_{02} = 22.8532$. On crossing this Hopf-point, populations converge to their positive steady-state. However, this situation no longer stays as another Hopf-bifurcation occurs at $\tau = \tau_{03} = 27.5091$, and consequently system becomes unstable with the generation of a stable limit cycle. The Hopf-bifurcation diagram in Fig. 2.9 depicts the stability change multiple times due to the occurrence of supercritical Hopf-bifurcation with respect to fear-response delay. Furthermore, to demonstrate the solution behavior for $\tau < \tau_{01}$ and $\tau > \tau_{01}$, we plot the phase portrait diagram in Fig. 2.10.

In the presence of delay, we vary the cost of fear K for the same parameters set (see Fig. 2.11). The interior equilibrium is initially stable for very low level of fear in the region R_1. However, an increase in K causes the instability of E^* through a supercritical Hopf-bifurcation

on crossing the blue curve. Therefore, both populations oscillate periodically between one maximum and one minimum value, showing the existence of limit cycle in the region R_2. When the fear level is comparatively high, the oscillations are controlled and limit cycle disappears leading to the stability of E^* again through another Hopf-bifurcation on crossing the red curve. Therefore, in the region R_3, the interior equilibrium E^* is stable.

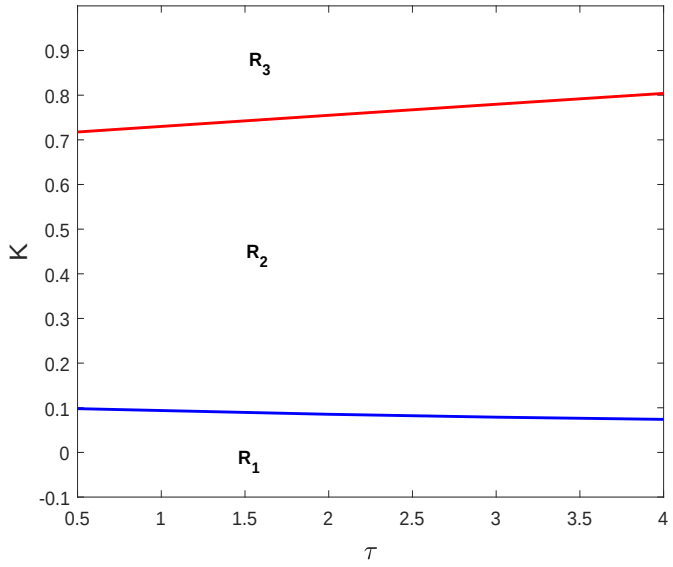

Fig. 2.11: Two Hopf-bifurcation curves dividing the τK-plane into three regions.

2.6 Discussion and conclusion

In the present manuscript, we proposed a modified Leslie-Gower predator-prey model employing ordinary differential equations. While formulation of the model, we considered that the birth rate of the prey population is reduced due to the fear induced by predators. Therefore we multiply the birth rate of the prey population with the decreasing function of the predator population size, $\phi(K,y) = \frac{1}{1+Ky}$. The effect of fear on prey population is not visible immediately, it takes a fear-response delay τ. Moreover, we assumed that predators cooperate for hunting a common target. This mechanism affects the predation rate significantly. Therefore, the group hunting term $\alpha + \lambda y$ is incorporated in the functional response term. Prey species perform group defense for their survival in this situation, which is shown in the model through simplified Holling type IV functional response.

To ensure the biological validity of the system, we proved that all solutions are positive and bounded in R^2_+. We determined all feasible equilibrium points and analyzed their stability. The extinction state $E_0(0,0)$ and predator-free state $E_1(K_1,0)$ are always unstable. When the prey's birth rate is less than a critical value, the prey-free equilibrium $E_2(0,\frac{bs}{\omega})$ is stable. All cases

of the existence of positive equilibrium E^* are discussed. The proposed system can exhibit at most three interior equilibrium points. We obtained sufficient conditions for the local and global stability of E^*.

It is noticed that the fear parameter K and the cooperation strength parameter λ play a crucial role in the system's dynamics. The system experiences transcritical bifurcation for the fear parameter. Moreover, we remarked that a high level of fear might cause the prey species to be extinct. The system shows a feature of bi-stability between two interior points, and it undergoes a saddle-node bifurcation with respect to λ. We noticed that both species start to fluctuate about their co-existence state when the cooperation strength λ is more than a critical value $\lambda^{[hf]}$. This change in dynamics is due to the Hopf-bifurcation at $\lambda = \lambda^{[hf]}$. Since our system has fear and cooperation strength as crucial parameters, we varied them simultaneously. Consequently, we obtained a Hopf-bifurcation curve in λK-plane.

We further extended our study to understand the traits of the delayed system. The increase in fear-response delay in system (2.1) caused several times stability change of the positive equilibrium through supercritical Hopf-bifurcation. We obtained a broad range of τ, for which both populations oscillate in a periodic manner. Furthermore, the change in stability occurs twice through Hopf-bifurcation on adjusting the fear level in the presence of time delay.

Chapter 3

Complex dynamics of Leslie–Gower prey–predator model with fear, refuge and additional food under multiple delays [1]

3.1 Introduction

Understanding prey-predator interactions via differential equations is a classical application of mathematics in ecology. It is trendy to study these interactions with different concepts like harvesting, functional response, a refuge for prey, time delays, additional food for predators, etc. Employing these ideas makes the system more consistent with the real world. The dynamics of a prey-predator system depend upon the feeding rate of a predator on prey. The predator's per capita feeding rate on prey is called functional response [61]. Holling type II functional response is a function of prey abundance which serves extensive literature on prey-predator theory [92].

Leslie [5] introduced a predator-prey model where the carrying capacity of the predator is directly proportional to the prey density. Many researchers have widely used this concept [9, 93, 94, 95, 96]. Aziz-Alaoui and Okiye [7] gave the first study of a prey-predator model with modified Leslie-Gower and Holling type II schemes. This concept was further used with delay differential equations by Nindjin *et al.* [90] and with stochastic perturbation by Ji *et al.* [96]. Aguirre *et al.* [97] obtained three limit cycles due to Hopf-bifurcation and homoclinic bifurcation in a Leslie-Gower model with Allee effect in prey population. Chen *et al.* [98] studied the Leslie-Gower model with refuge for prey. The work by Zhang *et al.* [10] gives an insight into the dynamics of the modified Leslie-Gower model with nonlinear harvesting and Holling type IV functional response.

[1] A considerable part of this chapter is published in *International Journal of Biomathematics*, **15**, 2250060, 2022.

Functional responses introduced in the system show direct killing only. But merely the presence of a predator can affect the prey physically and mentally as well [13]. Usually, there is a predation risk while searching for food, resulting in starvation [14]. The scared prey may not find a suitable environment to reproduce juveniles. And this indirect effect of fear can be more than the direct killing effect [15, 16, 17]. Experiments done by Zanette *et al.* [19] reflect that fear of predators alone led to a 40% reduction in the successor of the song sparrows could produce. Evidence of the fear effect can also be seen in snowshoe hares [18] and dugongs [99]. Sheriff *et al.* [18] monitored free-ranging female snowshoe hares and observed declination in their reproduction output. Dugongs sacrifice food by staying in deeper water where the encounter rate with tiger sharks is low [99].

The fear in prey causes declination in both species [100]. Extra food is offered to the predator to help them grow faster. Prey population increases as distraction caused by additional food to the predator reduce the level of fear in prey. A study done by Mondal *et al.* [38] shows providing additional food to the predator plays a crucial role in controlling the fear effect. Das and Samanta [39] studied a stochastic prey-predator model with refuge for prey and additional food for the predator. They observed that reserving prey can lead to predator extinction, but supplying an adequate amount of extra food can prevent their extinction. Some authors [101, 102] have investigated the consequences of providing additional food to the predator in a prey-predator system. Without the provision of additional food, prey and predator never co-exist, and predator goes to extinction in finite time [101]. van Baalen *et al.* [103] explored the link between optimal foraging theory and population dynamical consequences when foraging predators switch to alternative food either in the fine-grained environment or in the coarse-grained environment. They concluded that alternative food shows a stabilizing effect and promotes persistence. Holt [104] investigated that in the presence of supplementary food, predator increases, and prey decreases at the equilibrium level. This predator-mediated effect of extra food on prey density is "apparent competition" [104]. Some studies [105, 106] are available in the literature in favor of apparent competition. But some experimental studies show that additional food provided to the predator does not enhance the target predation [107, 108]. A recent study by Kaur *et al.* [102] shows that both populations survive at a stable level when the additional food is available for the predator in a sufficient amount; they grow continuously. Provision of additional food is undoubtedly beneficial for weak and struggling predators. For example, lionesses at AENP were provided with culled warthog carcasses while they were struggling to keep young cubs alive [37].

The work by Srinivasu *et al.* [109] reflects that providing the right kind of additional food to the predator can enhance the predation effect, leading to prey elimination. Also, supplying low-quality food at high density causes distraction to predators, and prey can be relieved from predation pressure. A recent study by Kumar and Dubey [36] reveals that both populations

oscillate in the absence of additional food. These oscillations can be completely controlled by increasing the predator dependency factor on additional food. The effect of additional food in the dynamics of a prey-predator system can also be seen in [40, 110, 111].

It is vital to consider prey refuge in the prey-predator system to maintain the ecological balance. By providing refuge, nature can offer a certain degree of protection to the prey. It prevents over-exploitation of prey. Increasing the amount of refuge can increase prey density. Kar [112] and Huang *et al.* [113] analyzed prey-predator interaction with prey refuge. They discovered that refugia stabilized the system. When prey is afraid of predators, Zhang *et al.* [27] examined the effect of prey refuge on predator density. The authors concluded that fear could suppress the predator population.

Every process has a time delay that cannot be ignored. The inclusion of time delay brings realism to the scheme by demonstrating the future state's reliance on the past state [55]. One of the main benefits of using a time-delayed term is that it can accurately explain the dietary energy transformation mechanism [114, 115]. The use of delay differential equations in modeling population dynamics is currently very active [88, 116, 117, 118]. Biological processes include time delays with various factors like maturation [119], gestation [11], prey hunting [119], anti-predator response [88], etc. Time delay can alter the stability dynamics of the system [56]. Liu *et al.* [120] examined the combined effect of maturation and gestation delay on the dynamics of a prey-predator model. Bandopadhyay and Banerjee [121] calculated the length of a time delay to preserve stability. The system shows richer dynamics in the presence of time delay. Therefore, it is vital to study time lag's impact on the system's dynamics.

Keeping the above aspects in mind, the main focus of our present study is to explore the following ecological issues:

1. How are the system's dynamics affected by fear and refuge factors?
2. What are the conditions for the persistence and extinction of both species?
3. Does additional food for predators promote richer biodiversity?
4. What is the range of time delay in which the prey-predator system shows stable dynamics?

In this paper, to explore the above issues, we propose a Leslie-Gower prey-predator model to study the impact of fear, refuge, additional food, fear-response delay, and gestation delay on the system's dynamics in Sec. 3.2. To the best of the authors' knowledge, such general models are not available in the literature. Sec. 3.3 discusses the non-delayed model and its well-posedness, equilibrium analysis, and local and global stability. Also, we show the existence of a limit cycle here. Sec. 3.4 presents the local stability and Hopf-bifurcation analysis of the

delayed system. We validate our analytical findings in Sec. 3.5. In the end, all the results are summarized in Sec. 3.6.

3.2 Construction of mathematical model

Onana *et al.* [11] studied the following model:

$$\begin{aligned}\frac{dx}{dt} &= r\left(1-\frac{x(t)}{K}\right)x(t) - q\lambda_1(1-m)x(t)y(t) - \phi(x(t)),\\ \frac{dy}{dt} &= sy(t)\left(1-\frac{y(t-\tau)}{q\alpha(1-m)x(t-\tau)+(1-q)\alpha_A K_A}\right),\end{aligned} \tag{3.1}$$

where $x(t)$ and $y(t)$ are the number of prey population and predator population, respectively. Using this work as inspiration, we develop a model (3.2) based on the following assumptions:

- It is assumed that the birth rate of the prey population is reduced due to the fear induced by predators. Therefore we multiply the birth rate of the prey population with the decreasing function of the predator population size, $\phi(K,y) = \frac{1}{1+Ky}$. A similar fear function was used by many authors [17, 88, 122]. In the absence of fear, the prey population grows logistically.

- As the feeding rate of predators decreases with prey density due to handling and searching time, we assume that the predators ingest prey by Holling type II functional response [9].

- Due to the fact that increment in predator population after ingesting prey is not an instantaneous phenomenon, we assume that a predator individual takes τ_2 time for gestation. Therefore, the rate of predator change depends on the number of individuals present at the time $(t-\tau_2)$ [123].

- The fear effect can stabilize the prey-predator system and promote the co-existence of all the populations. Due to the fear of predation risk, the birth rate of prey individuals decreases. In order to study the effect of fear response, we consider a time delay τ_1 in the specific growth rate of the prey species. This fear mechanism takes τ_1 units of time to respond to changes in the prey population [88].

With the above considerations in mind, the mathematical model integrating the fear effect, refuge, and additional food for the predator under multiple delays is as follows:

$$\begin{aligned}
\frac{dx}{dt} &= \frac{rx}{1+Ky(t-\tau_1)} - r_0 x - r_1 x^2 - \frac{q\alpha(1-m)xy}{a+q(1-m)x}, \\
\frac{dy}{dt} &= sy\left(1 - \frac{\beta y(t-\tau_2)}{q\alpha(1-m)x(t-\tau_2)+(1-q)\alpha_A K_A}\right), \\
x(s) &= \phi_1(s) \geq 0,\ y(s) = \phi_2(s) \geq 0,\ s \in [-\tau, 0],\ \tau = max\{\tau_1, \tau_2\}.
\end{aligned} \tag{3.2}$$

In the absence of both delays ($\tau_1 = \tau_2 = 0$), the model (3.2) takes the following form:

$$\begin{aligned}
\frac{dx}{dt} &= \frac{rx}{1+Ky} - r_0 x - r_1 x^2 - \frac{q\alpha(1-m)xy}{a+q(1-m)x}, \\
\frac{dy}{dt} &= sy\left(1 - \frac{\beta y}{q\alpha(1-m)x+(1-q)\alpha_A K_A}\right), \\
x(0) &\geq 0,\ \ y(0) \geq 0.
\end{aligned} \tag{3.3}$$

The biological meaning of parameters used in the proposed model is given in Table 3.1.

Remark. If $r < r_0$, then the prey population will die out. Therefore, we will consider $r > r_0$ throughout this article to avoid this situation.

Table 3.1: Biological explication of variables/parameters used in model (3.2)

Variables/Parameters	Biological explication	Dimension
x	Number of prey individuals	Biomass
y	Number of predator individuals	Biomass
r	Birth rate of prey	Time^{-1}
s	Intrinsic growth rate of predator	Time^{-1}
r_0	Natural death rate of prey	Time^{-1}
r_1	Death rate of prey due to competition among them	Biomass^{-1}Time^{-1}
a	Half saturation constant	Biomass
K	Cost of fear	Biomass^{-1}
q	Preference rate of predator for food and $q \in (0,1)$	Dimensionless
m	Refuge parameter and $m \in (0,1)$	Dimensionless
α_A	It measures the amount of energy of the additional food assimilate into the predator's energy	Time^{-1}
K_A	Additional food of constant density A	Biomass
α	Maximum rate of per capita removal of prey species due to predation	Time^{-1}
β	Maximum rate of per capita removal of predator species	Time^{-1}
τ_1	Fear response time delay	Time
τ_2	Gestation delay	Time

3.3 Dynamics of non-delayed model

In this section, we look at the dynamics of the system (3.3). First, we demonstrate that our model is biologically viable (refer to Subsec. 3.3.1). The steady-state solutions are then determined (refer to Subsec. 3.3.2), followed by the stability analysis (refer to Subsec. 3.3.3 and 3.3.6). We address the presence of a periodic solution in Subsec. 3.3.4 and then present an analysis for transcritical bifurcation in Subsec. 3.3.5.

3.3.1 Well-posedness of model

This subsection shows that all solutions of the system (3.3) are positive and bounded. Furthermore, we demonstrate that the system is uniformly persistent under a parametric condition.
Let $F = (f,g)^T$,
where

$$f = \frac{rx}{1+Ky} - r_0 x - r_1 x^2 - \frac{q\alpha(1-m)xy}{a+q(1-m)x}$$

and

$$g = sy\left(1 - \frac{\beta y}{q\alpha(1-m)x + (1-q)\alpha_A K_A}\right).$$

Since F and $Jacobian(F)$ are continuous in R^2_+, the IVP (3.3) has a unique solution by the standard theory of the ODE system.
Further, the model (3.3) can be re-written as

$$\frac{dx}{dt} = x\phi_1(x,y), \quad \frac{dy}{dt} = y\phi_2(x,y),$$

where

$$\phi_1(x,y) = \frac{r}{1+Ky} - r_0 - r_1 x - \frac{q\alpha(1-m)y}{a+q(1-m)x},$$
$$\phi_2(x,y) = s\left(1 - \frac{\beta y}{q\alpha(1-m)x + (1-q)\alpha_A K_A}\right).$$

It follows that

$$x(t) = x(0)e^{\int_0^t \phi_1(x,y)ds} \geq 0,$$
$$y(t) = y(0)e^{\int_0^t \phi_2(x,y)ds} \geq 0.$$

Thus, all solutions $(x(t),y(t))$ with initial condition $(x(0),y(0))$ remain positive throughout the region R^2_+.
The following lemma illustrates the boundedness of the system (3.3).

Lemma 3.3.1. *The set* $\Omega = \{(x,y) : 0 \le x \le K_1, 0 \le y \le \mu\}$ *is an invariant set for all solutions initiated in the positive quadrant, where* $K_1 = \frac{r-r_0}{r_1}$ *and* $\mu = \frac{1}{\beta}(q\alpha(1-m)K_1 + (1-q)\alpha_A K_A)$.

Proof. We may deduce the first equation of the model (3.3) as

$$\frac{dx}{dt} \le rx - r_1x^2 - r_0x,$$

which implies

$$\limsup_{t\to\infty} x(t) \le K_1,$$

where

$$K_1 = \frac{r-r_0}{r_1}.$$

Now, the second equation of the model gives

$$\frac{dy}{dt} \le sy\left(1 - \frac{\beta y}{(q\alpha(1-m)K_1 + (1-q)\alpha_A K_A)}\right),$$

which yields

$$\limsup_{t\to\infty} y(t) \le \mu,$$

where

$$\mu = \frac{1}{\beta}(q\alpha(1-m)K_1 + (1-q)\alpha_A K_A).$$

We also note that if $x(t) \ge K_1$ and $y(t) \ge \mu$, then $\frac{dx}{dt} \le 0$, $\frac{dy}{dt} \le 0$.
This shows that all solutions of the system (3.3) starting in the region Ω remain in Ω for all $t > 0$. □

Lemma 3.3.2. *If the following condition*

$$r > (1+K\mu)\left(r_0 + \frac{q\alpha(1-m)\mu}{a}\right)$$

holds, then the system (3.3) is uniformly persistent.

Proof. The persistence of the system ensures that the species will not become extinct and are present for all future time if they are present initially.
From the model (3.3) and using Lemma 3.3.1, we can write

$$\frac{dx}{dt} \ge \left(\frac{r}{1+K\mu} - r_0 - \frac{q\alpha(1-m)\mu}{a}\right)x - r_1x^2,$$

$$\frac{dy}{dt} \geq sy\left(1 - \frac{\beta y}{(1-q)\alpha_A K_A}\right),$$

which implies

$$\liminf_{t\to\infty} x(t) \geq \left(\frac{r}{1+K\mu} - r_0 - \frac{q\alpha(1-m)\mu}{a}\right)\frac{1}{r_1} =: x_a,$$

$$\liminf_{t\to\infty} y(t) \geq \frac{1}{\beta}(1-q)\alpha_A K_A =: y_a.$$

Let $M_a = min\{x_a, y_a\}, M_m = max\{K_1, \mu\}$ and $X(t) = \begin{pmatrix} x(t) \\ y(t) \end{pmatrix}$.

Then it follows that

$$M_a \leq \liminf X(t) \leq \limsup X(t) \leq M_m.$$

Hence the system is uniformly persistent. □

3.3.2 Equilibrium points

It can be investigated that the model (3.3) has four types of equilibria, namely, trivial extinction equilibrium $E_0(0,0)$, prey-free equilibrium $E_1\left(0, \frac{(1-q)\alpha_A K_A}{\beta}\right)$, predator-free equilibrium $E_2(\frac{r-r_0}{r_1}, 0)$, and co-existence equilibrium $E^*(x^*, y^*)$. The equilibria E_0, E_1, and E_2 exist unconditionally.

Existence of interior equilibrium $E^*(x^*, y^*)$: Here x^* and y^* are positive solutions of the following equations:

$$\frac{r}{1+Ky^*} - r_0 - r_1 x^* - \frac{q\alpha(1-m)y^*}{a + q(1-m)x^*} = 0, \tag{3.4}$$

$$s\left(1 - \frac{\beta y^*}{q\alpha(1-m)x^* + (1-q)\alpha_A K_A}\right) = 0. \tag{3.5}$$

From Eq. (3.5), we have

$$y^* = \frac{1}{\beta}(q\alpha(1-m)x^* + (1-q)\alpha_A K_A) > 0.$$

Substituting this value of y^* in Eq. (3.4), we get

$$P_1 {x^*}^3 + P_2 {x^*}^2 + P_3 x^* + P_4 = 0, \tag{3.6}$$

where

$$P_1 = \frac{K}{\beta} r_1 q^2 \alpha (1-m)^2,$$

$$P_2 = q(1-m)[r_1(1+\frac{K}{\beta}(1-q)\alpha_A K_A + \frac{K}{\beta} a\alpha) + \frac{K}{\beta} r_0 q\alpha(1-m) + \frac{K}{\beta^2} q^2\alpha^3(1-m)^2],$$

$$P_3 = \frac{K}{\beta}[r_0 a\alpha q(1-m) + \frac{2}{\beta} q^2\alpha^2(1-m)^2(1-q)\alpha_A K_A + r_0 q(1-q)(1-m)\alpha_A K_A$$
$$+ ar_1(1-q)\alpha_A K_A] + q^2\frac{\alpha^2}{\beta}(1-m)^2 + ar_1 - (r-r_0)q(1-m),$$

$$P_4 = \frac{K}{\beta}(1-q)\alpha_A K_A[\frac{\alpha q}{\beta}(1-m)(1-q)\alpha_A K_A + ar_0] + \frac{q\alpha}{\beta}(1-q)(1-m)\alpha_A K_A - (r-r_0)a.$$

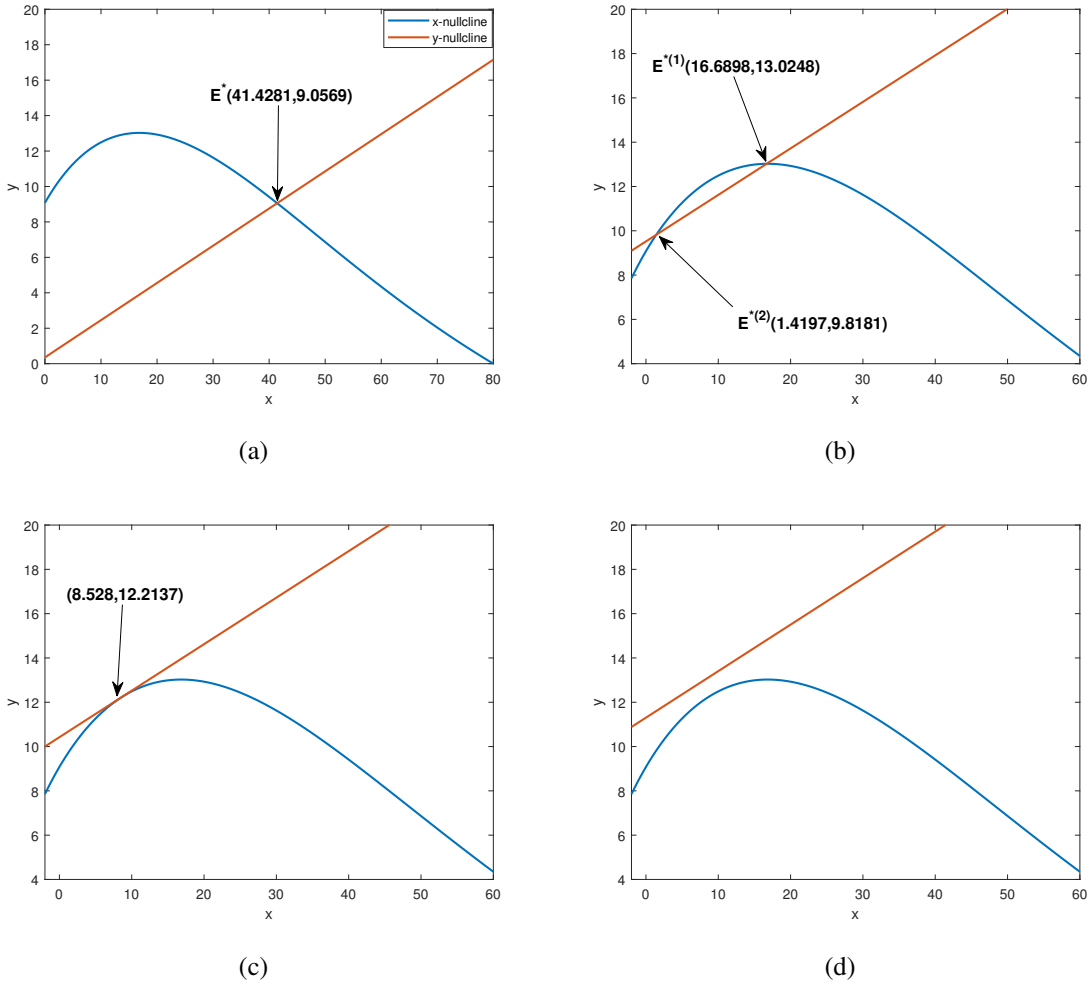

(a) (b)

(c) (d)

Fig. 3.1: Nullclines showing number of interior equilibria with varying α_A when (a)$\alpha_A = 0.3$, (b)$\alpha_A = 8$, (c)$\alpha_A = 8.758699$ and (d)$\alpha_A = 9.5$, fixing other parameters as $r = 3.5,\ K = 0.05,\ q = 0.3,\ r_0 = 0.5,\ r_1 = 0.0375,\ a = 1,\ K_A = 1.7,\ \alpha = 2,\ s = 0.2,\ m = 0.65,\ \beta = 1.$

The discriminant of Eq. (3.6) is given by:

$$\Delta = P_2^2 P_3^2 - 4P_1 P_3^3 - 4P_2^3 P_4 - 27P_1^2 P_4^2 + 18P_1 P_2 P_3 P_4.$$

Depending upon the sign of P_3, P_4, and Δ, the proposed system would have none, one, or two co-existence equilibria (refer to Fig. 3.1).

(a) Existence of unique positive equilibrium.
By Descarte's rule of sign, Eq. (3.6) will have a unique positive solution x^* if and only if $P_4 < 0$. The value of y^* can be conveniently calculated by substituting this value of x^* in Eq. (3.5). This implies that there exists a unique interior equilibrium $E^*(x^*, y^*)$.

(b) Existence of dual positive equilibria.
If $P_3 < 0$ and $P_4 > 0$, then by Descarte's rule of sign Eq. (3.6) will have at most two positive roots. Additionally, if $\Delta > 0$, then Eq. (3.6) will have exactly two positive roots.

(c) Existence of one positive solution of Eqs. (3.4) and (3.5) with multiplicity two.
When $P_3 < 0$, $P_4 > 0$ and $\Delta = 0$, Eq. (3.6) will have a positive double root.

(d) Non-existence of interior equilibrium.

- If P_3 and P_4 are positive, then Eq. (3.6) will not have a positive root.
- If $P_3 < 0$, $P_4 > 0$ and $\Delta < 0$, then the system (3.3) will not attain positive equilibrium.

Remark. In Fig. 3.1 (a), P_4 is negative for a smaller value of α_A ($\alpha_A = 0.3$), which implies $E_1(0, \frac{(1-q)\alpha_A K_A}{\xi})$ is unstable. Therefore, species are more likely to persist at a lower value of additional food parameter α_A. When α_A is increased to larger values (see Fig. 3.1 (b), (c), (d)), P_4 becomes positive, which implies that the prey-free equilibrium E_1 is always stable. Hence, at higher values of α_A, predators can use the additional food energy for predation, which might cause prey's extinction.

3.3.3 Local stability analysis

To examine the local stability behavior of the equilibrium, we compute the variational matrix corresponding to the system (3.3) at each equilibrium point. Based upon the sign of the real part of the eigenvalue of this matrix, we obtain the following results:

1. The equilibrium point $E_0(0,0)$ is unstable.

2. The variational matrix at $E_1\left(0, \frac{(1-q)\alpha_A K_A}{\beta}\right)$ is given by:

$$\begin{pmatrix} \frac{r\beta}{\beta+K\alpha_A K_A(1-q)} - r_0 - q(1-m)(1-q)\alpha_A K_A \frac{\alpha}{a\beta} & 0 \\ \frac{sq\alpha(1-m)}{\beta} & -s \end{pmatrix}.$$

It is noted that

- E_1 is locally asymptotically stable if

$$r\beta < \left(r_0 + q(1-m)(1-q)\alpha_A K_A \frac{\alpha}{a\beta}\right)(\beta + K\alpha_A K_A(1-q)).$$

- E_1 is a saddle point if

$$r\beta > \left(r_0 + q(1-m)(1-q)\alpha_A K_A \frac{\alpha}{a\beta}\right)(\beta + K\alpha_A K_A(1-q)).$$

3 $E_2(\frac{r-r_0}{r_1}, 0)$ is a saddle point with stable manifold in x direction and with unstable manifold in y direction.

Remark: It should be highlighted that the system (3.3) has a unique positive equilibrium if and only if prey-free equilibrium E_1 is unstable.

In order to study the local stability behavior of positive equilibrium, let $M|_{E^*}$ be the variational matrix evaluated at $E^*(x^*, y^*)$. Then

$$M|_{E^*} = \begin{pmatrix} -r_1 x^* + \frac{\alpha q^2 (1-m)^2 x^* y^*}{(a+q(1-m)x^*)^2} & -\frac{rKx^*}{(1+Ky^*)^2} - \frac{q\alpha(1-m)x^*}{(a+q(1-m)x^*)} \\ \frac{s\beta q\alpha(1-m){y^*}^2}{(q\alpha(1-m)x^* + (1-q)\alpha_A K_A)^2} & -\frac{s\beta y^*}{(q\alpha(1-m)x^* + (1-q)\alpha_A K_A)} \end{pmatrix}.$$

The characteristic equation corresponding to the above matrix is

$$\lambda^2 + A_1\lambda + A_2 = 0, \tag{3.7}$$

where

$$\begin{aligned} A_1 &= r_1 x^* - \frac{\alpha q^2 (1-m)^2 x^* y^*}{[a+q(1-m)x^*]^2} + \frac{\beta s y^*}{[q\alpha(1-m)x^* + (1-q)\alpha_A K_A]} = -tr(M|_{E^*}), \\ A_2 &= \frac{s\beta y^*}{[q\alpha(1-m)x^* + (1-q)\alpha_A K_A]}\left[r_1 x^* - \frac{\alpha q^2 (1-m)^2 x^* y^*}{(a+q(1-m)x^*)^2}\right] \\ &\quad + \frac{s\beta q\alpha(1-m){y^*}^2 x^*}{[q\alpha(1-m)x^* + (1-q)\alpha_A K_A]^2}\left[\frac{rK}{(1+Ky^*)^2} + \frac{q\alpha(1-m)}{(a+q(1-m)x^*)}\right] = det(M|_{E^*}). \end{aligned}$$

Using the Routh-Hurwitz criterion, all the eigenvalues of $M|_{E^*}$ have negative real part if and only if the following conditions hold:

$$A_1 > 0,\ A_2 > 0. \tag{3.8}$$

Thus, we can state the following theorem.

Theorem 3.3.3. *The positive equilibrium point E^* is locally asymptotically stable in the interior of the positive quadrant of the xy-plane if and only if (3.8) holds true.*

Remark: We can easily note that (3.8) holds true if

$$r_1 > \frac{\alpha q^2 (1-m)^2 y^*}{(a+q(1-m)x^*)^2}.$$

3.3.4 Limit cycle

Theorem 3.3.4. *Let E^* exists uniquely and any one of the following condition holds:*

(i) $A_1 < 0,\ A_2 > 0,$

(ii) $A_1 < 0,\ A_2 < 0.$

Then the model (3.3) has a limit cycle.

Proof. From Lemma 3.3.1, it follows that int(Ω) is a positively invariant set. If (i) or (ii) holds, then E^* is unstable. So, it is clear that the $\omega-$ limit set does not contain any stationary point. Hence, according to the Poincare-Bendixson theorem, the system has a limit cycle. □

Now, we investigate the possibility of Hopf-bifurcation around the interior equilibrium E^* by considering the parameter α_A as the bifurcation parameter.

The interior equilibrium E^* loses its stability through Hopf-bifurcation when the eigenvalues are complex conjugate with zero real parts. We consider α_A as the bifurcation parameter. Let $\lambda(\alpha_A) = \lambda_r(\alpha_A) + i\lambda_i(\alpha_A)$ be an eigenvalue of the characteristic equation (3.7). After substituting the value of $\lambda(\alpha_A)$ in Eq. (3.7) and separating the real and imaginary parts, we get

$$\lambda_r^2 - \lambda_i^2 + A_1\lambda_r + A_2 = 0 \tag{3.9}$$

$$2\lambda_r\lambda_i + A_1\lambda_i = 0 \tag{3.10}$$

At the Hopf-bifurcation point $\alpha_A = \alpha_A^*$, $\lambda_r(\alpha_A) = 0$. Therefore, we obtain

$$-\lambda_i^2 + A_2 = 0, \text{ where } \lambda_i \in R$$

and

$$A_1\lambda_i = 0, \text{ where } \lambda_i \neq 0.$$

Therefore, from the above equations, we have $A_1(\alpha_A) = 0$, and $A_2(\alpha_A) > 0$.
Thus at the bifurcation point, $A_1(\alpha_A) = 0$ yields

$$\alpha_A^* = \frac{1}{(1-q)K_A}\left[\frac{\beta s y^*}{\frac{\alpha q^2(1-m)^2x^*y^*}{(a+q(1-m)x^*)^2} - r_1x^*} - q\alpha(1-m)x^*\right].$$

Differentiating Eqs. (3.9) and (3.10) with respect to α_A and substituting $\lambda_r = 0$, we obtain

$$-2\lambda_i\frac{d\lambda_i}{d\alpha_A} + A_1\frac{d\lambda_r}{d\alpha_A} + \frac{dA_2}{d\alpha_A} = 0,$$

$$2\lambda_i\frac{d\lambda_r}{d\alpha_A} + \frac{dA_1}{d\alpha_A}\lambda_i + A_1\frac{d\lambda_i}{d\alpha_A} = 0.$$

Solving these equations, we get

$$\left.\frac{d\lambda_r}{d\alpha_A}\right|_{\alpha_A=\alpha_A^*} = -\frac{A_1\frac{dA_2}{d\alpha_A} + 2\frac{dA_1}{d\alpha_A}\lambda_i^2}{A_1^2 + 4\lambda_i^2} \neq 0,$$

provided $A_1\frac{dA_2}{d\alpha_A} + 2\frac{dA_1}{d\alpha_A}\lambda_i^2 \neq 0$.
Thus we can state the following result.

Theorem 3.3.5. *If $A_2 > 0$ and $\frac{d\lambda_r(\alpha_A)}{d\alpha_A}|_{\alpha_A=\alpha_A^*} \neq 0$, then the interior equilibrium E^* of the model (3.3) is locally asymptotically stable when $\alpha_A < \alpha_A^*$, and undergoes Hopf-bifurcation around E^* at $\alpha_A = \alpha_A^*$.*

3.3.5 Transcritical bifurcation

Theorem 3.3.6. *The non-delayed system undergoes a transcritical bifurcation between interior equilibrium E^* and prey-free equilibrium $E_1\left(0, \frac{(1-q)\alpha_A K_A}{\beta}\right)$ at*

$$K = K^{[tc]} = \frac{\beta}{(1-q)\alpha_A K_A}\left(\frac{r}{r_0 + \frac{q\alpha}{a\beta}(1-m)(1-q)\alpha_A K_A} - 1\right)$$

if $r > (r_0 + \frac{q\alpha}{a\beta}(1-m)(1-q)\alpha_A K_A)$ and $\delta_3 \neq 0$, where δ_3 is defined in the proof of this theorem.

Proof. The variational matrix corresponding to the system (3.3) at E_1 is given by

$$H = DF(E_1,K) = \begin{pmatrix} \frac{r\beta}{\beta+K\alpha_A K_A(1-q)} - r_0 - q(1-m)(1-q)\alpha_A K_A \frac{\alpha}{a\beta} & 0 \\ \frac{sq\alpha(1-m)}{\beta} & -s \end{pmatrix}.$$

E_1 is a non-hyperbolic equilibrium at $K = K^{[tc]}$. Therefore, the matrix at this point becomes

$$H = \begin{pmatrix} 0 & 0 \\ \frac{sq\alpha(1-m)}{\beta} & -s \end{pmatrix}.$$

The eigenvectors $v = (1, \frac{q\alpha(1-m)}{\beta})^T$ and $w = (1,0)^T$ are corresponding to the eigenvalue zero of matrix H and H^T, respectively.
Let $F = (f,g)^T$, where f and g are the same as mentioned earlier.

$$F_K = \begin{pmatrix} -\frac{rxy}{(1+Ky)^2} \\ 0 \end{pmatrix}.$$

Clearly,

$$\delta_1 = w^T F_K(E_1, K^{[tc]}) = 0.$$

Now, consider

$$\delta_2 = w^T[DF_K(E_1,K^{[tc]})v] = \begin{pmatrix} 1 & 0 \end{pmatrix} \begin{pmatrix} -\frac{r\beta(1-q)\alpha_A K_A}{(\beta+K^{[tc]}(1-q)\alpha_A KA)^2} & 0 \\ 0 & 0 \end{pmatrix} \begin{pmatrix} 1 \\ \frac{q\alpha(1-m)}{\beta} \end{pmatrix}$$

which yields

$$\delta_2 = -\frac{r\beta(1-q)\alpha_A K_A}{(\beta+K^{[tc]}(1-q)\alpha_A KA)^2} \neq 0.$$

Clearly, δ_2 is non-zero.
Let us define

$$\delta_3 = w^T[D^2F(E_1,K^{[tc]})(v,v)] = \begin{pmatrix} 1 & 0 \end{pmatrix} \begin{pmatrix} f_{xx} & f_{xy} & f_{yx} & f_{yy} \\ g_{xx} & g_{xy} & g_{yx} & g_{yy} \end{pmatrix}_{(E_1,K^{[tc]})} \begin{pmatrix} v_1v_1 \\ v_1v_2 \\ v_2v_1 \\ v_2v_2 \end{pmatrix}$$

$$= f_{xx}v_1v_1 + 2f_{xy}v_1v_2 + f_{yy}v_2v_2,$$

where

$$f_{xx}(E_1,K^{[tc]}) = -2r_1 + \frac{2q^2\alpha(1-m)^2(1-q)\alpha_A K_A}{\beta a^2},$$
$$f_{xy}(E_1,K^{[tc]}) = -\frac{rK^{[tc]}\beta^2}{(\beta+K^{[tc]}(1-q)\alpha_A K_A)^2} - \frac{q\alpha(1-m)}{a},$$
$$f_{yy}(E_1,K^{[tc]}) = 0,\ g_{xx}(E_1,K^{[tc]}) = -\frac{2sq^2\alpha^2(1-m)^2}{\beta(1-q)\alpha_A K_A},$$
$$g_{xy}(E_1,K^{[tc]}) = \frac{2sq\alpha(1-m)}{(1-q)\alpha_A K_A},\ g_{yy}(E_1,K^{[tc]}) = -\frac{2s\beta}{(1-q)\alpha_A K_A},$$
$$v_1v_1 = 1,\ v_1v_2 = \frac{q\alpha(1-m)}{\beta},\ v_2v_2 = \frac{q^2\alpha^2(1-m)^2}{\beta^2},$$

which entails that

$$\delta_3 = -2r_1 + \frac{2q^2\alpha(1-q)(1-m)^2\alpha_A K_A}{\beta a^2} - \frac{2q\alpha(1-m)}{\beta}\left(\frac{rK^{[tc]}\beta^2}{(\beta+K^{[tc]}(1-q)\alpha_A K_A)^2} + \frac{q\alpha(1-m)}{a}\right).$$

If $\delta_3 \neq 0$, then by the Sotomayor's theorem as mentioned by Perko [60], the non-delayed system experiences a transcritical bifurcation between E^* and E_1 at $K = K^{[tc]}$. □

3.3.6 Global stability analysis

Theorem 3.3.7. *If $\{P_3 > 0,\ P_4 > 0\}$ or $\{P_3 < 0,\ P_4 > 0$ and $\Delta < 0\}$, then the prey-free equilibrium E_1 is globally asymptotically stable.*

Proof. In Lemma 3.3.1, we have proved that the solutions starting in the first quadrant are bounded and lie in the invariant region Ω. The equilibrium points $E_0(0,0)$ and $E_2(K_1,0)$ are always unstable, and no positive equilibrium exists if $\{P_3 > 0,\ P_4 > 0\}$ or $\{P_3 < 0,\ P_4 > 0$ and $\Delta < 0\}$ (refer to Subsec. 3.3.2). Therefore, by the Poincare-Bendixson theorem, the equilibrium point E_1 is the only attractor in the first quadrant. □

Theorem 3.3.8. *The system (3.3) is globally asymptotically stable around the interior equilibrium E^* if the following inequality holds:*

$$L^2 < 4L_1L_2, \tag{3.11}$$

where L, L_1, and L_2 are defined in the proof of this theorem.

Proof. Let a positive definite Lyapunov function about E^* be

$$V(x,y) = x - x^* - x^* ln\frac{x}{x^*} + \left[y - y^* - y^* ln\frac{y}{y^*}\right].$$

Now, along with the solutions of the model (3.3), differentiate V with regard to time t to obtain

$$\frac{dV}{dt} = \frac{(x-x^*)}{x}\frac{dx}{dt} + \frac{(y-y^*)}{y}\frac{dy}{dt}.$$

Substituting the value of $\frac{dx}{dt}$ and $\frac{dy}{dt}$ from the model (3.3), we get

$$\frac{dV}{dt} = -a_{11}(x-x^*)^2 + a_{12}(x-x^*)(y-y^*) - a_{22}(y-y^*)^2,$$

where

$$a_{11} = r_1 - \frac{q^2\alpha(1-m)^2y^*}{(a+q(1-m)x)(a+q(1-m)x^*)},$$
$$a_{22} = \frac{s\beta}{(q\alpha(1-m)x^* + (1-q)\alpha_A K_A)},$$
$$a_{12} = \frac{s\beta q\alpha(1-m)y}{(q\alpha(1-m)x^* + (1-q)\alpha_A K_A)(q\alpha(1-m)x + (1-q)\alpha_A K_A)} - \frac{q\alpha(1-m)}{a+q(1-m)x} - \frac{rK}{(1+Ky)(1+Ky^*)}.$$

$\frac{dV}{dt}$ is negative definite under condition (3.11), where

$$L = \frac{s\beta q\alpha(1-m)\mu}{(q\alpha(1-m)x^* + (1-q)\alpha_A K_A)(1-q)\alpha_A K_A} - \frac{q\alpha(1-m)}{a+q(1-m)K_1} - \frac{rK}{(1+K\mu)(1+Ky^*)},$$
$$L_1 = r_1 - \frac{q^2\alpha(1-m)^2y^*}{a(a+q(1-m)x^*)},$$
$$L_2 = \frac{s\beta}{(q\alpha(1-m)x^* + (1-q)\alpha_A K_A)}.$$

Therefore, interior equilibrium $E^*(x^*,y^*)$ is globally asymptotically stable if condition (3.11) holds. □

3.4 Dynamics of the delayed model

In this section, we will investigate the dynamics of the delayed system (3.2).

3.4.1 Local stability and Hopf-bifurcation

The model (3.2) can be rewritten as

$$\frac{d\Psi(t)}{dt} = F((\Psi(t),\ \Psi(t-\tau_1), \Psi(t-\tau_2)),$$

where

$$\Psi(t) = [x(t), y(t)]^T, \Psi(t-\tau_i) = [x(t-\tau_i), y(t-\tau_i)]^T,\ \ i = 1,2.$$

Let the variational matrix of the model (3.2) with respect to $\Psi(t),\ \Psi(t-\tau_1),\ \Psi(t-\tau_2)$ at any point (u,v) be

$$V = P_1' + P_2' e^{-\lambda\tau_1} + P_3' e^{-\lambda\tau_2} = \begin{pmatrix} a_{11} & a_{12} \\ a_{21} & a_{22} \end{pmatrix},$$

where

$$P_1' = \left(\frac{\partial F}{\partial \Psi(t)}\right)_{(u,v)},\ P_2' = \left(\frac{\partial F}{\partial \Psi(t-\tau_1)}\right)_{(u,v)},\ P_3' = \left(\frac{\partial F}{\partial \Psi(t-\tau_2)}\right)_{(u,v)},$$

$$a_{11} = \frac{r}{1+Kv} - r_0 - 2r_1 u - \frac{aq\alpha(1-m)v}{(a+q(1-m)u)^2},$$

$$a_{12} = -\frac{q\alpha(1-m)u}{a+q(1-m)u} - \frac{rKue^{-\lambda\tau_1}}{(1+Kv)^2},\ a_{21} = -\frac{s\beta q\alpha(1-m)v^2 e^{-\lambda\tau_2}}{(q\alpha(1-m)u + (1-q)\alpha_a K_A)^2},$$

$$a_{22} = s\left(1 - \frac{\beta v}{q\alpha(1-m)u + (1-q)\alpha_A K_A}\right) - \frac{s\beta v e^{-\lambda\tau_2}}{q\alpha(1-m)u + (1-q)\alpha_A K_A}.$$

Remark. In the presence of delay, the local stability behavior of all the boundary equilibria remains unaltered. At E^*, we obtain

$$V = \begin{pmatrix} -r_1 x^* + \frac{b_1^2}{\alpha} x^* y^* & -b_1 x^* - b_2 e^{-\lambda\tau_1} \\ q\alpha(1-m)\frac{b_3^2}{s} e^{-\lambda\tau_2} & -b_3 e^{-\lambda\tau_2} \end{pmatrix},$$

where

$$b_1 = \frac{q\alpha(1-m)}{a+q(1-m)x^*},\ b_2 = \frac{rKx^*}{(1+Ky^*)^2},\ b_3 = \frac{s\beta y^*}{q\alpha(1-m)x^* + (1-q)\alpha_A K_A}.$$

The corresponding characteristic equation is

$$\lambda^2 + A\lambda + (E\lambda + F)e^{-\lambda\tau_2} + Ge^{-\lambda(\tau_1+\tau_2)} = 0, \tag{3.12}$$

where

$$A = \left(r_1 - \frac{b_1^2}{\alpha}y^*\right)x^*,\ E = b_3,\ F = b_3\left(r_1 - \frac{b_1^2}{\alpha}y^*\right)x^* + b_1b_3^2\frac{q\alpha(1-m)}{s}x^*,\ G = \frac{b_2b_3^2q\alpha(1-m)}{s}.$$

Case(1): $\tau_1 = \tau_2 = 0$. Then Eq. (3.12) becomes

$$\lambda^2 + (A+E)\lambda + F + G = 0. \tag{3.13}$$

The characteristic equation (3.13) is the same as the characteristic equation (3.7) of the non-delayed model (3.3) studied in Subsec. 3.3.3.
All the roots of Eq. (3.13) have negative real parts if and only if
(H_1): $A+E > 0$ and $F+G > 0$.
So the interior equilibrium $E^*(x^*, y^*)$ is locally asymptotically stable if and only if (H_1) holds.
Case(2): $\tau_1 = 0,\ \tau_2 > 0$. Then Eq. (3.12) becomes

$$\lambda^2 + A\lambda + (E\lambda + F + G)e^{-\lambda\tau_2} = 0. \tag{3.14}$$

This is a transcendental equation. So stability behavior of the system (3.2) cannot be determined by Routh-Hurwitz criteria. Let us assume $\lambda = \pm i\omega(\omega > 0)$; then the real and imaginary components are given below

$$E\omega\sin(\omega\tau_2) + (F+G)\cos(\omega\tau_2) = \omega^2, \tag{3.15}$$

$$E\omega\cos(\omega\tau_2) - (F+G)\sin(\omega\tau_2) = -A\omega, \tag{3.16}$$

Combining Eqs. (3.15) and (3.16) leads to a quadratic equation in ω^2 as

$$\omega^4 + (A^2 - E^2)\omega^2 - (F+G)^2 = 0. \tag{3.17}$$

If we put $\omega^2 = \rho$, then Eq. (3.17) becomes

$$\rho^2 + c_1\rho + c_2 = 0,$$

where $c_1 = A^2 - E^2$ and $c_2 = -(F+G)^2$.
Remark. Since Eq. (3.17) has a unique positive root (say ω_1), therefore, the stability of the system (3.2) with respect to τ_2 cannot be switched more than once.

Substituting ω_1^2 in Eq. (3.17), we get

$$\tau_{2_n} = \frac{1}{\omega_1}\cos^{-1}\left(\frac{(F+G-AE)\omega_1^2}{E^2\omega_1^2+(F+G)^2}\right)+\frac{2n\pi}{\omega_1}, \quad n=0,1,2,... \tag{3.18}$$

Now, we will verify the transversality condition of Hopf-bifurcation.
Put $\lambda = \xi + i\omega$ in Eq. (3.14), we get real and imaginary parts as follows:

$$\xi^2-\omega^2+A\xi+(E\xi+F+G)e^{-\xi\tau_2}\cos(\omega\tau_2)+E\omega\sin(\omega\tau_2)e^{-\xi\tau_2}=0, \tag{3.19}$$

$$2\omega\xi+A\omega+E\omega e^{-\xi\tau_2}\cos(\omega\tau_2)-(E\xi+F+G)e^{-\xi\tau_2}\sin(\omega\tau_2)=0. \tag{3.20}$$

Differentiating (3.19) and (3.20) with respect to τ_2 and substituting $\tau_2=\tau_{2_0}$, we get

$$P_1\xi_{\tau_{2_0}}+P_2\omega_{\tau_{2_0}}=R_1, \tag{3.21}$$

$$-P_2\xi_{\tau_{2_0}}+P_1\omega_{\tau_{2_0}}=R_2, \tag{3.22}$$

where

$$\begin{aligned}
P_1 &= A+(E-(F+G)\tau_{2_0})\cos(\omega_1\tau_{2_0})-\tau_{2_0}E\omega_1\sin(\omega_1\tau_{2_0}),\\
P_2 &= (E-\tau_{2_0}(F+G))\sin(\omega_1\tau_{2_0})+E\omega_1\tau_{2_0}\cos(\omega_1\tau_{2_0})-2\omega_1,\\
R_1 &= (F+G)\omega_1\sin(\omega_1\tau_{2_0})-E\omega_1^2\cos(\omega_1\tau_{2_0}),\\
R_2 &= (F+G)\omega_1\cos(\omega_1\tau_{2_0})+E\omega_1^2\sin(\omega_1\tau_{2_0}).
\end{aligned}$$

Solving (3.21) and (3.22), we get

$$\left(\frac{d(Re\lambda)}{d\tau_2}\right)_{\tau_2=\tau_{2_0},\lambda=i\omega_1}=\xi_{\tau_{2_0}}=\frac{R_1P_1-R_2P_2}{P_1^2+P_2^2}.$$

$$(H_2): R_1P_1-R_2P_2\neq 0.$$

If (H_2) holds, then stability switching of E^* occurs. The following theorem states the criteria for Hopf-bifurcation near E^*.

Theorem 3.4.1. *For the system (3.2), τ_2 as ordinate, assuming (H_2) holds, there exists a positive number τ_{2_0} such that E^* is locally asymptotically stable when $\tau_2<\tau_{2_0}$ and unstable when $\tau_2>\tau_{2_0}$. Furthermore, the system (3.2) undergoes a Hopf-bifurcation about E^* at $\tau_2=\tau_{2_0}$.*

Case(3): $\tau_1>0,\ \tau_2=0.$

We can state the following theorem under an analysis similar to Case(2).

Theorem 3.4.2. *For the system (3.2), with τ_1 as abscissa, the equilibrium point E^* is locally asymptotically stable when $\tau_1 < \tau_{1_0}$ and unstable when $\tau_1 > \tau_{1_0}$. Furthermore, the system (3.2) undergoes a Hopf-bifurcation near E^* at $\tau_1 = \tau_{1_0}$, where*

$$\tau_{1_0} = \frac{1}{\omega_2}\tan^{-1}\left(\frac{(A+E)\omega_2}{\omega_2^2 - F}\right).$$

Case(4): $\tau_1 > 0,\ \tau_2 > 0.$

We consider Eq. (3.12) keeping τ_1 fix in its stable range $(0, \tau_{1_0})$ and τ_2 to vary. Let $i\omega(\omega > 0)$ be a root of Eq. (3.12). Separating real and imaginary parts, we obtain

$$\omega^2 = [F + G\cos(\omega\tau_1)]\cos(\omega\tau_2) + [E\omega - G\sin(\omega\tau_1)]\sin(\omega\tau_2), \tag{3.23}$$

$$A\omega = [F + G\cos(\omega\tau_1)]\sin(\omega\tau_2) - [E\omega - G\sin(\omega\tau_1)]\cos(\omega\tau_2). \tag{3.24}$$

On eliminating τ_2, we get

$$\omega^4 + (A^2 - E^2)\omega^2 + (2GE\sin(\omega\tau_1))\omega - (2GF\cos(\omega\tau_1) + F^2 + G^2) = 0. \tag{3.25}$$

Without loss of generality, we can assume that there exists at least one positive root ω_0 of Eq. (3.25). So, rewriting Eqs. (3.23) and (3.24) as

$$\omega_0^2 = B_1\cos(\omega_0\tau_2) + B_2\sin(\omega_0\tau_2), \tag{3.26}$$

$$A\omega_0 = B_1\sin(\omega_0\tau_2) - B_2\cos(\omega_0\tau_2), \tag{3.27}$$

where

$$B_1 = F + G\cos(\omega_0\tau_1),$$

$$B_2 = E\omega_0 - G\sin(\omega_0\tau_1).$$

On solving Eqs. (3.26) and (3.27), we obtain the following critical value of τ_2 as

$$\tau_{2_i}' = \frac{1}{\omega_0}\cos^{-1}\left(\frac{B_1^2 - A^2\omega_0^2}{\omega_0^2 B_1 + A\omega_0 B_2}\right) + \frac{2i\pi}{\omega_0}, \quad i = 0, 1, 2... \tag{3.28}$$

Now, to verify the transversality condition for Hopf-bifurcation, put $\lambda = \xi + i\omega$ in Eq. (3.12) and then separating real and imaginary parts, we get

$$\xi^2 - \omega^2 + A\xi + (E\xi + F)e^{-\xi\tau_2}\cos(\omega\tau_2) + E\omega\sin(\omega\tau_2)e^{-\xi\tau_2} + G\cos(\omega(\tau_1+\tau_2))e^{-\xi(\tau_1+\tau_2)} = 0, \tag{3.29}$$

$$2\omega\xi + A\omega + E\omega e^{-\xi\tau_2}\cos(\omega\tau_2) - (E\xi + F)e^{-\xi\tau_2}\sin(\omega\tau_2) - G\sin(\omega(\tau_1+\tau_2))e^{-\xi(\tau_1+\tau_2)} = 0. \tag{3.30}$$

Differentiating (3.29) and (3.30) with respect to τ_2 and put $\xi = 0$ (the system changes stability when $Re(\lambda) = 0$) and $\tau_2 = \tau'_{2_0}$, we obtain

$$M_1\xi_{\tau'_{2_0}} + M_2\omega_{\tau'_{2_0}} = N_1, \tag{3.31}$$

$$-M_2\xi_{\tau'_{2_0}} + M_1\omega_{\tau'_{2_0}} = N_2, \tag{3.32}$$

where

$$\begin{aligned}
M_1 &= A + (E - F\tau'_{2_0})\cos(\omega_0\tau'_{2_0}) - \tau'_{2_0}E\omega_0\sin(\omega_0\tau'_{2_0}) - G(\tau_1+\tau'_{2_0})\cos(\omega_0(\tau_1+\tau'_{2_0})),\\
M_2 &= (E - \tau'_{2_0}F)\sin(\omega_0\tau'_{2_0}) + E\omega_0\tau'_{2_0}\cos(\omega_0\tau'_{2_0}) - 2\omega_0 - G(\tau_1+\tau'_{2_0})\sin(\omega_0(\tau_1+\tau'_{2_0})),\\
N_1 &= F\omega_0\sin(\omega_0\tau'_{2_0}) - E\omega_0^2\cos(\omega_0\tau'_{2_0}) + G\omega_0\sin(\omega_0(\tau_1+\tau'_{2_0})),\\
N_2 &= F\omega_0\cos(\omega_0\tau'_{2_0}) + E\omega_0^2\sin(\omega_0\tau'_{2_0}) + G\omega_0\cos(\omega_0(\tau_1+\tau'_{2_0})).
\end{aligned}$$

Solving (3.31) and (3.32), we get

$$\left(\frac{d(Re\lambda)}{d\tau_2}\right)_{\tau_2=\tau'_{2_0},\lambda=i\omega_0} = \xi_{\tau'_{2_0}} = \frac{N_1M_1 - N_2M_2}{M_1^2 + M_2^2}.$$

$$(H_3) : N_1M_1 - N_2M_2 \neq 0.$$

Theorem 3.4.3. *For the system (3.2), with $\tau_1 \in (0, \tau_{1_0})$ and assuming that (H_3) holds, there exists a positive number τ'_{2_0} such that E^* is locally asymptotically stable when $\tau_2 < \tau'_{2_0}$ and unstable when $\tau_2 > \tau'_{2_0}$. Furthermore, the system (3.2) undergoes a Hopf-bifurcation near E^* at $\tau_2 = \tau'_{2_0}$.*

3.4.2 Direction and stability of Hopf-bifurcation

In the previous subsection, we obtained conditions under which the system experiences Hopf-bifurcation with respect to delay parameters τ_1 and τ_2. Here, we will determine the direction of Hopf-bifurcation and stability of the bifurcated periodic solution at $\tau_2 = \tau'_{2_0}$ and $\tau_1 = \tau_1^* = \in (0, \tau_{1_0})$ using center manifold theorem and normal form theory as described by Hassard *et al.* [124].

Let $\tau_2 = \tau'_{2_0} + \mu,\ \mu \in R$ so that Hopf-bifurcation occurs at $\mu = 0$. Rescaling the time delay $t \mapsto \frac{t}{\tau_2}$, the system (3.2) can be written as

$$\dot{U} = \tau_2(P'U(t) + Q'U(t - \frac{\tau_1^*}{\tau_2}) + R'U(t-1) + f(x,y)),$$

where

$$U(t) = (x(t), y(t))^T.$$

$$P' = \begin{pmatrix} P_{11} & P_{12} \\ 0 & 0 \end{pmatrix},\ Q' = \begin{pmatrix} 0 & Q_{12} \\ 0 & 0 \end{pmatrix},\ R' = \begin{pmatrix} 0 & 0 \\ R_{21} & R_{22} \end{pmatrix},\ f = (f_1, f_2)^T,$$

such that $P_{11} = -r_1 x^* + \frac{b_1^2}{a} x^* y^*$, $P_{12} = -b_1 x^*$, $Q_{12} = -b_2$, $R_{21} = \frac{q\alpha(1-m)b_3^2}{s}$, $R_{22} = -b_3$.
The non-linear terms f_1, f_2 are given by

$$f_1 = \frac{rx(t)}{1 + Ky(t - \frac{\tau_1^*}{\tau_2})} - r_1 x^2(t) - \frac{q\alpha(1-m)x(t)y(t)}{a + q(1-m)x(t)},$$
$$f_2 = -\frac{sy(t)y(t-1)}{q\alpha(1-m)x(t-1) + (1-q)\alpha_A K_A}.$$

In functional form, the delayed system can be written as

$$L_\mu \phi = (\tau_2 + \mu)\left(P'\phi(0) + Q'\phi(-\frac{\tau_1^*}{\tau_2}) + R'\phi(-1) \right),$$

$$\phi = (\phi_1, \phi_2)^T \in C([-1, 0], R^2).$$

By the Riesz representation theorem, there exists a 2×2 matrix $\eta(\theta, \mu)$ such that its elements are function of bounded variation. Therefore,

$$L_\mu \phi = \int_{-1}^{0} d\eta(\theta, \mu)\phi(\theta).$$

In fact, choosing

$$\eta(\theta, \mu) = \begin{cases} (\tau_{2_0}' + \mu)(P' + Q' + R'), & \theta = 0, \\ (\tau_{2_0}' + \mu)(Q' + R'), & \theta \in [\frac{-\tau_1^*}{\tau_2}, 0), \\ (\tau_{2_0}' + \mu)R', & \theta \in (-1, \frac{-\tau_1^*}{\tau_2}), \\ 0, & \theta = -1, \end{cases}$$

for $\phi \in C^1([-1, 0], R^2)$, we define

$$A(\mu)\phi(\theta) = \begin{cases} \frac{d\phi(\theta)}{d\theta}, & -1 \le \theta < 0, \\ \\ \int_{-1}^{0} [d\eta(\xi, \mu)]\phi(\xi), & \theta = 0, \end{cases}$$

$$A^*\psi(s) = \begin{cases} -\frac{d\psi(s)}{ds}, & s \in (0,1], \\ \\ \int_{-1}^{0}[d\eta(\xi,0)]\psi(-\xi), & s = 0, \end{cases}$$

and the bilinear form

$$\langle \psi(s), \phi(\theta)\rangle = \overline{\psi(0)}\phi(0) - \int_{-1}^{0}\int_{\xi=0}^{\theta} \overline{\psi(\xi-\theta)}d\eta(\theta)\phi(\xi)d\xi,$$

where

$$\eta(\theta) = \eta(\theta,0).$$

We know that eigenvalues of $A(0)$ are $\pm i\omega^*\tau'_{2_0}$. Since A and A^* are adjoint. Therefore, eigenvalues of A and A^* are same. Now, we need to verify that

$$q(\theta) = (1,\alpha_1)^T e^{i\omega^*\tau'_{2_0}\theta} \ (\theta \in [-1,0])$$

and

$$q^*(s) = \frac{1}{D}(1,\alpha_1^*)e^{i\omega^*\tau'_{2_0}s} \ (s \in [0,1])$$

are the eigenvectors of $A(0)$ and A^* corresponding to the eigenvalue $i\omega^*\tau'_{2_0}$ and $-i\omega^*\tau'_{2_0}$, respectively, where

$$\langle q^*(s), q(\theta)\rangle = 1, \ \ \langle q^*(s), \overline{q(\theta)}\rangle = 1,$$

$$\alpha_1 = \frac{R_{21}}{i\omega^* e^{i\omega^*\tau'_{2_0}} - R_{22}},$$

$$\alpha_1^* = -\frac{(P_{12} + Q_{12}e^{\frac{i\omega^*\tau_1^*}{\tau'_{2_0}}})}{i\omega^* + R_{22}e^{i\omega^*\tau'_{2_0}}},$$

and

$$\overline{D} = 1 + \alpha_1\overline{\alpha_1^*} + \tau'_{2_0}\left[R_{21}\overline{\alpha_1^*}e^{-i\omega^*\tau'_{2_0}} + R_{22}\alpha_1\overline{\alpha_1^*}e^{-i\omega^*\tau'_{2_0}} + Q_{12}\frac{\alpha_1\tau_1^*}{\tau'_{2_0}}e^{\frac{-i\omega^*\tau_1^*}{\tau'_{2_0}}}\right].$$

Following the algorithms explained by Hassard *et al.* [124] and using a computation process similar to that in [125], which is used to obtain the properties of Hopf-bifurcation, we obtain

$$g_{20} = \tau'_{2_0}\overline{D}\left[rW_{20}^{(1)}(0) - 2rK\alpha_1 e^{-i\omega^*\tau_1^*} - 2r_1 - \frac{2\alpha\alpha_1 q(1-m)}{a} - \frac{2\overline{\alpha_1^*}s\alpha_1^2 e^{-i\omega^*\tau'_{2_0}}}{(1-q)\alpha_A K_A}\right],$$

$$g_{02} = \tau'_{2_0}\overline{D}\left[rW_{02}^{(1)}(0) - 2rK\overline{\alpha_1}e^{i\omega^*\tau_1^*} - 2r_1 - \frac{2\alpha\overline{\alpha_1}q(1-m)}{a} - \frac{2\overline{\alpha_1^*}s\overline{\alpha_1}^2 e^{i\omega^*\tau'_{2_0}}}{(1-q)\alpha_A K_A}\right],$$

$$g_{11} = \tau'_{2_0}\overline{D}\left[rW_{11}^{(1)}(0) - rK\alpha_1 e^{-i\omega^*\tau_1^*} - rK\overline{\alpha_1}e^{i\omega^*\tau_1^*} - 2r_1 - \frac{\alpha(\alpha_1+\overline{\alpha_1})q(1-m)}{a} - \frac{\overline{\alpha_1^*}s\alpha_1\overline{\alpha_1}e^{i\omega^*\tau'_{2_0}}}{(1-q)\alpha_A K_A}\right],$$

$$\begin{aligned} g_{21} = \tau'_{2_0}\overline{D}\Bigg[& r(-2K\alpha_1 W_{11}^{(1)}(0)e^{-i\omega^*\tau_1^*} - K\overline{\alpha_1}W_{20}^{(1)}(0)e^{i\omega^*\tau_1^*} + KW_{20}^{(2)}\frac{\tau_1^*}{\tau'_{2_0}} + 2KW_{11}^{(2)}\frac{\tau_1^*}{\tau'_{2_0}} \\ &+ 2K^2\alpha_1^2 e^{-2i\omega^*\tau_1^*} + 4K^2\alpha_1\overline{\alpha_1}) - r_1(W_{20}^{(1)}(0) + 2W_{11}^{(1)}(0)) - \frac{2\alpha q(1-m)}{a}\Bigg(\alpha_1 W_{11}^{(1)}(0) + \frac{\overline{\alpha_1}}{2}W_{20}^{(1)}(0) \\ &+ \frac{W_{20}^{(2)}(0)}{2} + W_{11}^{(2)}(0) - \frac{2\alpha_1 q(1-m)}{a} - \frac{\overline{\alpha_1}q(1-m)}{a}) - \frac{2\overline{\alpha_1^*}s}{(1-q)\alpha_A K_A}(\alpha_1 W_{11}^{(2)}(0)e^{-i\omega^*\tau'_{2_0}} \\ &+ \frac{\overline{\alpha_1}}{2}W_{20}^{(2)}(0)e^{i\omega^*\tau'_{2_0}} + \frac{\overline{\alpha_1}}{2}W_{20}^{(2)}(-1) + W_{11}^{(2)}(-1)\alpha_1 - \frac{\alpha q(1-m)\alpha_1\overline{\alpha_1}}{(1-q)\alpha_A K_A} - \frac{\alpha q(1-m)\alpha_1^2}{(1-q)\alpha_A K_A}\Bigg)\Bigg], \end{aligned}$$

where

$$\begin{aligned} W_{20}(\theta) &= \frac{ig_{20}}{\omega^*\tau'_{2_0}}q(0)e^{i\omega^*\tau'_{2_0}\theta} + \frac{i\overline{g_{02}}}{3\omega^*\tau'_{2_0}}\overline{q(0)}e^{-i\omega^*\tau'_{2_0}\theta} + M_1 e^{2i\omega^*\tau'_{2_0}\theta}, \\ W_{02}(\theta) &= -\frac{ig_{02}}{3\omega^*\tau'_{2_0}}q(0)e^{i\omega^*\tau'_{2_0}\theta} - \frac{i\overline{g_{20}}}{\omega^*\tau'_{2_0}}\overline{q(0)}e^{-i\omega^*\tau'_{2_0}\theta} + M_2 e^{-2i\omega^*\tau'_{2_0}\theta}, \\ W_{11}(\theta) &= -\frac{ig_{11}}{\omega^*\tau'_{2_0}}q(0)e^{i\omega^*\tau'_{2_0}\theta} + \frac{i\overline{g_{11}}}{\omega^*\tau'_{2_0}}\overline{q(0)}e^{-i\omega^*\tau'_{2_0}\theta} + M_3. \end{aligned}$$

M_1 and M_2 can be computed as

$$M_1 = 2\begin{pmatrix} 2i\omega^* - P_{11} & -P_{12} - Q_{12}e^{-2i\omega^*\tau_1^*} \\ -R_{21}e^{-2i\omega^*\tau'_{2_0}} & 2i\omega^* - R_{22}e^{-2i\omega^*\tau'_{2_0}} \end{pmatrix}^{-1}\begin{pmatrix} -r + r_1 + q\alpha(1-m)\alpha_1 \\ s\alpha_1^2 e^{-2i\omega^*\tau'_{2_0}} \end{pmatrix},$$

$$M_2 = 2\begin{pmatrix} -2i\omega^* - P_{11} & -P_{12} - Q_{12}e^{2i\omega^*\tau_1^*} \\ -R_{21}e^{2i\omega^*\tau'_{2_0}} & -2i\omega^* - R_{22}e^{2i\omega^*\tau'_{2_0}} \end{pmatrix}^{-1}\begin{pmatrix} -r + r_1 + q\alpha(1-m)\overline{\alpha_1} \\ s\overline{\alpha_1}^2 e^{2i\omega^*\tau'_{2_0}} \end{pmatrix},$$

$$M_3 = 2\begin{pmatrix} -P_{11} & -P_{12} - Q_{12} \\ -R_{21} & -R_{22} \end{pmatrix}^{-1}\begin{pmatrix} -r + r_1 + q\alpha(1-m)\frac{(\alpha_1+\overline{\alpha_1})}{2} \\ s\alpha_1\overline{\alpha_1} \end{pmatrix}.$$

Consequently, we can find g_{ij} in terms of delay parameter and other biological parameters. To determine characteristics of the bifurcated periodic solution, we can compute the following

coefficients:

$$C_1(0) = \frac{i}{2\tau'_{2_0}\omega^*}\left(g_{20}g_{11} - 2|g_{11}|^2 - \frac{|g_{02}|^2}{3}\right) + \frac{g_{21}}{3}, \ \ \mu_2 = -\frac{Re\{C_1(0)\}}{Re\{\lambda'(\tau'_{2_0})\}},$$

$$\beta_2 = 2Re\{C_1(0)\} \ \text{ and } \ T_2 = -\frac{Im\{C_1(0)\} + \mu_2\{Im(\lambda'(\tau'_{2_0}))\}}{\omega^*\tau'_{2_0}}.$$

Now we are able to state the following theorem.

Theorem 3.4.4. *1. The sign of μ_2 determines the direction of the Hopf-bifurcation. If $\mu_2 > 0 (< 0)$, then the Hopf-bifurcation is supercritical (subcritical).*

2. The sign of β_2 determines the stability of the bifurcating periodic solution. If $\beta_2 > 0 (< 0)$, then the obtained periodic solution is unstable (stable).

3. T_2 determines the period of the bifurcating periodic solution. If $T_2 > 0 (< 0)$, then the period increases (decreases).

3.5 Numerical simulation

In order to support the theoretical analysis, some numerical simulations are performed using MATLAB R2020b. The set of parameters is chosen as follows:

$$\begin{aligned} &r = 3.5, \ \ K = 1, \ \ q = 0.3, \ \ r_0 = 0.5, \ \ r_1 = 0.0375, \ \ a = 0.1, \\ &K_A = 1.7, \ \ \alpha = 2, \ \ s = 0.2, \ \ m = 0.65, \ \ \alpha_A = 0.3, \ \ \beta = 1. \end{aligned} \tag{3.33}$$

The corresponding equilibrium points and their stability behavior are given in Table 3.2.

Table 3.2: Equilibrium points of the proposed model and their stability behavior in the absence of delay.

Equilibrium points	Eigenvalues	Stability behavior
$E_0(0,0)$	$(3, 0.2)$	unstable
$E_1(0, 0.357)$	$(1.3295, -0.2)$	saddle point
$E_2(80, 0)$	$(-3, 0.2)$	saddle point
$E^*(7.13, 1.8543)$	$(-0.0312 \pm 0.4175i)$	stable focus

3.5.1 Computation for the non-delayed system

This subsection presents the numerical simulation for the system (3.3) with parameters given in (3.33). To examine the effect of fear, refuge, and additional food on the dynamics of the system

(3.3), we obtain exciting results concerning parameters: K, q, m, α_A. The effect of fear (on varying K) is shown in Fig. 3.2 and Fig. 3.3.

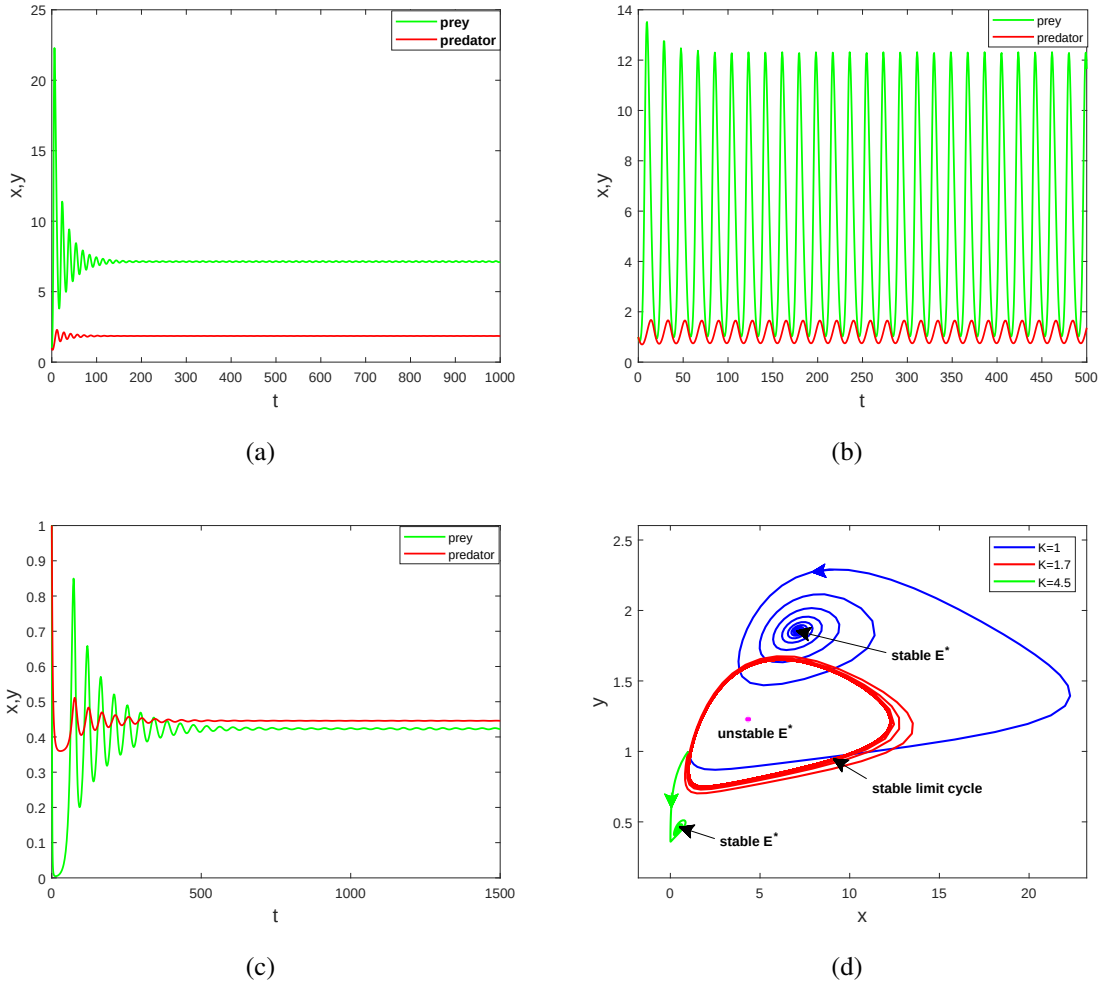

Fig. 3.2: Time series solution for system (3.3) around E^* for (a) $K = 1$, (b) $K = 1.7$, (c) $K = 4.5$. (d) Combined phase portrait corresponding to (a), (b) and (c) initiated from $(1, 1)$.

In Fig. 3.2 (a), initially, for some duration, the prey and predator population oscillate about their steady-state, and eventually, it converges to the co-existence equilibrium. On increasing the value of the fear parameter, at $K = K^{[H_1]} = 1.3576755$, the system undergoes Hopf-bifurcation resulting in instability of E^*, and a stable limit cycle is induced. At $K = 1.7$, the system is unstable about E^*, as shown in Fig.3.2 (b). Both populations fluctuate highly about their mean position between their maximum and minimum values. Further increase in K makes the system stable from periodic oscillations via Hopf-bifurcation at $K = K^{[H_2]} = 4.396743$. Hence at $K = 4.5$, the system shows stable behavior about E^*, shown in Fig. 3.2 (c). Phase portraits corresponding to Fig. 3.2 (a), 3.2 (b), and 3.2 (c) are shown in Fig. 3.2 (d). Therefore,

we conclude that the stability behavior of the co-existence equilibrium of the system (3.3) is sensitive to the fear parameter.

Now, to check the transversality condition for Hopf-bifurcation at $K^{[H_1]}$ and $K^{[H_2]}$, using Newton's forward difference formula, we obtain the following results:

$$\left.\frac{d(Re(\lambda))}{dK}\right|_{K=K^{[H_1]}} = 0.0671 > 0$$

and

$$\left.\frac{d(Re(\lambda))}{dK}\right|_{K=K^{[H_2]}} = -0.0729 < 0.$$

Also, at both the bifurcation points

$$Re(\lambda) = tr(M|_{E^*}) = 0,\ det(M|_{E^*}) > 0,$$

where λ is the characteristic root of Eq. (3.7). Therefore by the Andronov-Hopf-bifurcation theorem, the system (3.3) undergoes Hopf-bifurcation at $K^{[H_1]}$ and $K^{[H_2]}$ around the positive equilibrium E^*. At $K = K^{[tc]} = 5.04389962$, we obtain $\delta_3 = -0.3279 \neq 0$. Therefore, according to Theorem 3.3.6, the system (3.3) undergoes a transcritical bifurcation at $K = K^{[tc]}$.

In order to visualize Hopf-bifurcation and transcritical bifurcation with respect to the fear parameter K, we draw a bifurcation diagram in Fig. 3.3. According to Fig. 3.2, our system undergoes Hopf-bifurcation at $K^{[H_1]}$ and $K^{[H_2]}$. This situation is combinedly presented in Fig. 3.3.

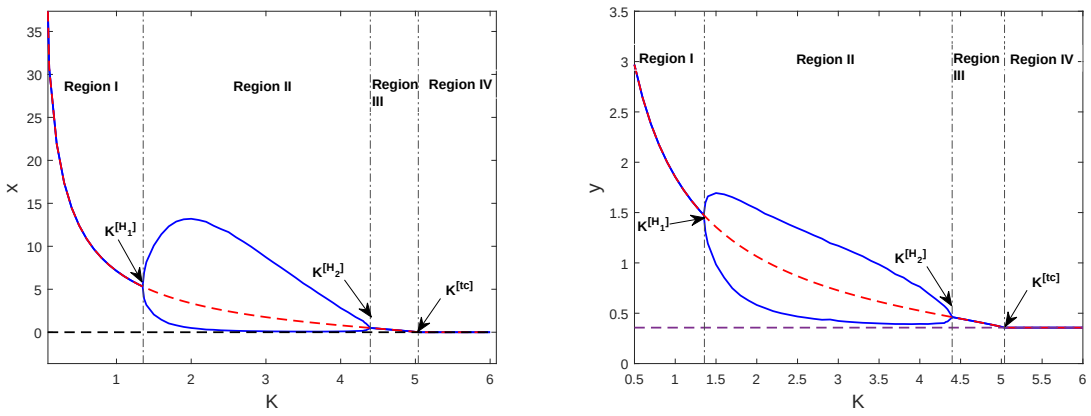

(a) (b)

Fig. 3.3: Bifurcation diagram with respect to fear parameter K and remaining parameters are same as in (3.33).

In Region I, the system is locally asymptotically stable around the interior equilibrium E^*

and unstable around prey-free equilibrium E_1. In Region II, E^* is unstable, and a stable limit cycle is born via Hopf-bifurcation at $K = K^{[H_1]}$. The axial equilibrium E_1 is also unstable in this region. In Region III, the positive equilibrium point E^* again switches its stability through Hopf-bifurcation at $K = K^{[H_2]}$, and E_1 is still unstable. At $K = K^{[tc]} = 5.04389962$, E^* disappears and transfers its stability to the prey-free equilibrium point E_1. The aforementioned phenomenon is transcritical bifurcation. Therefore, Region IV shows stable behavior of E_1, and E^* does not exist here.

To determine the direction of Hopf-bifurcation, we use the formula given in [17]. We obtain $\sigma^*|_{K=K^{[H_1]}} = -0.3148569566$ and $\sigma^*|_{K=K^{[H_2]}} = -3.6036317012$. Since these values are negative. Therefore, the direction of Hopf-bifurcation at $K = K^{[H_1]}$ and $K = K^{[H_2]}$ is supercritical.

Table 3.3: Effect of q on steady state of prey and predator population when $K = 0.1$ and all parameters are same as in (3.33).

value of q	x^*	y^*
0.1	49.6502	3.9345
0.2	38.1714	5.752
0.3	30.7263	6.8795
0.4	25.239	7.3729
0.5	20.941	7.5843
0.6	17.4666	7.54
0.7	14.6112	7.3175
0.8	12.2463	6.96
0.9	10.2826	6.529

From Table 3.3, one can see that on increasing the preference rate of the predator, the prey population decreases, and on consuming prey, the predator population grows. Now, for larger values of q, as the predator is highly dependent on prey and prey are lesser in number, the predator population decreases. This result justifies the negative feedback.

Effect of m: The effect of refuge parameter m is shown in Fig. 3.4. From this figure, we note that the prey population increases with an increase in the value of the refuge parameter. In contrast, the predator population initially increases up to $m = 0.39236$ and then decreases. This shows that reserving prey is beneficial for both prey and predator up to a threshold value of the refuge parameter. However, beyond this value, it causes a negative effect on the predator. The rate of change in predator population y^* with respect to m is determined, and we get

$$\left[\frac{dy^*}{dm}\right]_{m=m^*} = 0.$$

Predator population attain its maximum i.e., $y^*_{max} = 7.5957$ at $m = m^* = 0.39236$.

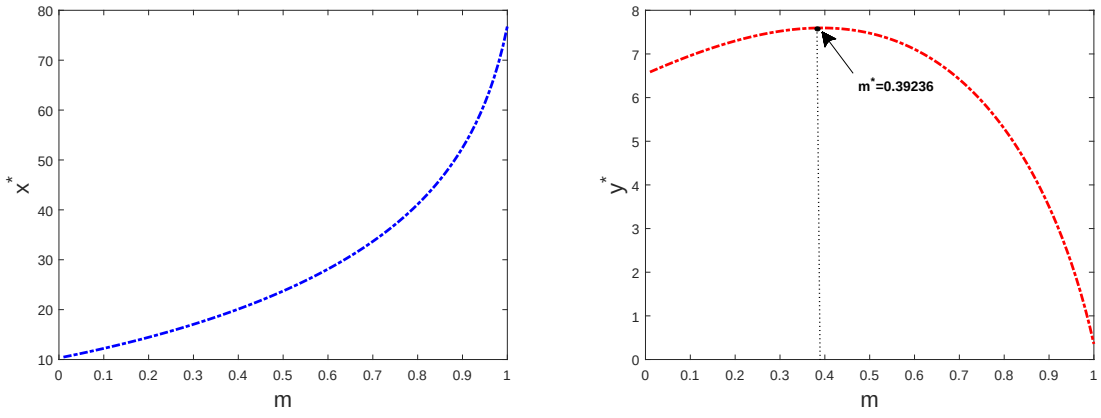

(a) (b)

Fig. 3.4: The effect of refuge on prey and predator population, other parameters are the same as in Eq. (3.33).

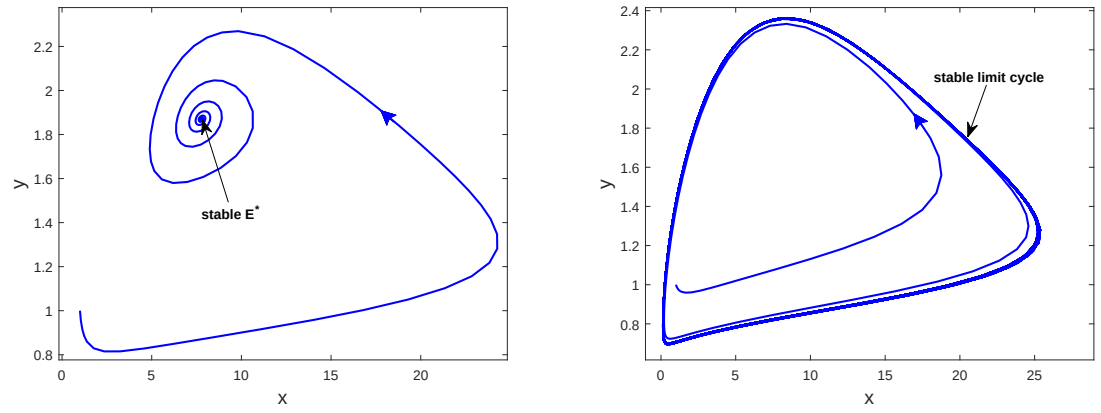

(a) (b)

Fig. 3.5: Switching of stability of E^*. (a) E^* is stable at $\alpha_A = 0.2 < \alpha_A^*$. (b) E^* is unstable at $\alpha_A = 0.5 > \alpha_A^*$.

Effect of α_A: The effect of additional food parameter α_A is depicted in Fig. 3.5 and Fig. 3.6 . From Fig. 3.5, it is observed that the positive equilibrium E^* is stable initially at $\alpha_A = 0.2$. On increasing the value of α_A, the system (3.3) undergoes Hopf-bifurcation at $\alpha_A = \alpha_A{}^* = 0.41983$, computed by the formula derived in Sec. 3.3. After this value, E^* becomes unstable, and a stable limit cycle is born. The direction of Hopf-bifurcation is obtained from the formula given in Wang [17], which gives $\sigma^* = -0.1884045609$. By Perko [60], it is a supercritical Hopf-bifurcation as $\sigma^* < 0$.

Initially, at $\alpha_A = 0.48$, a stable limit cycle around E^* and a saddle point E_1 are observed in Fig. 3.6 (a). With the increase in the value of α_A, at $\alpha_A = 0.51$, the limit cycle expands

and approaches towards the saddle point E_1. This can be seen in Fig. 3.6 (b). The limit cycle collides with saddle point E_1 at $\alpha_A = \alpha_A^{**} = 0.61091$, the homoclinic bifurcation point, and a closed trajectory with an infinite period termed homoclinic orbit is formed, in which the saddle point links itself, as seen in Fig. 3.6 (c). After homoclinic bifurcation, the limit cycle disappears, and the prey-free equilibrium E_1 is stable. Fig. 3.6 (d) shows the phase portrait after homoclinic bifurcation at $\alpha_A = 0.63$. It concludes that as we increase α_A, the prey population immediately collapses after homoclinic bifurcation [126].

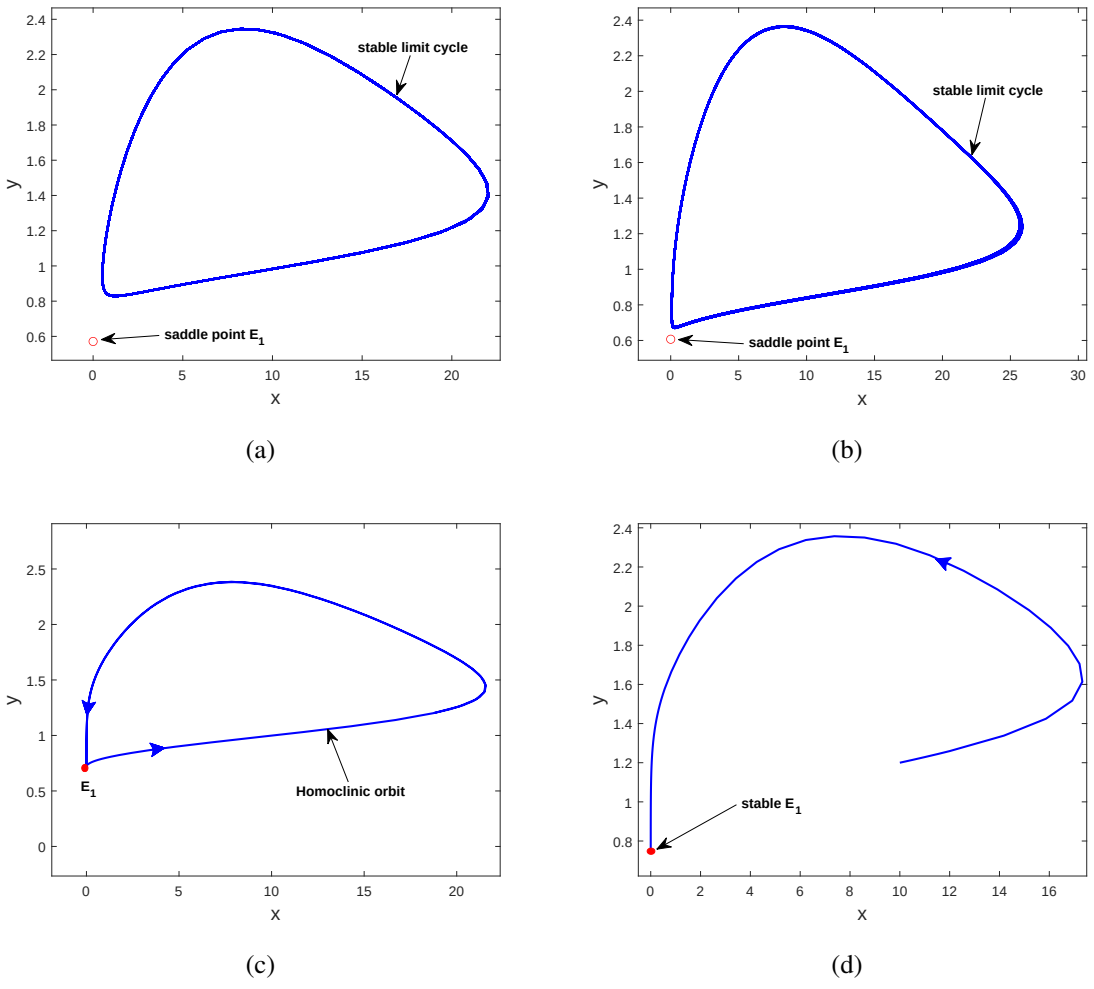

Fig. 3.6: Effect of α_A causes the system (3.3) to undergo a homoclinic bifurcation at $\alpha_A = \alpha_A^{**}$ between saddle point E_1 and stable limit cycle around E^*. The stable limit cycle approach towards saddle point E_1 before the homoclinic bifurcation (a), (b). The last vestige of the limit cycle: homoclinic orbit, is formed at the homoclinic bifurcation (c). After bifurcation, the trajectory tends towards E_1 (d).

The variation of the preference rate of predator with fear parameter is shown in Fig. 3.7. From this figure, it is observed that on increasing preference rate of the predator, the cost of

fear in prey varies such that the stability of E^* and E_1 is affected, which gives rise to four different regions. In region I, E^* is stable and E_1 is unstable. E^* changes its stability via Hopf-bifurcation, and a stable limit cycle occurs in region II. Region III represents the stability region of E^* as the system (3.3) undergoes Hopf-bifurcation again. In region IV, E_1 is stable by means of a transcritical bifurcation.

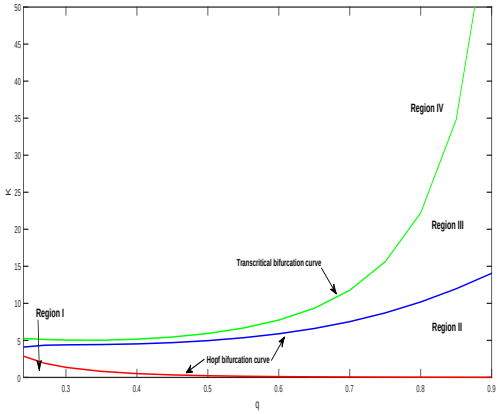

Fig. 3.7: Various stability regions of the model (3.3) in the $qK-$plane.

We can see from Fig. 3.1 (d) that no positive equilibrium exists for the chosen set of parameters, and $P_3 = -0.1274$, $P_4 = 0.9986$ and $\Delta = -1.2237 \times 10^{-6}$. Furthermore, all existing equilibria except the prey-free equilibrium are unstable. Hence by the Poincare-Bendixson's theorem, the equilibrium E_1 is globally asymptotically stable (shown in Fig. 3.8). This finding supports Theorem 3.3.7.

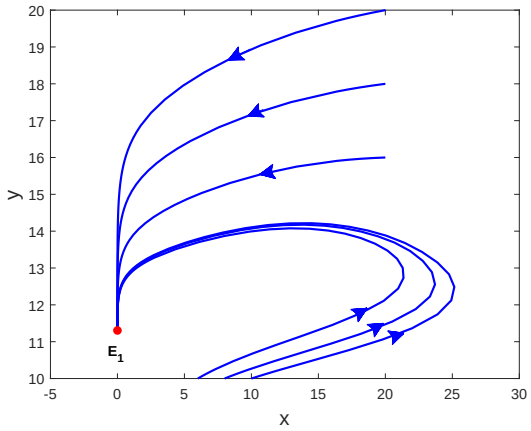

Fig. 3.8: E_1 is globally asymptotically stable where the parameters are the same as in Fig. 3.1 (d).

The co-existence between two stable attractors can be achieved using a control parameter. This phenomenon is bi-stability. The system can converge to two different attractors depending

upon the initial condition. Our system exhibits bi-stability between prey-free and interior equilibrium (see Fig. 3.9). The black dashed curve shown here is the separatrix; it separates the region of stability of both equilibria. It is clear from Fig. 3.9 that the trajectory (green curve) started from below the separatrix converges to E_1^*, and the blue curve started from above the separatrix approaches to E_1. For bi-stability, the range of α_A is $[7.631265, 8.585380]$.

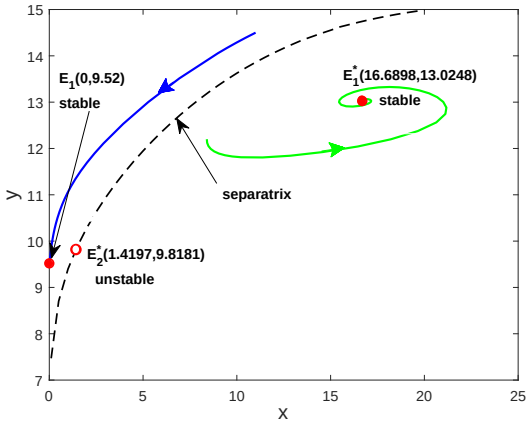

Fig. 3.9: Bi-stability phenomenon between equilibrium points E_1 and E_1^* for the system (3.3). Here $\alpha_A = 8$, $a = 1$, $K = 0.05$ and other parameters are from (3.33).

3.5.2 Computation for the delayed model

Here we shall perform numerical simulation for the delayed model (3.2) with the set of parameters (3.33). For the chosen parameters, the numerical value of equilibrium points is the same as in Table 3.2. In the absence of delay, condition (3.8) holds, which implies that the system is stable about the interior equilibrium E^*. Upon introducing delay, we shall investigate different cases discussed in Subsec. 3.4.1.

The effect of gestation delay: $\tau_1 = 0,\ \tau_2 > 0$. We can verify Theorem 3.4.1 numerically. We observe that the transversality condition (H_2) holds at τ_{2_0}. This value of τ_{2_0} can be determined using (3.18). Taking $n = 0$, we obtain

$$\tau_{2_0} = 0.345727 \ \text{ and } \ \frac{d(Re\lambda)}{d\tau_2}\bigg|_{\tau_2=\tau_{2_0}} = 0.014547 \neq 0.$$

This shows $Re(\lambda)$ is increasing function of τ_2 at $\tau_2 = \tau_{2_0}$. Thus, according to Theorem 3.4.1, the system (3.2) undergoes a Hopf-bifurcation around E^* at $\tau_2 = \tau_{2_0} = 0.345727$.

Fig. 3.10 (a) (time series curve) and Fig. 3.10 (c) (phase portrait) show that the solution trajectory oscillates about E^* at first and eventually converges to it. This behavior is the local

asymptotic stability of E^* at $\tau_2 = 0.2 < \tau_{2_0}$. On increasing the value of gestation delay, the system experiences a Hopf-bifurcation near E^* at $\tau_2 = \tau_{2_0}$. Consequently, E^* is no longer stable, and a stable limit cycle is induced at $\tau_2 = 0.52 > \tau_{2_0}$ (refer to Fig. 3.10 (b), (d)).

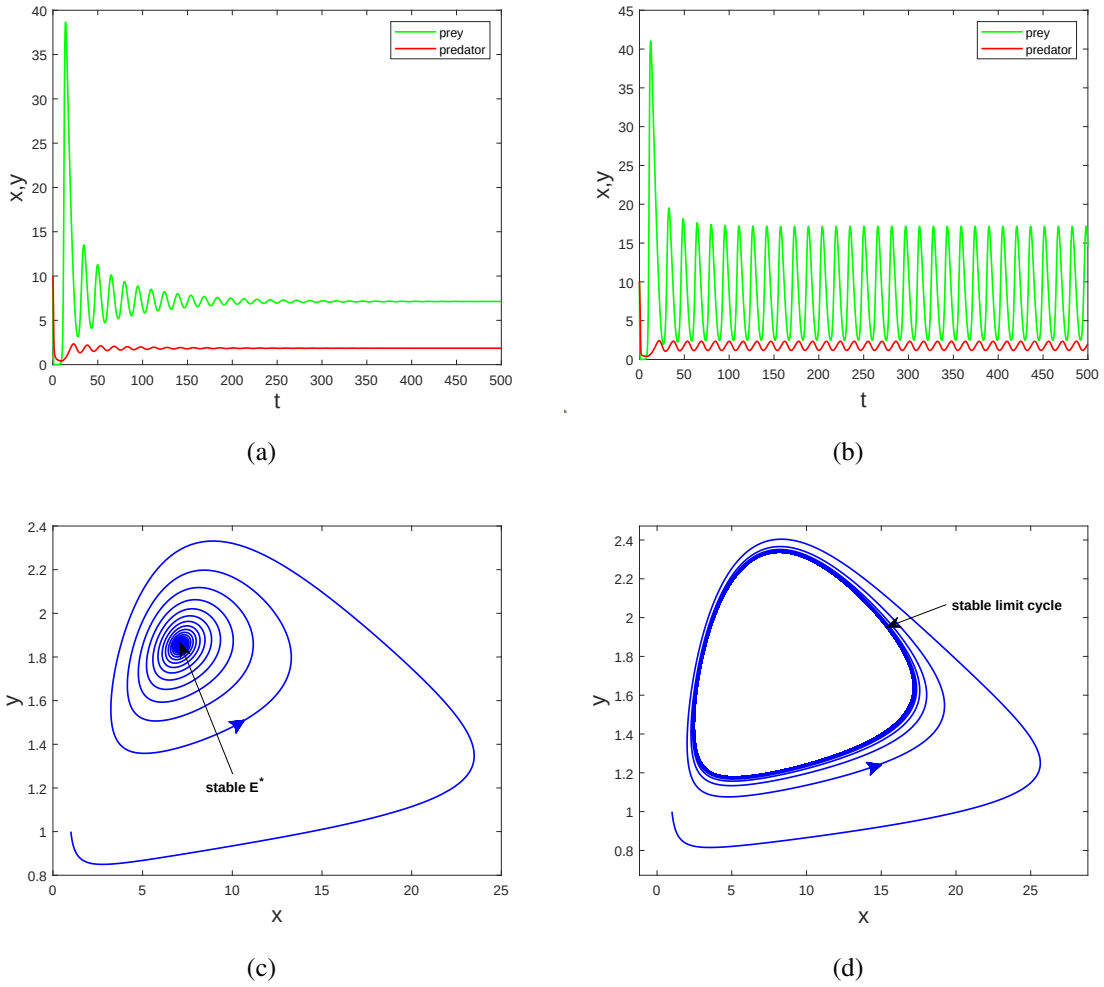

Fig. 3.10: When $\tau_2 = 0.2 < \tau_{2_0}$ and $\tau_1 = 0$, E^* is locally asymptotically stable (a,c). At $\tau_2 = 0.52 > \tau_{2_0}$ and $\tau_1 = 0$, E^* is unstable (b, d).

To demonstrate the Hopf-bifurcation in a better way, we constructed a bifurcation diagram in three dimensions (see Fig. 3.11). Trajectories of both populations are plotted against gestation delay. It is observed that before the critical value of τ_2, the positive equilibrium is stable, but when it crosses this value, the trajectory is attracted towards limit cycles. The colored closed orbits shown here are stable limit cycles.

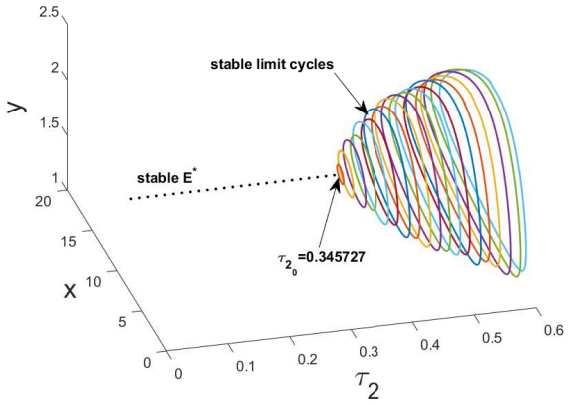

Fig. 3.11: Bifurcation diagram representing attractors (equilibrium points and limit cycles) for various values of gestation delay τ_2.

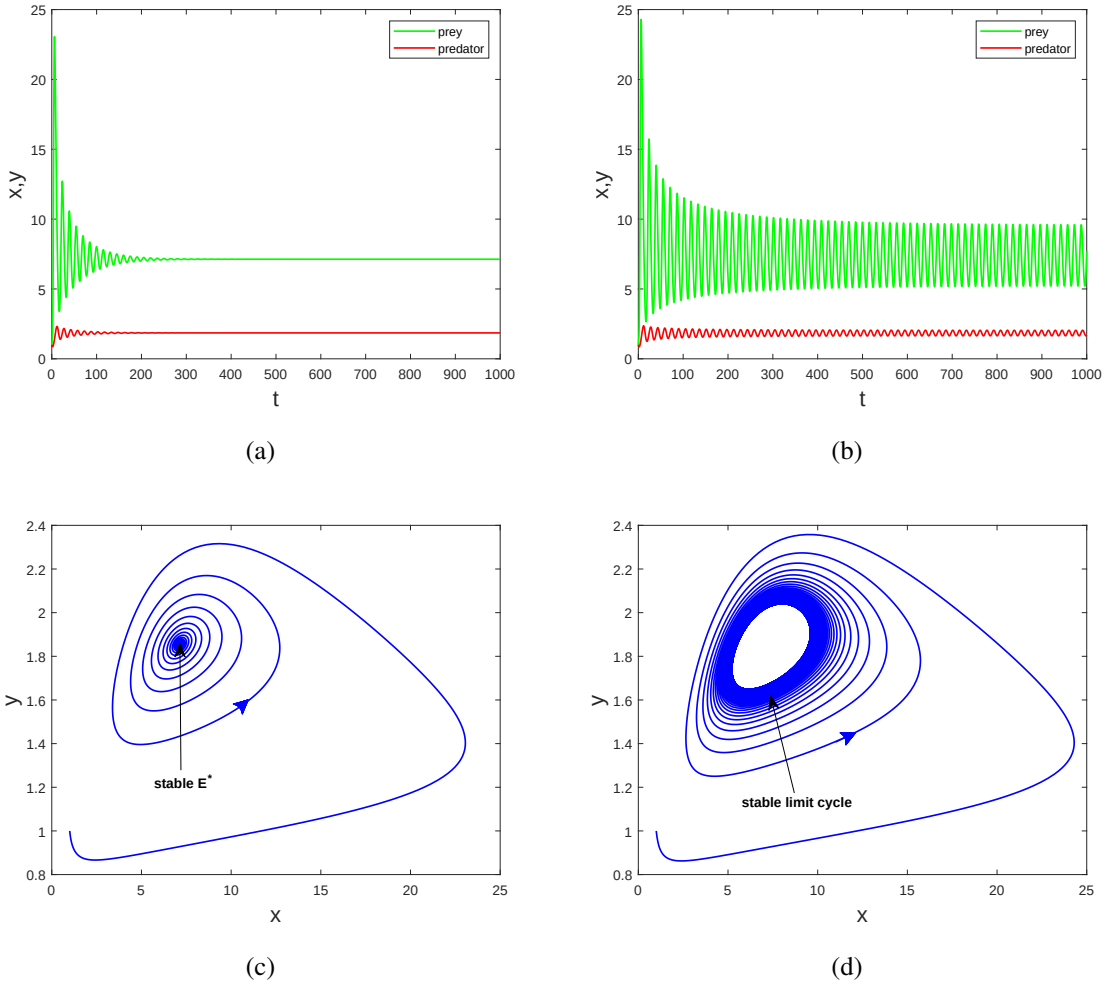

Fig. 3.12: When $\tau_1 = 0.2 < \tau_{1_0}$ and $\tau_2 = 0$, E^* is locally asymptotically stable (a,c). At $\tau_1 = 0.52 > \tau_{1_0}$ and $\tau_2 = 0$, E^* is unstable and a stable limit cycle is born (b, d).

The effect of fear-response delay: $\tau_1 > 0,\ \tau_2 = 0$. Fig. 3.12 gives the verification of Theorem 3.4.2. This shows Hopf-bifurcation near E^* at $\tau_1 = \tau_{1_0} = 0.489907$. When the prey's fear response is immediate, i.e., $\tau_1 = 0$, the co-existence equilibrium E^* is stable. When there is a time lag, such as $\tau_1 > 0$, E^* stays stable until τ_1 reaches τ_{1_0}. At this point, E^* loses its stability, and a stable limit cycle is born by means of a supercritical Hopf-bifurcation. This phenomenon is better demonstrated by the bifurcation diagram in Fig. 3.13. The colored closed trajectories shown here are the stable limit cycles.

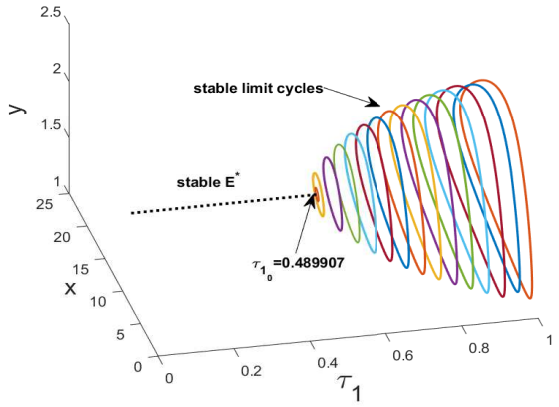

Fig. 3.13: Bifurcation diagram showing the effect of fear response delay on E^*.

How does the fear-response delay affect the system's bi-stability (shown in Fig. 3.9)? To find the answer to this question, we analyze the system in the presence of fear-response delay for parametric values similar to Fig. 3.9. Bi-stability is a phenomenon that relies on the initial condition. At $\tau_1 = 4$, the system is bi-stable between $E_1(0, 9.52)$ and $E^*(16.6898, 13.0248)$. If we start any trajectory inside the cyan region, it eventually converges to the co-existence equilibrium (see the yellow spiral). This closed area denotes the set of initial values for which the trajectory converges to E^*, while any trajectory starting outside of it goes to E_1 (see the green curve). The boundary of this region (black curve) forms the unstable limit cycle (see Fig. 3.14 (a)). On increasing the value of τ_1, the system undergoes a subcritical Hopf-bifurcation at $\tau_1 = \tau_1^{(1)} = 6.5576641808$ and becomes unstable about E^*. Fig. 3.14 (b) depicts instability of E^* and stability of E_1 at $\tau_1 = 7.1 > \tau_1^{(1)}$. In this case, the amplitude of the oscillations about E^* increases and becomes so high that it touches the stable manifold of E_1, resulting in almost everywhere stability of prey-free equilibrium. On further increasing τ_1, the system regains its stability via another subcritical Hopf-bifurcation at $\tau_1 = \tau_1^{(2)} = 23.30867546$, and an unstable limit cycle enclosing stable E^* is generated. Fig. 3.14 (c) illustrates this behavior at $\tau_1 = 30 > \tau_1^{(2)}$. However, the system remains no longer stable (via another subcritical Hopf-bifurcation) when the fear-response delay crosses another critical value $\tau_1 = \tau_1^{(3)} = 33.56175777054$. Fig.

3.14 (d) at $\tau_1 = 35 > \tau_1^{(3)}$ has the same explanation as Fig. 3.14 (b). In all these cases, the prey-free equilibrium E_1 is always stable. The range of τ_1 for the system to be bi-stable between E^* and E_1: $[0, \tau_1^{(1)}) \cup (\tau_1^{(2)}, \tau_1^{(3)})$. This multiple switching of stability with respect to the fear-response delay can be better explained through the bifurcation diagram plotted in Fig. 3.15. The phenomenon of bi-stability between E^* and E_1 remains unaffected by τ_1 until it reaches the first critical value, i.e., $\tau_1^{(1)}$. In fact, for a lower value of τ_1, E^* is stable for a broader range of y. E^* switches stability thrice via subcritical Hopf-bifurcation at $\tau_1^{(1)}$, $\tau_1^{(2)}$, and $\tau_1^{(3)}$.

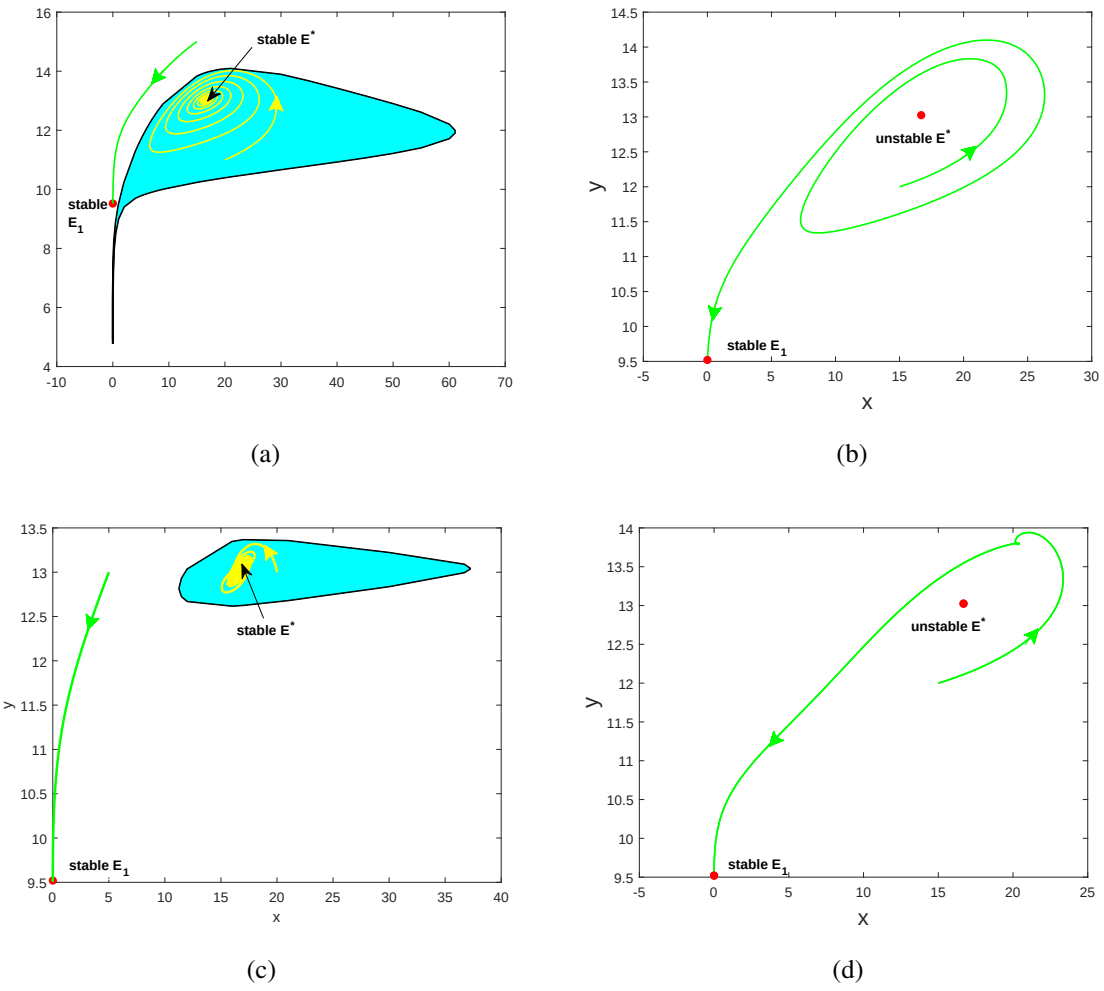

Fig. 3.14: Phase portrait at (a)$\tau_1 = 4 < \tau_1^{(1)}$, (b)$\tau_1^{(1)} < \tau_1 = 7.1 < \tau_1^{(2)}$, (c)$\tau_1^{(2)} < \tau_1 = 30 < \tau_1^{(3)}$ and (d)$\tau_1 = 35 > \tau_1^{(3)}$. Parametric values are same as chosen in Fig. 3.9.

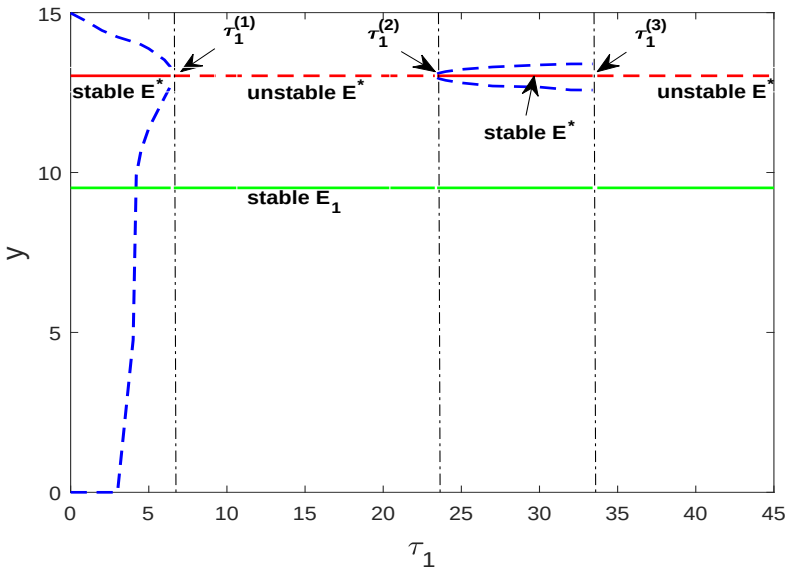

Fig. 3.15: Bifurcation diagram for y showing subcritical Hopf-bifurcation with respect to τ_1, other parameters are the same as chosen in Fig. 3.9 .

The first two critical values are obtained from the formula in Theorem 3.4.2 corresponding to $\omega_2^{(1)} = 0.23267529$ and $\omega_2^{(2)} = 0.11304208$. $\tau_1^{(3)}$ is determined from the numerical simulation. The solid red and green lines represent the stability of E^* and E_1, respectively. The blue and red dashed line or curve shows instability (see Fig. 3.15).

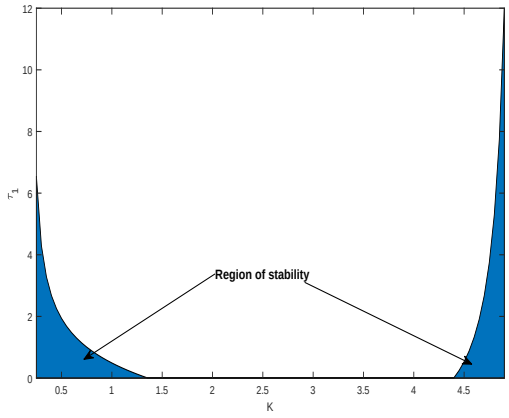

Fig. 3.16: Stability region for the system (3.2) in $K\tau_1-$ plane, other parameters are same as in (3.33).

Since the system shows Hopf-bifurcation regarding K and τ_1, we plotted Fig. 3.16. The values of K for which the system is stable around E^* are taken on the abscissa. For each value of such K, one can obtain a unique value of τ_1 at which the system starts showing oscillatory

behavior. This divides the $K\tau_1-$ plane into two different regions. E^* is locally asymptotically stable in the blue region, and in the white region, it is unstable and periodic solutions occur.

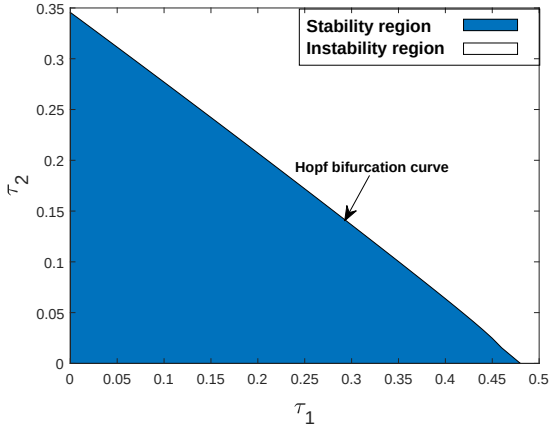

Fig. 3.17: Region of stability and instability in $\tau_1\tau_2-$plane.

Integrated effect of fear-response delay and gestation delay: $\tau_1 > 0,\ \tau_2 > 0$**.** For each value of τ_1 in its stable range $[0, \tau_{1_0})$, a unique value of τ_2 in its stable range $[0, \tau'_{2_0})$ is obtained at which the system switches its stability via Hopf-bifurcation. Below this point, the system is stable around positive equilibrium E^*, and at this point, it becomes unstable with born of a stable limit cycle. The collection of all such points forms the Hopf-bifurcation curve, as shown in Fig. 3.17.

Taking $\tau_1 = 0.3 \in (0, \tau_{1_0})$, we obtain a critical value of gestation delay at which the Hopf-bifurcation can occur. On substituting $i = 0$ in (3.28), we get $\tau'_{2_0} = 0.13631786$. The transversality condition also holds, viz.

$$\left.\frac{d(Re\lambda)}{d\tau_2}\right|_{\tau_2=\tau'_{2_0}} = (1.2393)10^{-4} \neq 0.$$

In the presence of fear-response delay, Fig. 3.18 (a) and (c) display the stability of positive equilibrium E^* when the value of τ_2 is less than its critical value τ'_{2_0}, and Fig. 3.18 (b) and (d) presents the stable limit cycle surrounding unstable E^* when $\tau_2 > \tau'_{2_0}$. All of these aspects verify Theorem 3.4.3. Hence, the system (3.2) experiences a Hopf-bifurcation in the presence of both delays.

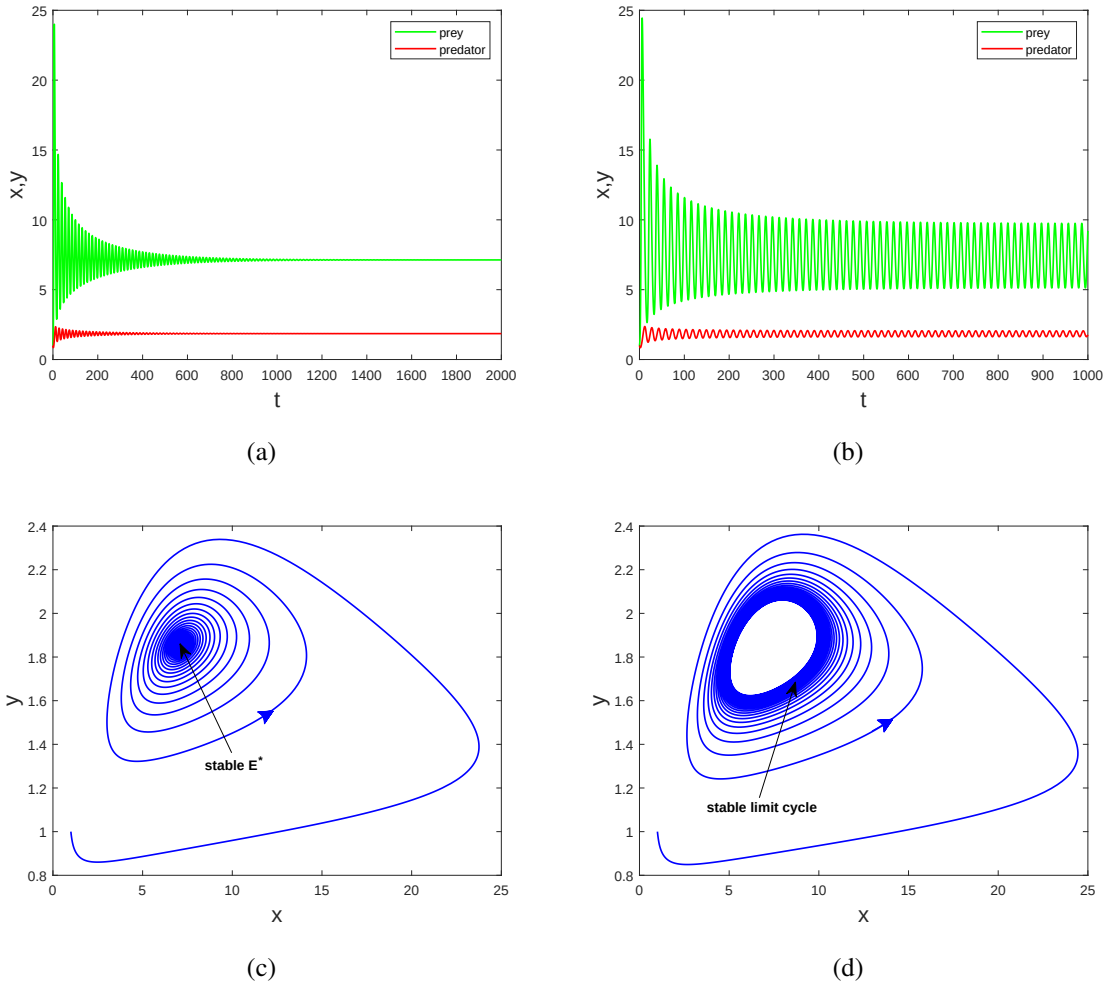

Fig. 3.18: Fixing $\tau_1 = 0.3 \in (0, \tau_{1_0})$ we obtained $\tau'_{2_0} = 0.13631786$ from (3.28).When $\tau_2 = 0.09 < \tau'_{2_0}$, E^* is locally asymptotically stable (a,c). At $\tau_2 = 0.16 > \tau'_{2_0}$ E^* is unstable and it is surrounded by a stable limit cycle (b,d).

3.6 Discussion and conclusion

In this article, we have studied the Leslie-Gower prey-predator model, assuming predators can consume prey as well as the constant additional food provided, according to their choice. The impact of prey's fear of being victimized is also considered. For prey conservation, some are protected, and hence the concept of refuge is taken into consideration. We have also analyzed this system in the presence of gestation delay and fear response delay. As per our knowledge, no literature shows dynamics for a prey-predator model with all these effects.

In the non-delayed model, we observed that when species are present initially, they will sustain for all time if the birth rate of prey is good enough. The system exhibits four equilibria: trivial equilibrium $E_0(0,0)$, prey-free equilibrium $E_1(0, \frac{(1-q)\alpha_A K_A}{\beta})$, predator-free equilibrium

$E_2(\frac{r-r_0}{r_1},0)$ and interior equilibrium $E^*(x^*,y^*)$. E_0 and E_2 are always unstable. Prey-free equilibrium is stable only when the birth rate of prey does not exceed a particular value. The stability of this equilibrium decides the number of positive steady-states. The instability of E_1 guarantees the existence of a unique positive equilibrium and vice versa. When E_1 is stable, the system acquires either two positive equilibria or none. When both species do not co-exist, the prey will become extinct, and the predator will survive, resulting in the global stability of E_1 (see Fig. 3.8). The stability of E^* can be achieved under a necessary and sufficient condition (3.8). Furthermore, we discussed the possibility of Hopf-bifurcation and transcritical bifurcation.

Many researchers have shown that cost of fear can alter the stability of the system [76, 127]. Therefore it is essential to investigate our model concerning the fear parameter K. We obtained fascinating results with respect to it. The system shows multiple Hopf-bifurcations and a transcritical bifurcation on varying K. In the absence of fear, both species converge to their positive steady-state. This behavior is unaltered until the fear reaches a certain level. At this level, both species start oscillating about the positive equilibrium. Taking K in a specific range can maintain the stability of the system. When prey individuals are too afraid, they may forage less, eventually leading to extinction. Although increasing fear reduces the predator density, they never go extinct (see Fig. 3.3). This result agrees with the recent findings demonstrated by Mishra and Upadhyay [128]. They remarked that the fear of wolf spiders reduces the density of insect pests and helps the plant ecosystem, strengthening the role of wolf spiders as biocontrol agents. In our system, it has been observed that extra food provided to the predator plays a significant role in governing the dynamics of the system.

Onana *et al.* [11] concluded that when predators' preference rate increases, they decline. On the other hand, our findings show that the increasing preference rate of predators results in their increment. However, when predators prefer prey more, they decline. Possibly, this diminution in predators is the consequence of the reduction in prey population (due to the lack of their favorite food) (refer to Table 3.3). Since the system shows extensive fear parameter and preference rate results, we divided the $qK-$ plane into various regions based on the stability of E^* and E_1. By looking at Fig. 3.7, one can determine the value of q and K for which the system attains Hopf-bifurcation and transcritical bifurcation.

The purpose of introducing refuge to prey is to control the biological imbalance. We obtained a result in favor of it viz. reserving prey up to a certain level can enhance both the species. It is also noted that predators never go extinct even when the prey refuge is strong. The presence of extra food could be the reason for the survival of predators. A study by Ghosh *et al.* [110] reveals that both species co-exist at the low value of prey refuge, but predators extinct at strong prey refuge.

The amount of energy obtained from additional food given to the predator can have a massive impact on the dynamics of the system. The system shows local as well as global dynamics with respect to α_A. As predators get more energy from additional food, they can consume more prey. The decrease in prey may lead to their extinction. As shown in Fig. 3.6, at a high value of α_A, the prey population extinct, and the predator population survives via a homoclinic global bifurcation. Prasad *et al.* [111] observed that a large quantity of additional food with high quality to predators could lead to prey eradication. Also, when both populations co-exist and the system is oscillatory, reducing the value of α_A can stabilize the system via a supercritical Hopf-bifurcation.

The system without delay exhibits bi-stability by adjusting the additional food parameter α_A. The solution trajectory converges to two different attractors depending on the initial state. One is the co-existence equilibrium, and the other is prey-free equilibrium. Their basin of attraction is separated by a curve called separatrix (see Fig. 3.9). Also, we obtained the range of α_A, for which the system stays bi-stable between E^* and E_1.

Destabilization of a prey-predator system with respect to time delay is frequent. To study the dynamics of the delayed system (3.2), we investigated analytically and numerically. We studied this model in the presence of gestation delay, fear response delay, and when both delays are present. In all these cases, we observed that a stable system undergoes a supercritical Hopf-bifurcation at a slightly high value of the delay parameter, resulting in oscillations of both species around their co-existence equilibrium. With a different set of parameters, we examined the effect of fear-response delay on the bi-stability of the non-delayed system. The delayed system experiences stability switching three times through subcritical Hopf-bifurcation as τ_1 varies. Consequently, we obtained a range of τ_1, for which the system is bi-stable between E^* and E_1. Panday *et al.* [88] analyzed that multiple switching of stability arises due to supercritical Hopf-bifurcation for fear-response delay. Moreover, they also observed a bi-stability phenomenon between interior equilibrium and limit cycle. Gestation delay introduced in the system ($\tau_1 = 0, \tau_2 > 0$) can cause at most one-time stability switching through Hopf-bifurcation. Analytically, we determined the direction of Hopf-bifurcation and stability of the bifurcated limit cycle. Since the system shows Hopf-bifurcation with respect to the fear parameter and both the delays, we mapped Hopf-bifurcation curve in $K\tau_1-$plane and $\tau_1\tau_2-$plane. To understand the bifurcation phenomenon clearly, bifurcation diagrams are constructed (see Figs. 3.11, 3.13 and 3.15).

Our findings might give a biological understanding of prey-predator relationships. This research can be expanded in the future by incorporating diffusion aspects. The impact of the reaction-diffusion effect on prey-predator interactions would be fascinating to investigate.

Chapter 4

Bifurcations and multi-stability in an eco-epidemic model with additional food [1]

4.1 Introduction

In the study of ecosystems, predator-prey interactions are a major topic of debate. Non-linear differential equations are frequently used to express the interaction between them. Complex phenomena such as bifurcation and chaos have been found in these sorts of dynamic systems [129]. When prey, or predator, or both are exposed to some infectious disease, the dynamics of the system are often altered. We direct interested readers to the pieces of literature [45, 130, 131] and relevant references therein. The study of illness in a prey-predator system falls under the umbrella of eco-epidemiology, a specialized branch of research. The fusion of ecology and epidemiology has made tremendous progress in recent decades. To examine the interaction among prey and predator, plenty of mathematical models are developed [33, 128, 132, 133, 134, 135, 136]. In 1986, Anderson and May [44] discovered that the virus in a prey-predator system is capable of changing the stability behavior. Many articles in the prior research focused solely on parasite infection in prey [137], while some addressed predator infection through prey consumption [138] or disease transmission in predators [139]. Recently, Majumder *et al.* [140] looked at the impact of ambient noise on species persistence and extinction in an eco-epidemic system. Due to the fact that infected preys are weak, the predator can hunt them easily. According to Joly and Messier [141], wolf hunts on moose are more likely to succeed if the moose is severely infested by Echinococcus granulosus. However, Saha and Samanta [84] revealed that if a predator consumes infected prey in a large amount, the predator population declines. This shows that feeding on sick prey can harm the predator. Several experimental investigations have demonstrated that parasitic mortality enhances predation susceptibility in the majority of eco-epidemic systems [142, 143]. When a predator feeds on healthy food, it

[1] A considerable part of this chapter is published in *The European Physical Journal Plus*, **137**, 118, 2022.

may do so out of fear of contracting a disease from the diseased prey. For example, dicyphus hesperus females rejected infected nymphs 96% of the time compared to non-infected nymphs 39% of the time [144].

The healthy prey may show a defense mechanism against predation. The effect of group defense on interacting populations is often presented through the Holling type IV functional response: $\frac{\omega x}{\frac{x^2}{i}+x+a}$ [48]. Calculations conducted by Yamauchi and Yamamura [145] showed that defensive evolution in prey tended to enhance harmonious cohabitation among the three species and, depending on parameter values, lowered the amplitude of population oscillations. A Leslie-Gower prey-predator model with group defense was investigated by Mishra *et al.* [81], they determined that greater prey defensive capacity leads to destabilization of the model, which can lead to periodic and chaotic fluctuations. In the presence of disease in prey, Bate and Hilker [146] hypothesized that prey performs group defense and found that the prey's sickness can aid the predator by lowering prey numbers. Banerjee *et al.* [46] performed extensive bifurcation analysis comprising local and global bifurcations for an eco-epidemic model with herd behavior of prey. Gimmelli *et al.* [147] investigated an ODE model with a sick predator interacting with the prey showing herd behavior. They observed a heteroclinic connection between saddle equilibrium points in the disease-free system.

An additional food given to the predators increases the density of predators which causes a decrease in the equilibrium level of prey species. It has been observed that additional food given to the predators may reduce or eliminate oscillations in the prey-predator system [109]. For species conservation, it is essential to eradicate the disease from a prey-predator system. Providing additional food to the predator is one of the non-chemical approaches for this aim. It is evident from the research done that extra food for the predator can control disease in the system. Sahoo's [40] numerical results indicate that in the absence of additional food, the system can not be disease-free above a threshold of infection rate but providing food can eliminate the disease even if the transmission rate is high. Plenty of eco-epidemiological models have been developed and analyzed in the last several decades with the goal of controlling the disease, and it has become a topic of great interest. Samanta *et al.* [148] observed that in the presence of alternative food, enrichment plays a significant role in reducing the diseased population. Sahoo and Poria [149] formulated a SEIP prey-predator model with disease in prey, and to control the disease in the system; they studied the consequences of providing alternative food to the predator. It does not matter whether the predator is infected or not, a predator species' population does not become extinct when they have access to an alternate food supply [45]. Providing alternative food to one of the interacting species has become an eco-friendly method with applications in a variety of disciplines, including biological conservation, bio-remediation, resource management, biological control, pest management, and so on. However, research shows that

studying predator–prey dynamics in the presence of increased food accessible to the predator alters the system's qualitative behavior. Therefore, it is important to investigate the effect of additional food on the dynamics of a prey-predator system.

The primary goal of the present article is to investigate the impact of additional food to control disease in a prey-predator system. To achieve this goal, firstly, we formulate a Leslie-Gower prey-predator initial value problem based upon some assumptions in Sect. 4.2. The biological viability of the proposed system is demonstrated in Sect. 4.3. Next, we analyze the disease-free subsystem substantially in Sect. 4.4. The results obtained in this section are helpful in determining the dynamics of the full system. Sect. 4.5 deals with equilibrium point analysis, local stability, Hopf-bifurcation, and global stability. Then, to confirm the analytical results derived, we perform numerical simulations in Sect. 4.6. Lastly, all findings of the chapter (theoretical and numerical) are summarized in Sect. 4.7.

4.2 The model with basic assumptions

In this section, we propose a formal model that depicts disease transmission in a prey-predator system based on the following assumptions:

1. In the presence of infection, the prey population is divided into two basic compartments: susceptible prey $S(t)$ and infected prey $I(t)$, with the predator's density represented by $P(t)$ at any time t.

2. Only susceptible prey can compete for the resources (limited). As a result, their growth is considered logistic growth. Infected prey, on the other hand, is supposed to be unable to reproduce. Therefore, their population growth is solely related to the infection of susceptible victims. The transmission among susceptible and infected classes obeys the mass-action law [133]. Nevertheless, the prey cannot transmit this disease to the predator in any case [150].

3. The predator cannot distinguish between healthy and infected prey, and thus predator utilizes healthy as well as infected prey, which is reasonably significant [84].

4. Susceptible preys are healthy and can defend themselves. Hence Holling type IV functional response is taken into consideration. In comparison, infected preys are not strong enough to defend themselves against predation. Therefore, we assume that the predator consumes infected prey employing Holling type II functional response.

5. The residual loss in infected prey is either due to its natural death (includes death due to infection also) or by predation, which means that the infected prey is not immune to the disease.

6. We presume that the predator is fed extra food of constant density K_A and gains energy in the form of biomass α_A. According to the proportions given by the parameter q, the predator consumes prey and the supplementary meal. Therefore, their development is reliant on both sources, and this relationship follows the modified Leslie-Gower scheme [11].

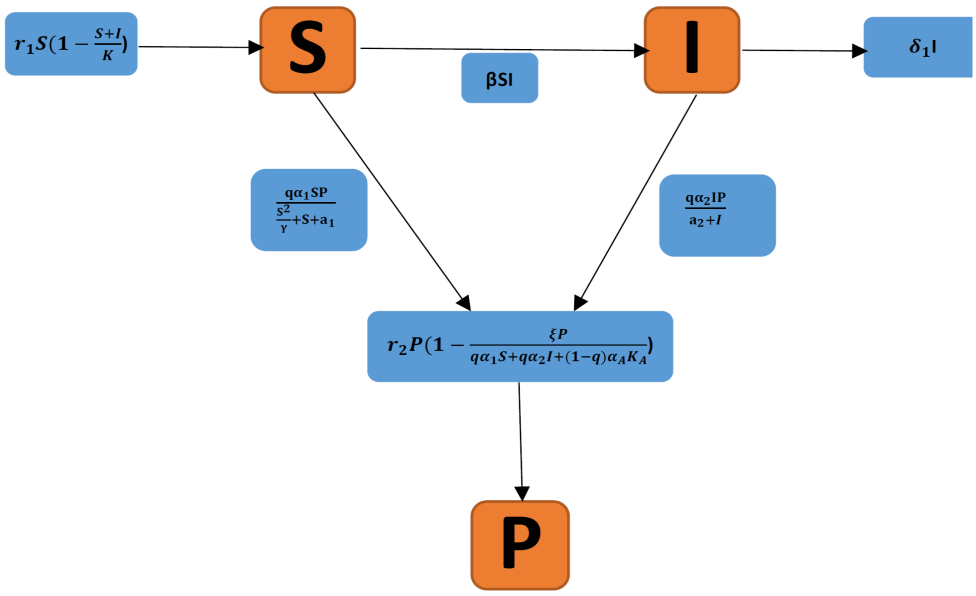

Fig. 4.1: Schematic flow chart showing model (4.1) formulation.

In light of the preceding assumptions, the interaction between susceptible prey, infected prey, and predators feeding on them is represented as

$$\begin{aligned}
\frac{dS}{dt} &= r_1 S\left(1-\frac{S+I}{K}\right) - \beta SI - \frac{q\alpha_1 SP}{\frac{S^2}{\gamma}+S+a_1} = f_1(S,I,P),\\
\frac{dI}{dt} &= \beta SI - \delta_1 I - \frac{q\alpha_2 IP}{a_2+I} = f_2(S,I,P),\\
\frac{dP}{dt} &= r_2 P\left(1-\frac{\xi P}{q\alpha_1 S+q\alpha_2 I+(1-q)\alpha_A K_A}\right) = f_3(S,I,P),
\end{aligned} \tag{4.1}$$

$$S(0)\geq 0,\ I(0)\geq 0\ P(0)\geq 0.$$

The biological meaning and dimension of parameters and variables involved in system (4.1) are listed in Table 4.1, and the formulation of this model is illustrated as a schematic view in Fig.

4.1. The proposed system (4.1) is composed of two subsystems: *SP* model (4.2) and *SI* model (4.3).

(i) In the absence of disease, i.e., $I = 0$, model (4.1) takes the following form:

$$\begin{aligned} \frac{dS}{dt} &= r_1 S\left(1-\frac{S}{K}\right) - \frac{q\alpha_1 SP}{\frac{S^2}{\gamma}+S+a_1} = h_1(S,P), \\ \frac{dP}{dt} &= r_2 P\left(1-\frac{\xi P}{q\alpha_1 S+(1-q)\alpha_A K_A}\right) = h_2(S,P), \end{aligned} \tag{4.2}$$

Investigating (4.2) would be very valuable in studying the intricate dynamics of (4.1). Model (4.2) is an interesting problem to study as it has not been addressed in the current literature. We will analyze this system in Sect. 4.4.

(ii) In the absence of predation, i.e., $P = 0$, model (4.1) is transformed into an epidemic model, given by:

$$\begin{aligned} \frac{dS}{dt} &= r_1 S\left(1-\frac{S+I}{K}\right) - \beta SI, \\ \frac{dI}{dt} &= \beta SI - \delta_1 I. \end{aligned} \tag{4.3}$$

Sahoo [40] thoroughly investigated this model (4.3).

Table 4.1: Biological explication of variables/parameters used in model (4.1)

Variables/Parameters	Biological explication	Dimension
S	Susceptible prey density	Biomass
I	Infected prey density	Biomass
P	Predator density	Biomass
r_1	Intrinsic growth rate of susceptible prey	Time^{-1}
K	Environmental carrying capacity of prey	Biomass
β	Rate of disease transmission at which the susceptible prey gets infected	$\text{Biomass}^{-1}\ \text{Time}^{-1}$
α_1	Maximum rate of per capita removal of susceptible prey due to predation	Time^{-1}
a_1	Half saturation constant for susceptible prey	Biomass
γ	Measure of predator's immunity from prey	Biomass
δ_1	Natural death rate of infected prey + death rate due to infection	Time^{-1}
q	Preference rate of predator for food and $q \in (0,1)$	Dimensionless
α_2	Maximum rate of per capita removal of infected prey due to predation	Time^{-1}
a_2	Half saturation constant for infected prey	Biomass
r_2	Intrinsic growth rate of predator	Time^{-1}
α_A	It measures the amount of energy of the additional food assimilate into the predator's energy	Time^{-1}
K_A	Additional food of constant density A	Biomass
ξ	Maximum rate of per capita removal of predator species	Time^{-1}

4.3 Positivity and boundedness of the proposed system

The other form of model (4.1) is

$$\frac{dS}{dt} = S\phi_1(S,I,P),\ \ \frac{dI}{dt} = I\phi_2(S,I,P),\ \ \frac{dP}{dt} = P\phi_3(S,I,P),$$

where

$$\phi_1(S,I,P) = r_1\left(1-\frac{S+I}{K}\right) - \beta I - \frac{q\alpha_1 P}{\frac{S^2}{\gamma}+S+a_1},\ \phi_2(S,I,P) = \beta S - \delta_1 - \frac{q\alpha_2 P}{a_2+I},$$

$$\phi_3(S,I,P) = r_2\left(1-\frac{\xi P}{q\alpha_1 S + q\alpha_2 I + (1-q)\alpha_A K_A}\right).$$

It follows that

$$S(t) = S(0)e^{\int_0^t \phi_1(S(\theta),I(\theta),P(\theta))d\theta} \geq 0,$$

$$I(t) = I(0)e^{\int_0^t \phi_2(S(\theta),I(\theta),P(\theta))d\theta} \geq 0,$$

$$P(t) = P(0)e^{\int_0^t \phi_3(S(\theta),I(\theta),P(\theta))d\theta} \geq 0.$$

Thus, all solutions $(S(t),I(t),P(t))$ with the positive initial condition remain positive throughout the region R^3_+.

Due to a scarcity of resources, nature does not allow any species to expand abruptly. Therefore, it is essential to check the boundedness of the formulated model.

Theorem 4.3.1. *All solutions of system (4.1) starting in R^3_+ are confined in the region $\Omega = \{(S,I,P) \in R^3_+ :\ 0 \leq S \leq K,\ 0 \leq S+I \leq \frac{2r_1K}{\delta_*},\ 0 \leq P \leq \mu\}$, where δ_* and μ are defined in the proof of this theorem.*

Proof. From the first equation of the model

$$\frac{dS}{dt} \leq r_1 S\left(1-\frac{S}{K}\right),$$

which implies

$$\limsup_{t\to\infty} S(t) \leq K.$$

Combining first and second equations of the model gives

$$\begin{aligned}\frac{dS}{dt}+\frac{dI}{dt} &\leq 2r_1S - r_1S - \delta_1 I,\\ &\leq 2r_1K - \delta_*(S+I),\end{aligned}$$

where $\delta_* = min\{\delta_1, r_1\}$. This implies

$$\limsup_{t\to\infty}(S(t)+I(t)) \leq \frac{2r_1K}{\delta_*}.$$

Now, to show the boundedness of predator population, we can write

$$\frac{dP}{dt} \leq r_2P\left(1-\frac{\xi P}{(qK(\alpha_1+\frac{2\alpha_2r_1}{\delta_*})+(1-q)\alpha_AK_A)}\right),$$

Using differential inequality theory, we arrive at

$$\limsup_{t\to\infty}P(t) \leq \frac{1}{\xi}\left(qK(\alpha_1+\frac{2\alpha_2r_1}{\delta_*})+(1-q)\alpha_AK_A\right) = \mu.$$

Therefore, we can conclude that all solutions of system (4.1) remain attracted in the region Ω. □

When a population is present at the beginning, it has the potential to live under certain conditions. The following theorem determines these requirements.

Theorem 4.3.2. *Assume that the following inequalities are true:*

(i) $\frac{2(r_1+\beta K)}{\delta_*}+\frac{q\alpha_1\mu}{a_1r_1} < 1,$

(ii) $\frac{1}{S_a}(\frac{q\alpha_1K\mu}{a_1r_1}+\frac{2\delta_1K}{\delta_*}+\frac{2q\alpha_2K\mu}{a_2\delta_*}) < 1,$
then the system (4.1) persists uniformly.

Proof. If each component population survives, the system is considered to perpetuate. Analytically, the system is said to be persistent if there exists $M_a > 0$, $M_b > 0$ such that

$$M_a \leq \liminf X(t) \leq \limsup X(t) \leq M_b.$$

In order to prove the above condition, we manipulate the first equation of the model as

$$\frac{dS}{dt} \geq \left(r_1-(\frac{r_1}{K}+\beta)\frac{2r_1K}{\delta_*}-\frac{q\alpha_1\mu}{a_1}\right)S-\frac{r_1S^2}{K}$$

which implies

$$\liminf_{t\to\infty}S(t) \geq \left(r_1-(\frac{r_1}{K}+\beta)\frac{2r_1K}{\delta_*}-\frac{q\alpha_1\mu}{a_1}\right)\frac{K}{r_1} =: S_a.$$

Now, from first two equations of model (4.1), we can write

$$\frac{d(S+I)}{dt}+r_1(S+I) \geq r_1S_a-\frac{q\alpha_1K\mu}{a_1}-\frac{2\delta_1r_1K}{\delta_*}-\frac{2qr_1\alpha_2K\mu}{a_2\delta_*}.$$

Therefore,

$$\liminf_{t\to\infty}(S+I)(t) \geq S_a - \frac{q\alpha_1 K\mu}{a_1 r_1} - \frac{2\delta_1 K}{\delta_*} - \frac{2q\alpha_2 K\mu}{a_2\delta_*} =: I_a.$$

From the third equation of the model we directly obtain

$$\liminf_{t\to\infty} P(t) \geq \frac{(1-q)\alpha_A K_A}{\xi} = P_a.$$

Let $M_a = min\{S_a, I_a, P_a\}$, $M_b = max\{K, \frac{2r_1K}{\delta_*}, \mu\}$ and $X(t) = (S(t), I(t), P(t))'$. If both conditions mentioned in the theorem are satisfied, then it follows that

$$M_a \leq \liminf X(t) \leq \limsup X(t) \leq M_b.$$

As a result of this, the theorem is established. □

4.4 Dynamics of subsystem (4.2)

The boundedness of system (4.1) results into the boundedness of subsystem (4.2). The possible four steady-states of system (4.2) are: $(i)E_0(0,0)$, $(ii)E_1(K,0)$, $(iii)E_2(0, \frac{(1-q)\alpha_A K_A}{\xi})$, $(iv)E_*(S_*, P_*)$, here (S_*, P_*) is the unique positive solution of following equations:

$$r_1\left(1-\frac{S}{K}\right) - \frac{q\alpha_1 P}{\frac{S^2}{\gamma}+S+a_1} = 0, \tag{4.4}$$

$$P = \frac{1}{\xi}(q\alpha_1 S + (1-q)\alpha_A K_A). \tag{4.5}$$

Solving Eqs. (4.4) and (4.5) we obtain

$$B_1 S^3 + B_3 S^2 + B_5 S + B_7 = 0, \tag{4.6}$$

where $B_1 = r_1\xi > 0$, $B_3 = r_1\xi(\gamma - K)$, $B_5 = -r_1\gamma\xi K + r_1 a_1\gamma\xi + q^2\alpha_1^2\gamma K$, $B_7 = q\alpha_1\gamma K(1-q)\alpha_A K_A - r_1 a_1\gamma\xi K$.

The possible cases for the uniqueness of E_* are following:

	B_1	B_3	B_5	B_7
(i)	+	+	+	-
(ii)	+	+	-	-
(iii)	+	-	-	-
(iv)	+	-	+	-

- In cases (i), (ii) and (iii), using the Descarte's rule, the existence of unique positive root of Eq. (4.6) is guaranteed.
- In case (iv), by Descarte's rule of sign Eq. (4.6) may have three positive roots or one positive root and two complex roots. Moreover, if the discriminant of the cubic equation, i.e., $\Delta = B_3^2B_5^2 - 4B_1B_5^3 - 4B_3^3B_7 - 27B_1^2B_7^2 + 18B_1B_3B_5B_7$ is negative, then it assures that Eq. (4.6) has exactly one positive root. This provides us the next theorem.

Theorem 4.4.1. (a) *Let any one of the following holds:*

(i) $B_3 > 0$, $B_5 > 0$ *and* $B_7 < 0$,

(ii) $B_3 > 0$, $B_5 < 0$ *and* $B_7 < 0$,

(iii) $B_3 < 0$, $B_5 < 0$ *and* $B_7 < 0$.

Then subsystem (4.2) has a unique positive equilibrium $E_*(S_*, P_*)$.
(b) *Let the following inequalities hold:* $B_3 < 0$, $B_5 > 0$, $B_7 < 0$ *and* $\Delta < 0$. *Then* $E_*(S_*, P_*)$ *exists uniquely.*

Remark. $B_7 < 0$ is the necessary condition for the uniqueness of $E_*(S_*, P_*)$.

Local stability: Based on the eigenvalue theory, the local stability behavior of any equilibrium is determined. Table 4.2 describes the boundary equilibria and their local stability behavior of subsystem (4.2).

Table 4.2: The local stability behavior of boundary equilibria of subsystem (4.2)

Equilibrium point	Stability behavior
$(0,0)$	Unconditionally unstable
$(K,0)$	Always saddle
$(0, \frac{(1-q)\alpha_A K_A}{\xi})$	Asymptotically stable if $r_1 < \frac{q\alpha_1(1-q)\alpha_A K_A}{a_1\xi}$; saddle if $r_1 > \frac{q\alpha_1(1-q)\alpha_A K_A}{a_1\xi}$

For the stability behavior of $E_*(S_*, P_*)$, we can state the following theorem.

Theorem 4.4.2. $E_*(S_*, P_*)$ *is locally asymptotically stable if and only if* $\Theta_1 > 0$ *and* $\Theta_2 > 0$, *where* Θ_1 *and* Θ_2 *are defined in the proof of this theorem.*

Proof. The variational matrix for (4.2) about $E_*(S_*, P_*)$ is

$$M|_{E_*} = \begin{pmatrix} -\frac{r_1 S_*}{K} + \frac{q\alpha_1 S_* P_* (\frac{2S_*}{\gamma}+1)}{(\frac{S_*^2}{\gamma}+S_*+a_1)^2} & -\frac{q\alpha_1 S_*}{\frac{S_*^2}{\gamma}+S_*+a_1} \\ \frac{r_2\xi P_*^2 q\alpha_1}{(q\alpha_1 S_*+(1-q)\alpha_A K_A)^2} & -\frac{r_2\xi P_*}{q\alpha_1 S_*+(1-q)\alpha_A K_A}. \end{pmatrix}.$$

The characteristic equation corresponding to above matrix is

$$\lambda^2 + \Theta_1\lambda + \Theta_2 = 0,$$

where $\Theta_1 = -tr(M|_{E_*})$ and $\Theta_2 = det(M|_{E_*})$.
According to Routh-Hurwitz criteria, $E_*(S_*, P_*)$ is locally asymptotically stable if and only if $\Theta_1 > 0$ and $\Theta_2 > 0$. □

Remark. If $r_1 > \frac{Kq\alpha_1 P_*(\frac{2S_*}{\gamma}+1)}{(\frac{S_*}{\gamma}^2+S_*+a_1)^2}$, the stability of $E_*(S_*, P_*)$ is confirmed.
Now let us discuss the global stability of subsystem (4.2) in the next theorem.

Theorem 4.4.3. *Let $E_*(S_*, P_*)$ exists uniquely, and it will be the global attractor if $\nabla_1 < 0$, where ∇_1 is defined in the proof of this theorem.*

Proof. The uniqueness of $E_*(S_*, P_*)$ yields $r_1 > \frac{q\alpha_1(1-q)\alpha_A K_A}{a_1\xi}$ which implies that the prey-free equilibrium is unstable. Now, the possible attractors in the positive quadrant of the $SP-$ plane are E_* and the limit cycle. Let us consider a continuously differentiable function in R^2_+ as $H_1 = \frac{(\frac{S^2}{\gamma}+S+a_1)}{SP}$.
Now,

$$\nabla_1 = \frac{\partial}{\partial S}(h_1 H_1) + \frac{\partial}{\partial P}(h_2 H_1),$$

which gives

$$\nabla_1 = -\frac{r_1}{P}\left[\frac{3S^2}{K\gamma} + 2S(\frac{1}{K} - \frac{1}{\gamma}) + \frac{a_1}{K}\right] - \frac{r_2\xi(\frac{S^2}{\gamma}+S+a_1)}{S(q\alpha_1 S + (1-q)\alpha_A K_A)}.$$

If $\nabla_1 < 0$, then by the Bendixson-Dulac's criteria, the system (4.2) can not have a limit cycle. Therefore, in this case, $E_*(S_*, P_*)$ will be the global attractor. □

Remark. If $\gamma > K$, then ∇_1 is always negative.

4.5 Dynamics of the proposed system (4.1)

The equilibrium points of system (4.1) are $E_0(0,0,0)$, $E_S(K,0,0)$, $E_P(0,0,\frac{(1-q)\alpha_A K_A}{\xi})$, $E_{SI}(\frac{\delta_1}{\beta}, \frac{r_1(\beta K-\delta_1)}{\beta(r_1+\beta K)}, 0)$, $E_{SP}(S_{SP}, 0, P_{SP})$ and $E^*(S^*, I^*, P^*)$. The existence of $E_{SP}(S_{SP}, 0, P_{SP})$ is same as discussed in the previous section. The axial equilibria: E_S and E_P exist unconditionally. E_{SI} exists if $K > \frac{\delta_1}{\beta}$, and the disease in this case can be eradicated if $K < \frac{\delta_1}{\beta}$.

Existence of $E^*(S^*,I^*,P^*)$: Here (S^*, I^*, P^*) is the unique positive solution of the following algebraic equations:

$$r_1\left(1-\frac{S+I}{K}\right)-\beta I-\frac{q\alpha_1 P}{\frac{S^2}{\gamma}+S+a_1}=0, \tag{4.7}$$

$$\beta S-\delta_1-\frac{q\alpha_2 P}{a_2+I}=0, \tag{4.8}$$

$$r_2\left(1-\frac{\xi P}{q\alpha_1 S+q\alpha_2 I+(1-q)\alpha_A K_A}\right)=0. \tag{4.9}$$

Eq. (4.9) can be rewritten as

$$P=\frac{1}{\xi}(q\alpha_1 S+q\alpha_2 I+(1-q)\alpha_A K_A).$$

Substituting this value in (4.7) and (4.8), we obtain

$$A_1S+A_2I+A_3SI+A_4=0=\psi_1(S,I), \tag{4.10}$$

$$B_1S^3+B_2S^2I+B_3S^2+B_4SI+B_5S+B_6I+B_7=0=\psi_2(S,I), \tag{4.11}$$

where
$A_1=q^2\alpha_1\alpha_2-\beta a_2\xi, A_2=q^2\alpha_2^2+\xi\delta_1>0, A_3=-\xi\beta<0, A_4=\xi\delta_1 a_2+q(1-q)\alpha_2\alpha_A K_A>0,$
$B_1=r_1\xi>0,\ B_2=r_1\xi+\beta K\xi>0,\ B_3=r_1\xi(\gamma-K),\ B_4=r_1\gamma\xi+\beta\gamma\xi K>0,$
$B_5=-r_1\gamma\xi K+r_1a_1\gamma\xi+q^2\alpha_1^2\gamma K,\ B_6=r_1a_1\gamma\xi+\beta a_1\gamma\xi K+q^2\alpha_1\alpha_2\gamma K>0,$
$B_7=q\alpha_1\gamma K(1-q)\alpha_A K_A-r_1a_1\gamma\xi K.$
The curve ψ_1 passes through $(0,\bar{I_1})$ and $(\bar{S_1},0)$, where $\bar{I_1}=-\frac{A_4}{A_2}<0$ and $\bar{S_1}=-\frac{A_4}{A_1}>0$ (if $A_1<0$), and we also assume that its slope

$$\frac{dI}{dS}=-\frac{A_1+IA_3}{A_2+SA_3}$$

is positive. The curve ψ_2 passes through $(0,\bar{I_2})$ and $(\bar{S_2},0)$, where $\bar{I_2}=-\frac{B_7}{B_6}>0$, if $B_7<0$ and let $\bar{S_2}$ be the unique positive root of the equation:

$$B_1S^3+B_3S^2+B_5S+B_7=0.$$

The slope of ψ_2

$$\frac{dI}{dS}=-\frac{3B_1S^2+2SIB_2+2SB_3+B_4I+B_5}{B_2S^2+B_4S+B_6}$$

is assumed to be negative. If $\bar{S_1}<\bar{S_2}$, then curves ψ_1 and ψ_2 intersect at a unique positive point (S^*,I^*). Substituting it in (4.9) yields a unique positive equilibrium $E^*(S^*,I^*,P^*)$. All

the sufficient conditions for existence of E^* are mentioned in the theorem below.

Theorem 4.5.1. *The interior equilibrium $E^*(S^*,I^*,P^*)$ of the proposed system (4.1) exists uniquely under the following conditions:* (i) $A_1 < 0$,
(ii) $\frac{A_1+IA_3}{A_2+SA_3} < 0$,
(iii) $3B_1S^2 + 2SIB_2 + 2SB_3 + B_4I + B_5 > 0$,
(iv) $B_7 < 0$,
(v) $\bar{S_1} < \bar{S_2}$.

To verify Theorem 4.5.1, we consider a set of parameters as
$K = 5,\ r_1 = 2.5,\ \alpha_1 = 0.1539,\ \alpha_2 = 0.04,\ a_1 = 0.1,\ a_2 = 0.1,\ \gamma = 0.1,\ r_2 = 2,\ K_A = 10,\ q = 0.6,\ \delta_1 = 0.05,\ \beta = 0.3,\ \xi = 1.$

For this set, all conditions in Theorem 4.5.1 are fulfilled viz., $(i) - 0.0919 < 0$, $(ii) - 51.2557 < 0$, $(iii) 12.1502 > 0$, $(iv) - 0.1214 < 0$ and (v) condition can be verified from Fig. 4.2. As a result, a unique interior equilibrium $E^*(S^*,I^*,P^*)$ of system (4.1) is obtained. Here P^* is determined on substituting values of S^* and I^* in Eq. (4.9). Thus, the interior equilibrium is $E^*(2.154, 1.778, 1.6644)$.

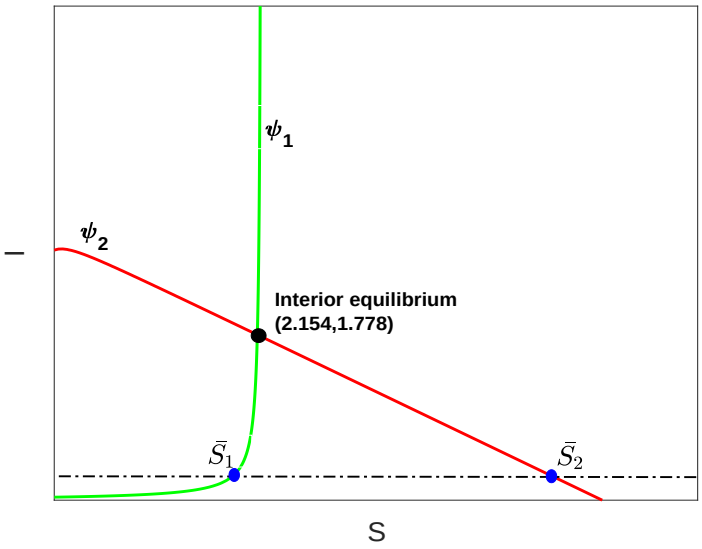

Fig. 4.2: Intersection of isoclines is a unique interior equilibrium (S^*,I^*).

4.5.1 Local stability

Local stability refers to the stability of an equilibrium point in the near vicinity. The Routh-Hurwitz criterion and the Jacobian matrix will be used to investigate this phenomenon. The

characteristics of extinction equilibrium $E_0(0,0,0)$, prey-only equilibrium $E_S(S,0,0)$ and predator-only equilibrium $E_P(0,0,\frac{(1-q)\alpha_A K_A}{\xi})$ are the same as mentioned in Table 4.2. Now let us discuss the stabilizing property of all feasible planar and interior equilibrium points of system (4.1).

Stability behavior of $E_{SI}(S_{SI},I_{SI},0)$: The variational matrix about E_{SI} is

$$M|_{E_{SI}} = \begin{pmatrix} -\frac{r_1 S_{SI}}{K} & -\frac{r_1 S_{SI}}{K} - \delta_1 & -\frac{q\alpha_1 S_{SI}}{\frac{S_{SI}^2}{\gamma}+S_{SI}+a_1} \\ \beta I_{SI} & 0 & -\frac{q\alpha_2 I_{SI}}{a_2+I_{SI}} \\ 0 & 0 & r_2 \end{pmatrix}.$$

The determinant of above matrix is $r_2\beta I_{SI}(\frac{r_1 S_{SI}}{K}+\delta_1) > 0$. For the stability of E_{SI}, determinant of $M|_{E_{SI}}$ must be negative. Hence E_{SI} is always unstable.

Stability behavior of $E_{SP}(S_{SP},0,P_{SP})$: The variational matrix about E_{SP} is

$$M|_{E_{SP}} = \begin{pmatrix} -\frac{r_1 S_{SP}}{K} + \frac{q\alpha_1 S_{SP} P_{SP}(\frac{2S_{SP}}{\gamma}+1)}{(\frac{S_{SP}^2}{\gamma}+S_{SP}+a_1)^2} & -\frac{r_1 S_{SP}}{K} - \beta S_{SP} & -\frac{q\alpha_1 S_{SP}}{\frac{S_{SP}^2}{\gamma}+S_{SP}+a_1} \\ 0 & \beta S_{SP} - \delta_1 - \frac{q\alpha_2 P_{SP}}{a_2} & 0 \\ \frac{r_2\xi P_{SP}^2 q\alpha_1}{(q\alpha_1 S_{SP}+(1-q)\alpha_A K_A)^2} & \frac{r_2\xi P_{SP}^2 q\alpha_2}{(q\alpha_1 S_{SP}+(1-q)\alpha_A K_A)^2} & -\frac{r_2\xi P_{SP}}{q\alpha_1 S_{SP}+(1-q)\alpha_A K_A} \end{pmatrix},$$

Clearly, one eigenvalue of the above matrix is $\beta S_{SP} - \delta_1 - \frac{q\alpha_2 P_{SP}}{a_2}$. The other two eigenvalues are the roots of the characteristic equation given in Theorem 4.4.2. Therefore, for stability conditions of E_{SP}, we can establish the next theorem.

Theorem 4.5.2. *E_{SP} is locally asymptotically stable if the following conditions hold true:*

(i) $\delta_1 > \beta S_{SP} - \frac{q\alpha_2 P_{SP}}{a_2}$,

(ii) $r_1 > \frac{Kq\alpha_1 P_{SP}(\frac{2S_{SP}}{\gamma}+1)}{(\frac{S_{SP}^2}{\gamma}+S_{SP}+a_1)^2}$.

Biological meaning: The disease from the considered eco-epidemic problem can be completely eradicated if the death rate of the infected prey is greater than a threshold value. Also, birth rate of susceptible prey must exceed a critical value so that the susceptible prey and the predator can survive.

Remark.

(i) E_P is stable $\Rightarrow$ E_{SP} does not exist uniquely. The contrapositive of this statement is also true.

(ii) E_{SP} is stable $\Rightarrow E_*(S_*,P_*)$ is stable. The converse of this statement is not true.

Stability behavior of $E^*(S^*,I^*,P^*)$: The variational matrix about E^* is

$$M|_{E^*} = \begin{pmatrix} m_{11} & m_{12} & m_{13} \\ m_{21} & m_{22} & m_{23} \\ m_{31} & m_{32} & m_{33} \end{pmatrix}$$

$$= \begin{pmatrix} -\frac{r_1 S^*}{K} + \frac{q\alpha_1 S^* P^* (\frac{2S^*}{\gamma}+1)}{(\frac{S^{*2}}{\gamma}+S^*+a_1)^2} & -\frac{r_1 S^*}{K} - \beta S^* & -\frac{q\alpha_1 S^*}{\frac{S^{*2}}{\gamma}+S^*+a_1} \\ \beta I^* & \frac{q\alpha_2 I^* P^*}{(a_2+I^*)^2} & -\frac{q\alpha_2 I^*}{a_2+I^*} \\ \frac{r_2 \xi P^{*2} q\alpha_1}{(q\alpha_1 S^*+q\alpha_2 I^*+(1-q)\alpha_A K_A)^2} & \frac{r_2 \xi P^{*2} q\alpha_2}{(q\alpha_1 S^*+q\alpha_2 I^*+(1-q)\alpha_A K_A)^2} & -\frac{r_2 \xi P^*}{q\alpha_1 S^*+q\alpha_2 I^*+(1-q)\alpha_A K_A} \end{pmatrix},$$

The characteristic equation corresponding to $M|_{E^*}$ is

$$\lambda^3 + D_1\lambda^2 + D_2\lambda + D_3 = 0,$$

where
$D_1 = -(m_{11}+m_{22}+m_{33})$, $D_2 = m_{11}m_{22}+m_{11}m_{33}+m_{22}m_{33}-m_{12}m_{21}-m_{13}m_{31}-m_{32}m_{23}$,
$D_3 = m_{11}m_{23}m_{32}+m_{12}m_{21}m_{33}+m_{13}m_{31}m_{22}-m_{11}m_{22}m_{33}-m_{12}m_{23}m_{31}-m_{13}m_{21}m_{32}$.
According to Routh-Hurwitz criteria, $E^*(S^*,I^*,P^*)$ is locally asymptotically stable if and only if $D_1 > 0$, $D_3 > 0$, and $D_1D_2 - D_3 > 0$. In the next theorem, we study the Hopf-bifurcation behavior of the system taking α_A as a bifurcation parameter.

Theorem 4.5.3. *The system (4.1) undergoes Hopf-bifurcation at $\alpha_A = \alpha_A^{[hf]}$ around E^* (if it exists) where $\alpha_A^{[hf]}$ is the unique positive root of the equation $D_1(\alpha_A)D_2(\alpha_A) - D_3(\alpha_A) = 0$ with $D_1(\alpha_A) > 0$, $D_2(\alpha_A) > 0$ and $D_2 \neq 1$ holds.*

Proof. The characteristic equation of the Jacobian matrix of E^* is

$$\lambda^3 + D_1(\alpha_A)\lambda^2 + D_2(\alpha_A)\lambda + D_3(\alpha_A) = 0, \tag{4.12}$$

For $\alpha_A = \alpha_A^{[hf]}$, the above characteristic equation is transformed as

$$(\lambda^2 + D_2)(\lambda + D_1) = 0,$$

which entails $\lambda_{1,2} = \pm i\sqrt{D_2}$, $\lambda_3 = -D_1$. Differentiating Eq. (4.12) with respect to α_A, we obtain

$$\frac{d\lambda}{d\alpha_A} = -\frac{D_1'\lambda^2 + D_2'\lambda + D_3'}{3\lambda^2 + 2D_1\lambda + D_2}.$$

Now,

$$\left.\frac{d\lambda}{d\alpha_A}\right|_{\lambda=i\sqrt{D_2}} = \frac{-D_1'D_2 + D_3' + iD_2'\sqrt{D_2}}{2D_2 - 2iD_1\sqrt{D_2}}.$$

$$= \frac{(-D_1'D_2^2 + D_2D_3' - D_1D_2'D_2^{3/2}) + i(D_2^2D_2' + D_1\sqrt{D_2}D_3' - D_1D_1'D_2^{3/2})}{2(D_2^2 + D_1^2D_2)},$$

which implies

$$\left.\frac{dRe(\lambda)}{d\alpha_A}\right|_{\alpha_A=\alpha_A^{[hf]}} = -\left.\frac{D_1D_2'(\sqrt{D_2}-1)}{2(D_2+D_1^2)}\right|_{\alpha_A=\alpha_A^{[hf]}} \neq 0.$$

Hence, the transversality condition, i.e., $\frac{dRe(\lambda)}{d\alpha_A}|_{\alpha_A=\alpha_A^{[hf]}} \neq 0$ holds if $D_2 \neq 1$. This brings the theorem to a close. □

Remark. With regard to any other parameter, the Hopf-bifurcation analysis will be analogous to that provided in the previous Theorem 4.5.3.

4.5.2 Global stability

In this section, global stability behavior of the unique positive equilibrium $E^*(S^*,I^*,P^*)$ is studied. We are able to find some sufficient conditions under which $E^*(S^*,I^*,P^*)$ is globally asymptotically stable.

Theorem 4.5.4. *$E^*(S^*,I^*,P^*)$ is globally asymptotically stable if the following conditions hold true:*

(i) $\frac{4r_1^2\beta^2K^2}{\delta_*^2} + (\frac{r_1}{K}+\beta)^2 < \left[\frac{r_1}{K} - \frac{(1+K+S^*)q\alpha_1P^*}{a_1(\frac{S^{*2}}{\gamma}+S^*+a_1)}\right](\delta_1 - \beta S^*)$,

(ii) $\left[\frac{r_2\xi q\alpha_2P^*}{(1-q)\alpha_AK_A(q\alpha_1S^*+q\alpha_2I^*+(1-q)\alpha_AK_A)} - \frac{q\alpha_2I^*}{a_2+I^*}\right]^2 < \frac{r_2\xi}{(qK(\alpha_1+\frac{2\alpha_2r_1}{\delta_*})+(1-q)\alpha_AK_A)}(\delta_1-\beta S^*)$,

(iii) $\left[\frac{r_2\xi q\alpha_2P^*}{(1-q)\alpha_AK_A(q\alpha_1S^*+q\alpha_2I^*+(1-q)\alpha_AK_A)} - \frac{q\alpha_1}{a_1}\right]^2 < \frac{r_2\xi}{(qK(\alpha_1+\frac{2\alpha_2r_1}{\delta_*})+(1-q)\alpha_AK_A)}\left[\frac{r_1}{K} - \frac{(1+K+S^*)q\alpha_1P^*}{a_1(\frac{S^{*2}}{\gamma}+S^*+a_1)}\right]$.

Proof. We consider a positive definite Lyapunov function about $E^*(S^*,I^*,P^*)$ as

$$V_1 = S - S^* - S^*ln\frac{S}{S^*} + \frac{1}{2}(I-I^*)^2 + (P - P^* - P^*ln\frac{P}{P^*}).$$

Differentiating V_1 with respect to time along the solutions of (4.1), we obtain

$$\dot{V}_1 = \frac{S-S^*}{S}\frac{dS}{dt} + (I-I^*)\frac{dI}{dt} + \frac{(P-P^*)}{P}\frac{dP}{dt}.$$

Further, some algebraic manipulation yields

$$\begin{aligned}\dot{V}_1 = &\frac{a_{11}}{2}(S-S^*)^2 + a_{12}(S-S^*)(I-I^*) + \frac{a_{22}}{2}(I-I^*)^2 \\ &+ \frac{a_{22}}{2}(I-I^*)^2 + a_{23}(I-I^*)(P-P^*) + \frac{a_{33}}{2}(P-P^*)^2 \\ &+ \frac{a_{33}}{2}(P-P^*)^2 + a_{13}(P-P^*)(S-S^*) + \frac{a_{11}}{2}(S-S^*)^2,\end{aligned}$$

where

$$a_{11} = -\frac{r_1}{K} + \frac{(1+S+S^*)q\alpha_1 P^*}{(\frac{S^{*2}}{\gamma}+S^*+a_1)(\frac{S^2}{\gamma}+S+a_1)},\ a_{22} = \beta S^* - \delta_1 - \frac{q\alpha_2 a_2 P}{(a_2+I)(a_2+I^*)},$$

$$a_{33} = -\frac{r_2\xi}{(q\alpha_1 S + q\alpha_2 I + (1-q)\alpha_A K_A)},\ a_{12} = \beta I - (\frac{r_1}{K}+\beta),$$

$$a_{13} = -\frac{q\alpha_1}{\frac{S^2}{\gamma}+S+a_1} + \frac{r_2\xi q\alpha_1 P^*}{q\alpha_1 S + q\alpha_2 I + (1-q)\alpha_A K_A)(q\alpha_1 S^* + q\alpha_2 I^* + (1-q)\alpha_A K_A)},$$

$$a_{23} = -\frac{q\alpha_2 I^*}{a_2+I^*} + \frac{r_2\xi q\alpha_2 P^*}{q\alpha_1 S + q\alpha_2 I + (1-q)\alpha_A K_A)(q\alpha_1 S^* + q\alpha_2 I^* + (1-q)\alpha_A K_A)}.$$

As per the Sylvester's criterion, $\dot{V}_1$ is negative definite if

$a_{11} < 0, \quad a_{22} < 0, \quad a_{33} < 0, \quad a_{12}^2 < a_{11}a_{22}, \quad a_{23}^2 < a_{22}a_{33}$ & $a_{13}^2 < a_{11}a_{33}$.

If (i), (ii), (iii) holds, then the Sylvester's criterion is satisfied. Hence the theorem follows. □

4.6 Numerical simulation

We begin by numerically simulating the subsystem (4.2) using the parameter values given in Table 4.3. We construct nullclines and the system phase diagram for various values of α_A. With the increment in α_A, the system changes its stability through double Hopf-bifurcation and a transcritical bifurcation. At $\alpha_A = 0.3$, the system exhibits a stable focus at the positive equilibrium $E_*(S_*, P_*)$ (Fig. 4.3(a)). However, this stability no longer sustains as the system undergoes Hopf-bifurcation at $\alpha_A^{[H_1]} = 0.667092$, which causes the born of a stable limit cycle enclosing E_*. At $\alpha_A = 1$, the system displays a stable limit cycle around E_* (Fig. 4.3(b)). The aforementioned limit cycle vanishes when the system experiences another Hopf-bifurcation at $\alpha_A^{[H_2]} = 1.419495$, and E_* becomes stable. For $\alpha_A = 2$, the system shows stable dynamics around the co-existence state E_* (Fig. 4.3(c)). With a further rise in α_A, the system experiences another type of bifurcation, i.e., transcritical bifurcation at $\alpha_A^{[tc]} = 3.125$. The positive steady-state dissipate at this point, transferring stability to the prey-free state. Therefore, at $\alpha_A = 3.5$, the prey-free equilibrium E_2 is a stable node (Fig. 4.3(d)).

Table 4.3: Data set of parameters used in (4.2) with references.

Parameters	Numerical value	Reference(s)
r_1	5	[150]
K	8.3	[48]
α_1	5	[40]
a_1	5	Assumed
γ	1	[48]
r_2	2	[150]
K_A	10	Assumed
q	0.8	[11]
ξ	1	[150]
α_A	0.3	Assumed

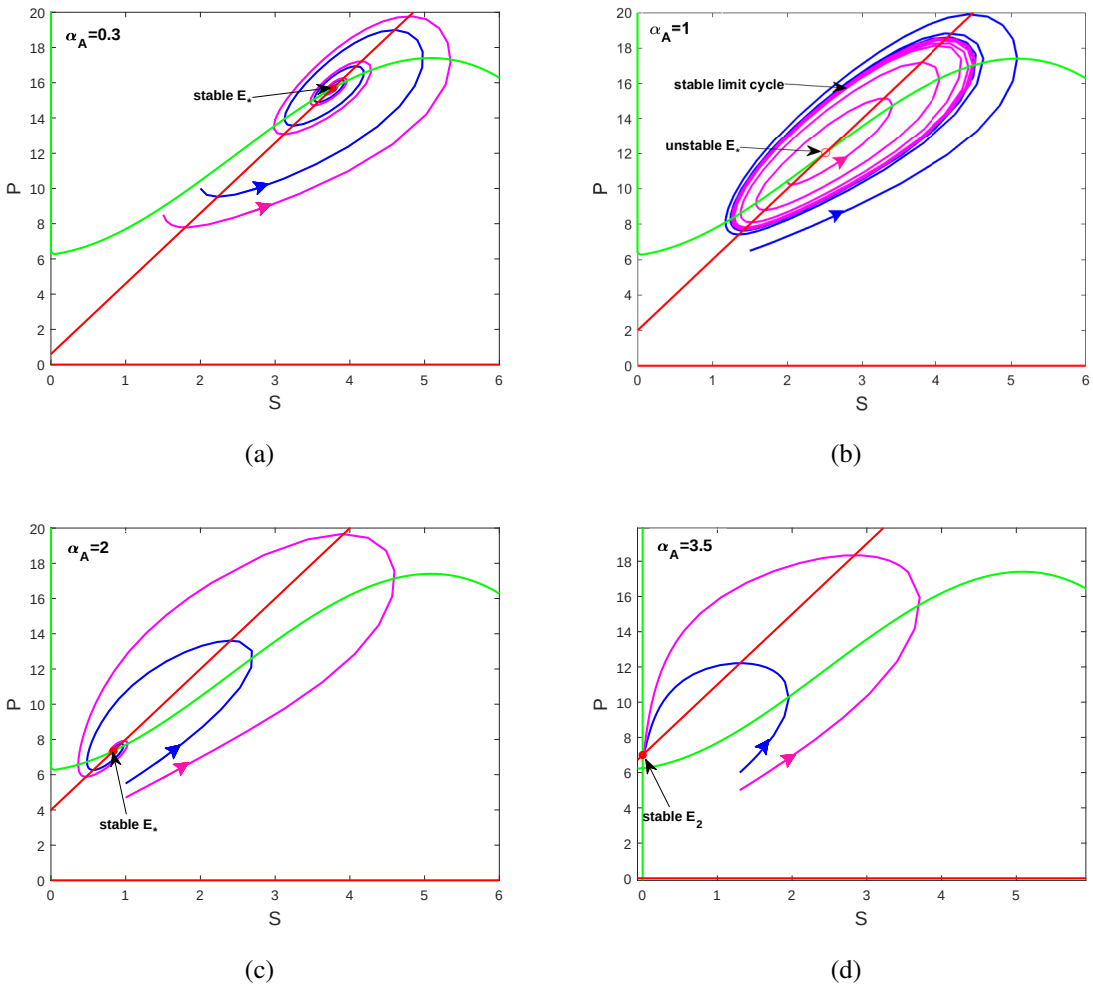

Fig. 4.3: Nullclines and phase portrait of *SP* subsystem (4.2) for different values of α_A. Green curve represent the prey nullclines and red lines represent the predator nullclines. Two trajectories starting from different initial points are shown by magenta and blue color.

To visualize these bifurcations in a better way, we plotted bifurcation diagram with regard to α_A for S (left) and P (right) in Fig. 4.4. Here blue curve represents E_* and oscillations about it and red is for E_2; solid curve shows stable nature and dashed curve denotes instability. At $\alpha_A^{[H_1]}$ and $\alpha_A^{[H_2]}$, $\Theta_1 = 0$ and $\Theta_2 > 0 \implies Re(\lambda) = 0$. The transversality condition for Hopf-bifurcation at $\alpha_A^{[H_1]}$ and $\alpha_A^{[H_2]}$ can be checked using the Newton's forward difference formula, which results:

$$\left.\frac{Re(\lambda)}{d\alpha_A}\right|_{\alpha_A^{[H_1]}} = 6 > 0 \text{ and } \left.\frac{Re(\lambda)}{d\alpha_A}\right|_{\alpha_A^{[H_2]}} = -0.75 < 0.$$

Therefore, $Re(\lambda)$ is a monotonic function of α_A at both the bifurcation points. All these conditions verify the occurrence of Hopf-bifurcation at $\alpha_A^{[H_1]}$ and $\alpha_A^{[H_2]}$.

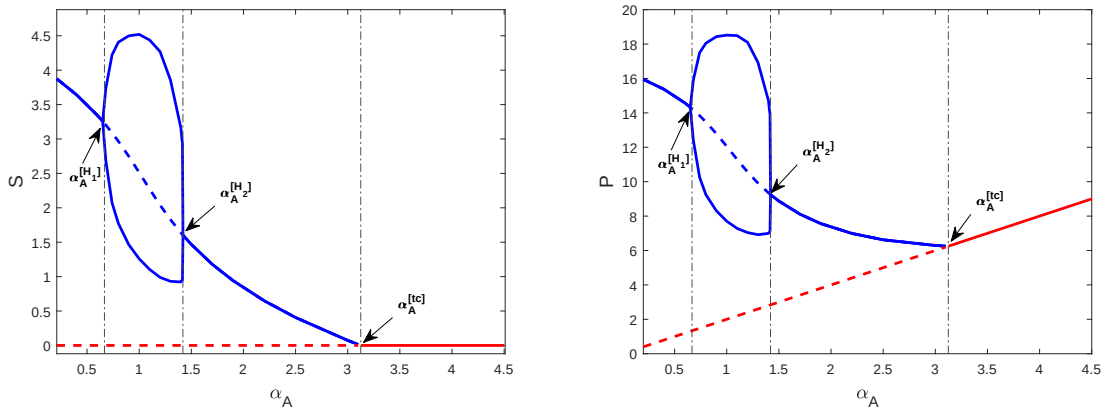

(a) (b)

Fig. 4.4: Bifurcation diagram showing double Hopf-bifurcation and a transcritical bifurcation in SP subsystem (4.2) with respect to α_A.

For the set of parameters given in Table (4.3), we obtain $E_*(3.7697, 15.6791)$ and the eigenvalues corresponding to it are: $-0.224 \pm 1.4474i$. The prey-free equilibrium $(0, 0.6)$ is a saddle point as $r_1 - (\frac{q\alpha_1(1-q)\alpha_A K_A}{a_1\xi}) = 4.52 > 0$. Furthermore, $\nabla_1 = -0.493 < 0$ shows that system (4.2) does not exhibit any periodic orbit. This confirms the global stability of $E_*(S_*, P_*)$ (refer to Theorem 4.4.3). Attraction of trajectories towards the global attractor E_* is shown in Fig. 4.5.

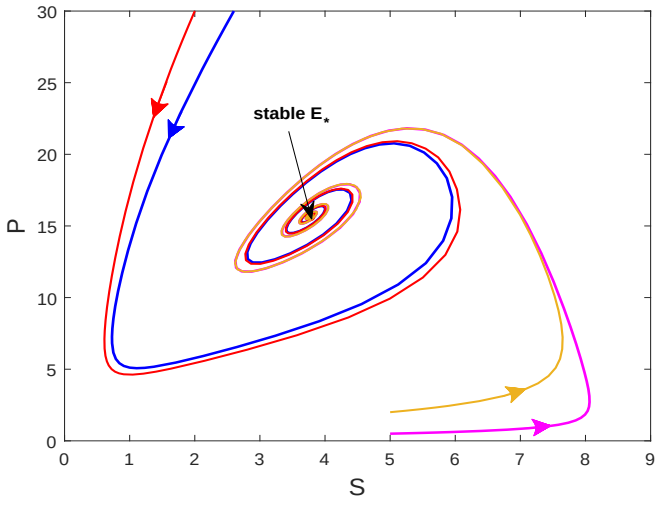

Fig. 4.5: Global stability of subsystem (4.2) about $E_*(S_*, P_*)$ for parameters set given in Table 4.3.

Let us examine the effect of additional food parameter α_A on the dynamics of full system (4.1) with a different set of parameters:

$$K = 5,\ r_1 = 2.5,\ \alpha_1 = 0.1539,\ \alpha_2 = 0.04,\ a_1 = a_2 = \gamma = 0.1,\ r_2 = 2,\ K_A = 10,\ q = 0.6,$$
$$\delta_1 = 0.05,\ \beta = 0.3,\ \xi = 1. \tag{4.13}$$

We plot a series of phase diagrams with the variation in α_A (Fig. 4.6). When the predator does not get energy from the provided additional food, i.e., $\alpha_A = 0$ in such case, the positive steady state of the *SIP* system is locally asymptotically stable, and the disease-free state E_{SP} is saddle (Fig. 4.6 (a)). For positive values of α_A, the predator-only steady-state E_P comes into existence, and it remains saddle for initial values. With the increase in α_A, the oscillations about the positive equilibrium E^* are turned on, i.e., a stable limit cycle occurs through a supercritical Hopf-bifurcation at $\alpha_A^{(1)} = 0.08261$. However, the disease-free equilibrium E_{SP} remains saddle (Fig. 4.6(b)). The limit cycle swells with the rise in α_A, and gradually it connects the predator-only saddle point E_P forming a homoclinic orbit (Fig. 4.6 (c)), which is stable. This coalesces of limit cycle, and E_P is the homoclinic bifurcation. It occurs in our system (4.1) at $\alpha_A^{(2)} = 0.3739$. The homoclinic orbit surrounding E^* stays for $\alpha_A \in [0.3739, 0.4146)$. After that, it integrates another saddle point E_{SP} into it by the heteroclinic bifurcation at $\alpha_A^{(3)} = 0.4146$. This closed trajectory formed connecting two saddle points E_P & E_{SP} is the heteroclinic orbit (Fig. 4.6 (d)). The connection between the two saddles is such that the stable manifold of E_P coincides with the unstable manifold of E_{SP} and the period of the heteroclinic cycle becomes infinite. Furthermore, only the predator population survives (E_P is stable) when the heteroclinic cycle

or the saddle-saddle connection breaks at $\alpha_A^{(4)} = 0.6769$. E_P's stability promotes the formation of another planar equilibrium, $E_{SP}^{(1)}$, which is a saddle node (Fig. 4.6 (e)). As α_A is boosted more, the system achieves bi-stability between axial and planar equilibrium (E_P & E_{SP}) for $\alpha_A = 4.5$ (Fig. 4.6 (f)). In this case, the basin of attraction for the stable steady-states in shown in Fig. (4.9 (a)). The critical value of α_A for which the system becomes stable about E_{SP} is $\alpha_A^{(5)} = 1.3938$. Later on, the system attains tri-stability between the axial E_P , planar E_{SP} and the interior equilibrium E^* at $\alpha_A^{(6)} = 7.5238$.

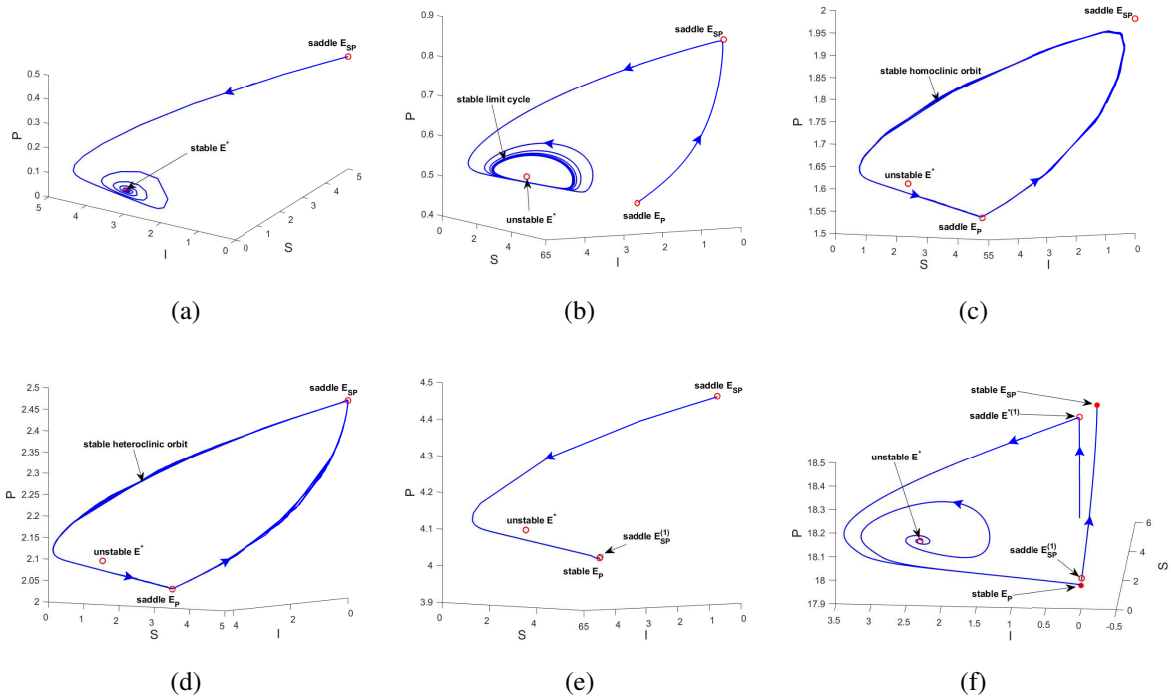

Fig. 4.6: Series of phase portraits with regard to α_A. (a) $\alpha_A = 0$, (b) $\alpha_A = 0.1$, (c) $\alpha_A = 0.38$, (d) $\alpha_A = 0.5$, (e) $\alpha_A = 1$, (f) $\alpha_A = 4.5$. The other parameters are same as (4.13).

Multi-stability: The concept of multi-stability between different attractors is based on their presence and stability criteria. Ecological models may exhibit more than one interior equilibrium points. All feasible interior equilibrium points may have different stability behavior which depends on the combination of model parameters. In many prey-predator systems, only one or a few states exist where all species persist with different abundances; in most other states, some species become extinct. The latter phases are undesirable because they result in a decrease in biodiversity in the model system. This type of multi-stability can be linked to very convoluted fractal basins of attraction of the various equilibria, resulting in a shift in biodiversity induced by the transition to a state in which part of the species has died out [151]. A multi-stable system can adopt several stable states, in the same ecological conditions. The presence of many

stable states allows for a considerable deal of system performance flexibility without requiring large parameter adjustments [152]. Knowlton [153] presented the experimental evidence of conservation of marine ecosystem due to the existence of multiple attractors. Understanding the complex behavior of interacting populations such as multi-stability pattern is an important aspect to study for managing ecological systems. In the present work, system (4.1) is tri-stable between predator-only equilibrium E_P, disease-free equilibrium E_{SP}, and the positive equilibrium E^* if all the four conditions stated below are satisfied.

(i) $r_1 - \frac{q\alpha_1(1-q)\alpha_A K_A}{a_1\xi} < 0,$

(ii) $\delta_1 - \beta S_{SP} + \frac{q\alpha_2 P_{SP}}{a_2} > 0,$

(iii) $r_1 - \frac{Kq\alpha_1 P_{SP}(\frac{2S_{SP}}{\gamma}+1)}{(\frac{S_{SP}^2}{\gamma}+S_{SP}+a_1)^2} > 0,$

(iv) $D_1 > 0, D_3 > 0$ and $D_1D_2 - D_3 > 0.$

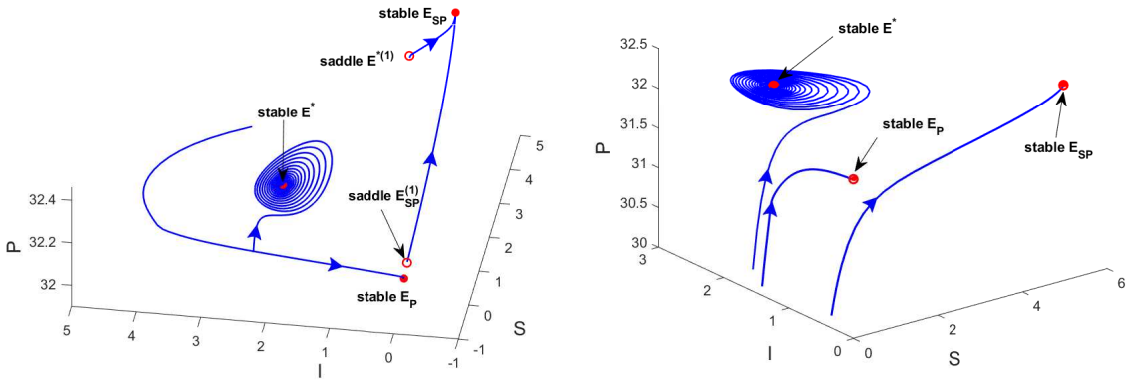

(a) (b)

Fig. 4.7: Multi-stability among steady-states E_P, E_{SP} and E^* at $\alpha_A = 8$ and other parameters are taken from (4.13).

At $\alpha_A = 8$, the steady-states with their nature are listed as:

$(4.0596, 0.5655, 32.388)$	*saddle node*	$E^{*(1)}$
$(1.3384, 2.0965, 32.1739)$	*stable spiral*	E^*
$(0.2937, 0, 32.0271)$	*saddle node*	$E_{SP}^{(1)}$
$(4.9762, 0, 32.4595)$	*stable node*	E_{SP}
$(0, 0, 32)$	*stable node*	E_P

Simple calculation yields $(i): -27.0488 < 0,\ (ii): 6.3473 > 0,\ (iii): 2.4764 > 0,\ (iv): D_1 = 2.0388 > 0,\ D_3 = 0.62787 > 0,\ D_1D_2 - D_3 = 1.5973 > 0$. This shows that the system is tri-stable for E_P, E_{SP} and E^*. Moreover, the system (4.1) attains multi-stability for all $\alpha_A \in [7.5238, 11.5438]$. Beyond this value, the interior equilibrium does not exist. For $\alpha_A = 8$, we plot the phase portrait showing all steady-states (whose nature may alter) in Fig. 4.7 (a), while Fig. 4.7 (b) displays attractors only. Since the dynamical behavior of multi-stable systems is influenced by the initial circumstances, it is possible to find coexisting attractors by choosing suitable initial conditions [154]. The creation of the attractor is accompanied by the emergence of its basin of attraction, the limits of which might be smooth or fractal. A bi-stable system with only two coexisting attractors usually has smooth boundaries of their respective basins of attraction, whereas a multi-stable system frequently has fractal basin boundaries [152]. The basin of attraction for the three steady-states is shown by different colors; green color for E^*, blue color for E_{SP} and red color represent initial values for E_P in Fig. 4.10.

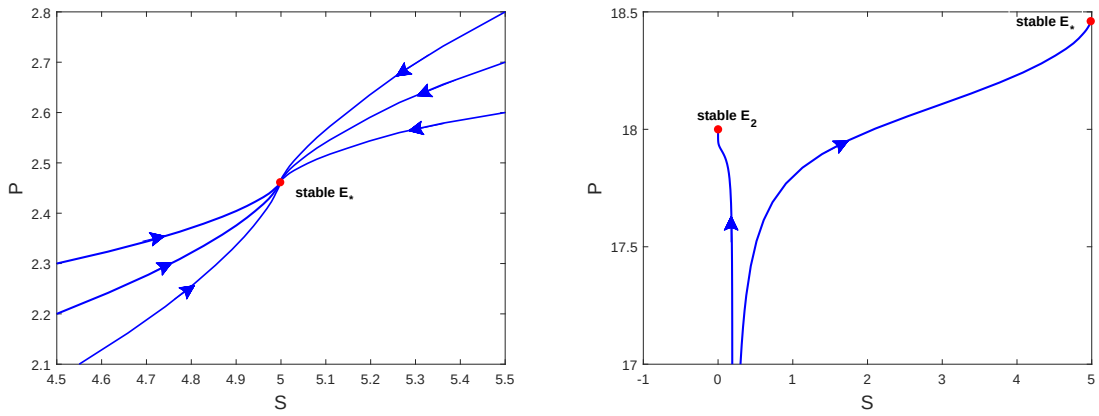

(a) (b)

Fig. 4.8: Phase portrait showing stability dynamics of *SP*- subsystem at (a) $\alpha_A = 0.5$ and (b) $\alpha_A = 4.5$. Here the parameters are same as in (4.13).

The dynamics of the *SP* subsystem are considerably different with respect to α_A, for the set (4.13). The system (4.2) is globally asymptotically stable about $E_*(S_*P_*)$ for $\alpha_A \in [0, 0.6769)$. Additionally, Theorem 4.4.3 holds for the mentioned range. At $\alpha_A = 0.6769$ and onwards, the system attains bi-stability between prey-free equilibrium E_2 and the positive equilibrium E_*. In Fig. 4.8 (a), for $\alpha_A = 0.5$, trajectories starting from six different initial pairs eventually converge to the $E_*(4.9982, 2.46150)$. Corresponding to it the eigenvalues are $-2.4966, -2$, $\nabla_1 = -94.19904$ and $r_1 - (\frac{q\alpha_1(1-q)\alpha_A K_A}{a_1\xi}) = 0.6532 > 0$. Therefore, Theorem 4.4.3 holds and E_* attracts all trajectories globally in the positive quadrant of the $SP-$ plane. In Fig. 4.8 (b), two trajectories starting from different initial points converge to two different attractors resulting in

bi-stability between $E_*(4.9865, 18.46045)$ and $E_2(0, 18)$ at $\alpha_A = 4.5$. The set of initial values for which the trajectories eventually converge to E_* (blue color dots) and E_2 (red color dots) is displayed in Fig. 4.9 (b).

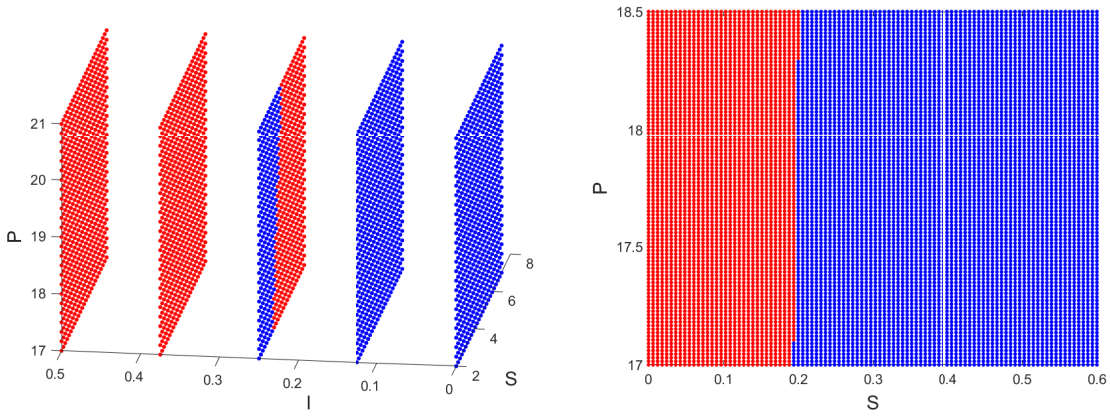

(a) (b)

Fig. 4.9: Basin of attraction at $\alpha_A = 4.5$ for system (4.1) (left) and (4.2) (right), respectively. Here red and blue dots represent initial values for which the predator-only equilibrium is stable, whereas blue dots are corresponding to the disease-free equilibrium, i.e., E_{SP} (in full system) and E_* (in SP subsystem). This figure is corresponding to the Fig. 4.6 (f) and Fig. 4.8 (b), respectively.

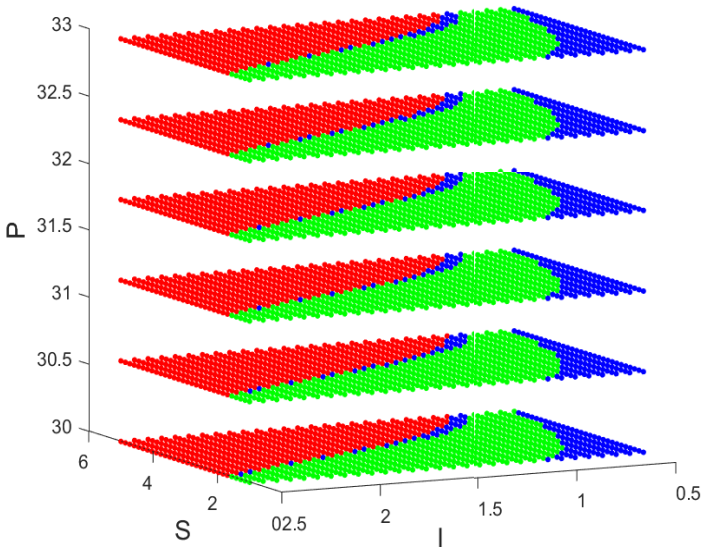

Fig. 4.10: Basin of attraction for multi-stable equilibrium points E_P (red dots), E_{SP} (blue dots) and E^* (green dots). This illustration is associated with Fig. 4.7.

It can be depicted from Fig. 4.11 that for lower values of parameter α_A two inner equilibrium points E^* and $E^{*(1)}$ coexist. E^* denotes a stable point, while $E^{*(1)}$ denotes a saddle point. When we raise the value of α_A, both equilibrium points approach towards one another until they clash and obliterate each other via a saddle-node bifurcation at the threshold value $\alpha_A^{[sn]} = 11.5438$. For $\alpha_A > \alpha_A^{[sn]}$, neither of the interior equilibria exists. For the chosen set of parameters, at $\alpha_A = \alpha_A^{[sn]} = 11.5438$ we have coexistence equilibrium $\bar{E}(2.7051, 1.3637, 46.4577)$ and $det(M|_{\bar{E}}) = 0$.

The variational matrix around $\bar{E}$ at the saddle-node bifurcation point $\alpha_A = \alpha_A^{[sn]}$ is

$$A = M|_{\bar{E}} = \begin{pmatrix} -1.2419 & -2.1642 & -0.0032 \\ 0.4090 & 0.7095 & -0.02236 \\ 0.1846 & 0.048 & -1.9999 \end{pmatrix}.$$

The eigenvectors corresponding to the eigenvalue zero of matrix A and A^T are $v = (1, -0.5739, 0.0794)^T$ and $w = (1, 3.0535, 0.0478)^T$, respectively. Our computation yields

$$F_{\alpha_A}(\bar{E}, \alpha_A^{[sn]}) = \begin{pmatrix} 0 \\ 0 \\ 7.9999 \end{pmatrix} \text{ and } D^2F(\bar{E}, \alpha_A^{[sn]})(v, v) = \begin{pmatrix} -0.12 \\ 0.3208 \\ 0.00057 \end{pmatrix}.$$

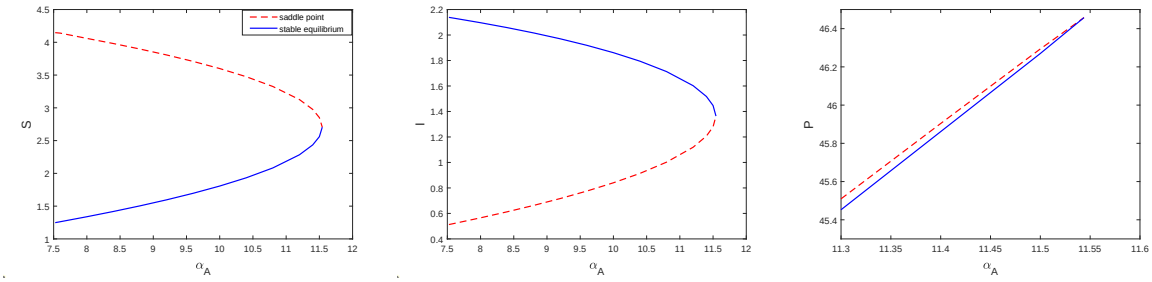

(a) (b) (c)

Fig. 4.11: Saddle-node bifurcation diagram concerning α_A.

Here $F = (f_1, f_2, f_3)^T$, and F_{α_A} is the partial derivative of F with respect to α_A.

$$w^T F_{\alpha_A}(\bar{E}, \alpha_A^{[sn]}) = 0.3824 \neq 0 \text{ and } w^T[D^2F(\bar{E}, \alpha_A^{[sn]})(v, v)] = -1.0995 \neq 0.$$

Therefore, according to the Sotomayor's theorem [60], system (4.1) undergoes saddle-node bifurcation at $\alpha_A = \alpha_A^{[sn]} = 11.5438$ around $\bar{E}((2.7051, 1.3637, 46.4577))$.

The effect of α_A on the dynamics of system (4.1) is presented in Fig. 4.12. Different sectors of the circle contain various attractors. The explanation for all the sectors in the circle is summarized in Table 4.4. We now study the characteristics of system (4.1) concerning the infection rate β with $\alpha_A = 0.5$ and other parameters are from (4.13). β does not affect the stability of predator-only equilibrium but affects the nature of disease-free state and co-existence state of equilibria. It is noticed from Fig. 4.13 (a) that E^* and E_{SP} are co-stable for $\beta = 0.1$. For the initial values from the blue dots in Fig. 4.14 (a), the trajectory converges towards E_{SP}, which indicates that the disease can be eliminated when the trajectory is started from any blue dot. The stability of E_{SP} is lost at $\beta = 0.1282$, and it becomes saddle. At $\beta = 0.13$, high oscillations occur around stable equilibrium E^* for the initial time, and eventually, the trajectory goes to the stable focus. Moreover, the trajectory experiences a pull towards stable manifold of E_P and E_{SP} (Fig. 4.13 (b)). On small increment in β, the system exhibits focus-cycle bi-stability (Fig. 4.13 (c), and in between them, there is an invisible repeller (limit cycle) which separates the basins of attraction of heteroclinic cycle and the focus steady-state E^*. The basin of attraction at $\beta = 0.14$ is plotted in Fig. 4.14. With a slight increment in β, the interior equilibrium loses its stability by means of a subcritical Hopf-bifurcation at $\beta = 0.1732$, while the saddle-saddle connection remains stable. This feature is presented in Fig. 4.13 (d).

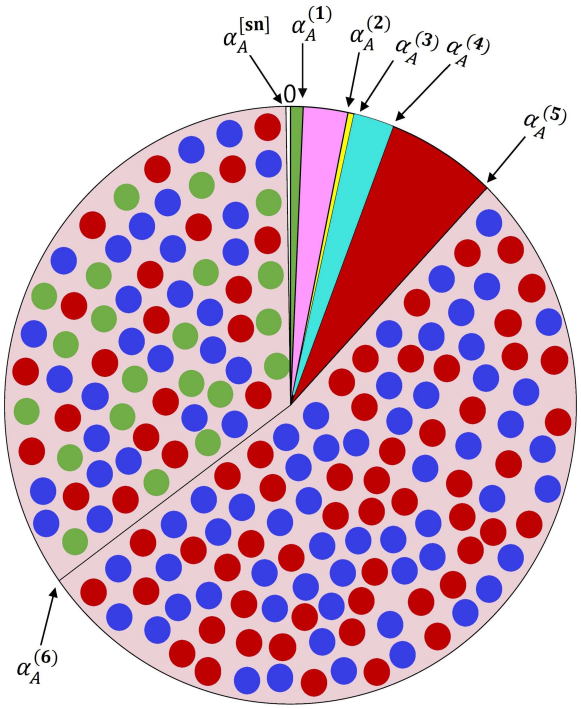

Fig. 4.12: Circle graph representing different attractors concerning α_A for all parameters from (4.13).

Table 4.4: A brief description of attractors based on intervals of α_A, as seen in Fig. 4.12.

Range of α_A	Attractor(s)	Color(s)(respectively)
$[0, \alpha_A^{(1)})$	E^*	green
$(\alpha_A^{(1)}, \alpha_A^{(2)})$	limit cycle	pink
$(\alpha_A^{(2)}, \alpha_A^{(3)})$	homoclinic orbit	yellow
$(\alpha_A^{(3)}, \alpha_A^{(4)})$	heteroclinic orbit	aqua
$(\alpha_A^{(4)}, \alpha_A^{(5)})$	E_P	red
$(\alpha_A^{(5)}, \alpha_A^{(6)})$	E_P, E_{SP}	red, blue (circles)
$(\alpha_A^{(6)}, \alpha_A^{[sn]})$	$E_P,\ E_{SP},\ E^*$	red, blue, green (circles)

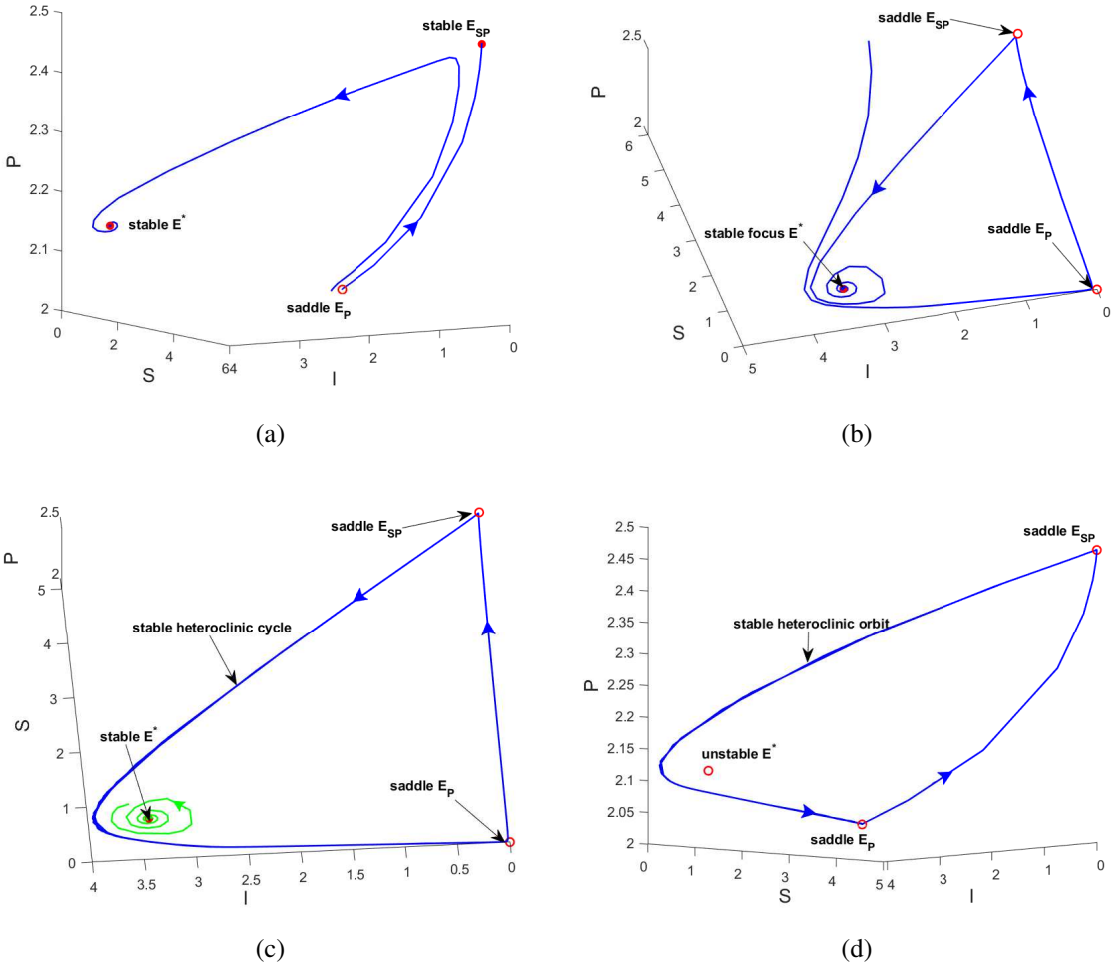

Fig. 4.13: The effect of disease transmission rate β on system (4.1)'s dynamics when $\alpha_A = 0.5$ and the parameters other than β, & α_A are same as (4.13). (a)Focus-node bi-stability for $\beta = 0.1$, (b)stable focus E^* at $\beta = 0.13$, (c)focus-cycle bi-stability for $\beta = 0.14$, (d) stable heteroclinic orbit at $\beta = 0.18$,

The system shows complex dynamics for additional food parameter α_A and infection rate β, which motivates us to observe the combined effect of both the parameters. The integrated effect of β and α_A is shown in Fig. 4.15. We obtain three critical values of α_A corresponding to a single value of β for which the system (4.1) undergoes Hopf-bifurcation twice followed by a saddle-node bifurcation about the co-existence equilibria. As a result, the $\beta\alpha_A$- plane is divided into various regions. In Region I, the interior equilibrium of (4.1) exists uniquely and is locally asymptotically stable. However, it loses its stability at the first Hopf-bifurcation point on the red-colored curve. Therefore in Region II, the interior equilibrium behaves as a repeller, surrounded by a closed trajectory. Boosting α_A again stabilizes the system about co-existence equilibrium by means of a supercritical Hopf-bifurcation on the blue-colored curve. On crossing this curve, there are two interior equilibria one is stable (it was unstable in Region II), and the other is a saddle in Region III. On increment in α_A, these two equilibria approach each other to perform a saddle-node bifurcation. Upon reaching the saddle-node bifurcation curve (green), both positive equilibria destroy each other and finally disappear. Region IV has no interior equilibrium because of this. In Fig. 4.15, the predator-only state and the disease-free state of equilibria always exist, but their stability behavior changes from the saddle to stable with respect to α_A (when β is fix). Below the cyan-colored dashed line, E_P is a saddle, and above this line, E_P gains stability. E_{SP} is a saddle in the region below the yellow-colored dashed curve, but beyond this curve, the E_{SP} becomes stable. Therefore, we can say that in between the yellow (dashed) and blue curve, the system attains bi-stability about E_P and E_{SP}, and the system is tri-stable between E_P, E_{SP} and E^* in Region III.

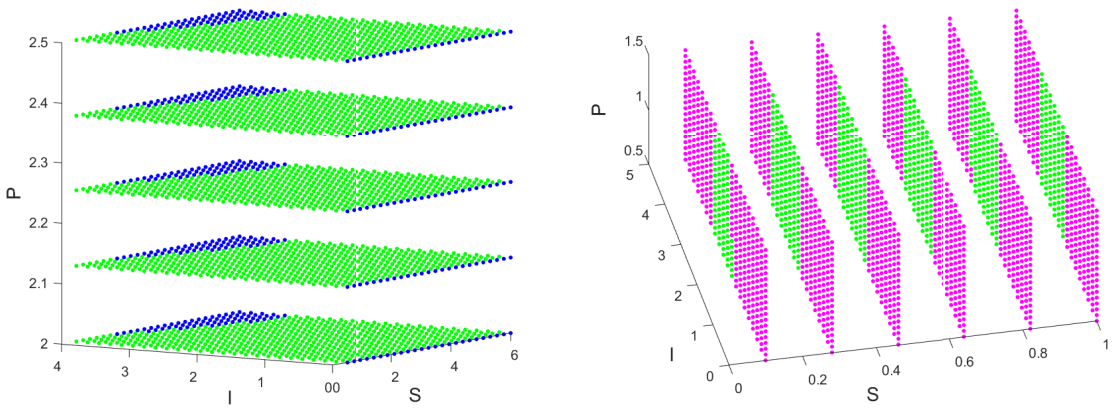

(a) (b)

Fig. 4.14: Basins of attraction corresponding to Fig. 4.13 (a) and (c). Green dots are the initial values for which the system is stable around E^*, blue dots show the basin of pull for E_{SP} and magenta dots display the basin of attraction of heteroclinic cycle.

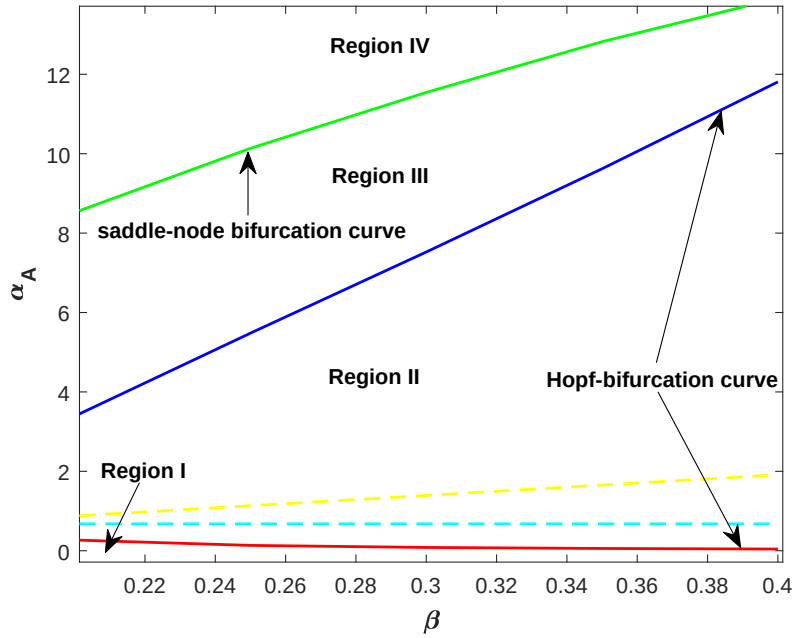

Fig. 4.15: Bi-parametric graph showing Hopf-bifurcation curves and saddle-node curve in the $\beta\alpha_A$- plane.

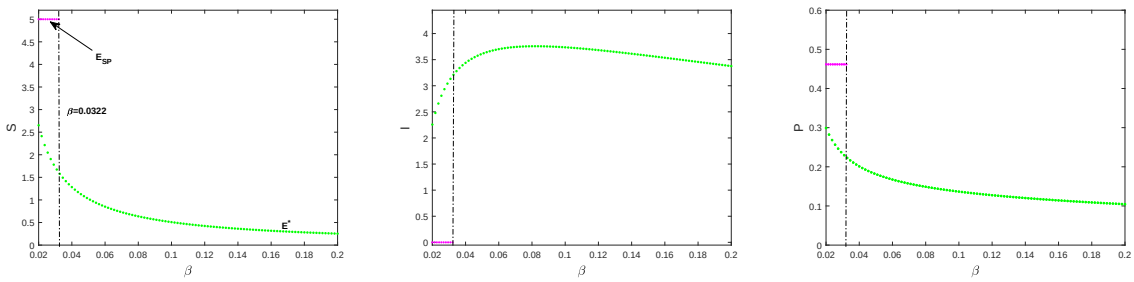

(a) (b) (c)

Fig. 4.16: Effect of infection rate β on the population density for $\alpha_A = 0$.

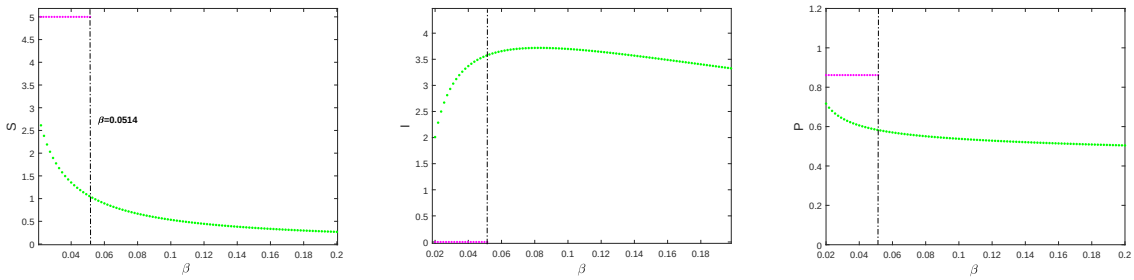

(a) (b) (c)

Fig. 4.17: Effect of infection rate β on the population density for $\alpha_A = 0.1$.

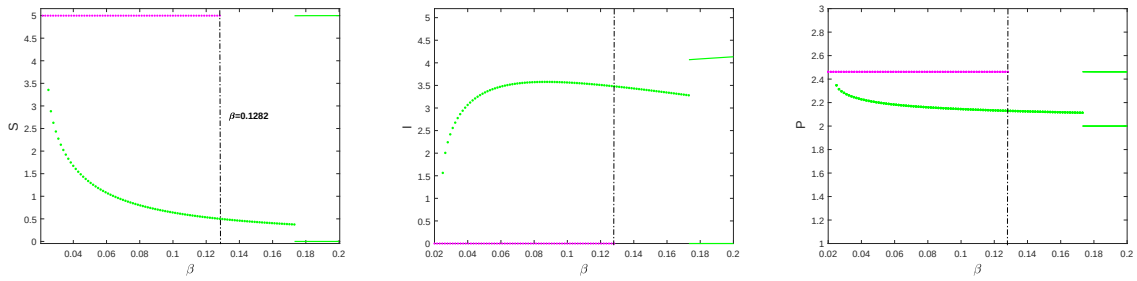

(a) (b) (c)

Fig. 4.18: Effect of infection rate β on the population density for $\alpha_A = 0.5$.

In the absence of extra food $\alpha_A = 0$, the system can be made disease-free (E_{SP} is stable) only when $\beta \in [0.02, 0.0322)$ (Fig. 4.16). The elimination of the disease for this range depends on the initial condition. However, for a higher infection rate, the disease persists in the system (E^* is stable). If the predator receives energy from the additional meal, at $\alpha_A = 0.1$, the illness can be managed for a higher infection rate $\beta \in [0.02, 0.0514)$ (Fig. 4.17). Furthermore, if the predator obtains more energy from the given food, disease eradication is better. At $\alpha_A = 0.5$, E_{SP} is stable for the higher range of infection rate, i.e., $\beta \in [0.02, 0.1282)$ (Fig. 4.18). It can be depicted from Figs. 4.16, 4.17 and 4.18 that the population numbers remarkably vary for $\beta \in [0.02, 0.2)$. The susceptible population decline for ascending infection rates and is added to the infected class simultaneously. However, the disease gets deadly for higher infection rates; consequently, the infected prey declines. Due to the lack of the favorite food of the predator, viz., healthy prey, predator numbers decrease significantly. There is a rapid declination in predators when there is no provision of alternative food. However, when they gain energy from the extra food, the decrement is not so fast. The rise in α_A does not affect this behavior up to some extent. Nevertheless, species start to oscillate about their positive steady-state for a higher infection rate $\beta > 0.1731$ at $\alpha_A = 0.5$. The green curve in Figs. 4.16, 4.17 and 4.18 denotes the co-existence equilibrium E^* of system (4.1), whereas magenta color line displays the disease-free equilibrium E_{SP}.

4.7 Discussion and conclusion

Though there are many ways to control the disease in species, mostly are the chemical approaches like treatment [155], vaccination [156], etc. In literature, a considerable amount of work has been done on prey-predator models with additional food. However, a few demonstrated the application of additional food to control the disease in the system [40, 149]. The present article deals with a prey-predator model where prey develops an untreatable infectious disease, and the predator can switch to the different food provided. Therefore, we formulated

a Leslie-Gower model where the predator depends on more than one food source to realize this effect. Generally, the epidemic models are divided into a finite number of compartments. When prey catches the disease, we assumed that the whole prey population is classified into two compartments: susceptible (S) and infected (I). Furthermore, we hypothesized that the susceptible prey is strong enough to defend themselves from the predator. Thus, this interaction is incorporated as Holling type IV functional response. Since the infected prey population may be weak and thus the interaction between infected prey and predator is taken as Holling type II functional response.

Firstly, we established the well-posedness of the proposed model. Then, we used the isoclines method to determine sufficient conditions for the uniqueness and existence of the positive steady-state. We analyzed the disease-free subsystem in order to study the proposed model finely. Consequently, we discovered that if the prey birth rate is above a certain threshold, the disease-free equilibrium (E_* or E_{SP}) occurs. The present article contains extensive work on the long-term behavior of all feasible states of the system (4.1) and (4.2). We used eigenvalue theory and Lyapunov stability theory to determine local and global stability, respectively. If the birth rate of prey exceeds a certain threshold value and the mortality rate of infected prey exceeds a different threshold value, in that situation, the disease can be completely eradicated from the system. Mathematically, the E_{SP} is stable in such a case.

Our model analysis shows that stability behavior of all feasible steady-states depends on the value of additional food parameter. Both systems (4.1) and (4.2) show rich dynamics with respect to the additional food parameter α_A. For a considered set of parameters given in the text and with the increment in α_A, the subsystem (4.2) switches stability thrice through double Hopf-bifurcation and a transcritical bifurcation. It is also observed that all trajectories initiated from different points in the positive quadrant of the SP-plane converge to the positive equilibrium of (4.2) for the same set. This global attraction towards E_* is proven theoretically and numerically as well. Now, for a different set of parameters, we discovered fascinating results regarding additional food energy parameter. The system (4.1)'s stability about E_P, E_{SP} and E^* is not always same. The stability dynamics of these equilibria are highly sensitive to the change in α_A. The system undergoes different types of local and global bifurcations for α_A; Hopf-bifurcation, saddle-node bifurcation, homoclinic and heteroclinic bifurcation. The roller-coaster of these bifurcations makes the system bi-stable and tri-stable for different ranges of α_A. The presence of attractors of (4.1) for different values of α_A is uniquely presented through a circle graph Fig. 4.12. For the same set of parameters, subsystem (4.2) is either globally asymptotically stable about E_* or bi-stable between E_* and E_2. We have plotted basins of attraction whenever the system is bi-stable or tri-stable. If any solution trajectory starts from the blue-colored point, the system will go disease-free (see Figs. 4.9, 4.10, 4.14). Due to the disease eradication, both healthy prey and predator will survive, resulting in the richer biodiversity of the system.

Moreover, the flexibility provided by the multi-stability of steady-states may result in species conservation.

The disease-transmission rate β is also a crucial parameter to study. It is capable of altering system (4.1)'s kinetics. For lower values of infection rate, the system is bi-stable between co-existence and disease-free steady-states (E^* and E_{SP}). For a greater infection rate, the system performs a subcritical Hopf-bifurcation, and periodic oscillations occur about E^*. Moreover, these oscillations go to the stable manifolds of two saddle points, forming a stable heteroclinic orbit.

Since the system shows captivating dynamics for α_A and β, we constructed a bi-parametric curve concerning it (Fig. 4.15). As a result, we found distinct regions depending on whether the solution trajectory converges to steady-state attractor(s) or cyclic attractor on undergoing Hopf-bifurcation and saddle-node bifurcation. We can conclude from Fig. 4.15 that the disease elimination is achievable in the region above the yellow-dashed line in the $\beta\alpha_A$-plane.

When there is no additional food for the predator, the disease extermination is feasible at lower infection rates only (refer to Fig. 4.16). However, in the presence of extra food, the predator gains energy from it. In such a case, disease control is possible even for higher infection rates (see Figs. 4.17 and 4.18). In this way, the disease in a prey-predator system can be managed if the predator's energy (obtained from additional food) is boosted more. Sahoo [40] discovered a similar kind of strategy to control disease in the prey-predator system. The author observed that supplying an adequate amount of extra food quantity to the predator can make the system disease-free.

Chapter 5

Bifurcation and chaos in a delayed eco-epidemic model induced by prey configuration [1]

5.1 Introduction

Ecology and epidemiology, individually, are prominent areas of study. Nowadays, significant research is also going on in the interdisciplinary field of eco-epidemiology. It contains assessments of interactions between hosts and their viruses, parasites, and illnesses of both people and wildlife at the population and community level. On the other hand, diseases can have a considerable impact not only on their host populations but also on other species that interact with them [44]. The invasion of disease has far-reaching effects on the structure and stability of ecosystems [157]. Eco-epidemiology research aids in identifying the critical elements that contribute to the spread of infectious illnesses and determining the most effective control tactics. Studying a mathematical model of ordinary differential equations is a standard way to know an eco-epidemic system. An eco-epidemic model hybridizes an ecological and epidemic model.

In the prey population, the link between predation and infection is multifaceted. According to Lafferty and Morris [158], due to a fatal disease, killifish (Fundulus parvipinnis) comes to the surface and becomes more vulnerable to predation. Infection among prey or predator or both can regulate their co-existence as well as stability dynamics. The incidence rate plays a crucial role in analyzing the disease transmission among prey-predator species. The incidence rate refers to the number of infected people in a particular period (per unit of time). In classic epidemic models, the bilinear incidence rate is widely used [159, 160]. However, the implementation of a saturated incidence rate can explain the diverse dynamics of the system [150]. The non-linear incidence function incorporates the saturation of disease transmission at high infective levels [161]. Han *et al.* [162] analyzed four eco-epidemic models with standard incidence and mass-action incidence. They demonstrated that when the sickness remains in the

[1] A considerable part of this chapter is published in *Chaos Solitons and Fractals*, **165**, 112785, 2022.

prey population and the predators ingest enough to survive, the disease continues in the predator population. According to Haque *et al.* [163], a sufficiently significant sickness in the prey may prevent predator extinction. Similar findings have been reported in another eco-epidemiological model [164], in which enhanced susceptibility of diseased prey is proven to allow the predator population to survive. Some experimental shreds of evidence show that infectious mortality increases the chance of predation in many eco-epidemiological systems [141, 143]. Nevertheless, too much dependence on diseased prey can harm the predator, decreasing their number [84]. The fear of contracting the disease diverts the predator toward the consumption of healthy prey [144]. An ecosystem is likely to show unpredictability in real. Many ecological and eco-epidemiological systems offer complex dynamics like bifurcation and chaos [165, 166, 167, 168]. Eilersen *et al.* [169] predicted chaos when the disease among prey is contagious enough to last. Shaikh *et al.* [166] detected chaos through the period-doubling route in an eco-epidemic system with additional food.

When predation is a threat, many animals organize groups to protect themselves. There is a plethora of research on ecological systems in which the prey population demonstrates herd behavior [32, 80, 170]. An experimental study reveals that the shoaling behavior of Minnows dilutes the predation risk [78]. The basic model displaying herd behavior was introduced by Ajraldi *et al.* [29]. The fundamental premise is that the predator will not be able to reach the interior prey of the herd. Therefore the predator would only target the nearest prey within the prey group's boundaries. Mathematically, they represented this type of interaction by using the square root of the prey population ($\sqrt{X}$) rather than simply the prey population (X). Such algorithms are limited to 2D pack forms found in prey such as buffalos, lambs, and other animals. However, those algorithms cannot deal with 3D herd forms like birds, fish, and other species. In 2013, Venturino and Petrovskii [30] came up with the elementary concept of generalized herd shape and replaced $\sqrt{X}$ with X^{α}, where $0 < \alpha < 1$. Their study was further extended by Xu *et al.*[31], and then by Bulai and Venturino [32].

Apart from using the herd behavior concept in ecology, many researchers implement it in eco-epidemiology [171, 172]. In the presence of infectious disease, the sound prey can show herd behavior against predation. Gupta and Dubey [80] observed fascinating dynamics in their eco-epidemic model with herd behavior. Banerjee *et al.* [46] used the square root function to show the herd behavior of prey and remarked on the impact of simultaneous feeding of the predator on healthy and sick prey. Time delay integrated with an ODE system makes the model more practicable. A small change in time delay can lead to bifurcation and chaos in the associated system [173]. Moreover, the research on delayed prey-predator models with herd behavior is gaining much attention [170]. Wu and Meng [174] constructed a model incorporating several ecological factors like herd behavior, time delay, etc. They discussed local and

global stability and determined the basic reproduction number associated. Djilali [175] incorporated the concept of generalized herd shape in the classic Holling type II functional response in a time-delayed prey-predator model. The author examined the effect of prey herd shape on the system's dynamics. As the prey herd shape changes, the predator's hunting strategy also modifies, which causes variation in both population densities.

In the physical realm, coordinated behavior by a prey herd has the potential to injure the predator, particularly in the case of larger prey like buffaloes, elephants, and hippopotami, which are incredibly harmful to the predator (lions and hyenas as an example). Every year, many predators die from buffalo horns or hippopotamus bites, demonstrating the enormous strength of the herd's cooperative behavior, and this is the primary purpose for living in congregations that prior studies had overlooked. This is only a sampling of the creatures that may demonstrate this behavior; we can also name other living beings, such as bees, which guard the herd and employs this cooperative method to defend the group, and the ant population, which does the same. In an experimental study by Choh *et al.* [176], it was found that young prey exposed to adult predators modifies their behavior later in life: as adults, they kill juvenile predators at a higher rate. Djilali *et al.* [33] conducted the first investigation to demonstrate that powerful prey might kill the predator. Furthermore, they believed that some time is necessary between the injury of a predator during predation and the predator's death. Motivated by their work, we have the current piece of research.

It is worth noting that none of the research described above discusses the association between various aspects such as generalized herd structure, sickness, prey defense boosting predator lethality, and the time delay between predator injury and death. The current study is an attempt to fill this void.

5.2 The eco-epidemiological framework

Mathematic modeling is commonly used to analyze population dynamics better and understand natural occurrences. Ordinary differential equations are frequently used to study the interaction between prey and predator, which can help with species conservation and population management. This section discusses the formulation of a three-dimensional prey-predator model, where the prey exhibits herd behavior and has an infectious disease, predicated on the following assumptions.

1. We assume that the diseased prey population dies quickly, and reproduction is only evaluated for the vulnerable prey species. However, sick prey contributes to the ecosystem's carrying capacity. The afflicted classes are unable to recover or develop immunity. Either predation or natural death eliminates them. The prey is assumed to grow logistically in

the absence of disease and predator. Thus we have

$$\frac{dS}{dt} = rS\left(1 - \frac{S}{K}\right),$$

where r is the intrinsic growth rate of susceptible prey and K denotes the environmental carrying capacity of prey.

2. The fatal contagious disease divides the prey population into two sub-populations: susceptible prey (S) and infected prey (I). Direct contact is the only way for infection to spread. The saturated incidence rate, i.e., $\frac{\beta SI}{b+S}$, where β is the rate of disease transmission, and b is the half-saturation constant, shows the disease transmission mechanism. Therefore, the basic epidemic model exhibiting prey(S)-prey(I) interaction is given by the set of differential equations below:

$$\begin{aligned}\frac{dS}{dt} &= rS\left(1 - \frac{S+I}{K}\right) - \frac{\beta SI}{b+S},\\ \frac{dI}{dt} &= \frac{\beta SI}{b+S} - \mu_1 I.\end{aligned}$$

Here μ_1 is the natural death rate of infected prey.

3. We believe that the prey's disease cannot be passed on to the predator. Furthermore, the predator cannot differentiate between healthy and diseased prey; it uses both healthy and sick prey, which is reasonable.

4. The weakness in infected prey makes them highly vulnerable to predation. Due to this, the predator's feeding rate for infected prey is reflected by the Holling type I functional response.

5. The healthy prey population forms a herd, and so exhibits social behavior. We consider that prey and predator individuals interact mainly around the perimeter (border) of the pack (herd) produced in 2D space or along the whole surface area of the herd in 3D space. When prey is herded, the interaction between prey and predator is confined to the prey exposed on the herd's exterior. This behavior is reflected through the modified Holling type II functional response. Based on this concept, Djilali *et al.* [33] recently created and studied the following model :

$$\begin{aligned}\frac{dS}{dt} &= rS\left(1 - \frac{S}{K}\right) - \frac{a_1 S^\alpha P}{1 + a_1 \sigma S^\alpha},\\ \frac{dP}{dt} &= \frac{c_1 a_1 S^\alpha P}{1 + a_1 \sigma S^\alpha} - \mu_2 P - \delta_1 S^\alpha P.\end{aligned}$$

Here α is the rate of herd shape such that $\alpha \in (0,1)$.

- When $\alpha = \frac{1}{2}$, the herd shape is a square or circle,
- When $\alpha = \frac{2}{3}$, the herd shape is a sphere or cube.

The last term in the above model displays the role reversal of prey and predator. The strong prey on the outer herd can injure the predator, which can result in the predator's death.

In this chapter, we are using this idea to show the interaction between healthy prey and predator.

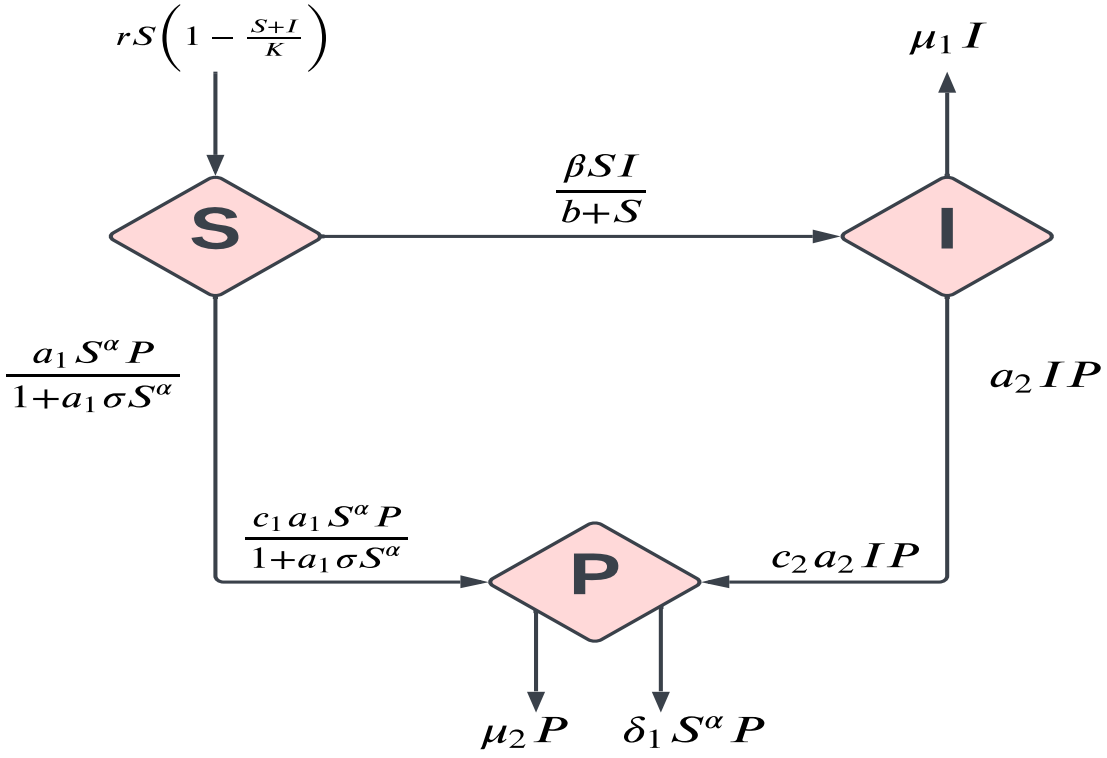

Fig. 5.1: Schematic flowchart for model (5.1).

Fusing all the aforementioned aspects of ecology and epidemiology gives us the following system of ordinary differential equations:

$$\begin{aligned}
\frac{dS}{dt} &= rS\left(1-\frac{S+I}{K}\right) - \frac{\beta SI}{b+S} - \frac{a_1 S^\alpha P}{1+a_1\sigma S^\alpha} = f_1(S,I,P),\\
\frac{dI}{dt} &= \frac{\beta SI}{b+S} - \mu_1 I - a_2 IP = f_2(S,I,P),\\
\frac{dP}{dt} &= \frac{c_1 a_1 S^\alpha P}{1+a_1\sigma S^\alpha} + c_2 a_2 IP - \mu_2 P - \delta_1 S^\alpha P = f_3(S,I,P),
\end{aligned} \tag{5.1}$$

$$S(0) > 0,\ I(0) \geq 0\ P(0) \geq 0.$$

Table 5.1 summarizes the biological meaning and dimension of the parameters and variables used in system (5.1), and Fig. 5.1 depicts the model formulation as a schematic view.

5.3 Well-posedness of the formulated system

In the real world, neither the population number can go negative nor can they grow abruptly. Therefore, well-posedness of the formulated system must be verified first.

Table 5.1: Biological explanation of variables/parameters used in model (5.1)

Variables/Parameters	Biological explanation	Dimension
S	Susceptible prey density	Biomass
I	Infected prey density	Biomass
P	Predator density	Biomass
β	Rate of disease transmission at which the susceptible prey gets infected	Time^{-1}
r	Intrinsic growth rate of susceptible prey	Time^{-1}
K	Environmental carrying capacity of prey	Biomass
a_1	Maximum rate of per capita removal of susceptible prey due to predation	$\text{Biomass}^{-\alpha}\ \text{Time}^{-1}$
a_2	Maximum rate of per capita removal of infected prey due to predation	$\text{Biomass}^{-1}\text{Time}^{-1}$
δ_1	Mortality rate of the predator due to prey group	$\text{Biomass}^{-\alpha}\ \text{Time}^{-1}$
c_1	Conversion rate of the healthy prey to a predator	Dimensionless
c_2	Conversion rate of the infected prey to a predator	Dimensionless
α	Rate of the herd shape	Dimensionless
σ	Time spent by predator in handling healthy prey	Time
b	Half-saturation constant for disease transmission	Biomass
μ_1	Natural death rate of infected prey	Time^{-1}
μ_2	Natural death rate of predator	Time^{-1}

Theorem 5.3.1. *Every solution of system (5.1) beginning from the stated initial condition is unique and positive in* Γ*, where* Γ *is defined in the proof.*

Proof. The concept of herd behavior is based on the case in which the prey population is sufficiently dense to permit a herd formation. Therefore it is biologically reasonable to consider that susceptible prey density is far from zero. Now, we can see that the functions $f_1,\ f_2$ and f_3 in the right-hand side (RHS) of the formulated model system (5.1) are locally Lipschitz-continuous in the region $\Gamma = \{(S,I,P) \in [q,A] \times [0,B] \times [0,C]\}$, with q is a positive real constant. In fact,

it can easily be seen that $\forall S_1,\ S_2 \in \Gamma$,

$$\begin{aligned}|f_1(S_1,I,P)-f_1(S_2,I,P)| &\leq r|S_1-S_2|+\frac{r}{K}|S_1-S_2||S_1+S_2|+\frac{r|I|}{K}|S_1-S_2|+\frac{\beta b|I||S_1-S_2|}{|b+S_1||b+S_2|}\\ &\quad+\frac{a_1|P||S_1-S_2||S_1^{\alpha}-S_2^{\alpha}|}{|S_1-S_2||1+a_1\sigma S_1^{\alpha}||1+a_1\sigma S_2^{\alpha}|}\\ &\leq |S_1-S_2|\Bigg(r+\frac{r(|S_1|+|S_2|)}{K}+\frac{r|I|}{K}+\frac{\beta b|I|}{|b+S_1||b+S_2|}\\ &\quad+\frac{a_1|P|(|S_1|^{\alpha}+|S_2|^{\alpha})}{|1+a_1\sigma S_1^{\alpha}||1+a_1\sigma S_2^{\alpha}||(|S_1|-|S_2|)|}\Bigg)\\ &\leq L|S_1-S_2|,\end{aligned}$$

where

$$L=r+\frac{2rA}{K}+\frac{rB}{K}+\frac{\beta bB}{(b+q)^2}+\frac{2a_1A^{\alpha}C}{(A-q)}>0$$

is the Lipschitz constant. Therefore, $f_1(S,I,P)$ is locally Lipschitz-continuous with respect to S. Similar explanation can be given for f_2 and f_3. Hence the system has a unique solution in the region Γ.

Now, to show the positivity of the solutions, first we need to prove that $S(t)>0\ \forall t>0$. If it is not true, then there exist a $t_1>0$ with $t_1=inf\{t:\ S(t)=0,\ t>0\}$, such that $\frac{dS}{dt}\Big|_{t=t_1}<0$ and $S(t)>0,\ \forall t\in[0,t_1)$. From the first equation of the model (5.1), we observe that

$$\frac{dS}{dt}\Big|_{t=t_1}=rS(t_1)\left(1-\frac{S(t_1)+I(t_1)}{K}\right)-\frac{\beta S(t_1)I(t_1)}{b+S(t_1)}-\frac{a_1S^{\alpha}(t_1)P(t_1)}{1+a_1\sigma S^{\alpha}(t_1)}=0,$$

which contradicts the condition $\frac{dS}{dt}\Big|_{t=t_1}<0$. So, $S(t)>0\ \forall t\geq 0$.
Next, the second and third equations of the model can be written as

$$\frac{dI}{dt}=I\phi_1(S,I,P),\ \ \frac{dP}{dt}=P\phi_2(S,I,P),$$

where

$$\phi_1(S,I,P)=\frac{\beta S}{b+S}-\mu_1-a_2P,\quad \phi_2(S,I,P)=\frac{c_1a_1S^{\alpha}}{1+a_1\sigma S^{\alpha}}+c_2a_2I-\mu_2-\delta_1S^{\alpha}.$$

It follows that

$$I(t)=I(0)e^{\int_0^t\phi_1(S(\theta),I(\theta),P(\theta))d\theta}\geq 0,\ P(t)=P(0)e^{\int_0^t\phi_2(S(\theta),I(\theta),P(\theta))d\theta}\geq 0.$$

Thus, all solutions $(S(t),I(t),P(t))$ with the stated initial condition remain positive $\forall t>0$ [177]. □

Theorem 5.3.2. *All solutions of system (5.1) beginning in R^3_+ stay enclosed in the region $\Omega = \{(S,I,P) : 0 < S+I \leq \frac{(r+\eta_1)^2K}{4r\eta_1},\ 0 < S+\frac{1}{c_1}P \leq \frac{(r+\eta_2)^2K}{4r\eta_2}\}$, where η_1 and η_2 are some real numbers satisfying $0<\eta_1<\mu_1$, $0<\eta_2<\mu_2-\frac{(r+\eta_1)^2Kc_2a_2}{4r\eta_1}$.*

Proof. From the first equation of the model, we can write

$$\frac{dS}{dt} \leq rS\left(1-\frac{S}{K}\right)$$

which implies that

$$\limsup_{t\to\infty} S(t) \leq K.$$

Let $z_1 = S+I$ and $\eta_1 > 0$. Then

$$\begin{aligned}
\frac{dz_1}{dt}+\eta_1 z_1 &= rS\left(1-\frac{S+I}{K}\right)-\frac{a_1S^\alpha P}{1+a_1\sigma S^\alpha}-\mu_1 I-a_2IP+\eta_1(S+I)\\
&\leq rS\left(1-\frac{S}{K}\right)-\mu_1 I+\eta_1(S+I)\\
&\leq (r+\eta_1)S-\frac{rS^2}{K}-(\mu_1-\eta_1)I\\
&\leq (r+\eta_1)S-\frac{rS^2}{K}, \text{ for } \eta_1<\mu_1.
\end{aligned}$$

Define $\kappa(S) = (r+\eta_1)S-\frac{rS^2}{K}$. Then

$$\max_{S\geq 0} \kappa(S) = \frac{(r+\eta_1)^2K}{4r}.$$

Therefore,

$$\frac{dz_1}{dt}+\eta_1 z_1 \leq \frac{(r+\eta_1)^2K}{4r},$$

which implies

$$\limsup_{t\to\infty}(S(t)+I(t)) \leq \frac{(r+\eta_1)^2K}{4r\eta_1}.$$

Now, to check the boundedness of $P(t)$, we consider $z_2 = S+\frac{1}{c_1}P$ and $\eta_2>0$. Then

$$\begin{aligned}
\frac{dz_2}{dt}+\eta_2 z_2 &= rS\left(1-\frac{S+I}{K}\right)-\frac{\beta SI}{b+S}+\frac{c_2a_2}{c_1}IP-\frac{\mu_2}{c_1}P-\frac{\delta_1}{c_1}S^\alpha P+\eta_2 S+\frac{\eta_2}{c_1}P,\\
&\leq (r+\eta_2)S-\frac{rS^2}{K}-\left(\frac{\mu_2}{c_1}-\frac{\eta_2}{c_1}-\frac{c_2a_2I_{max}}{c_1}\right)P, \text{ where } I_{max}=\frac{(r+\eta_1)^2K}{4r\eta_1}.
\end{aligned}$$

Now, for $0 < \eta_2 < \mu_2 - c_2 a_2 I_{max}$, we can write

$$\frac{dz_2}{dt} + \eta_2 z_2 \leq (r+\eta_2)S - \frac{rS^2}{K}$$

which entails that

$$\limsup_{t\to\infty}\left(S(t) + \frac{1}{c_1}P(t)\right) \leq \frac{(r+\eta_2)^2 K}{4r\eta_2}.$$

Hence the theorem follows. □

5.4 Equilibrium points

The proposed system has the following feasible equilibrium points:

$$E_0(0,0,0),\ E_1(K,0,0),\ E_{SI}(S_{SI},I_{SI},0),\ E_{SP}(S_{SP},0,P_{SP}), \text{and } E^*(S^*,I^*,P^*),$$

where $S_{SI} = \frac{\mu_1 b}{\beta-\mu_1}$, $I_{SI} = \frac{rb(K(\beta-\mu_1)-\mu_1 b)}{(K(\beta-\mu_1)+rb)}$. Therefore, the epidemic equilibrium exists if and only if the basic reproduction number $\left(R_0 = \frac{\beta K}{\mu_1(b+K)}\right) > 1$.
The disease-free equilibrium E_{SP} has been extensively studied by Djilali *et al.* [33].
Remark.

(i) If $R_0 < 1$, disease cannot invade.

(ii) If $R_0 > 1$, disease may invade.

The interior equilibrium $E^*(S^*,I^*,P^*)$ of system (5.1) is the positive solution of the following equations:

$$r\left(1 - \frac{S+I}{K}\right) - \frac{\beta I}{b+S} - \frac{a_1 S^{\alpha-1} P}{1+a_1\sigma S^\alpha} = 0,$$

$$\frac{\beta S}{b+S} - \mu_1 - a_2 P = 0,$$

$$\frac{c_1 a_1 S^\alpha}{1+a_1\sigma S^\alpha} + c_2 a_2 I - \mu_2 - \delta_1 S^\alpha = 0.$$

On solving these equations, we obtain

$$I = \frac{1}{c_2 a_2}\left(\mu_2 + \delta_1 S^\alpha - \frac{c_1 a_1 S^\alpha}{1+a_1\sigma S^\alpha}\right), \tag{5.2}$$

$$P = \frac{1}{a_2}\left(\frac{\beta S}{b+S} - \mu_1\right), \tag{5.3}$$

$$f(S) = A_1 S^{\alpha+2} + A_2 S^{\alpha+1} + A_3 S^{2\alpha+1} + A_4 S^{2\alpha} + A_5 S^\alpha + A_6 S^2 + A_7 S + A_8 S^{\alpha-1} + A_9, \tag{5.4}$$

where

$A_1 = rc_2a_2a_1\sigma, A_2 = (rc_2a_2a_1\sigma(b-K)+r(\delta_1-c_1a_1+\mu_2\sigma a_1)), A_3 = ra_1\sigma\delta_1,$
$A_4 = (a_1\sigma\delta_1(\beta K+rb)), A_5 = (a_1c_2K(\beta-\mu_1)+(\beta K+rb)(\delta_1-c_1a_1+\mu_2a_1\sigma)-rKbc_2a_2a_1\sigma),$
$A_6 = rc_2a_2, A_7 = (brc_2a_2-rKc_2a_2+r\mu_2), A_8 = -a_1c_2K\mu_1b, A_9 = -rKbc_2a_2+rb\mu_2+\beta K\mu_2.$

Theorem 5.4.1. *Eq. (5.4) will have a unique positive root S^* if $f(K) > 0$ and $f'(S) > 0$. Furthermore, we can obtain I^* and P^* from Eqs. (5.2) and (5.3), respectively.*

Proof. We can easily observe that as $S \to 0$, $f(S) \to -\infty$. Assume that $f(K)$ is positive and $f(S)$ is an increasing function of S. Then $f(S)$ will intersect at exactly one point on the positive S- axis. For the better realization of this theorem, we consider a numerical example. We take the following set of parameters:

$$r = 0.4,\ K = 30,\ a_1 = 0.5,\ \sigma = 2,\ \mu_2 = 0.5,\ \alpha = 0.1,\ c_1 = 0.85,\ \delta_1 = 0.0145,\ \beta = 5.5,$$
$$b = 12,\ \mu_1 = 2.1,\ a_2 = 2,\ c_2 = 0.17. \tag{5.5}$$

Simple computation yields $f(K) = 128.13996 > 0$ and $f(S)$ is an increasing function. With the help of MATLAB, we obtain Fig. 5.2 showing $f(S)$ crosses the positive S- axis exactly once at $S^* = 16.8232$. Corresponding to this S^*, we obtain $I^* = 0.8145$ and $P^* = 0.55509$ from Eqs. (5.2) and (5.3), respectively.

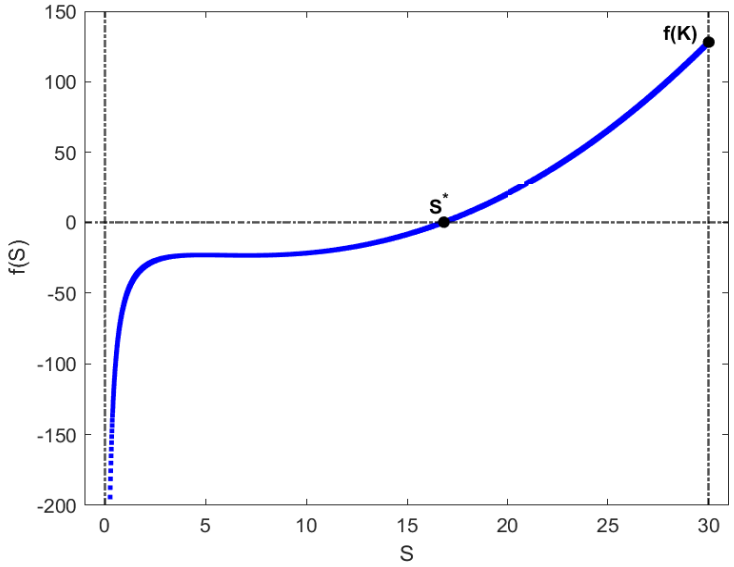

Fig. 5.2: The plot of $f(S)$ vs. S showing unique positive root S^* of Eq. (5.4).

□

Remark. It may be noted here that A_1, A_3, A_4 and A_6 are positive, A_8 is negative and $0 < \alpha < 1$. By computing $f'(S)$, it can be easily be seen that $f'(S) > 0$ if the following conditions hold:

$$A_2 > 0,\ A_5 > 0, \text{and } A_7 > 0.$$

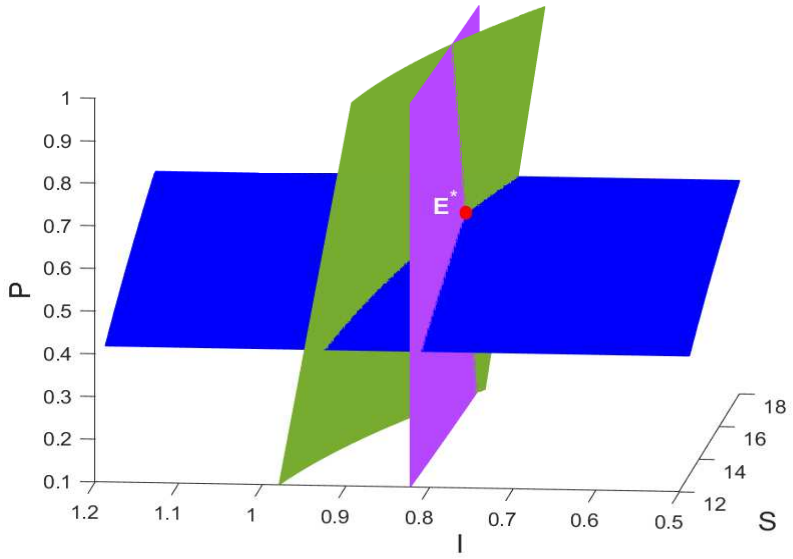

Fig. 5.3: Surface plot displaying existence of $E^*(16.8232, 0.8145, 0.55509)$. Here green color surface is S-nullcline ($f_1(S,I,P) = 0$), blue surface denotes I-nullcline ($f_2(S,I,P) = 0$) and voilet color surface represents P-nullcline ($f_3(S,I,P) = 0$).

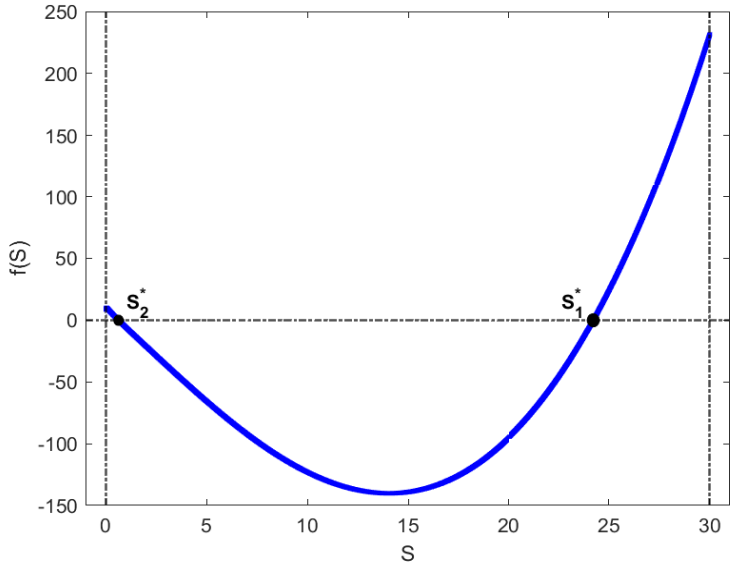

Fig. 5.4: The plot of $f(S)$ vs. S showing two positive roots S_1^* and S_2^* of Eq. (5.4).

To support a unique positive equilibrium, we have a surface plot showing the junction of three nullclines as an interior equilibrium point $E^*(16.8232, 0.8145, 0.55509)$ (see Fig. 5.3).

Due to the complexity of Eq. (5.4), theoretically, it is difficult to determine the number and nature of its roots. However, we can observe numerically that the system can have multiple interior equilibrium points. For the parameter values from Table 5.2, Eq. (5.4) has two positive roots $S_1^* = 24.2275$ and $S_2^* = 0.6339$ (see Fig. 5.4). The corresponding steady-states are $E_1^*(24.2275, 0.6513, 1.1772)$ and $E_2^*(0.6339, 0.9567, 0.118)$.

5.5 Stability assessment

It is appropriate to check the eigenvalues of the variational matrix at each equilibrium point to obtain the local stability requirements. Based on this, we have the following results:

- If $R_0 < 1$ and $\left(R_0^P = \frac{c_1 a_1 K^\alpha}{(1+a_1\sigma K^\alpha)(\mu_2+\delta_1 K^\alpha)}\right) < 1$, then $E_1(K,0,0)$ is locally asymptotically stable. Here R_0^P is the disease-free demographic reproduction number for the predator.
- If $r > \frac{\beta K I_{SI}}{(b+S_{SI})^2}$ and $\frac{c_1 a_1 S_{SI}^\alpha}{1+a_1\sigma S_{SI}} + c_2 a_2 I_{SI} < \mu_2 + \delta_1 S_{SI}^\alpha$, then $E_{SI}(S_{SI}, I_{SI}, 0)$ is locally asymptotically stable.

Remark.

(i) When going through the variational matrix method, we get singularity at the extinction equilibrium E_0. Therefore, we cannot determine the stability behavior of E_0 by this method. However, we obtained the phase portrait displaying E_0 as the saddle point (see Fig. 5.5).

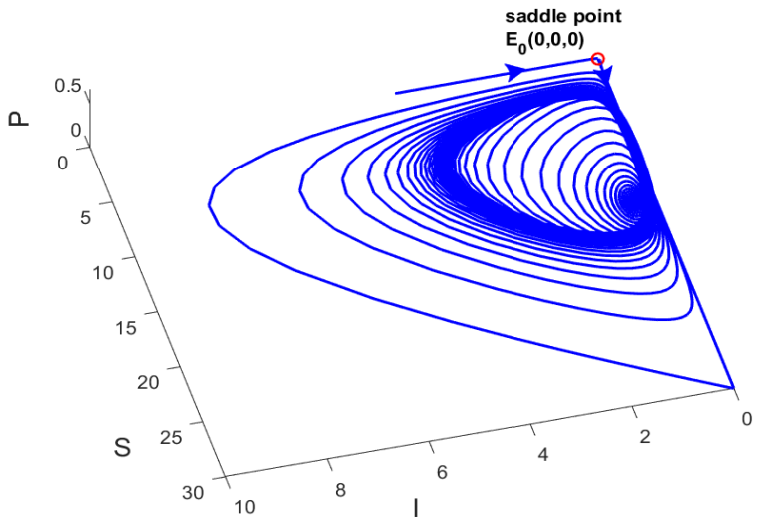

Fig. 5.5: Phase portrait demonstrating saddle nature of $E_0(0,0,0)$ for the parameters set (5.5).

(ii) The existence of predator-free equilibrium E_{SI} directs that E_1 cannot be stable.

(iii) When $R_0^P < 1$, the predator cannot capture prey.

(iv) When $R_0^P > 1$, the predator may capture prey.

Stability of E^*: The variational matrix about the positive equilibrium E^* is

$$M|_{E^*} = \begin{pmatrix} m_{11} & m_{12} & m_{13} \\ m_{21} & m_{22} & m_{23} \\ m_{31} & m_{32} & m_{33} \end{pmatrix},$$

where
$m_{11} = -\frac{rS^*}{K} + \frac{\beta S^* I^*}{(b+S^*)^2} + \frac{a_1(1-\alpha)S^{*(\alpha-1)}P^*}{1+a_1\sigma S^{*\alpha}} + \frac{\alpha a_1^2 \sigma S^{*(2\alpha-1)}P^*}{(1+a_1\sigma S^{*\alpha})^2}$, $m_{12} = -\frac{rS^*}{K} - \frac{\beta S^*}{b+S^*}$,
$m_{13} = -\frac{a_1 S^{*\alpha}}{1+a_1\sigma S^{*\alpha}}$, $m_{21} = \frac{b\beta I^*}{(b+S^*)^2}$, $m_{22} = 0$, $m_{23} = -a_2 I^*$,
$m_{31} = \frac{\alpha c_1 a_1 S^{*(\alpha-1)}P^*}{(1+a_1\sigma S^{*\alpha})^2} - \delta_1 \alpha S^{*(\alpha-1)}P^*$, $m_{32} = c_2 a_2 P^*$, $m_{33} = 0$.
The characteristic equation corresponding to the above matrix is

$$\lambda^3 + B_1\lambda^2 + B_2\lambda + B_3 = 0, \tag{5.6}$$

where $B_1 = -m_{11}$, $B_2 = -m_{23}m_{32} - m_{13}m_{31} - m_{12}m_{21}$ and $B_3 = -det(M|_{E^*})$.
According to the Routh-Hurwitz criteria, E^* is locally asymptotically stable if and only if $B_1 > 0$, $B_3 > 0$, and $B_1B_2 - B_3 > 0$.

Theorem 5.5.1. *The necessary and sufficient conditions for the existence of Hopf-bifurcation around E^* at $\delta_1 = \delta_1^*$ are the following:*

(i) $B_1 > 0$, $B_3 > 0$,

(ii) $B_1B_2 - B_3 = 0$,

(iii) $\left.\frac{dR}{d\delta_1}\right|_{\delta_1=\delta_1^*} \neq 0$, *where* $R = B_1B_2 - B_3$.

Proof. At $\delta_1 = \delta_1^*$, $B_1B_2 - B_3 = 0$, Eq. (5.6) becomes

$$(\lambda + B_1)(\lambda^2 + B_2) = 0.$$

This implies $\lambda_{1,2} = \pm i\sqrt{B_2}$ and $\lambda_3 = -B_1$, where $B_2(\delta_1) > 0$.
Differentiate Eq. (5.6) with respect to δ_1, we obtain

$$\left.\frac{d\lambda}{d\delta_1}\right|_{\delta_1=\delta_1^*} = -\left[\frac{B_1'\lambda^2 + B_2'\lambda + B_3'}{3\lambda^2 + 2B_1\lambda + B_2}\right]_{\delta_1=\delta_1^*}.$$

This implies

$$Re\left[\frac{d\lambda}{d\delta_1}\right]_{\delta_1=\delta_1^*} = -\frac{\frac{dR}{d\delta_1}}{2(B_1^2+B_2)}.$$

Thus, $Re\left[\frac{d\lambda}{d\delta_1}\right]_{\delta_1=\delta_1^*} \neq 0$ if $\frac{dR}{d\delta_1} \neq 0$. Hence the theorem follows. □

Remark. The analysis of Hopf-bifurcation for any other parameter will be identical to that presented in Theorem 5.5.1.

5.6 The effect of time delay on the proposed system

Djilali *et al.* [33] considered a time lag between injury and death of the injured predator. Believing in their idea, we would like to see the effect of such time delay on our proposed model. Model (5.1) in the presence of time delay reduces to the following delay differential equations:

$$\begin{aligned}
\frac{dS}{dt} &= rS\left(1-\frac{S+I}{K}\right) - \frac{\beta SI}{b+S} - \frac{a_1 S^\alpha P}{1+a_1\sigma S^\alpha} = f_1(S,I,P),\\
\frac{dI}{dt} &= \frac{\beta SI}{b+S} - \mu_1 I - a_2 IP = f_2(S,I,P),\\
\frac{dP}{dt} &= \frac{c_1 a_1 S^\alpha P}{1+a_1\sigma S^\alpha} + c_2 a_2 IP - \mu_2 P - \delta_1 (S(t-\tau))^\alpha P(t-\tau) = f_3'(S,I,P),
\end{aligned} \tag{5.7}$$

subject to the non-negative conditions $S(s) = \phi_1(s) > 0$, $I(s) = \phi_2(s) \geq 0$, $P(s) = \phi_3(s) \geq 0$ for $s \in [-\tau, 0]$, where τ is the time duration between injury and the passing away of the predator. System (5.7) can be written in the vector form as

$$\frac{d\psi(t)}{dt} = F_1(\psi(t), \psi(t-\tau)),$$

where

$$\psi(t) = [S(t), I(t), P(t)]^T,\ \psi(t-\tau) = [S(t-\tau), I(t-\tau), P(t-\tau)]^T \text{ and } F_1 = [f_1, f_2, f_3']^T.$$

Let the variational matrix of the delayed system with respect to $\psi(t)$, $\psi(t-\tau)$ at $E^*(S^*, I^*, P^*)$ be

$$V = U_1' + U_2' e^{-\lambda\tau} = \begin{pmatrix} a_{11} & a_{12} & a_{13} \\ a_{21} & a_{22} & a_{23} \\ a_{31} & a_{32} & a_{33} \end{pmatrix},$$

where

$$U_1' = \frac{\partial F_1}{\partial \psi}\bigg|_{(S^*,I^*,P^*)},\ U_2' = \frac{\partial F_1}{\partial \psi(t-\tau)}\bigg|_{(S^*,I^*,P^*)},$$

$$a_{11} = -\frac{rS^*}{K} + \frac{\beta S^* I^*}{(b+S^*)^2} + \frac{a_1 S^{*\alpha-1} P^*(1-\alpha+a_1\sigma S^{*\alpha})}{(1+a_1\sigma S^{*\alpha})^2},\ a_{12} = -\frac{rS^*}{K} - \frac{\beta S^*}{b+S^*},$$

$$a_{13} = -\frac{a_1 S^{*\alpha}}{(1+a_1\sigma S^{*\alpha})},\ a_{21} = \frac{b\beta I^*}{(b+S^*)^2},\ a_{22} = 0,\ a_{23} = -a_2 I^*,$$

$$a_{31} = \alpha S^{*(\alpha-1)} P^*(\frac{c_1 a_1}{(1+a_1\sigma S^{*\alpha})^2} - \delta_1 e^{-\lambda\tau}),\ a_{32} = c_2 a_2 P^*,\ a_{33} = \delta_1 S^{*\alpha}(P^* - e^{-\lambda\tau}).$$

The characteristic equation of the above matrix is given by following equation:

$$\lambda^3 + n_1\lambda^2 + n_2\lambda + n_3 + (\lambda^2 + n_4\lambda + n_5)\rho e^{-\lambda\tau} = 0, \tag{5.8}$$

where

$$n_1 = -a_{11} - \rho P^*,\ n_2 = c_2 a_2^2 I^* P^* + a_{11}\rho P^* + \frac{c_1 a_1^2 \alpha S^{*2\alpha-1} P^*}{(1+a_1\sigma S^{*\alpha})^3} + \left(\frac{r}{K} + \frac{\beta}{b+S^*}\right)\frac{b\beta S^* I^*}{(b+S^*)^2},$$

$$n_3 = -a_{11}c_2 a_2^2 I^* P^* - \left(\frac{rS^*}{K} + \frac{\beta S^*}{b+S^*}\right)\left(\frac{b\beta\rho I^* P^*}{(b+S^*)^2} + \frac{c_1 a_1 a_2 \alpha S^{*\alpha-1} I^* P^*}{(1+a_1\sigma S^{*\alpha})^2}\right) + \frac{a_1 a_2 c_2 b\beta S^{*\alpha} I^* P^*}{(b+S^*)^2(1+a_1\sigma S^{*\alpha})},$$

$$n_4 = \frac{rS^*}{K} - \frac{\beta S^* I^*}{(b+S^*)^2} - \frac{a_1 S^{*\alpha-1} P^*(1-\alpha+a_1\sigma S^{*\alpha})}{(1+a_1\sigma S^{*\alpha})^2} - a_1 a_2 \alpha S^{*\alpha-1} P^*,$$

$$n_5 = (\frac{r}{K} + \frac{\beta}{b+S^*})(\frac{b\beta S^* I^*}{(b+S^*)^2} + a_2\alpha I^* P^*),\ \rho = \delta_1 S^{*\alpha},.$$

System (5.7) is stable around the positive equilibrium point $E^*(S^*, I^*, P^*)$ if all the characteristic roots of Eq. (5.8) have a negative real component. In order to show switching of stability via Hopf-bifurcation, the characteristic root must cross the imaginary axis. As a result, we suppose that $i\omega$ $(\omega > 0)$ is the root of Eq. (5.8). Then the real and imaginary parts of Eq. (5.8) is given by

$$(n_5 - \omega^2)\rho cos(\omega\tau) + n_4\omega\rho sin(\omega\tau) = n_1\omega^2 - n_3, \tag{5.9}$$

$$\rho n_4\omega cos(\omega\tau) - \rho(n_5 - \omega^2)sin(\omega\tau) = \omega^3 - n_2\omega. \tag{5.10}$$

Squaring and adding the above two equations, we get the following sextic equation:

$$\omega^6 + q_1\omega^4 + q_2\omega^2 + q_3 = 0, \tag{5.11}$$

where

$$q_1 = n_1^2 - 2n_2 - \rho^2,\ q_2 = n_2^2 - 2n_1 n_3 + 2n_5\rho^2 - n_4^2\rho^2,\ q_3 = n_3^2 - n_5^2\rho^2.$$

The critical value of τ can be determined by calculating $\{[Eq.(5.9)] \times n_4\omega - [Eq.(5.10)] \times (n_5 - \omega^2)\}$, which results

$$\tau_j = \frac{1}{\omega_1}\left\{ sin^{-1}\left[\frac{(n_1\omega_1^2 - n_3)n_4\omega_1 + \omega_1(n_2 - \omega_1^2)(n_5 - \omega_1^2)}{\rho((n_5 - \omega_1^2)^2 + n_4^2\omega_1^2)}\right] + 2\pi j\right\}, \quad j = 0,1,2,... \tag{5.12}$$

For the positivity of τ_j, the range of $sin(\omega\tau)$ should be positive. Therefore, τ_j is positive if the following inequality holds:

$$(n_1n_4 - n_2 - n_5)^2 < 4(n_2n_5 - n_3n_4).$$

To test the transversality criterion for Hopf-bifurcation, substitute $\lambda = \xi + i\omega$ in Eq. (5.8), and then separate real and imaginary components to obtain

$$\begin{aligned}&\xi^3 - 3\omega^2\xi + n_1(\xi^2 - \omega^2) + n_2\xi + n_3 + \rho(\xi^2 - \omega^2 + n_4\xi + n_5)e^{-\xi\tau}cos(\omega\tau)\\ &+ \rho\omega e^{-\xi\tau}sin(\omega\tau)(2\xi + n_4) = 0,\end{aligned} \tag{5.13}$$

$$\begin{aligned}&-\omega^3 + 3\xi^2\omega + 2n_1\xi\omega + n_2\omega - \rho e^{-\xi\tau}sin(\omega\tau)(\xi^2 - \omega^2 + n_4\xi + n_5)\\ &+ \rho\omega e^{-\xi\tau}cos(\omega\tau)(2n_3\xi + n_4) = 0.\end{aligned} \tag{5.14}$$

When we differentiate Eqs. (5.13) and (5.14) with regard to τ and set $\xi = 0$ (the system loses stability when $Re(\lambda) = 0$) and $\tau = \tau_0$, we get

$$M_1\xi_{\tau_0} + M_2\omega_{\tau_0} = N_1, \tag{5.15}$$

$$-M_2\xi_{\tau_0} + M_1\omega_{\tau_0} = N_2, \tag{5.16}$$

where

$$M_1 = \rho(\tau_0(\omega_1^2 - n_5) + n_4)cos(\omega_1\tau_0) + \rho\omega_1(2 - \tau_0n_4)sin(\omega_1\tau_0) + n_2 - 3\omega_1^2,$$

$$M_2 = \rho\omega_1(-2 + \tau_0n_4)cos(\omega_1\tau_0) + \rho(n_4 + \tau_0(\omega_1^2 - n_5))sin(\omega_1\tau_0) - 2n_1\omega_1,$$

$$N_1 = \rho\omega_1(n_5 - \omega_1^2)sin(\omega_1\tau_0) - n_4\omega_1^2cos(\omega_1\tau_0),$$

$$N_2 = \rho\omega_1(n_5 - \omega_1^2)cos(\omega_1\tau_0) + n_4\omega_1^2sin(\omega_1\tau_0).$$

Solving Eqs. (5.15) and (5.16), we obtain

$$\left.\frac{d(Re(\lambda))}{d\tau}\right|_{\tau=\tau_0} = \xi_{\tau_0} = \frac{N_1M_1 - N_2M_2}{M_1^2 + M_2^2}.$$

Hence the transversality condition

$$\left.\frac{d(Re(\lambda))}{d\tau}\right|_{\tau=\tau_0} \neq 0 \text{ holds, if } N_1M_1 \neq N_2M_2.$$

Theorem 5.6.1. *System (5.7) undergoes Hopf-bifurcation with respect to τ at $\tau = \tau_0(\tau_0 > 0)$ such that E^* is locally asymptotically stable when $\tau < \tau_0$, and unstable when $\tau > \tau_0$, if $N_1M_1 \neq N_2M_2$ at $\tau = \tau_0$.*

5.7 Numerical simulation

We begin by numerically simulating system (5.1) using the parameter values given in Table 5.2. The system exhibits four equilibrium points listed in Table 5.3 with eigenvalues. Figure 5.6 displays the phase portrait diagram corresponding to the Table 5.3. It shows the bi-stability between an interior equilibrium and a limit cycle surrounding a planar equilibrium and other points' stability behavior based on the eigenvalues mentioned in Table 5.3.

Table 5.2: Data set of parameters involved in (5.1) with sources.

Parameters	Numerical value	Source(s)
r	0.5	[33]
K	30	Assumed
a_1	0.5	[175]
a_2	2	[130]
σ	2	[175]
μ_1	0.05	[80]
μ_2	0.5	[33]
c_1	0.85	[33]
c_2	0.17	Assumed
β	3	[178]
b	6	Assumed
δ_1	0.0145	[33]
α	0.55	[33]

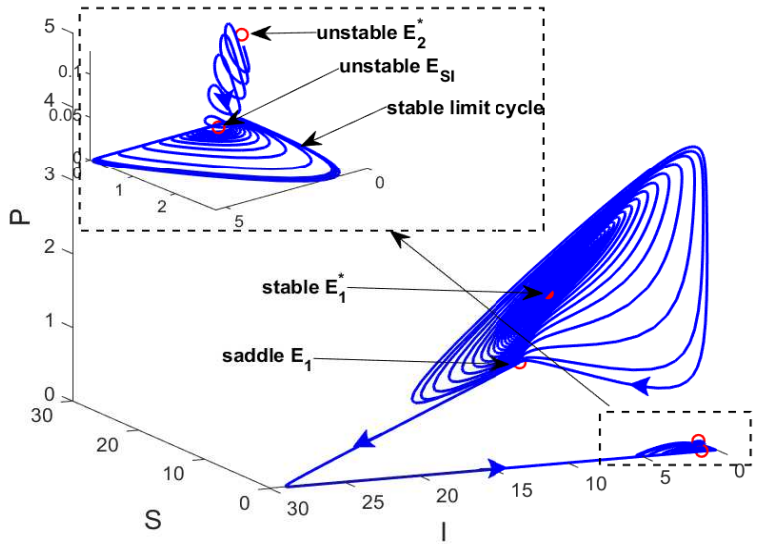

Fig. 5.6: Phase portrait showing all existing steady-states for the parametric values given in Table 5.2.

Table 5.3: Eigenvalues of equilibrium points associated with dataset given in Table 5.2.

Equilibrium points	Eigenvalues
$E_1^*(24.2275, 0.6513, 1.1772)$	$-0.322,\ -0.005 \pm 0.744i$
$E_2^*(0.6339, 0.9567, 0.118)$	$0.012 \pm 0.4408i,\ 0.0336$
$E_1(30, 0, 0)$	$-0.5,\ 2.45,\ -0.2258$
$E_{SI}(0.1016, 0.9802, 0)$	$0.0031 \pm 0.1564i,\ -0.0767$

Effect of predator mortality due to prey group (δ_1): Initially, for low values of δ_1, system (5.1) is locally asymptotically stable about the positive equilibrium E^* (see Fig. 5.7 (a)). With a slight increase in the value of δ_1, system (5.1) undergoes Hopf-bifurcation at $\delta_1 = \delta_1^* = 0.077446$. At the Hopf-bifurcation point, $E^*(24.008731, 0.832865, 1.150008)$ exists with $B_1 = 0.3307591$, $B_2 = 0.295172175$, and $B_3 = 0.09763095$, which yields all conditions mentioned in Theorem 5.5.1 are fulfilled. Then afterward, interior equilibrium E^* is unstable, and a stable limit cycle is observed around it for $\delta_1 \in (0.077446, 0.219583)$ (see Fig. 5.7 (b)). In this range, the oscillations in the system become so high that eventually, it touches the axis of predator-free equilibrium $E_{SI}(14, 1.6, 0)$ at $\delta_1^{**} = 0.219583$. Therefore, the epidemic state $E_{SI}(14, 1.6, 0)$ is a

stable focus for the higher values of δ_1 (see Fig. 5.7 (c)). We generated bifurcation diagrams for all three populations S, I, and P with respect to δ_1 to comprehend better the system's dynamics owing to Hopf-bifurcation (see Fig. 5.8).

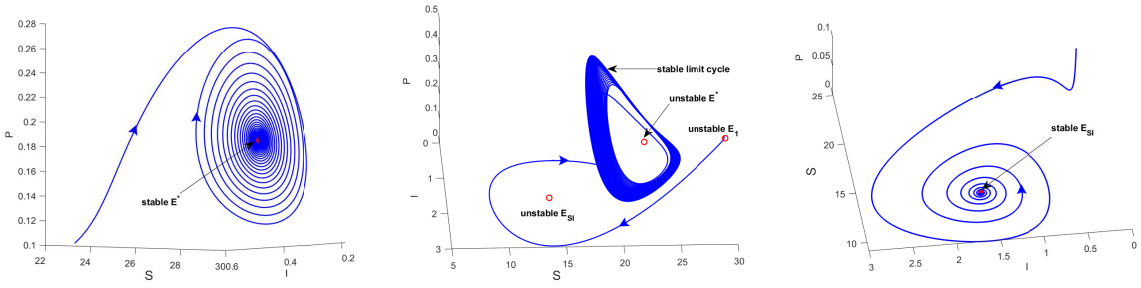

(a) (b) (c)

Fig. 5.7: Effect of δ_1 on system (5.1)'s dynamics at (a) $\delta_1 = 0.02$, (b) $\delta_1 = 0.1$, (c) $\delta_1 = 0.5$. The parameter values are: $\alpha = 0.7,\ \mu_1 = 2.1,\ c_2 = 0.5$, rest of the parameters are taken from Table 5.2.

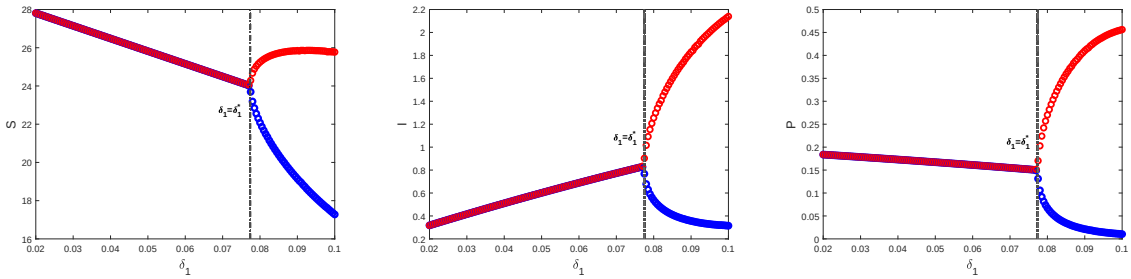

(a) (b) (c)

Fig. 5.8: Hopf-bifurcation diagram for δ_1 exhibiting the emergence of periodic oscillations after the bifurcation point $\delta_1 = \delta_1^* = 0.077446$. Red and blue colors represent the maximum and minimum of the positive solution in the non-transient period, respectively. For $\delta_1 < \delta_1^*$, the coinciding of maximum and minimum values demonstrate the stability of E^*. After that, the solution fluctuates between its maximum and minimum values, becoming unstable.

Effect of herd shape (α): In Fig. 5.9, the impact of different herd shapes on temporal dynamics of system (5.1) is highlighted. For multiple values of α, we plot the time series curve of healthy prey (S), infected prey (I), and predator (P). For $\alpha = 0.1,\ 0.5$, the system shows stable dynamics around interior equilibrium E^*. Whereas the system shows periodic oscillations around E^* for $\alpha = 0.67$. This switching of stability occurs via a supercritical Hopf-bifurcation at $\alpha = \alpha^* = 0.6621$. To demonstrate this phenomenon in a better way, we plot bifurcation diagrams for S, I and P concerning α as the bifurcation parameter (see Fig. 5.10).

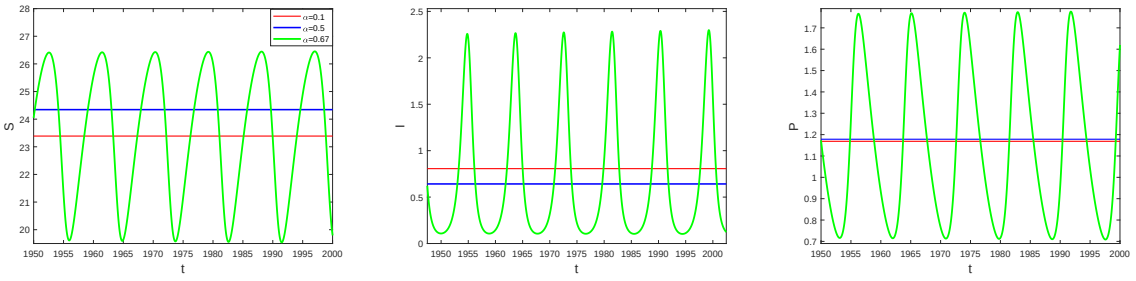

(a) (b) (c)

Fig. 5.9: Time series curve depicting the influence of the prey's herd shape α on the population density (a) Susceptible prey, (b) Infected prey and (c) Predator. The parameters values are taken from Table 5.2.

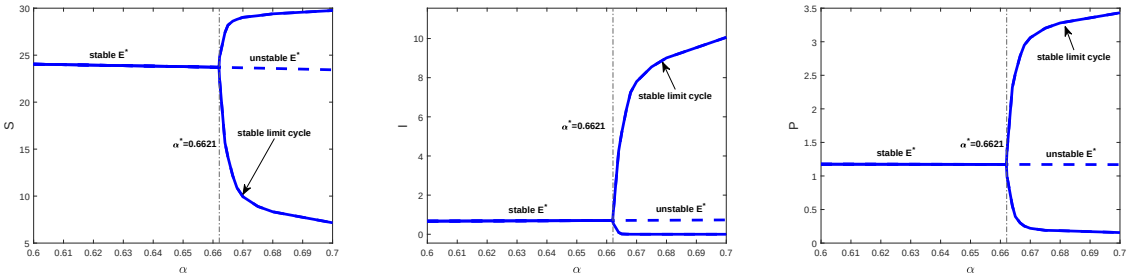

(a) (b) (c)

Fig. 5.10: Bifurcation diagram with respect to α.

Effect of disease transmission (β): The infectious disease among prey has an immense impact on the dynamics of the proposed model. The system experiences transcritical bifurcation twice with the variation in the disease transmission rate β for different steady-states. We can see from Fig. 5.11 that for high values of β, such that $\beta \in (2.58, 2.9)$, three steady-states are present: Disease-free and predator-free state E_1, epidemic state E_{SI}, and co-existence state E^*. Out of these three states, E^* is locally asymptotically stable, and the rest two are saddle points. Each color in Fig. 5.11 represents different equilibrium. Red color denotes E^*, blue color denotes E_{SI}, and magenta color is for E_1. A stable state is represented by the solid curve, whereas a dashed curve shows the saddle nature of an equilibrium point. With a decrease in β, the interior equilibrium E^* transfers its stability to the epidemic state E_{SI} through a transcritical bifurcation at $\beta = \beta^{**} = 2.58$ (shown by green color point). Meanwhile, E_1 remains a saddle-point. The saddle nature of E_1 changes when β further decreases. The system undergoes another transcritical bifurcation when E_{SI} passes stability to E_1 at $\beta = \beta^* = 2.52$.

Sotomayor's theorem validation for transcritical bifurcation: In order to show the transcritical bifurcation for system (5.1), concerning disease transmission rate β, we consider $\mu_1 = 2.1$, and other parameters from Table 5.2. For the chosen set, $E_1(30,0,0)$ is a non-hyperbolic equilibrium at $\beta = \beta^* = 2.52$. The Jacobian matrix about E_1 at $\beta = \beta^*$ is given by

$$H = \begin{pmatrix} -0.5 & -2.6 & -0.43326 \\ 0 & 0 & 0 \\ 0 & 0 & -0.2258 \end{pmatrix}.$$

The eigenvectors corresponding to zero eigenvalue of H and H^T are $v = (-5.2,\ 1,\ 0)^T$ and $w = (0,\ 1,\ 0)^T$, respectively. Now, we define

$$\Delta_1 = w^T F_\beta(E_1, \beta^*),$$

$$\Delta_2 = w^T DF_\beta(E_1, \beta^*)v,$$

and

$$\Delta_3 = w^T [D^2F(E_1, \beta^*)(v,v)],$$

where $F = (f_1, f_2, f_3)^T$, F_β is the derivative of F with respect to β, DF and D^2F are first order and second order derivatives of F.
Simple calculation yields

$$F_\beta(E_1, \beta^*) = (0,0,0)^T \text{ which implies } \Delta_1 = 0,$$

$$DF_\beta(E_1, \beta^*) = \begin{pmatrix} 0 & -0.83333 & 0 \\ 0 & 0.83333 & 0 \\ 0 & 0 & 0 \end{pmatrix} \text{ which implies } \Delta_2 = 0.83333 \neq 0,$$

$$D^2F_\beta(E_1, \beta^*)(v,v) = \begin{pmatrix} f_{1_{SS}} v_1^2 + 2f_{1_{SI}} v_1 v_2 + 2f_{1_{SP}} v_1 v_3 \\ 2f_{2_{SI}} v_1 v_2 + 2f_{2_{IP}} v_2 v_3 \\ 2f_{3_{SP}} v_1 v_3 + 2f_{3_{IP}} v_2 v_3 \end{pmatrix} \text{ which implies } \Delta_3 = -0.121333 \neq 0.$$

All conditions of the Sotomayor's theorem [60] are satisfied. Therefore, system (5.1) experiences transcritical bifurcation about $E_1(30,0,0)$ at $\beta = \beta^* = 2.52$.
Remark. The validation of Sotomayor's theorem for transcritical bifurcation at $\beta = \beta^{**}$ will be the same as the above process.

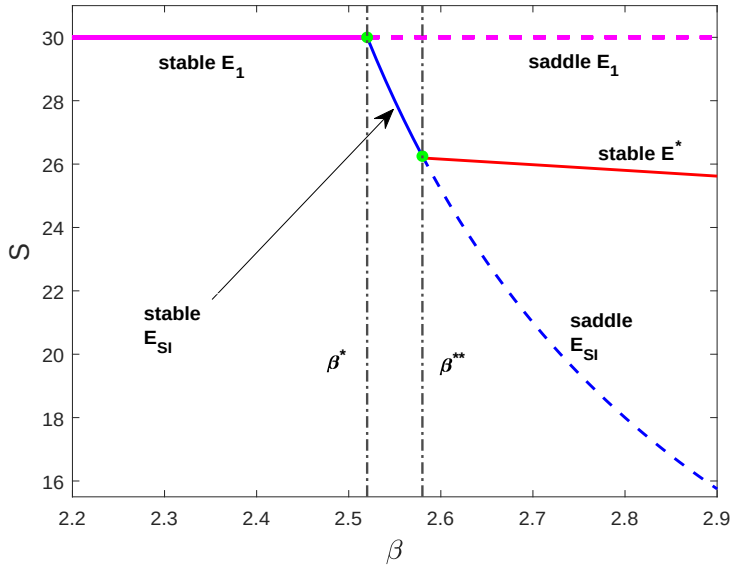

Fig. 5.11: Transcritical bifurcation diagram demonstrating the transition of stability between E_1, E_{SI} and E^* with respect to β, where $\mu_1 = 2.1$ and other parameters are same as in Table 5.2. The green dots denote the bifurcation points $\beta^* = 2.52$ and $\beta^{**} = 2.58$

Effect of predation rate for susceptible prey (a_1): The attack rate of the predator to hunt the healthy prey (predation rate) is a crucial parameter that governs the intricate dynamics of the system. Fig 5.12 depicts the geometric representations of system (5.1)'s solutions with the minor change in a_1. When a_1 is small, at $a_1 = 0.08$, the system is stable about the positive steady-state E^* (Fig. 5.12 (a)). Due to the Hopf-bifurcation, species begin to oscillate periodically at the bifurcation point $a_1 = a_1^* = 0.1593$. The phase portrait at $a_1 = 0.3$ (Fig. 5.12 (b)) displays the after bifurcation scenario. The limit cycle approach to the saddle point creates a homoclinic loop as we move from Fig. 5.12 (b) to (c). With the further increase in a_1, species oscillate between two maximum and two minimum values. Therefore, the stable limit cycle of period two occurs (Fig. 5.12 (d)). Furthermore, the period of oscillation increases with the rise in a_1. At $a_1 = 0.6$, the system has a period four stable limit cycle (see Fig5.12 (e)). When the attack rate is sufficiently large, the system enters a chaotic regime. We can see from the phase portrait diagram at $a_1 = 0.9$ (Fig. 5.12 (f)) that the presence of a chaotic attractor shows the unpredictability of the solution. For the chaos detection, we checked the sensitivity of the solution toward the initial condition. A slight adjustment to the initial solution can yield considerable variation in the final solution. Fig. 5.13 depicts the sensitivity of solution (S,I,P) for initial conditions $(10,0.5,0.5)$ and $(10,0.51,0.51)$. Moreover, the maximum Lyapunov exponent sketched in Fig. 5.14 is a standard method to verify the existence of chaos. For $a_1 \in (0.8,1.5)$, the positivity of the maximum Lyapunov exponent confirms the chaotic trait.

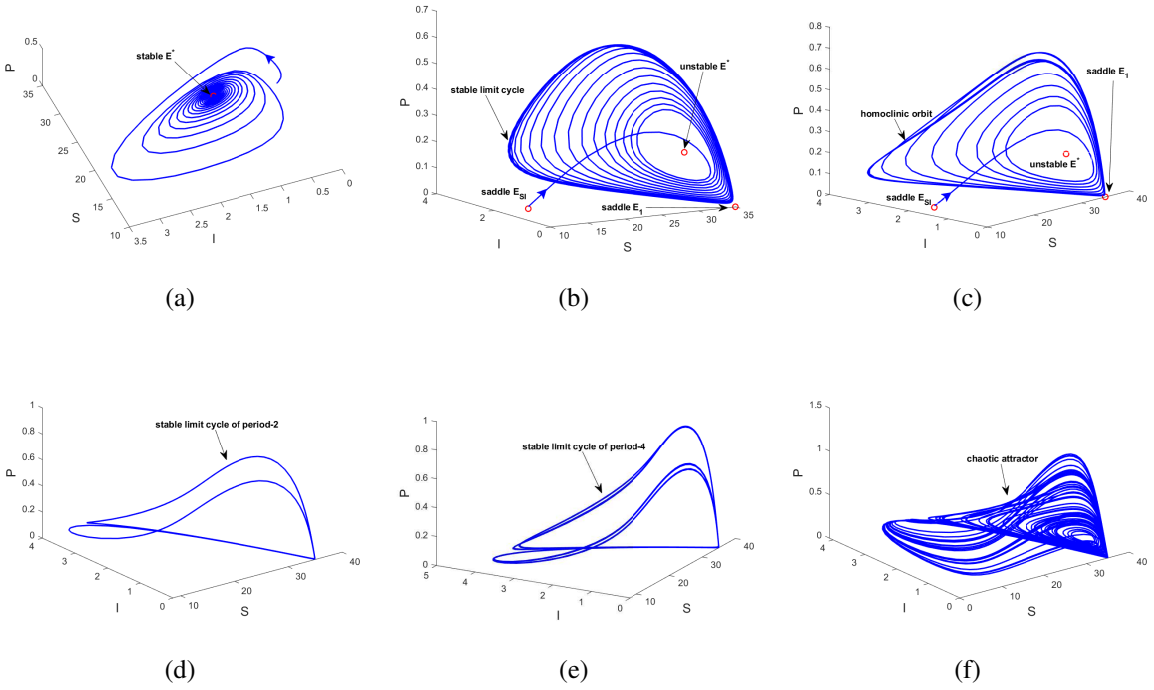

(a) (b) (c)

(d) (e) (f)

Fig. 5.12: Phase portraits showing complex dynamics of system (5.1) for different values of a_1 at (a) $a_1 = 0.08$, (b)$a_1 = 0.3$, (c) $a_1 = 0.4$, (d) $a_1 = 0.55$, (e) $a_1 = 0.6$, (f) $a_1 = 0.9$.

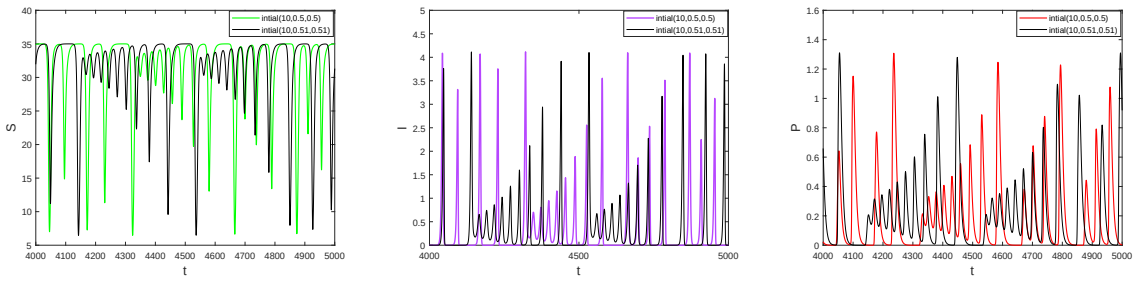

(a) (b) (c)

Fig. 5.13: Sensitivity of trajectories with initial condition at $a_1 = 0.9$.

Effect of time delay (τ): Every procedure has a time lag that must be taken into account. The addition of time delay to the system adds realism by emphasizing the future state's dependency on the past form [55]. The dynamical behavior of delayed systems has been the subject of several studies [156, 179, 180, 181].

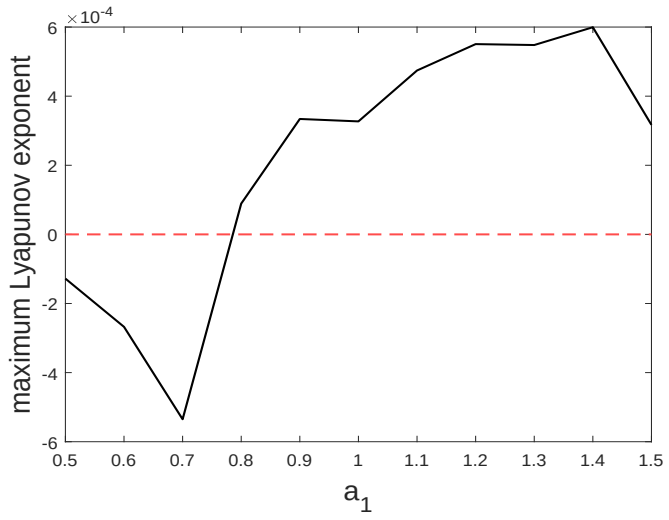

Fig. 5.14: Maximum Lyapunov exponent with respect to a_1.

Here we present the numerical simulation for the theoretical results obtained in Section 5.6. The numeric value of the interior equilibrium is unaffected by the variation of the delay parameter. Therefore, for the parameters in Table 5.2, $E^*(24.2275304, 0.6513395, 1.1772581)$ exists irrespective of time lag. However, its stability is tremendously affected by death delay τ. Initially for $\tau = 0$, $E^*(24.2275304, 0.6513395, 1.1772581)$ is locally asymptotically stable (see Fig. 5.6). With the rise in the value of τ, the magnitude of the real part of the complex eigenvalue decreases and becomes zero at $\tau = \tau_0 = 0.611518$. On crossing this critical value of τ, all populations oscillate about the positive steady state by means of Hopf-bifurcation. To determine the critical value of τ, we find the positive root $\omega_1 = 0.759011$ from the six degree equation (5.11), and corresponding to it, we calculate the value of τ_0 (the critical value of τ for Hopf-bifurcation) from the formula stated in (5.12), which is obtained as $\tau_0 = 0.611518$. Moreover, the transversality condition holds at $\tau = \tau_0$ as $N_1M_1 - N_2M_2 = 0.223011 \neq 0$ The dynamics of system (5.7) before (at $\tau = 0.5$) and after (at $\tau = 0.7$) Hopf-bifurcation are demonstrated in Fig. 5.15 and Fig. 5.16, respectively.

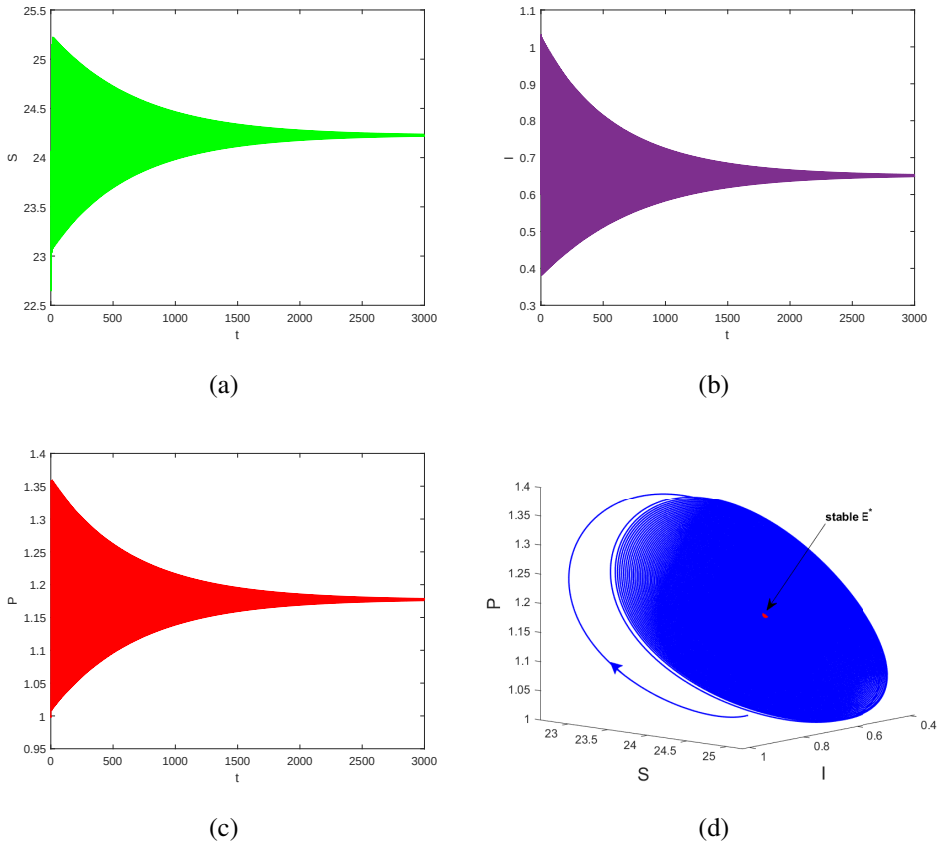

(a) (b)

(c) (d)

Fig. 5.15: Graphical demonstration of system (5.7)'s solutions at $\tau = 0.5$. Here (a), (b), and (c) display the temporal dynamics for all interacting species. (d) is the phase portrait instancing the convergence of solution towards E^*.

Based on the preceding findings, we have observed that α and δ_1 are the crucial parameters that contribute to the complex dynamics of the proposed eco-epidemic system. This inspires us to perform the bi-parametric analysis in the $\delta_1\alpha$-plane. We find a critical value of α for each value of δ_1 (and vice-versa), at which the system suffers Hopf-bifurcation. Connecting all these points forms a Hopf-bifurcation curve. We have drawn these curves in absence and presence of time delay for three different values of τ, $\tau = 0,\ 0.5,\ 1$ in Fig. 5.17. It can be observed from the figure that when τ increases, the Hopf-bifurcation curve shifts downwards with the almost same shape. The internal equilibrium E^* is stable below the curve, but unstable above it, with a stable limit cycle surrounding it.

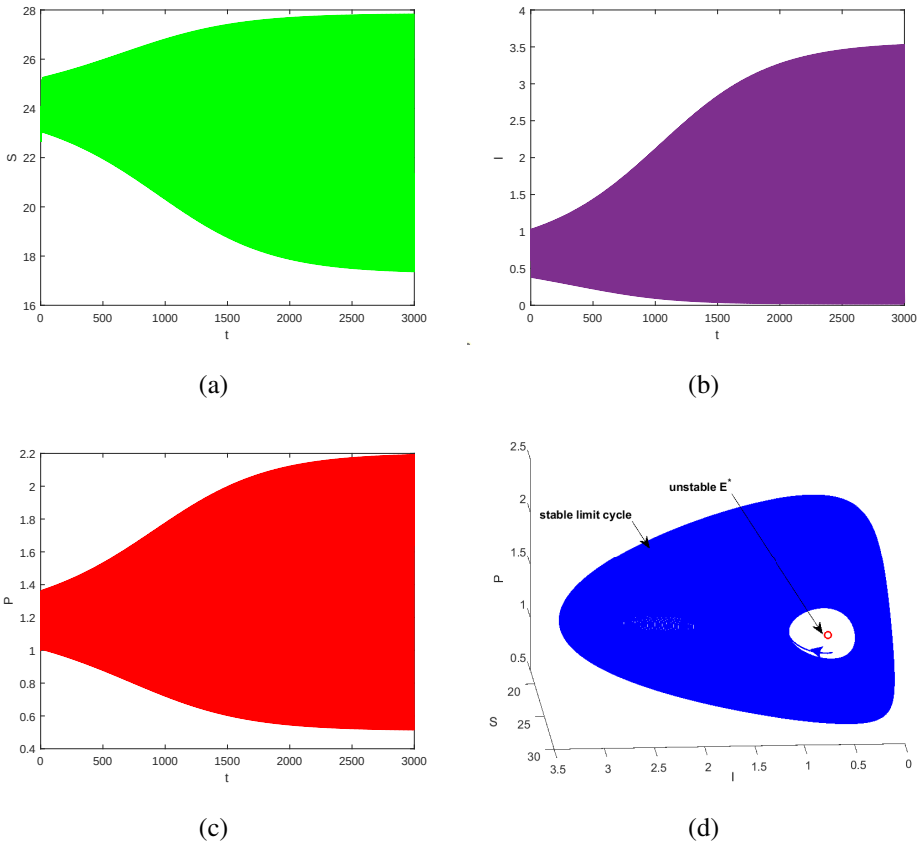

(a) (b)

(c) (d)

Fig. 5.16: Graphical illustration of system (5.7)'s solutions at $\tau = 0.7$. (a), (b) and (c) show that all solutions oscillate between maximum and minimum values as a consequence of Hopf-bifurcation. The corresponding phase portrait (d) represents the existence of a stable limit cycle around repelling E^*.

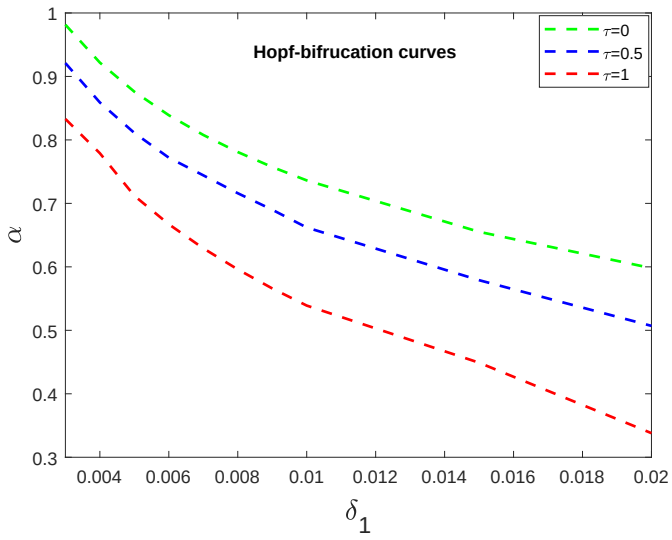

Fig. 5.17: Two parameter bifurcation diagram in $\delta_1\,\alpha$- plane for distinct values of τ.

Sensitivity analysis

In epidemiology, the basic reproduction number R_0 is a pivotal metric. Another reproduction number named disease-free demographic reproduction number R_0^P is an important figure in eco-epidemiology. Both reproduction numbers are influential to the characteristics of an eco-epidemic model. Model (5.1) must be subjected to sensitivity analysis to determine the relative change in the reproduction numbers R_0 and R_0^P to the relative change in its control attributes. The normalized forward sensitivity index of differentiable R_0 and R_0^P dependent on any of its parameters p is defined as follows.

$$\gamma_p^{R_0} = \frac{\partial R_0}{\partial p}\frac{p}{R_0},\ \gamma_p^{R_0^P} = \frac{\partial R_0^P}{\partial p}\frac{p}{R_0^P}, \tag{5.17}$$

where $\gamma_p^{R_0}$ and $\gamma_p^{R_0^P}$ represent the sensitivity level with regard to any parameter p for R_0 and R_0^P, respectively. In our model system, we have

$$R_0 = \frac{\beta K}{\mu_1(b+K)},\ R_0^P = \frac{c_1 a_1 K^\alpha}{(1+a_1\sigma K^\alpha)(\mu_2+\delta_1 K^\alpha)}.$$

Considering the parameter values from Table 5.2, we can calculate $\gamma_p^{R_0}$ and $\gamma_p^{R_0^P}$ for the associated parameters using (5.17). As a result, Fig. 5.18 visually depicts the sensitivity indexes for model (5.1). A positive sensitivity index implies that an increase (or decrease) in the value of a parameter corresponds to an increase (or decrease) in the reproduction number. In contrast, negative index parameters indicate that a rise (or reduction) in the value of the parameter results in a drop (or increase) in the reproduction number [182].

Observations from Fig. 5.18:

- β, μ_1 are the most sensitive parameters for R_0, and c_1 is most sensitive for R_0^P, i.e., 100% influential.
- R_0 will drop (or rise) by 16.66% if the value of b or K is increased.
- The most sensitive metric of all the negative indices in Fig. 5.18 (right) is the predator's handling time for healthy prey, denoted by σ. It means that changing the value of σ lowers (or raises) the value of R_0^P by 86.65%.
- System is least sensitive for R_0^P with respect to K, i.e., 1.37%.

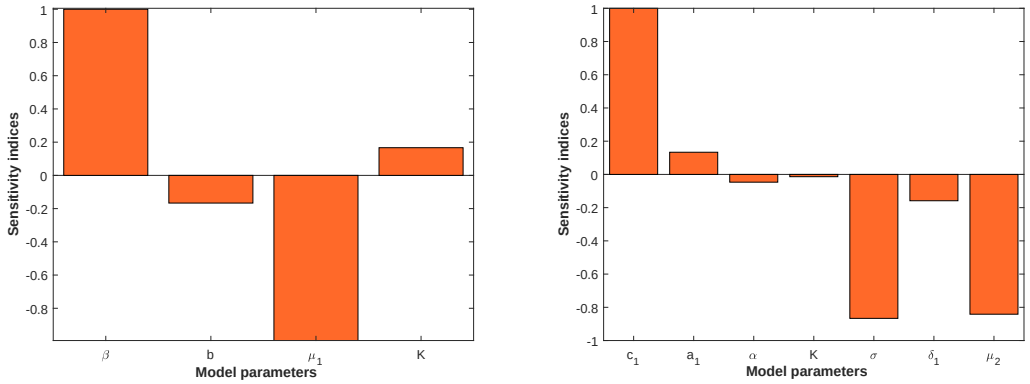

(a) (b)

Fig. 5.18: Sensitivity of R_0 (left) and R_0^P (right) for the associated parameters.

5.8 Discussion and conclusion

This article investigates the dynamical behavior of a prey-predator system where the prey develops an infectious disease. This illness cannot be communicated to their progeny and predators consuming them. The prey unaffected by the disease is assumed to be strong, therefore, performs group defense against the predator. Many animals, including buffaloes, gnus, bees, ants, elephants, sardines, and tunas, engage in this activity. This behavior may be observed in nature when prey moves in large herds. The most appealing aspect of this behavior is the slightly odd interaction between the two species (prey and predator); the predator hunts the prey on the herd's borders, leading to the conclusion that the number of prey victimized by a predator is proportional to the number of prey on the group's confinement. The herd form is square or circle when $\alpha = 1/2$. Some species, such as birds and fish, do not always follow this regular pattern; instead, they create spherical or cubical formations; hence, the rate of herd shape α is $2/3$. To generalize the forms, we assumed that the rate of herd shape α is between 0 and 1. Recently, Djilali *et al.* [33] highlighted the external competition between strong prey and predator. According to them, the prey on the fence of the herd can injure or kill the predator. Moreover, they used the fact that injury and passing away of the predator are not instantaneous and therefore investigated the system for the time delay. We incorporated these aspects of ecology in our model to fit the real-life situation better.

The proposed model behaves well, as all solutions are positive and bounded. We determined all feasible steady-states of the system and examined the co-existence of species S, I, and P. Theoretically and numerically, their local stability behavior has been explored enormously. When predator-free equilibrium E_{SI} exists, the healthy-prey only state E_1 cannot be stable. Sauna *et al.* [183] designed and analyzed the interaction of grouped prey, solitary prey,

and predator for $\alpha = 0.5$. Their mathematical results reveal that grouped prey will go extinct when lone prey and predator are absent. On the other hand, our work proves the survival of prey exhibiting herd behavior even when lone prey and predator die out ($E_1(K,0,0)$ is locally asymptotically stable under some conditions). The stability of E_1 depends on the two key numerals: the basic reproduction number R_0 and the disease-free demographic reproduction number for the predator R_0^P. The grouped prey can survive (E_1 is stable) when these numerals are less than unity, which conveys the benefit of living in herds. We observed that the system experiences Hopf-bifurcation about E^* for herd shape rate at $\alpha = 0.6621$. Djilali *et al.* [33] reported a similar phenomenon at $\alpha \in (0.6, 0.7)$ in the absence of disease. Furthermore, our work and their research show that an increase in predator mortality due to prey herd δ_1 or time delay τ can cause population fluctuations. Our study expresses that the high value of δ_1 can lead to predator elimination, which is biologically practicable. Due to the criticality of α, δ_1 and τ, we determined the effect of time delay τ on the Hopf-bifurcation curves in $\alpha\delta_1$-plane. With an increment in τ, the Hopf-bifurcation curve shifts downwards (see Fig. 5.17).

A certain herd shape is advantageous to either prey or predator. The predator's strategy to attack the target varies with the form of the herd [175]. Therefore, the attack rate plays a vital role in regulating the system's dynamics. Our work looked at the influence of a_1 (attack rate for healthy prey) and found some intriguing outcomes. Fig. 5.13 depicts a variety of system traits concerning a_1. For lower a_1, the system undergoes Hopf-bifurcation, and stable E^* bifurcates into a stable limit cycle. Gradually, the limit cycle links saddle E_1 in the form of a homoclinic loop. The system experiences period-doubling and eventually reaches a chaotic regime with the increment in a_1. Therefore, we can conclude that the formulated system is sensitive to the initial condition.

Next, we looked at the impact of disease on interacting populations. Though the infection does not spread among predators, their number varies due to the illness among prey. Three steady-states axial E_1, planar E_{SI}, and interior E^* are affected when the infection rate β changes (see Fig. 5.11). Controlling the infection among prey can manage the predator population [80]. In the current study, when the infection rate lies in a particular range ($\beta \in (\beta^*, \beta^{**})$), predators can be removed (E_{SI} is stable). Moreover, when β is less than a threshold, the disease can also be eradicated, i.e., $E_1(K,0,0)$ becomes stable. Our findings reveal that disease transmission rate and attack rate on vulnerable prey play a significant role in controlling the system's dynamics, and the system undergoes various bifurcations. Our observation also agrees with those reported by Saha and Samanta [172] for $\alpha = 0.5$.

In the end, we conducted a sensitivity analysis on the proposed model for basic reproduction number R_0 and disease-free demographic reproduction number R_0^P to identify the factors that might regulate the dynamics of the system and give insights into species conservation.

Chapter 6

Role reversal in a stage-structured prey–predator model with fear, delay, and carry-over effects [1]

6.1 Introduction

In classical prey-predator models, there is a misconception that every predator chases prey with the same strength. However, this does not always fit with the real world as the species behaves differently during the juvenile and adult life phases [184]. Predators weaned during adolescence lack foraging or hunting skills, which makes predation during juvenility an arduous endeavor. This scenario is investigated using the concept of stage structure in predator-prey models [185, 186, 187, 188, 189]. The mathematical incorporation of stages of any species is generally done by constructing a system of differential equations.

One thing that is common in the aforementioned literature is that young predators are nurtured by their adult parents in a relatively secure habitat. Nevertheless, in the real world, these assumptions are overly idealistic, as juvenile predator survival is significantly more difficult. The ability of prey to kill vulnerable predators that pose no threat to them is less well recognized. Due to size changes throughout maturation, adult predators are resistant to large prey, but juvenile predators are susceptible to attack by prey [190]. Mature lions hunt buffaloes for food, but juvenile lions cannot fight buffaloes until they are about one year old, and they also rely on their parents for survival. Furthermore, buffaloes attack and sometimes kill infant lions [191]. Frankliniella occidentalis, a worldwide prey species, is said to engage in anti-predator behaviour by ingesting phytoseiid mite eggs[192]. A study by Kaushik and Banerjee [193] suggests that counter-attacking controls heavy predation. Moreover, they draw the conclusion from their research that excessive counter-attacking can completely eliminate the predators. Li *et al.*

[1] A considerable part of this chapter is published in *Chaos: An Interdisciplinary Journal of Nonlinear Science*, **33**, 093114, 2023.

[34] believed that the counter-attacking on juvenile predators directly benefits the prey population. This situation of the role reversal of prey and predator brings out ecologically plausible complex dynamics.

Prey-predator interactions are generally studied to understand direct killing. Nevertheless, fear of predators among prey can hamper their reproduction rate [17, 194]. Therefore, it is better to explore the dynamics of a prey-predator system in the presence of fear. A large piece of the literature shows that fear among prey can stabilize or destabilize the system [21, 26, 58, 195, 196, 197]. In addition, fear above a threshold can cause the system to enter a state of chaos [122]. To overcome the fear of predation, prey often exhibits anti-predator behavior. When prey has no chance of escape, the last option left is to counter-attack. Recently, Prasad and Sasmal [195] studied a system of ordinary differential equations with fear and counter-attacking strategy as the anti-predator response. Their findings uncover fascinating dynamics like bi-stability, Hopf-bifurcation, and Bogdanov-Takens bifurcation.

The term "carry-over effect" came to light from repeated clinical experiment evaluations. In an ecological scenario, any circumstance in which an individual's prior history and experiences explain their current performance is a carry-over effect [198]. The incorporation of the carry-over effect into a population model can aid in understanding the relationship between life-history trade-offs and reproduction costs. Thus there is an increasing trend of investigating the prey-predator model with carry-over effect [21, 25].

Almost every biological process has some time lag, and integration of such time delay makes the model more realistic and engaging [55]. The study of delay differential equations has become popular as it provides rich dynamics. Many researchers discovered that the system undergoes Hopf-bifurcation with respect to time delay [199, 200]. Sajan *et al.* [21] found that the carry-over effect of fear in prey is not observed instantly. So, they introduced a carry-over effect delay in the three-species model and found that the large value of time delay transforms the chaotic system into a stable one.

Based on the aforementioned discussion, we formulate and study a mathematical model showing the interaction of prey, immature predator, and mature predator in the presence of fear and its carry-over effect with two discrete time delays. The purpose of our research is to look into the following problems:

1. How does fear, its COE and time delay impact population density and stability traits?
2. Does the phenomenon of bi-stability occur for our system?
3. In what way does the role reversal influence the co-existence of species?
4. How can the paradox of enrichment phenomenon be observed in our model, and under what circumstances can it be ruled out?

Further part of the manuscript is organized as follows: Section 6.2 shows the basic assumptions and the formulation of the model. The mathematical preliminaries including well-posedness, existence and stability of equilibrium points of the model system are discussed in Section 6.3. Moreover, we explore the possible bifurcations occurring in the system. Next, we investigate the local stability behavior and Hopf-bifurcation for the time-delayed system in Section 6.4. In Section 6.5, we observe the system dynamics through computational work. We use MATLAB R2021a to validate our analytical findings. Lastly, we summarize all our findings in Section 6.6.

6.2 The model construction

We develop a system of differential equations governing the continuous time interaction of prey $x(t)$, juvenile predator $y(t)$, and adult predator $z(t)$. Based on the literature survey done in Section 6.1, we formulate a mathematical model with the following assumptions:

1. When predator is absent, the prey population grows logistically with intrinsic growth rate $r - r_0 (> 0)$ and carrying capacity $K_1 = \frac{r-r_0}{r_1}$, here r, r_0, and r_1 are the birth, death, and intraspecific interference rates, respectively. Therefore the single species model is given by
$$\frac{dx}{dt} = (r - r_0)x\left(1 - \frac{x}{K_1}\right).$$

2. We assume that the predators are of specialist nature and their growth completely depends on the prey density consumed. To demonstrate the interaction of adult predator and prey, we use the Holling type II functional response, given by
$$p(x) = \frac{\alpha x}{1 + \alpha h x},$$
where α is the attack rate and h is the handling time.

3. The juvenile predator is incapable of reproducing and hunting. So they completely rely on their parents for survival [201]. A fraction of the consumed biomass by mature predator gets transferred into the young ones. The immature predator is transformed to the mature class with the constant rate β. d_1 and d_2 are the mortality rates of juvenile and adult predator, respectively.

4. In addition to the direct killing, adult predator induce fear in prey, which hampers the birth rate of prey negatively. Moreover, this fear has some carry-over effects on the prey density. Thus we incorporate these ecological factors into our model using the function

$\phi(c,k,x,z) = \frac{1+cx}{1+cx+kz}$, where k and c are the fear and its COE parameters [21]. From the ecological point of view, $\phi(c,k,x,z)$ must satisfy the following properties.

(i) In the absence of predator or fear effect, the function ϕ makes no sense, and the birth rate of the prey is unaffected. Therefore,

$$\phi(c,0,x,z) = \phi(c,k,x,0) = 1.$$

(ii) Increasing the level of fear or predator density lowers the prey growth. In mathematical terms, we have

$$\frac{\partial \phi}{\partial k} = -\frac{(1+cx)z}{(1+cx+kz)^2} < 0, \ \frac{\partial \phi}{\partial z} = -\frac{(1+cx)k}{(1+cx+kz)^2} < 0.$$

(iii) When fear level or the predator density is extremely high, prey species might be eliminated. Thus,

$$\lim_{k\to\infty} \phi(c,k,x,z) = \lim_{z\to\infty} \phi(c,k,x,z) = 0.$$

(iv) An increase in COE has a beneficial impact on prey growth as a result of lessons learned from past experiences. Mathematically, we can write

$$\frac{\partial \phi}{\partial c} = \frac{kxz}{(1+cx+kz)^2} > 0.$$

(v) The reproduction rate of the prey naturally increases with the rise in population density. Therefore,

$$\frac{\partial \phi}{\partial x} = \frac{ckz}{(1+cx+kz)^2} > 0.$$

(vi) When the COE or the prey density is too large, there will be no impact of fear on the reproduction rate. Hence, we obtain

$$\lim_{c\to\infty} \phi(c,k,x,z) = \lim_{x\to\infty} \phi(c,k,x,z) = 1.$$

5. The COEs caused by fear are not instantaneous, and the effects of the induced fear on the prey population will inevitably be delayed [21]. Consequently, including a COEs delay τ_1 in our system is ecologically reasonable.

6. The effect of fear does not retard the prey's birth rate immediately. Therefore, we incorporate the fear delay τ_2 to show a more realistic approach [22].

7. Further, we assume the prey takes revenge by counter-attacking the vulnerable juvenile predator with the constant rate e. A fraction of biomass intake by the prey helps them to reproduce new ones with the rate f. The counter-attack by prey causes the adult predator to show parental concern and hunt on prey. In a basic ecological sense, the juveniles of z are consumed by x, but adult predators of density z consume x. When the size structures of prey and predator coincide, it is challenging to identify the predator and the prey, which results in their role reversal [34].

Combining all the aspects mentioned above, we establish a mathematical model given by

$$\begin{aligned}
\frac{dx}{dt} &= rx\left(\frac{1+cx(t-\tau_1)}{1+cx(t-\tau_1)+kz(t-\tau_2)}\right) - r_0x - r_1x^2 - \frac{\alpha xz}{1+\alpha hx} + fxy,\\
\frac{dy}{dt} &= \frac{c_1\alpha xz}{1+\alpha hx} - \beta y - d_1y - exy,\\
\frac{dz}{dt} &= \beta y - d_2z,
\end{aligned} \tag{6.1}$$

$$x(s) = \phi_1(s) \geq 0,\ y(s) = \phi_2(s) \geq 0,\ z(s) = \phi_3(s) \geq 0,\ s \in [-\tau, 0], \tau = max\{\tau_1, \tau_2\}.$$

In the absence of time delay ($\tau_1 = 0,\ \tau_2 = 0$), model (6.1) is converted into the following three-dimensional system. All parameters included in the proposed system are explained in Table 6.1.

$$\begin{aligned}
\frac{dx}{dt} &= rx\left(\frac{1+cx}{1+cx+kz}\right) - r_0x - r_1x^2 - \frac{\alpha xz}{1+\alpha hx} + fxy = f_1(x,y,z),\\
\frac{dy}{dt} &= \frac{c_1\alpha xz}{1+\alpha hx} - \beta y - d_1y - exy = f_2(x,y,z),\\
\frac{dz}{dt} &= \beta y - d_2z = f_3(x,y,z),
\end{aligned} \tag{6.2}$$

$$x(0) \geq 0,\ y(0) \geq 0,\ z(0) \geq 0.$$

6.3 Mathematical preliminaries

In this part, firstly, we will check if the model is well-posed or not by ensuring the positivity and boundedness of solutions. Next, we investigate the equilibrium points and their stability behavior. Furthermore, we explore numerous bifurcations with respect to the significant parameters.

Table 6.1: Data set of parameters used in (6.1) with references.

Parameters	Ecological meaning	Numerical value	Reference(s)
r	Birth rate of the prey	2.6	[25]
r_0	Natural death rate of the prey	0.75	[22]
r_1	Intra-specific competition coefficient	0.35	Assumed
K	Level of fear	4	[21]
α	Predation rate of the adult predator	6.5	Assumed
d_1	Natural death rate of immature predator	0.2	[34, 202]
d_2	Natural death rate of mature predator	0.7	Assumed
c	Carry-over effect	0.001	[21]
β	Growth rate of immature predator	1.1	Assumed
c_1	Conversion efficiency	0.8	[193]
h	Handling time	0.65	[202]
e	Predation rate of the prey	0.25	[193]
f	Reproduction rate of the prey	0.001	Assumed

6.3.1 Positivity and boundedness

It is simply clear from the equations of model (6.2) that

$$\left.\frac{dx}{dt}\right|_{x=0} = 0, \qquad \left.\frac{dy}{dt}\right|_{y=0} = \frac{c_1\alpha xz}{1+\alpha hx}, \qquad \left.\frac{dz}{dt}\right|_{z=0} = \beta y.$$

Since $\left.\frac{dx}{dt}\right|_{x=0} \geq 0$, it implies that $x(t) \geq 0 \,\forall\, t \geq 0$. Now, we assert that $\left.\frac{dy}{dt}\right|_{y=0} = \frac{c_1\alpha xz}{1+\alpha hx} \geq 0$ hence $y(t) \geq 0 \,\forall\, t \geq 0$. If this is not the case, then suppose that $\exists$ a $t_1 > 0$ with $t_1 = inf\{t : y(t) = 0,\ t > 0\}$, such that $\left.\frac{dy(t_1)}{dt}\right|_{y(t_1)=0} = \frac{c_1\alpha x(t_1)z(t_1)}{1+\alpha hx(t_1)} < 0$. Furthermore, we also have $y(t_1) = 0,\ y(t) > 0$ with $t \in [0, t_1)$ and $z(t_1) < 0$. Since $z(0) \geq 0$, there is a $t_2 > 0$ with $t_2 = inf\{t : z(t) = 0,\ t \in [0, t_1)\}$. Therefore, by the definition of t_2, $\frac{dz(t_2)}{dt} \leq 0$. However $\frac{dz(t_2)}{dt} = \beta y(t_2) > 0$, which contradicts our premise. Hence $\left.\frac{dy}{dt}\right|_{y=0} \geq 0$, which follows that $y(t) \geq 0 \,\forall\, t \geq 0$. Finally, from the third equation of the model $\left.\frac{dz}{dt}\right|_{z=0} = \beta y \geq 0$, it follows that $z(t) \geq 0 \,\forall\, t \geq 0$.

Theorem 6.3.1. *The set* $\Omega = \{(x, y, z) : 0 < c_1x + y + z \leq \frac{c_1 r^2}{4\eta r_1}\}$ *is a region of attraction for all solutions initiating in the interior of the positive quadrant, where* $\eta \leq min\{r_0,\ d_1,\ d_2\}$.

Proof. Let $W = c_1x + y + z$ and choose $\eta > 0$ such that

$$\begin{aligned}\frac{dW}{dt} + \eta W &= \frac{c_1 rx(1+cx)}{1+cx+kz} - c_1 r_0 x - c_1 r_1 x^2 + c_1 fxy - d_1 y - d_2 z - exy + \eta(c_1 x + y + z) \\ &\leq c_1 rx - c_1 r_1 x^2 - (e - c_1 f)xy - c_1(r_0 - \eta)x - (d_1 - \eta)y - (d_2 - \eta)z.\end{aligned}$$

Let $e > c_1 f$ and for $\eta \leq min\{r_0,\ d_1,\ d_2\}$, we can write

$$\begin{aligned}\frac{dW}{dt} + \eta W &\leq c_1 rx - r_1 c_1 x^2 \\ &\leq \frac{c_1 r^2}{4r_1}.\end{aligned}$$

Therefore,

$$\limsup_{t\to\infty} (c_1 x + y + z) \leq \frac{c_1 r^2}{4\eta r_1}.$$

Hence the theorem is established. □

6.3.2 Equilibrium points and local stability

It is easy to see that the system has two boundary steady-states: $E_0(0,0,0)$ and $E_1(K_1,0,0)$, where $K_1 = \frac{r-r_0}{r_1}$. The predator-free state E_1 exists when $r > r_0$. Furthermore, the system exhibits a unique interior equilibrium point $E^*(x^*, y^*, z^*)$, which can be obtained by solving following equations.

$$r\left(\frac{1+cx}{1+cx+kz}\right) - r_0 - r_1 x - \frac{\alpha z}{1+\alpha hx} + fy = 0, \tag{6.3}$$

$$\frac{c_1 \alpha xz}{1+\alpha hx} - \beta y - d_1 y - ex = 0, \tag{6.4}$$

$$z = \frac{\beta y}{d_2}. \tag{6.5}$$

Solving Eqs. (6.3), (6.4), (6.5), we obtain following two quadratic equations.

$$A_1 x^2 + A_2 x + A_3 = 0, \tag{6.6}$$

where $A_1 = \alpha hed_2$, $A_2 = d_2(e + \alpha\beta h + \alpha h d_1) - c_1\alpha\beta$, $A_3 = d_2(\beta + d_1)$.

$$B_1 y^2 + B_2 y + B_3 = 0, \tag{6.7}$$

where $B_1 = \frac{\beta k \gamma}{d_2}$, $B_2 = \gamma(1+cx^*) + \frac{k\beta(r_0+r_1x^*)}{d_2}$, $B_3 = (1+cx^*)r_1(x^*-K_1)$, $\gamma = \frac{\beta\alpha}{d_2(1+\alpha h x^*)} - f$. Using Descarte's rule of sign, we can discuss the number of positive solutions of Eqs. (6.6) and (6.7). Therefore, to state the existence of the interior equilibrium, we have the following three theorems.

Theorem 6.3.2. *The system acquire two positive equilibrium points if the following conditions hold.*

(i) $A_2 < -2\sqrt{A_1A_3}$,

(ii) $\gamma > 0$ *and* $x_i^* < K_1 \ \forall i = 1,2$.

Proof. It is easy to note from Eq. (6.6) that the sign of A_1 and A_3 is always positive. The Descarte's rule suggests that for the existence of roots of Eq. (6.6), the negativity of the sign of A_2 is necessary. In such a case, number of roots can be two or zero. Moreover, if the discriminant of the quadratic equation is positive, the equation has exactly two positive roots. Therefore, for the existence of the positive root, we obtain the following necessary condition.

$$A_2 < 0, \text{ and } A_2^2 > 4A_1A_3.$$

Now, after calculating roots x_i^* from Eq. (6.6) , we need to determine y_i^* from Eq. (6.7). If γ is positive and $x_i^* < K_1$ for each $i = 1,2$, then $B_1 > 0$, $B_2 > 0$ and $B_3 < 0$. Therefore, for each x_i^*, we can determine unique y_i^* from Eq. (6.7), and z_i^* from Eq. (6.5). □

Theorem 6.3.3. *The system acquires a unique positive equilibrium if the following conditions hold.*

(i) $A_2 < -2\sqrt{A_1A_3}$,

(ii) $\gamma > 0$ *and*

(iii) $x_i^* > K_1$, $i = 1$ *or* 2.

Proof. In addition to the previous theorem, if one of the roots obtained from Eq. (6.6) is bigger than K_1 and the other root is lesser than K_1. Then in such a case, $x^* > K_1$ is not acceptable for our ecological system as the prey density cannot exceed its carrying capacity. Therefore, the system has a unique positive equilibrium if the conditions of the theorem are satisfied. □

Remark.

(i) If $A_2 = -2\sqrt{A_1A_3}$, then we note that A_2 is negative and Eq. (6.6) has a unique positive root of multiplicity two.

(ii) If $\gamma > 0$ and $x^* < K_1$, then Eq. (6.7) has a unique positive root.

(iii) If $A_2 = -2\sqrt{A_1 A_3}$, $\gamma > 0$ and $x^* < K_1$, then the proposed system has a unique positive equilibrium.

When conditions of both Theorems 6.3.2 and 6.3.3 are not satisfied, the system has no positive equilibrium. Therefore, we can establish the next theorem.

Theorem 6.3.4. *The system has no positive equilibrium if any one of the following cases is true.*

(i) $A_2 \geq 0$,

(ii) $-2\sqrt{A_1 A_3} < A_2 < 0$,

(iii) $A_2 < -2\sqrt{A_1 A_3}$, $B_2(x_i^*) > 0$ *and* $x_i^* > K_1$ $\forall i = 1,2$,

(iv) $A_2 < -2\sqrt{A_1 A_3}$, $B_1 < 0$, $B_2(x_i^*) < 0$ *and* $x_i^* < K_1$ $\forall i = 1,2$.

All these three theorems can be illustrated numerically by varying e and α in Fig. 6.1. The pair (e, α) for which the conditions of Theorem 6.3.2 are satisfied is colored red, and this region has exactly two interior equilibrium points. The blue color region points satisfy all conditions of Theorem 6.3.3, corresponding to a unique interior equilibrium. The green color region meets up the requirement of Theorem 6.3.4, and hence there does not exist any positive equilibrium.

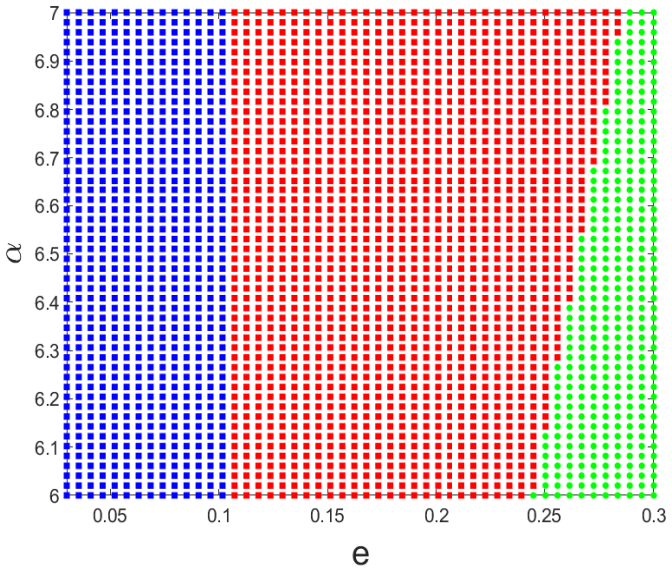

Fig. 6.1: $e\alpha$-plane divided based on the number of interior equilibrium points. Red, blue, and green color depicts the set of (e, α) values for which the system exhibits two, one, and zero positive equilibrium points, respectively. The rest of the parameters are taken from Table 6.1.

Remark.

- It is important to note here that the necessary mathematical condition for the existence of E^* is $A_2 < -2\sqrt{A_1 A_3}$, which yields the following inequality:

$$d_2 < \frac{c_1 \alpha \beta}{[\sqrt{e} + \sqrt{\alpha h(\beta + d_1)}]^2}.$$

- It is natural that any population number cannot exceed its environmental carrying capacity. Since prey density x^* is less than its carrying capacity K_1, it implies $B_3 < 0$. All other cases of B_3 are not permissible for our system.

- The proposed system can have at most two interior equilibrium points, and the existence of positive equilibrium is independent of fear (k) and carry-over effect (c).

The local stability behavior of an autonomous system's equilibrium point is determined by the sign of the eigenvalues of the associated jacobian matrix. Let J_1 be the Jacobian matrix corresponding to the positive steady-state E^*, which is given by the following.

$$J_1 = \begin{pmatrix} j_{11} & j_{12} & j_{13} \\ j_{21} & j_{22} & j_{23} \\ j_{31} & j_{32} & j_{33} \end{pmatrix} = \begin{pmatrix} \frac{kcrx^*z^*}{(1+cx^*+kz^*)^2} - r_1 x^* + \frac{h\alpha^2 x^* z^*}{(1+\alpha h x^*)^2} & fx^* & -\frac{rkx^*(1+cx^*)}{(1+cx^*+kz^*)^2} - \frac{\alpha x^*}{1+\alpha h x^*} \\ \frac{c_1 \alpha z^*}{(1+\alpha h x^*)^2} - ey^* & -d_1 - \beta - ex^* & \frac{c_1 \alpha x^*}{1+\alpha h x^*} \\ 0 & \beta & -d_2 \end{pmatrix}$$

Let $\Theta_1 = -(j_{11} + j_{22} + j_{33})$, $\Theta_2 = j_{22}j_{33} - j_{23}j_{32} + j_{11}j_{33} + j_{11}j_{22} - j_{12}j_{21}$, $\Theta_3 = -j_{11}(j_{22}j_{33} - j_{23}j_{32}) + j_{21}(j_{12}j_{33} - j_{13}j_{32})$. Then the local stability behavior of the non-negative equilibria is summarized in Table 6.2.

Table 6.2: Equilibrium points of the proposed model and their stability behavior in the absence of delay.

Equilibrium points	Eigenvalues	Stability behavior
$E_0(0,0,0)$	$r - r_0,\ -d_1 - \beta,\ d_2$	saddle point
$E_1(K_1,0,0)$	$-r_1 K_1$, other two are the roots of	
	$\lambda^2 + \Gamma_1 \lambda + \Gamma_2$, where $\Gamma_1 = d_1 + \beta + eK_1 + d_2$	stable $\Leftrightarrow \Gamma_2 > 0$
	and $\Gamma_2 = d_2(d_1 + \beta + eK_1) - \frac{c_1 \alpha \beta K_1}{1+\alpha h K_1}$	
$E^*(x^*,y^*,z^*)$	roots of $\lambda^3 + \Theta_1 \lambda^2 + \Theta_2 \lambda + \Theta_3 = 0$,	stable $\Leftrightarrow \Theta_1 > 0, \Theta_3 > 0$
		$\Theta_1 \Theta_2 - \Theta_3 > 0$

Remark. The stability of E_1 is independent of the reproduction rate of prey (f), fear (k), and the carry-over effect (c). Moreover, the necessary and sufficient condition for the stability

is given by

$$d_2 > \frac{c_1\alpha\beta K_1}{(1+\alpha hK_1)(d_1+\beta+eK_1)}.$$

In an ecological sense, when the death rate of the mature predator exceeds a threshold, the predator population will die out, and the prey will survive, resulting in the stability of E_1.

6.3.3 Hopf-bifurcation

Theorem 6.3.5. *System (1) experiences Hopf-bifurcation at $e = e^*$ about the co-existence state E^* if the following conditions hold:*

(i) $\Theta_1(e^*)\Theta_2(e^*) - \Theta_3(e^*) = 0,$

(ii) $\Theta_1(e^*) > 0,\ \Theta_3(e^*) > 0,$

(iii) $\left(\Theta_1\frac{d\Theta_2}{de} + \Theta_2\frac{d\Theta_1}{de} - \frac{d\Theta_3}{de}\right)_{e=e^*} \neq 0.$

Proof. At the Hopf-bifurcation point $e = e^*$, $\Theta_1\Theta_2 - \Theta_3 = 0$, the characteristic equation of J_1 can be re-written as

$$(\lambda + \Theta_1)(\lambda^2 + \Theta_2) = 0.$$

This yields $\lambda_1 = -\Theta_1$ and $\lambda_{2,3} = \pm i\sqrt{\Theta_2}$, where $\Theta_1 > 0, \Theta_2 > 0$. To evaluate the transversality condition, we assume that $\lambda_{2,3}(e) = \xi_1(e) + i\xi_2(e)$ and substitute $\lambda = \xi_1 + i\xi_2$ in the characteristic equation to obtain the real and imaginary parts as follows:

$$\xi_1^3 - 3\xi_1\xi_2^2 + \Theta_1(\xi_1^2 - \xi_2^2) + \Theta_2\xi_1 + B_3 = 0, \tag{6.8}$$

$$-\xi_2^3 + 3\xi_2\xi_1^2 + 2\Theta_1\xi_1\xi_2 + \Theta_2\xi_2 = 0. \tag{6.9}$$

Combining Eqs. (6.8) and (6.9), we get

$$8\xi_1^3 + 8\Theta_1\xi_1^2 + 2\xi_1(\Theta_2 + \Theta_1^2) + \Theta_1\Theta_2 - \Theta_3 = 0. \tag{6.10}$$

Now, differentiating Eq. (6.10) with respect to e, then at $e = e^*$, we obtain

$$\left.\frac{d\xi_1}{de}\right|_{e=e^*} = -\frac{1}{2(\Theta_2+\Theta_1^2)}\left[\Theta_1\frac{d\Theta_2}{de} + \Theta_2\frac{d\Theta_1}{de} - \frac{d\Theta_3}{de}\right]_{e=e^*}.$$

Therefore, the transversality condition is

$$\left[\Theta_1\frac{d\Theta_2}{de} + \Theta_2\frac{d\Theta_1}{de} - \frac{d\Theta_3}{de}\right]_{e=e^*} \neq 0.$$

Hence the theorem follows. □

Direction and stability of Hopf-bifurcation

To find the direction and stability of the bifurcating periodic solution, we need to determine Lyapunov's first coefficient. At the Hopf-bifurcation point, we shift the interior equilibrium point $E^*(x^*,y^*,z^*)$ to the origin using the transformation:

$$u_1 = x - x^*,\ u_2 = y - y^*, u_3 = z - z^*.$$

System (6.2) can also be written as

$$U' = J_1 U + \rho(U), \tag{6.11}$$

where $U = (U_1,U_2,U_3)^T$ and $\rho(U) = (g_1,g_2,g_3)^T$. Here g_1, g_2 and g_3 are the second order terms of the Taylor's expansion of f_1, f_2 and f_3 about $(0,0,0)$, respectively.

$$g_1 = \frac{1}{2}\Bigg\{\left[\frac{2rckz^*(1+kz^*)}{(1+cx^*+kz^*)^3} - 2r_1 + \frac{2h\alpha^2 z^*}{(1+\alpha hx^*)^3}\right]u_1^2 + \frac{2k^2rx^*(1+cx^*)}{(1+cx^*+kz^*)^3}u_3^2 + fu_1u_2 - \Bigg[\frac{rk}{(1+cx^*+kz^*)^2} + \frac{2crk^2x^*z^*}{(1+cx^*+kz^*)^3} - \frac{\alpha}{(1+\alpha hx^*)^2}\Bigg]u_1u_3\Bigg\},$$

$$g_2 = \frac{1}{2}\Bigg\{-\frac{2c_1\alpha^2hz^*}{(1+\alpha hx^*)^3}u_1^2 - eu_1u_2 + \frac{c_1\alpha}{(1+\alpha hx^*)^2}u_1u_3\Bigg\},\ g_3 = 0.$$

The eigenvectors corresponding to the eigenvalues $i\omega$, λ_3 are $\Xi_1 = (\xi_{11},\xi_{21},\xi_{31})^T$ and $\Xi_2 = (\xi_{12},\xi_{22},\xi_{32})^T$, respectively, where

$$\xi_{11} = \alpha_1 + i\beta_1,\ \xi_{21} = \alpha_2 + i\beta_2,\ \xi_{31} = 1,$$

$$\alpha_1 = \frac{x^*\{[\frac{rk(1+cx^*)}{(1+cx^*+kz^*)^2} + \frac{\alpha}{1+\alpha hx^*} - \frac{fd_2}{\beta}][\frac{kcrx^*z^*}{(1+cx^*+kz^*)^2} - r_1x^* + \frac{h\alpha^2x^*z^*}{(1+\alpha hx^*)^2}] + \frac{f\omega^2}{\beta}\}}{[\frac{kcrx^*z^*}{(1+cx^*+kz^*)^2} - r_1x^* + \frac{h\alpha^2x^*z^*}{(1+\alpha hx^*)^2}]^2 + \omega^2},$$

$$\beta_1 = \omega x^*\frac{-\frac{f}{\beta}[\frac{kcrx^*z^*}{(1+cx^*+kz^*)^2} - r_1x^* + \frac{h\alpha^2x^*z^*}{(1+\alpha hx^*)^2}] + [\frac{rk(1+cx^*)}{(1+cx^*+Kz^*)^2} + \frac{\alpha}{1+\alpha hx^*} - \frac{fd_2}{\beta}]}{[\frac{kcrx^*z^*}{(1+cx^*+kz^*)^2} - r_1x^* + \frac{h\alpha^2x^*z^*}{(1+\alpha hx^*)^2}]^2 + \omega^2},$$

$$\alpha_2 = \frac{d_2}{\beta},\ \beta_2 = \frac{\omega}{\beta},\ \xi_{31} = 1,$$

$$\xi_{12} = \frac{x^*\{[\frac{rk(1+cx^*)}{(1+cx^*+kz^*)^2} + \frac{\alpha}{1+\alpha hx^*}] - \frac{f(d_2+\lambda_3}{\beta}\}}{[\frac{kcrx^*z^*}{(1+cx^*+kz^*)^2} - r_1x^* + \frac{h\alpha^2x^*z^*}{(1+\alpha hx^*)^2} - \lambda_3]},\ \xi_{22} = \frac{d_2+\lambda_3}{\beta},\ \xi_{32} = 1.$$

Now, let us define $\mathscr{B} = [Re(\Xi_1), -Im(\Xi_1), \Xi_2]$, and $M = \mathscr{B}^{-1}U$, where $M = (M_1, M_2, M_3)^T$, then system (6.11) takes the following form:

$$M' = [\mathscr{B}^{-1} J_1 \mathscr{B}]M + \delta(M), \tag{6.12}$$

where

$$\delta(M) = \begin{pmatrix} \kappa^1 \\ \kappa^2 \\ \kappa^3 \end{pmatrix} = \mathscr{B}^{-1}\rho(\mathscr{B}M).$$

As per the Central Manifold Theorem [203], we can write

$$\begin{pmatrix} M_1 \\ M_2 \end{pmatrix}' = \begin{pmatrix} 0 & -\omega \\ \omega & 0 \end{pmatrix} \begin{pmatrix} M_1 \\ M_2 \end{pmatrix} + \begin{pmatrix} \kappa^1(M_1, M_2; e = e^*) \\ \kappa^2(M_1, M_2; e = e^*) \end{pmatrix}. \tag{6.13}$$

Here $\begin{pmatrix} \kappa_1 \\ \kappa_2 \end{pmatrix} = \frac{1}{\Delta} \begin{pmatrix} -\beta_2\xi_{32}g_1(\mathscr{B}M) + \beta_1\xi_{32}g_2(\mathscr{B}M) \\ (\xi_{22} - \alpha_2\xi_{32})g_1(\mathscr{B}M) + (\alpha_1\xi_{32} - \xi_{12})g_2(\mathscr{B}M) \end{pmatrix}$, where $\Delta = -\alpha_1\beta_2\xi_{32} + \beta_1(\alpha_2\xi_{32} - \xi_{22}) + \xi_{12}\beta_2$.

Next, we evaluate the first Lyapunov coefficient based on the normal form (6.13), which is given as

$$\mathscr{L} = \frac{1}{16}\left[\kappa^1_{M_1M_1M_1} + \kappa^1_{M_1M_2M_2} + \kappa^2_{M_1M_1M_2} + \kappa^2_{M_2M_2M_2}\right] + \frac{1}{16\omega}\left[\kappa^1_{M_1M_2}(\kappa^1_{M_1M_1} + \kappa^1_{M_2M_2}) - \kappa^2_{M_1M_2}(\kappa^2_{M_1M_1} + \kappa^2_{M_2M_2}) - \kappa^1_{M_1M_1}\kappa^2_{M_1M_1} + \kappa^1_{M_2M_2}\kappa^2_{M_2M_2}\right].$$

The sign of $\mathscr{L}$ determines the direction of Hopf-bifurcation. For this, we have our next theorem.

Theorem 6.3.6. *The system (6.2) experiences a*

(i) supercritical Hopf-bifurcation if $\mathscr{L} < 0$,

(ii) subcritical Hopf-bifurcation if $\mathscr{L} > 0$, and

(iii) generalized Hopf-bifurcation if $\mathscr{L} = 0$

around a positive equilibrium E^* at $e = e^*$.

6.3.4 Transcritical bifurcation

Theorem 6.3.7. *The system experiences transcritical bifurcation around predator-free equilibrium $E_1(K_1, 0, 0)$ at $e = e^{[tc]} = \left(\frac{c_1K_1\alpha\beta}{d_2(1+\alpha hK_1)} - \beta - d_1\right)\frac{1}{K_1}$ if $v_1 \neq 0$, where v_1 is defined in the proof.*

Proof. The variational matrix around E_1 at $e = e^{[tc]}$ is

$$A = \begin{pmatrix} -(r-r_0) & fK_1 & -\frac{krK_1}{(1+cK_1)} - \frac{\alpha K_1}{(1+\alpha hK_1)} \\ 0 & -\beta - d_1 - e^{[tc]}K_1 & \frac{c_1K_1\alpha}{1+\alpha hK_1} \\ 0 & \beta & -d_2 \end{pmatrix}.$$

Let the eigenvectors corresponding to the matrices A and A^T for eigenvalue zero be $v = \left(\frac{1}{r_1}(\frac{fd_2}{\beta} - \left(\frac{kr}{1+cK_1} + \frac{\alpha}{1+\alpha hK_1}\right)),\ \frac{d_2}{\beta},\ 1\right)^T$ and $w = \left(0,\ 1,\ \frac{c_1K_1\alpha}{d_2(1+\alpha hK_1)}\right)^T$, respectively. Now, simple calculation yields the following.

$$\Delta_1 = w^T F_e(E_1, e^{[tc]}) = 0,$$

$$\Delta_2 = w^T DF_e(E_1, e^{[tc]})v = -\frac{d_2K_1}{\beta} \neq 0,$$

and

$$\Delta_3 = w^T[D^2F(E_1, e^{[tc]})](v,v) = 2v_1\left(\frac{c_1\alpha^2hK_1}{(1+\alpha hK_1)^2} + \frac{d_2(d_1+\beta)}{\beta K_1}\right),$$

where

$$v_1 = \frac{1}{r_1}\left[\frac{fd_2}{\beta} - \left(\frac{kr}{1+cK_1} + \frac{\alpha}{1+\alpha hK_1}\right)\right].$$

Now we can note that $v_1 \neq 0 \implies \Delta_3 \neq 0$. Hence, we can conclude that all conditions of the Sotomayor's Theorem [60] are satisfied. Therefore, the system undergoes transcritical bifurcation around E_1 at $e = e^{[tc]} = \left(\frac{c_1K_1\alpha\beta}{d_2(1+\alpha hK_1)} - \beta - d_1\right)\frac{1}{K_1}$ if $v_1 \neq 0$. □

6.4 Stability analysis of delayed model (6.1)

It may be noted that our model's equilibrium density level is independent of the time delay. The analysis for the positivity and boundedness of the delayed model is similar to the non-delayed model, as performed in Section 6.3. The detail analysis is outlined in [200]. Thus, we omit the proof.

The equilibrium points of the proposed model do not change with respect to the time delay. Nevertheless, stability may alter. Therefore, we now linearize system (6.1) to investigate its stability behavior about the positive equilibrium. The linearized form of system (6.1) is given by the following matrix.

$$J_2 = P_1' + P_2'e^{-\lambda\tau_1} + P_3'e^{-\lambda\tau_2},$$

where P_1', P_2', P_3' are the Jacobian matrices about $E^*(x^*,y^*,z^*)$ in the direction of t, $(t-\tau_1)$, $(t-\tau_2)$, respectively. Therefore, the final matrix is given by

$$J_2 = \begin{pmatrix} v_{11}+v_{11}^* e^{-\lambda\tau_1} & j_{12} & v_{13}+v_{13}^* e^{-\lambda\tau_2} \\ j_{21} & j_{22} & j_{23} \\ j_{31} & j_{32} & j_{33} \end{pmatrix},$$

where $v_{11} = -r_1x^* + \frac{h\alpha^2x^*z^*}{(1+\alpha hx^*)^2}$, $v_{11}^* = \frac{crkx^*z^*}{(1+cx^*+kz^*)^2}$, $v_{13} = -\frac{\alpha x^*}{1+\alpha hx^*}$, $v_{13}^* = -\frac{rkx^*(1+cx^*)}{(1+cx^*+kz^*)^2}$, and rest of the entries are same as of the non-delayed system matrix J_1.
The transcendental characteristic equation about E^* in the form of λ is as follows.

$$\lambda^3+\mu_1\lambda^2+\mu_2\lambda+\mu_3+(\lambda^2+\eta_1\lambda+\eta_2)\rho e^{-\lambda\tau_1}+\rho\eta_3 e^{-\lambda\tau_2}=0, \tag{6.14}$$

where

$$\mu_1 = r_1x^* - \frac{h\alpha^2x^*z^*}{(1+\alpha hx^*)^2} + d_1+\beta+ex^*+d_2,$$

$$\mu_2 = d_2(d_1+\beta+ex^*) - \frac{c_1\alpha\beta x^*}{(1+\alpha hx^*)} + (d_2+d_1+\beta+ex^*)\left(r_1x^* - \frac{h\alpha^2x^*z^*}{(1+\alpha hx^*)^2}\right) + fx^*\left(ey^* - \frac{c_1\alpha z^*}{(1+\alpha hx^*)^2}\right),$$

$$\mu_3 = \left(r_1x^* - \frac{h\alpha^2x^*z^*}{(1+\alpha hx^*)^2}\right)\left(d_2(d_1+\beta+ex^*) - \frac{c_1\alpha\beta x^*}{(1+\alpha hx^*)}\right) + x^*\left(fd_2 - \frac{\alpha\beta}{1+\alpha hx^*}\right)\left(ey^* - \frac{c_1\alpha z^*}{(1+\alpha hx^*)^2}\right),$$

$$\eta_1 = d_1+\beta+ex^*+d_2,$$

$$\eta_2 = d_2(d_1+\beta+ex^*) - \frac{c_1\alpha\beta x^*}{(1+\alpha hx^*)},$$

$$\eta_3 = \frac{\beta(1+cx^*)}{cz^*}\left(ey^* - \frac{c_1\alpha z^*}{(1+\alpha hx^*)^2}\right).$$

Case I: $\tau_1=\tau_2=0$ **:** In the absence of delay, Eq. (6.14) reduces to the characteristic equation of system (6.2), and therefore the local stability behavior of both systems (6.1) and (6.2) is identical.

Case II: $\tau_1>0,\ \tau_2=0$ **:** In this case, Eq. (6.14) takes the following form.

$$\lambda^3+\mu_1\lambda^2+\mu_2\lambda+\mu_3+(\lambda^2+\eta_1\lambda+\eta_2)\rho e^{-\lambda\tau_1}+\rho\eta_3=0. \tag{6.15}$$

Finding the exact solution to the above transcendental equation is difficult. Nevertheless, we

can determine the critical value of carry-over effect delay at which system (6.1) experiences stability switching through Hopf-bifurcation. At the Hopf-bifurcation point, the two eigenvalues of Eq. (6.14) must be purely imaginary. Therefore, we substitute $\lambda = i\zeta$ in Eq. (6.14) to obtain following equations:

$$\rho(\eta_2 - \zeta^2)cos(\zeta\tau) + \rho\eta_1\zeta sin(\zeta\tau) = \mu_1\zeta^2 - \mu_3 - \rho\eta_3, \tag{6.16}$$

$$\rho\eta_1\zeta cos(\zeta\tau) - \rho(\eta_2 - \zeta^2)sin(\zeta\tau) = \zeta^3 - \mu_2\zeta. \tag{6.17}$$

Squaring and adding Eqs. (6.16) and (6.17), we get

$$\zeta^6 + \zeta^4(\mu_1^2 - 2\mu_2 - \rho^2) + \zeta^2(\mu_2^2 - 2\mu_1(\mu_3 + \rho\eta_3) + \rho^2(2\eta_2 - \eta_1^2)) + (\mu_3 + \rho\eta_3)^2 - \rho^2\eta_2^2 = 0. \tag{6.18}$$

Furthermore, manipulating Eqs. (6.16) and (6.17) yields the following formula to determine the critical value of τ_1 at which the Hopf-bifurcation occurs.

$$\tau_{1_i}^* = \frac{1}{\zeta}cos^{-1}\left\{\frac{(\eta_2 - \zeta^2)(\mu_1\zeta^2 - (\mu_3 + \rho\eta_3)) + \eta_1\zeta^2(\zeta^2 - \mu_2)}{\rho[(\eta_2 - \zeta^2)^2 + \eta_1^2\zeta^2]}\right\} + \frac{2i\pi}{\zeta}, \quad \forall i = 0, 1, 2, ... \tag{6.19}$$

The transversality condition required for the Hopf-bifurcation can be obtained under an analysis similar to the analysis obtained in [204], and it is given by

$$\left.\frac{dRe(\lambda)}{d\tau_1}\right|_{\tau_1 = \tau_{1_0}^*} = \frac{R_1S_1 - R_2S_2}{S_1^2 + S_2^2} \neq 0 \text{ when } R_1S_1 \neq R_2S_2, \tag{6.20}$$

where

$$R_1 = \rho\zeta(\eta_2 - \zeta^2)sin(\zeta\tau_{1_0}^*) - \eta_1\zeta^2 cos(\zeta\tau_{1_0}^*),$$

$$R_2 = \rho\zeta(\eta_2 - \zeta^2)cos(\zeta\tau_{1_0}^*) + \eta_1\zeta^2 sin(\zeta\tau_{1_0}^*),$$

$$S_1 = \rho(\tau_{1_0}^*(\zeta^2 - \eta_2) + \eta_1)cos(\zeta\tau_{1_0}^*) + \rho\zeta(2 - \tau_0^*\eta_1)sin(\zeta\tau_{1_0}^*) + \mu_2 - 3\zeta^2,$$

$$S_2 = \rho\zeta(-2 + \tau_{1_0}^*\eta_1)cos(\zeta\tau_{1_0}^*) + \rho(\eta_1 + \tau_0^*(\zeta^2 - \eta_2))sin(\zeta\tau_{1_0}^*) - 2\mu_1\zeta.$$

Thus, we can state the following theorem.

Theorem 6.4.1. *System (6.1) undergoes Hopf-bifurcation with respect to the carry-over effect delay τ_1 at $\tau_1 = \tau_{1_0}^* > 0$ if its transversality condition (6.20) holds.*

Case III: $\tau_1 = 0,\ \tau_2 > 0$ In this case, Eq. (6.14) takes the following form.

$$\lambda^3 + (\mu_1 + \rho)\lambda^2 + (\mu_2 + \eta_1\rho)\lambda + \mu_3 + \rho\eta_2 + \rho\eta_3 e^{-\lambda\tau_2} = 0. \tag{6.21}$$

Now, we proceed similarly to the previous case to obtain the critical value of fear-response delay at which the Hopf-bifurcation can occur.

$$\tau_2^* = \frac{1}{\zeta} cos^{-1} \frac{\zeta^2(\mu_1+\rho)-\mu_3-\rho\eta_2}{\rho\eta_3}.$$

Theorem 6.4.2. *For System (6.1), E^* is stable when $\tau_2 < \tau_2{}^*$ and unstable when $\tau_2 > \tau_2{}^*$. Moreover, the system experiences Hopf-bifurcation with respect to the fear-response delay τ_2 at $\tau_2 = \tau_2{}^*$.*

Case IV: $\tau_1 > 0,\ \tau_2 \in (0, \tau_2^*)$ **:** In this case, we choose τ_2 from its stable interval $(0, \tau_2^*)$. Now, we need to determine the critical value of τ_1 while fixing τ_2. As per the requirement of Hopf-bifurcation we substitute $\lambda = i\zeta$ in Eq. (6.14) to obtain the following equations.

$$\rho(\eta_2-\zeta^2)cos(\zeta\tau_1)+\rho\eta_1\zeta sin(\zeta\tau_1) = \mu_1\zeta^2-\mu_3-\rho\eta_3 cos(\zeta\tau_2). \tag{6.22}$$

$$\rho\eta_1\zeta cos(\zeta\tau_1)-\rho(\eta_2-\zeta^2)sin(\zeta\tau_1) = \zeta^3-\mu_2\zeta-\rho\eta_3 sin(\zeta\tau_2). \tag{6.23}$$

Solving Eqs. (6.22) and (6.23), we get

$$\tau_1^* = \frac{1}{\zeta} cos^{-1}\left[\frac{(\eta_2-\zeta^2)(\mu_1\zeta^2-\mu_3-\rho\eta_3 cos(\zeta\tau_2))+\eta_1\zeta(\zeta^3-\mu_2\zeta-\rho\eta_3 sin(\zeta\tau_2))}{\rho[(\eta_2-\zeta^2)^2+\eta_1^2\zeta^2].}\right]$$

In order to test the transversality condition for the Hopf-bifurcation, we substitute $\lambda = \chi + i\zeta$ in Eq. (6.14). Now, separating real and imaginary parts, we obtain following equations.

$$\begin{aligned}&\chi^3-3\zeta^2\chi+\mu_1(\chi^2-\zeta^2)+\mu_2\chi+\mu_3+\rho\eta_3+\rho(\chi^2-\zeta^2+\eta_1\chi+\eta_2)e^{-\chi\tau_1}cos(\zeta\tau_1)\\&+\rho\zeta(\eta_1+2\chi)e^{-\chi\tau_1}sin(\zeta\tau_1)+\rho\eta_3 e^{-\chi\tau_2}cos(\zeta\tau_2)=0\end{aligned} \tag{6.24}$$

$$\begin{aligned}&-\zeta^3+3\zeta\chi^2+2\zeta\chi\mu_1+\mu_2\zeta+\rho\zeta e^{-\chi\tau_1}(2\chi+\eta_1)cos(\zeta\tau_1)\\&-\rho(\chi^2-\zeta^2+\eta_1\chi+\eta_2)e^{-\chi\tau_1}sin(\zeta\tau_1)-\rho\eta_3 e^{-\chi\tau_2}sin(\zeta\tau_2)=0\end{aligned} \tag{6.25}$$

Differentiating Eqs. (6.24) and (6.25) with respect to τ_1 and then substitute $\chi = 0$, we get

$$Q_1\chi_{\tau_1}+Q_2\zeta_{\tau_1} = W_1, \tag{6.26}$$

$$-Q_2\chi_{\tau_1}+Q_1\zeta_{\tau_1} = W_2, \tag{6.27}$$

where

$$Q_1 = \mu_2-3\zeta^2+(\eta_1-\tau_1(\eta_2-\zeta^2))\rho cos(\zeta\tau_1)+(2-\eta_1\tau_1)\rho\zeta sin(\zeta\tau_1)-\rho\eta_3\tau_2 cos(\zeta\tau_2),$$

$$Q_2 = -2\zeta\mu_1 + (\eta_1\tau_1 - 2)\zeta\rho cos(\zeta\tau_1) + (\eta_1 - \tau_1(\eta_2 - \zeta^2))\rho sin(\zeta\tau_1) - \rho\eta_3\tau_2 sin(\zeta\tau_2),$$

$$W_1 = \rho\zeta(\eta_2 - \zeta^2)sin(\zeta\tau_1) - \rho\eta_1\zeta^2 cos(\zeta\tau_1),$$

$$W_2 = \rho\eta_1\zeta^2 sin(\zeta\tau_1) + \rho\zeta(\eta_2 - \zeta^2)cos(\zeta\tau_1).$$

Solving Eqs. (6.26) and (6.27), we obtain

$$\chi_{\tau_1} = \frac{dRe(\lambda)}{d\tau_1}\bigg|_{\tau_1=\tau_1^*} = \frac{W_1Q_1 - W_2Q_2}{Q_1^2 + Q_2^2} \neq 0. \tag{6.28}$$

Theorem 6.4.3. *When τ_2 is fixed in its stable interval $[0, \tau_2^*)$, system (6.1) undergoes Hopf-bifurcation at $\tau_1 = \tau_1^*$ if the transversality condition (6.28) holds.*

Case V: $\tau_1 \in (0, \tau_1^*),\ \tau_2 > 0$ **:** The analysis for this case is analogous to that of Case IV.

Remark. It is important to note here that the inequalities (6.20) and (6.28) must hold for the occurrence of Hopf-bifurcation with respect to τ_1 and τ_2, respectively. However, in the case of equality, a pair of complex-conjugate eigenvalues does not cross the imaginary axis with non-zero speed [69].

6.4.1 Direction and stability of Hopf-bifurcation

Here, we determine the direction of Hopf-bifurcation and stability of the bifurcated periodic solution at $\tau_1 = \tau_{1_0}^*$ and $\tau_2 \in (0, \tau_2{}^*)$ using the center manifold theorem and normal form theory as described by Hassard *et al.* [124]. Under an analysis similar to [179], we determine the following expressions for our model.

$$C_1(0) = \frac{i}{2\tau_{1_0}^*\zeta}\left(g_{20}g_{11} - 2|g_{11}|^2 - \frac{|g_{02}|^2}{3}\right) + \frac{g_{21}}{3},\ \ \mu_2 = -\frac{Re\{C_1(0)\}}{Re\{\lambda'(\tau_{1_0}^*)\}},$$

$$\beta_2 = 2Re\{C_1(0)\}\ \text{ and }\ T_2 = -\frac{Im\{C_1(0)\} + \mu_2\{Im(\lambda'(\tau_{1_0}^*))\}}{\zeta\tau_{1_0}^*},$$

where

$$g_{20} = \frac{\tau_{1_0}^*}{\overline{D}}\left[rW_{20}^{(1)}(0) - 2rk\beta_1 e^{-i\zeta\tau_2^*} - 2r_1 - 2\alpha\beta_1 + 2f\alpha_1 + 2\overline{\alpha_1^*}(\alpha c_1\beta_1 - e\alpha_1)\right],$$

$$g_{02} = \frac{\tau_{1_0}^*}{\overline{D}}\left[rW_{02}^{(1)}(0) - 2rk\overline{\beta_1} e^{-i\zeta\tau_2^*} - 2r_1 - 2\alpha\overline{\beta_1} + 2f\overline{\alpha_1} + 2\overline{\alpha_1^*}(\alpha c_1\overline{\beta_1} - e\overline{\alpha_1})\right],$$

$$g_{11} = \frac{\tau_{1_0}^*}{\overline{D}}\Bigg[rW_{11}^{(1)}(0) - rk(\beta_1+\overline{\beta_1})e^{-i\zeta\tau_2^*} - 2r_1 - \alpha(\beta_1+\overline{\beta_1}) + f(\alpha_1+\overline{\alpha_1}) + \overline{\alpha_1^*}(\alpha c_1(\beta_1+\overline{\beta_1}) - e(\alpha_1+\overline{\alpha_1}))\Bigg],$$

$$g_{21} = \frac{\tau_{1_0}^*}{\overline{D}}\Bigg[2rk(-\overline{\beta_1}W_{20}^{(1)}(0)e^{-i\zeta\tau_2^*} - W_{20}^{(3)}(\frac{-\tau_2^*}{\tau_{1_0}^*}) - W_{11}^{(3)}(\frac{-\tau_2^*}{\tau_{1_0}^*}) - \beta_1 W_{11}^{(1)}(0)e^{-i\zeta\tau_2^*} + k\beta_1(\beta_1 + \overline{\beta_1})e^{-2i\zeta\tau_2^*} + ce^{-i\zeta(\tau_{1_0}^*+\tau_2^*)}(2\beta_1+\overline{\beta_1})) - 4r_1W_{11}^{(1)}(0) - 2(\alpha + c_1\overline{\alpha_1^*})(W_{11}^{(3)}(0) + W_{11}^{(1)}(0)\beta_1 + \frac{\beta_1}{2}W_{20}^{(1)}(0) + \frac{W_{20}^{(3)}(0)}{2}) + 2\alpha^2 h(2\beta_1+\overline{\beta_1}) + 2(f - e\overline{\alpha_1^*})(W_{11}^{(2)}(0) + W_{11}^{(1)}(0)\alpha_1 + \frac{\overline{\alpha_1}}{2}W_{20}^{(1)}(0) + \frac{W_{20}^{(2)}(0)}{2}) + \overline{\alpha_1^*}(W_{11}^{(3)}(0) + W_{11}^{(1)}(0)\beta_1 + \frac{\beta_1}{2}W_{20}^{(1)}(0) + \frac{W_{20}^{(3)}(0)}{2}) - 2\alpha^2 c_1 h(2\beta_1+\overline{\beta_1})\Bigg].$$

Here $W_{20}(\theta)$, $W_{02}(\theta)$, $W_{11}(\theta)$, $\overline{D}$, α_1, β_1, α_1^*, β_1^* can be determined following the procedure used in [179].

Now we are able to state the following theorem.

Theorem 6.4.4. *1. The sign of μ_2 determines the direction of the Hopf-bifurcation. If $\mu_2 > 0 (< 0)$, then the Hopf-bifurcation is supercritical (subcritical).*

2. The sign of β_2 determines the stability of the bifurcating periodic solution. If $\beta_2 > 0 (< 0)$, then the obtained periodic solution is unstable (stable).

3. T_2 determines the period of the bifurcating periodic solution. If $T_2 > 0 (< 0)$, then the period increases (decreases).

6.5 Numerical simulation

Let us consider the parameter values from Table 6.1. For this set, the system exhibits two interior equilibrium points $E_1^*(0.8475, 0.1436, 0.2255)$, $E_2^*(1.4512, 0.128, 0.2012)$, and a predator-free equilibrium $E_1(5.2857, 0, 0)$. From Fig. 6.2 (c), we observe that both E_1^* and E_1 are attractors, depending upon the initial condition. E_2^* is a saddle point, which ecologically signifies that species appear to converge in this state, but it does not.

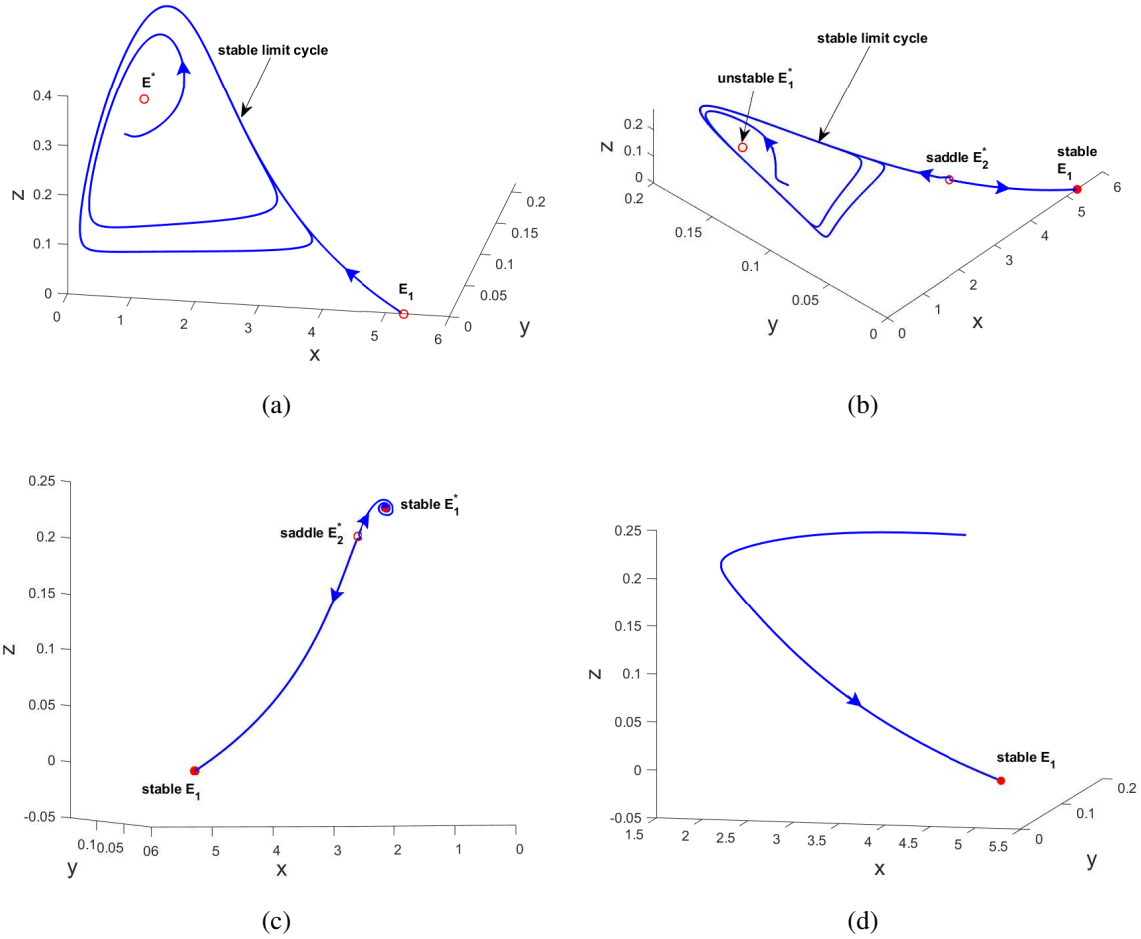

Fig. 6.2: Three-dimensional geometric plot illustrating the non-delayed system's solution behavior for different attack rates of prey, i.e., (a) $e = 0.05$, (b) $e = 0.15$, (c) $e = 0.25$, (d) $e = 0.28$. Other parameters are taken from Table 6.1.

Role reversal effect: We examine our system with respect to the role reversal parameter (e) theoretically and numerically. A series of phase portraits are plotted for different values of e in Fig. 6.2 (a)-(d). This Figure demonstrates the bi-stability phenomenon and several local bifurcations occurring in the system. Role reversal of prey and predator can cause the change in stability of E_1 and E_1^*, and number of positive steady-states. Consequently, the system experiences Hopf-bifurcation, saddle-node bifurcation and transcritical bifurcation (see Fig. 6.3).

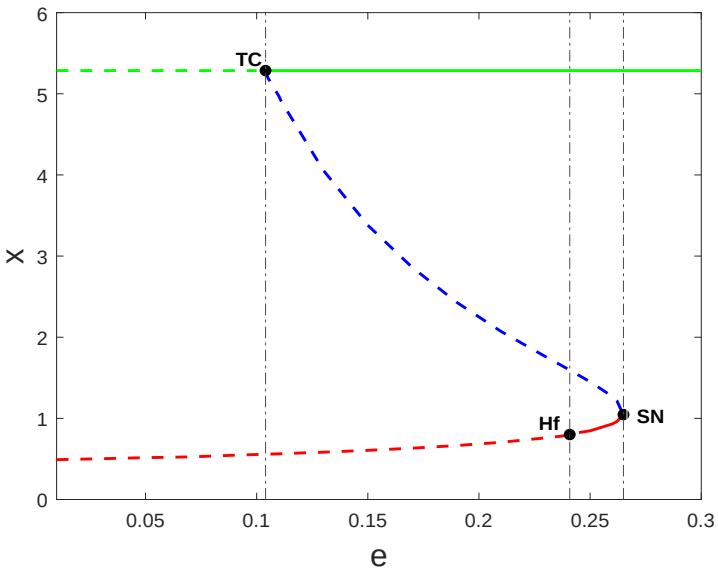

Fig. 6.3: Bifurcation diagram for prey density with respect to the role reversal parameter e in the absence of time delay. Here TC is the transcritical bifurcation point, SN is saddle-node bifurcation point, and Hf is the Hopf-bifurcation point. Dashed and solid curve represent the unstable and stable nature of an equilibrium point. Green color denotes the predator-free equilibrium E_1 and the two interior equilibrium points E_1^* and E_2^* are shown by red and blue colors, respectively.

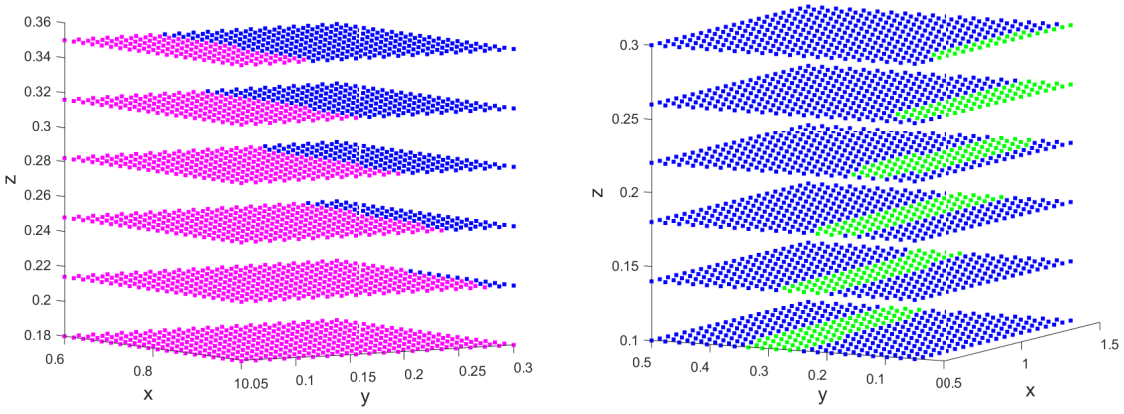

(a) (b)

Fig. 6.4: This figure displays the basin of attraction for two attractors corresponding to Fig. 6.2 (b) and Fig. 6.2 (c) in (a) and (b), respectively. The green color dots represent the basin of attraction for E_1^*, set of blue color dots is basin for E_1, and magenta color dots forms the basin for the limit cycle.

When the attack rate of prey (e) is low, all species oscillate about their positive steady-state

(see Fig. 6.2 (a)). When e increases, the possibility of predator extinction arises as the prey-only state becomes stable through transcritical bifurcation. Due to this, the system acquires bi-stability between the limit cycle and prey-only state E_1, and one more interior equilibrium comes into existence (see Fig. 6.2 (b)). The set of initial values for which the solution converges to a particular attractor is its basin of attraction. The three-dimensional basin for E_1 and limit cycle are represented with different colors in Fig. 6.4 (a). The limit cycle suffers Hopf-bifurcation and loses stability when e is further increased. After this, the system is bi-stable again, but this time it is node-focus bi-stability (see Fig. 6.2 (c)). We can visualize the basin of attraction for interior (focus) and axial (node) equilibrium in Fig. 6.4 (b). In addition, when the counter-attack rate is sufficiently high, the saddle-node bifurcation prohibits species from coexisting. However, the stability of the prey-only state remains unchanged. Therefore, predators can be eradicated when prey becomes more violent (see Fig. 6.2 (d)).

We have explored the Hopf and transcritical bifurcations in Section 6.3. In the following example, we are able to show the occurrence of the saddle-node bifurcation with respect to the role reversal parameter (e).

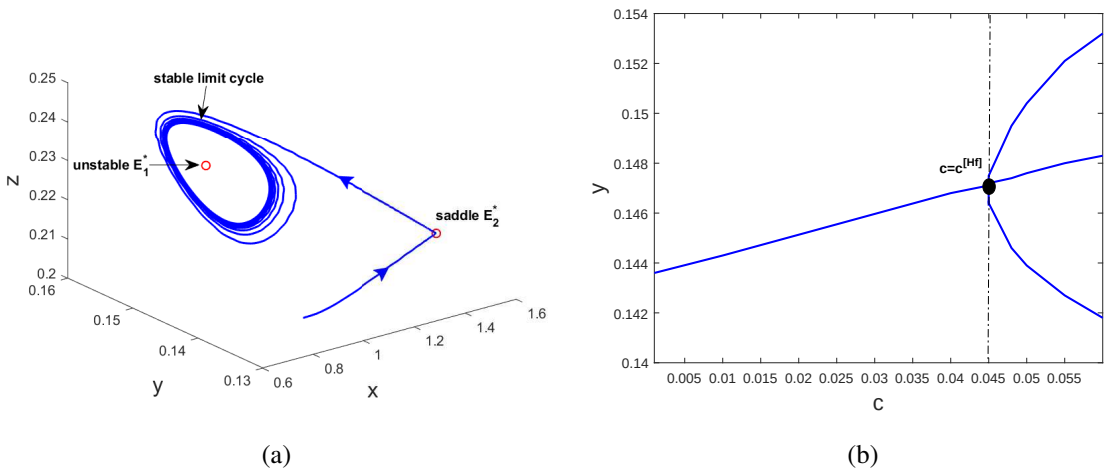

(a) (b)

Fig. 6.5: (a) Solution trajectory of system (6.2) converging to the limit cycle for $c = 0.06$ after the Hopf-bifurcation. (b) Hopf-bifurcation diagram of y regarding c.

Example 1: Consider $e = e^{[sn]} = 0.265283$ and other parameters from Table 6.1, the Jacobian matrix around $E^*(1.0464, 0.1405, 0.2209)$ is obtained as follows:

$$J_1 = \begin{pmatrix} -0.163 & 0.001 & -4.417 \\ 0 & -1.58 & 1.008 \\ 0 & 1.1 & -0.7 \end{pmatrix}.$$

The eigenvectors corresponding to the eigenvalue zero of matrix J_1 and J_1^T are $v = (-0.999,\ 0.022,\ 0.036)^T$ and $w = (0,\ -0.571,\ -0.82)^T$, respectively.
Now, we calculate

$$F_e(E^*, e^{[sn]}) = (0,\ -0.1501,\ 0)^T,$$

which yields

$$\nabla_1 = w^T F_e(E^*, e^{[sn]}) = 0.0857 \neq 0.$$

Some calculation yields another quantity

$$\nabla_2 = w^T [D^2 F(E^*, e^{[sn]})](v, v) = 0.032756 \neq 0.$$

All conditions of Sotomayor's Theorem for saddle-node bifurcation are satisfied [60]. Hence, system undergoes saddle-node bifurcation at $e = e^{[sn]} = 0.265283$ around $E^*(1.0464, 0.1405, 0.2209)$.

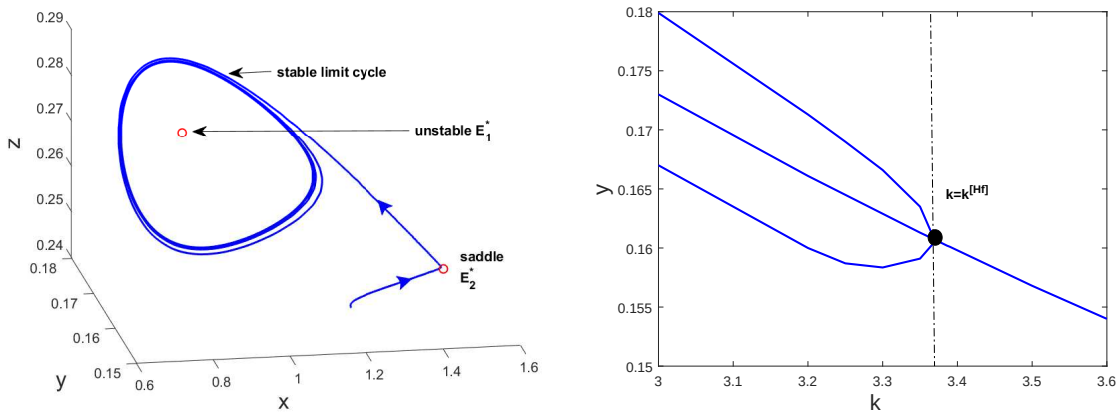

(a) (b)

Fig. 6.6: (a) Solution trajectory of system (6.2) converging to the limit cycle for $k = 3$ after the Hopf-bifurcation. (b) Hopf-bifurcation diagram of y regarding k.

Fear and carry-over effect: From the theoretical analysis done in the previous section, we can remark that the existence of any equilibrium and stability of extinction and predator-free equilibrium is unaffected by the fear (k) and its carry-over effect (c). Since, the stability of an interior equilibrium depends on k and c, the system can undergo Hopf-bifurcation under fear and carry-over effect. Figs. 6.5 (a) and 6.6 (a) show the stable nature of limit cycle surrounding unstable E_1^*, and saddle nature of E_2^* at $c = 0.06$ and $k = 3$, respectively. The instability of E_1^* is due to the supercritical Hopf-bifurcation with respect to c and k at $c^{[Hf]} = 0.044966$ and $k^{[Hf]} = 3.3859$, respectively. The bifurcation diagrams taking maximum and minimum values of y for different values of c and k are sketched in Fig. 6.5 (b) and 6.6 (b), respectively. It is important to note here that the population number is not much affected by the variation in

c. Switching of stability regarding fear and its carry-over effect motivates us to plot the Hopf-bifurcation curve in ck-plane. According to Fig. 6.7, for each value of c, one can determine K at which the system switches stability through Hopf-bifurcation.

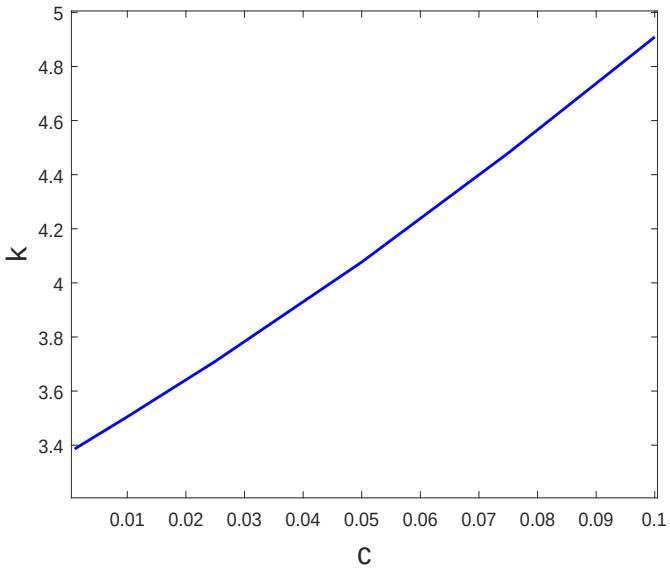

Fig. 6.7: Hopf-bifurcation curve in cK-plane for system (6.2).

Paradox of enrichment: Expansion of carrying capacity may not always support the enrichment of the ecosystem. Moreover, an increase in carrying capacity may destabilize the system (instead of stabilizing). This phenomenon is termed as "Paradox of enrichment." In our model, we can observe the paradox of enrichment with respect to the birth rate of the prey population (r) (see Fig. 6.8). The reason for choosing r to be the enrichment parameter is the expression for the carrying capacity of prey, i.e., $K_1 = \frac{r-r_0}{r_1}$. So, adjusting carrying capacity or birth rate works the same for our model. For the parameters chosen from Table 6.1, the co-existence state $E^*(0.8475, 0.1436, 0.2255)$ has eigenvalues $-2.228393,\ -0.014662 \pm 0.18895i$. The negativity of the real part of eigenvalues confirms the local stability of E^*, and graphically solution trajectory converges to it. When we increase the value of r, species oscillate about their mean state, generating a stable limit cycle. Mathematically, the magnitude of the real part of complex eigenvalues decreases up to zero and then increases. This phenomenon takes place due to a supercritical Hopf-bifurcation at $r = r^{[Hf]} = 2.809619$.

The paradox of enrichment can be completely precluded by adjusting the fear level (k) or the predator's attack rate (α). We can see from Figure 6.9 (a) that at a certain level of fear (at $k = 4$), system is unstable around its co-existence state. However, a slight increment in fear level can control the oscillations demonstrating elimination of the paradox. Therefore, at $k = 4.2$, E^* becomes a stable focus (see Fig. 6.9 (b)). Moreover, keeping the fear level same (at

$k = 4$), and a slight decrease in the attack rate of the predator (α) can also resolve the paradox. Fig. 6.9 (c) depicts that the trajectory converges to the attractor E^* for $\alpha = 6.4$.

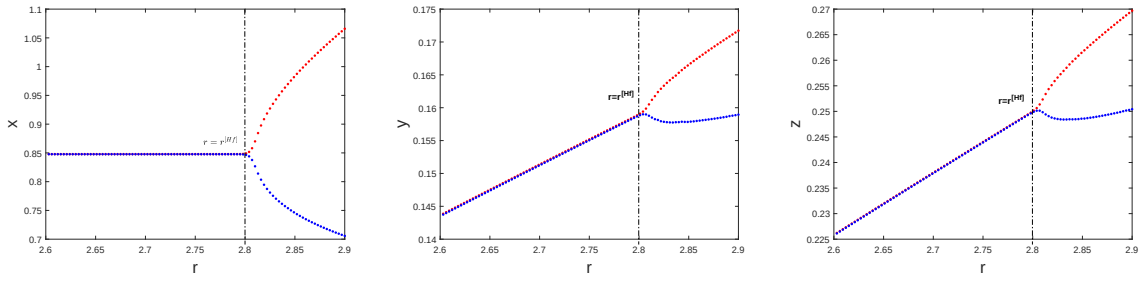

(a) (b) (c)

Fig. 6.8: Bifurcation diagram for (a) x, (b) y, and (c) z species with respect to r. When $r < {}^{[Hf]}$, the maximum and minimum of the solution coincide at the positive steady-state E^*, showing the stable nature of E^*. The difference between the maximum (red color) and minimum (blue color) solution increases with the rise in r after the Hopf point $r < {}^{[Hf]}$. This figure depicts the instability of the non-delayed system's solution when r increases.

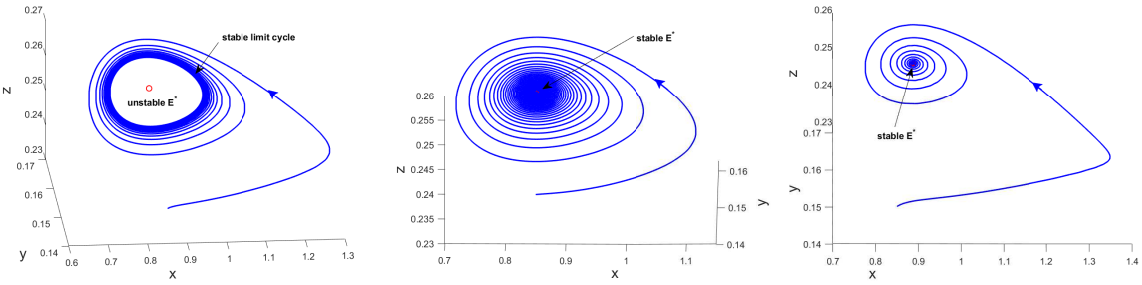

(a) (b) (c)

Fig. 6.9: Phase portrait showing (a) instability of the interior equilibrium E^* as a consequence of paradox of enrichment at $k = 4$, $\alpha = 6.5$. The paradox is resolved for (b) $k = 4.2$ and (c)$\alpha = 6.4$, making system (6.2) stable around E^*. Here $r = 2.85$ and other parameters are the same as in Table 6.1.

Effect of predation rate of prey and predator: We have already seen that our system possesses complex dynamics with respect to the predation rate of prey (e). What if we vary the predation rate of predator (α) and prey (e) together? Variation of two parameters simultaneously can provide intriguing system dynamics, an important one is Bogdanov-Takens bifurcation. This bifurcation is an exciting combination of Hopf-bifurcation, saddle-node bifurcation, and homoclinic bifurcation (see BT marked in Fig. 6.10). At the Bogdanov-Takens bifurcation

point, the Jacobian matrix evaluated at an interior equilibrium has an eigenvalue zero of multiplicity two, and another eigenvalue is negative. To derive the normal form of BT-bifurcation, we follow the steps mentioned in [69].

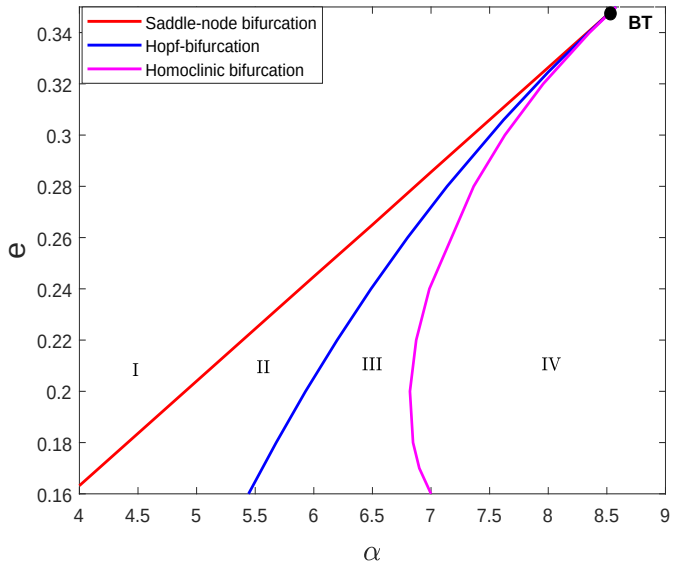

Fig. 6.10: Intersection of Hopf curve, saddle-node curve, and homoclinic curve at the Bogdanov-Takens bifurcation point. All these bifurcations occur with respect to e and α for system (6.2).

Firstly, we shift the interior equilibrium $E^*(x^*,y^*,z^*)$ to the origin using the transformation:

$$x-x^*=u_1,\;\; y-y^*=u_2,\;\; z-z^*=u_3.$$

Then system (6.2) is reduced as

$$\begin{aligned}
\frac{du_1}{dt} &= (u_1+x^*)\left[\frac{r(1+c(u_1+x^*))}{1+c(u_1+x^*)+k(u_3+z^*)} - r_0 - r_1(u_1+x^*) - \frac{\alpha(u_3+z^*)}{1+\alpha h(u_1+x^*)} + f(u_2+y^*)\right] \\
&= f_1(u_1,u_2,u_3), \\
\frac{du_2}{dt} &= \frac{c_1\alpha(u_1+x^*)(u_3+z^*)}{1+\alpha h(u_1+x^*)} - \beta(u_2+y^*) - d_1(u_2+y^*) - e(u_1+x^*)(u_2+y^*) = f_2(u_1,u_2,u_3), \\
\frac{du_3}{dt} &= \beta(u_2+y^*) - d_2(u_3+z^*) = f_3(u_1,u_2,u_3).
\end{aligned} \tag{6.29}$$

System (6.29) can also be written as system (6.11). Due to the complexity of the model, it is difficult to find the eigenvectors of J_1 explicitly in analytical manner. Therefore, we have our next example for the further explanation.

Example 2: At $\alpha = \alpha^{[bt]} = 8.577806$, $e = e^{[bt]} = 8.577806$ and other parameters from Table 6.1, the eigenvectors of the Jacobian matrix about $E^*(0.8156, 0.1411, 0.2217)$ are the columns of the following matrix.

$$P = \begin{array}{c} \begin{matrix} \Xi_1 & \Xi_2 & \Xi_3 \end{matrix} \\ \begin{pmatrix} 1 & 1 & 1.592 \\ 0 & -0.174 & -1.435 \\ 0 & -0.274 & 1 \end{pmatrix} \end{array},$$

where Ξ_1, Ξ_2, and Ξ_3 satisfy $J_1\Xi_1 = 0$, $J_1\Xi_2 = \Xi_1$, and $(J_1 - \lambda I)\Xi_3 = 0$, where $\lambda = -2.285$. Now, we use the following transformation.

$$\begin{pmatrix} u_1 \\ u_2 \\ u_3 \end{pmatrix} = P \begin{pmatrix} w_1 \\ w_2 \\ w_3 \end{pmatrix} = \begin{pmatrix} w_1 + w_2 + 1.592w_3 \\ -0.174w_2 - 1.435w_3 \\ -0.274w_2 + w_3 \end{pmatrix}.$$

From (6.11), we get

$$\begin{pmatrix} w_1 \\ w_2 \\ w_3 \end{pmatrix}' = P^{-1} \begin{pmatrix} u_1 \\ u_2 \\ u_3 \end{pmatrix}' = P^{-1} \left\{ J_1 \begin{pmatrix} u_1 \\ u_2 \\ u_3 \end{pmatrix} + \begin{pmatrix} g_1 \\ g_2 \\ 0 \end{pmatrix} \right\}.$$

Some mathematical calculation yields

$$\begin{aligned} \frac{dw_1}{dt} &= w_2 - 0.4129w_1^2 + 0.05236w_2^2 - 0.6225w_1w_2 + \mathscr{O}(|w_1, w_2, w_3|^2), \\ \frac{dw_2}{dt} &= 0.4202w_1w_2 + 0.0875w_1^2 + 0.3325w_2^2 + \mathscr{O}(|w_1, w_2, w_3|^2), \\ \frac{dw_3}{dt} &= -2.285w_3 + \mathscr{O}(|w_1, w_2, w_3|^2). \end{aligned} \quad . \tag{6.30}$$

Using the steps given in [203], system (6.30) is transformed to the normal form as

$$\begin{aligned} \frac{dw_1}{dt} &= w_2, \\ \frac{dw_2}{dt} &= 0.0875w_1^2 - 0.4056w_1w_2 + \mathscr{O}(|w_1, w_2|^2). \end{aligned} \tag{6.31}$$

In system (6.31), the coefficient of w_1^2 and w_1w_2 are non-zero, it concludes that the Bogdanov-Takens bifurcation of codimension two occur in the proposed system at $(\alpha, e) = (8.577806, 0.35)$. At this point, eigenvalues of the Jacobian matrix about $E^*(0.8156, 0.1411, 0.2217)$ are $0,\ 0, -2.2855$, and consequently, the Hopf curve, saddle-node curve, and Homoclinic curve intersect here (see Fig. 6.10).

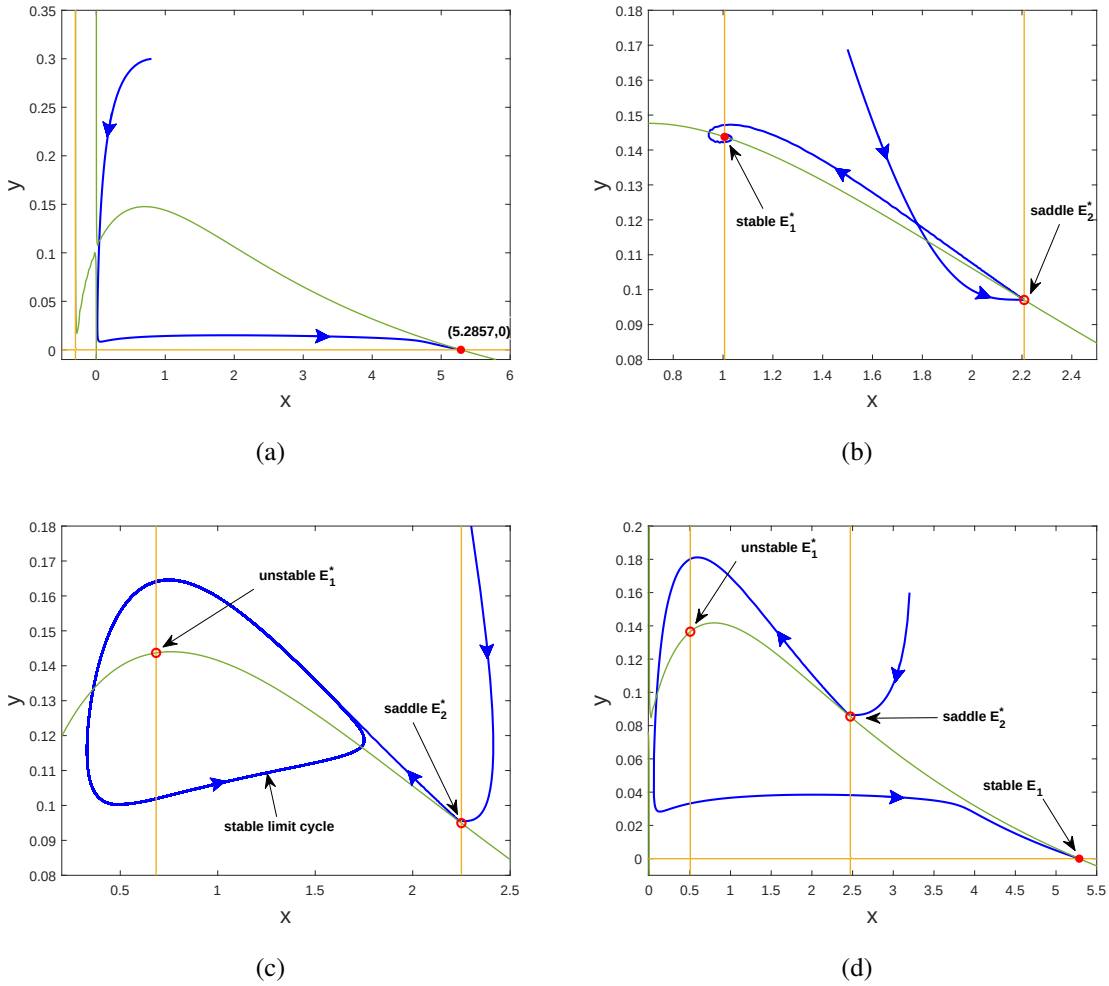

Fig. 6.11: Phaseportraits showing (x, y) solutions passing through various equilibrium points corresponding to (a) Region I, (b) Region II, (c) Region III, (d) Region IV displayed in Fig. 6.10. Green color represents the prey (x) nullcline and yellow color represents the juvenile predator (y) nullcline.

Various bifurcations occurring in the system divide the αe region into four regions. Region I has no interior equilibrium due to the occurrence of the saddle-node bifurcation at the red curve. Region II displays the scenario before the saddle-node bifurcation, where one stable and one saddle equilibrium exist. As we move across the blue Hopf curve, a positive equilibrium loses its stability through a supercritical Hopf-bifurcation and generates a stable limit cycle in Region III. This limit cycle expands and eventually connects the existing saddle interior equilibrium at the magenta curve through a homoclinic global bifurcation. After this, the limit cycle disappears, and the solution goes to the already stable E_1 in Region IV (see Fig. 6.10).

We can plot x and y nullclines of the reduced system obtained by substituting the value of z from Eq.(6.5) in (6.3) and (6.4). The intersection of nullclines is the x and y coordinate of an equilibrium point. We have plotted the solution trajectory and nullclines corresponding to

Regions I, II, III, and IV in Fig. 6.10. For $\alpha = 5$ and $e = 0.25$, positive equilibrium does not exist, and all trajectories converge to the predator-free equilibrium (see Fig. 6.11 (a)). Now, with the same value of α and $e = 0.18$, two positive equilibrium points E_1^* and E_2^* exist; one is a saddle, and the other is stable (see Fig. 6.11 (b)). After experiencing the supercritical Hopf-bifurcation, E_1^* becomes a repeller enclosed within a stable limit cycle for $\alpha = 6.5$ and $e = 0.2$ (see Fig. 6.11 (c)). Increasing the value of α takes us toward the global homoclinic bifurcation. For $\alpha = 8$, the solution finally converges to the predator-free state E_1 (see Fig. 6.11 (d)).

Effect of carry-over delay ($\tau_1 > 0, \tau_2 = 0$)**:** Let us consider the following set of parameters.

$$r = 3,\ r_0 = 0.4,\ r_1 = 0.6,\ k = 0.5,\ d_1 = 0.08,\ d_2 = 0.1,\ c = 0.15,\ \beta = 0.8,\ c_1 = 0.5,\ h = 1,$$
$$f = 0.001,\ e = 0.05,\ \alpha = 0.57 \tag{6.32}$$

For the above set of parameters, the proposed system is unstable about $E^*(0.5134, 0.2448, 1.9583)$ in the absence of time delay. Moreover, there are oscillations about the positive steady-state. These oscillations in the system are controlled for a particular value of τ_1. Consequently, the system becomes stable, and all solutions converge to E^*. The stability no longer sustains when the time delay is further increased. Limit cycle oscillations occur for a certain range of τ_1. The stability switching dynamics goes on when the value of τ_1 is higher. The visual of the aforementioned properties is demonstrated in Fig. 6.12. This figure shows six times stability switching for the different critical values of τ_1 at $\tau_1 = \tau_{1_i}^*$, for $i = 0, 1, 2, 3, 4, 5$. At these bifurcation points, the pair of complex eigenvalues becomes purely imaginary.

For the chosen set of parameters, the stability behavior of the interior equilibrium keeps on changing, but predator-free equilibrium remains saddle for all $\tau_1 \geq 0$.

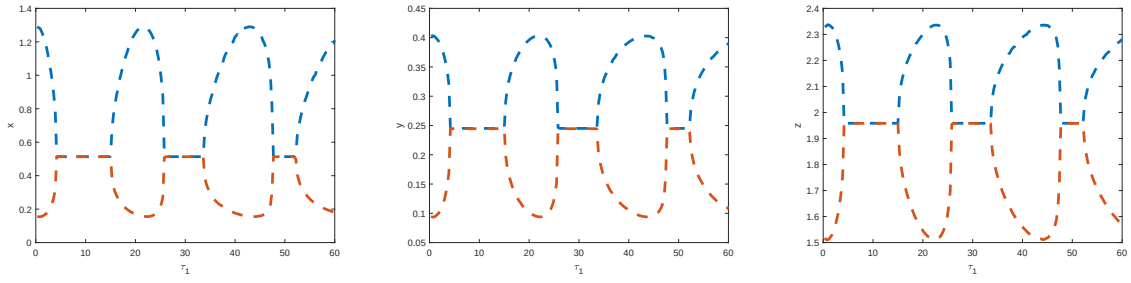

(a) (b) (c)

Fig. 6.12: (a), (b), and (c) depicts the bifurcation diagram for $x, y,$ and z species, respectively, with respect to the COE delay τ_1. This figure illustrates how oscillations about positive equilibrium can occur and be controlled repeatedly in the presence of COE delay.

Effect of fear-response delay ($\tau_1 = 0, \tau_2 > 0$): The system without time delay has a stable limit cycle for the parameters set (6.32). When we impose fear-response delay, E^* is unstable, and the limit cycle enclosing it persists for an intermediate range of τ_2. In a specific range of τ_2, chaos and two-periodic and higher periodic solutions emerge. The high periodicity of solutions and the occurrence of chaos enrich the system's dynamics with fear-response delay.

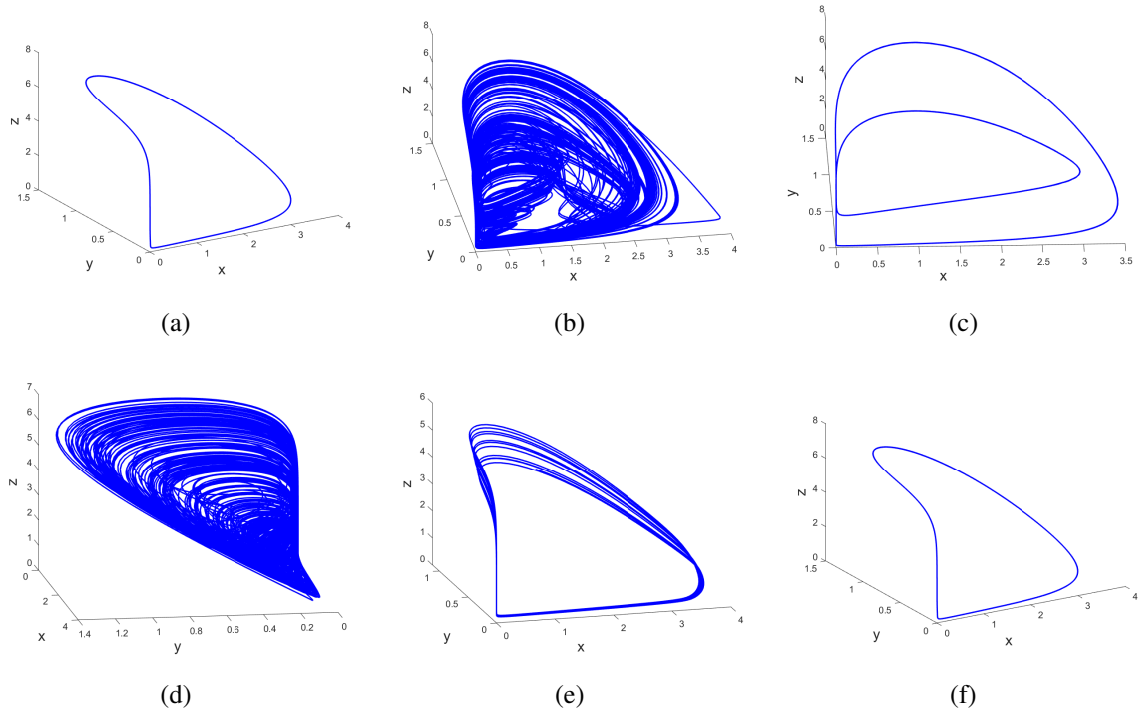

Fig. 6.13: Behavior of solution for distinct values of τ_2 at (a)$\tau_2 = 30$, (b)$\tau_2 = 32$, (c)$\tau_2 = 45$, (d)$\tau_2 = 57$, (e)$\tau_2 = 77$, (f)$\tau_2 = 82$.

The series of phase portraits are drawn in Fig. 6.13. We note that the solutions oscillate about their positive steady-state in the form of a limit cycle at $\tau_2 = 30$. When τ_2 is increased, we observe the unpredictability of the solution indicating the phenomenon of chaos at $\tau_2 = 32$ (see Fig. 6.13 (b)). The chaos is controlled, and a limit cycle of period-2 occurs for $\tau_2 = 45$ (see Fig. 6.13 (c)). Further increase in delay makes the system chaotic again at $\tau_2 = 57$ (see Fig. 6.13 (d)), and this chaos can be controlled again for higher values of τ_2. After leaving the chaotic behavior, oscillations of a high period occur (at $\tau_2 = 77$) in the system (see Fig. 6.13 (e)), and finally, the system has a limit cycle attractor at $\tau_2 = 82$ (see Fig. 6.13 (f)).

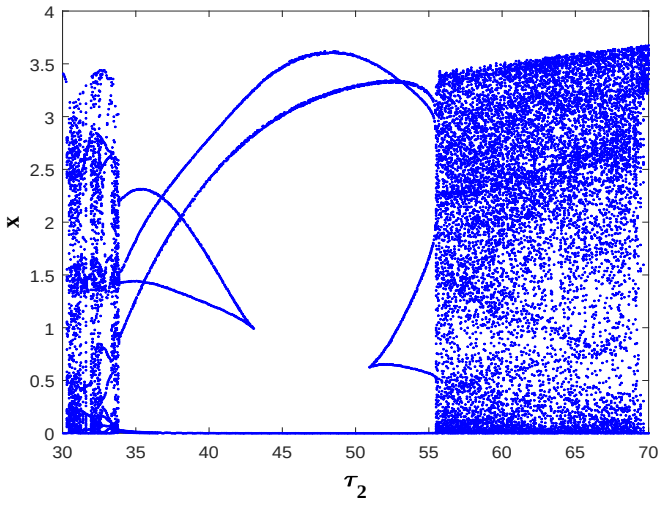

Fig. 6.14: Bifurcation diagram showing the emergence of chaos for an intermediate range of τ_2, when $\tau_1 = 0$.

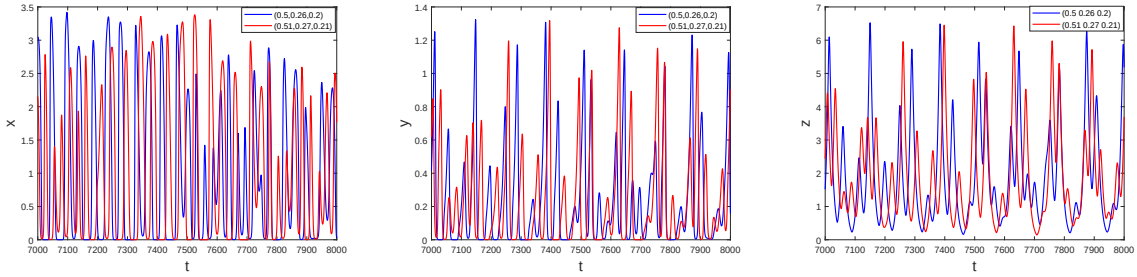

(a) (b) (c)

Fig. 6.15: The time evolution of species (a) x, (b) y, and (c) z, illustrating the sensitivity towards the initial point chosen at $\tau_2 = 57$, and other parameters are same as in (6.32).

For better visualization of the change in dynamics of system (6.1) regarding fear-response delay, we draw the bifurcation diagram for prey density with respect to τ_2 (see Fig. 6.14). To detect chaos, we perform sensitivity analysis concerning the initial condition. A slight perturbation in the initial solution $(0.5, 0.26, 0.2) \rightarrow (0.51, 0.27, 0.21)$ causes a large deviation in the final solution (shown by blue and red color in Fig. 6.15). In support of this, we draw the maximum Lyapunov exponent (MLE) to confirm the chaotic phenomenon (see Fig. 6.16). The positivity of the MLE shows the chaotic trait of the system with respect to the fear-response delay.

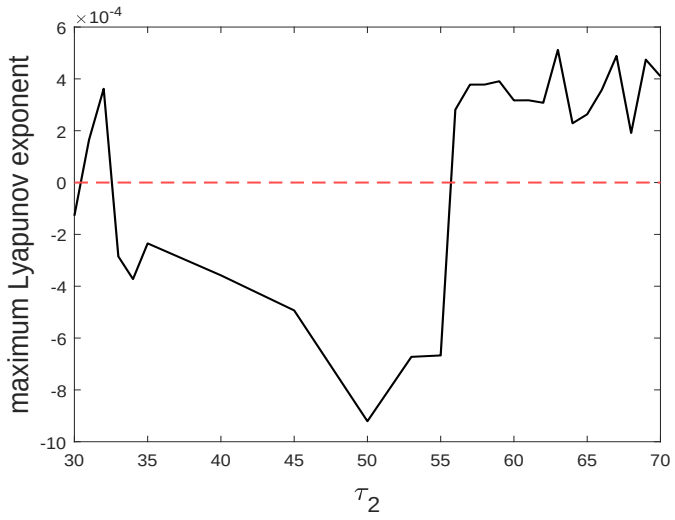

Fig. 6.16: The plot of Maximum Lyapunov Exponent with respect to τ_2, when $\tau_1 = 0$.

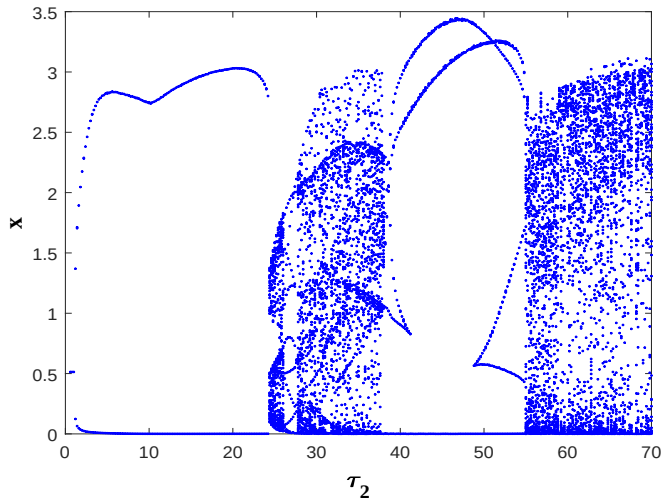

Fig. 6.17: Bifurcation diagram demonstrating the occurrence of Hopf-bifurcation and chaos with respect to τ_2, when $\tau_1 = 30$.

Combined effect of fear-response and COE delays: Let us fix τ_1 in its stable range from Fig. 6.12 say $\tau_1 = 30$. Now, vary τ_2 while keeping all parameters the same from (6.32). When $\tau_2 = 0$, E^* is stable, and it switches stability through Hopf-bifurcation at $\tau_2 = \tau_2^* = 1.145$. Going for large values of τ_2, the solution of system (6.1) shows chaotic trait, and then it becomes predictable for a certain range. Furthermore, the system again enters into a state of chaos for comparatively large values of τ_2. The non-linear phenomena such as Hopf-bifurcation and chaos can be visualized through a bifurcation diagram. Therefore, we plot the prey density against the carry-over delay for a non-transient period in Fig. 6.17. Furthermore, we perform the sensitivity analysis at $\tau_2 = 57$ to show that the system is sensitive to the small change in its

initial condition (see Fig. 6.18). Consequently, our non-linear multi-delayed system shows the attribute of chaos for fear-response delay when the COE delay is fixed. Moreover, we sketch the MLE against τ_2, and its positivity verifies the chaotic trait of the system (see Fig. 6.19).

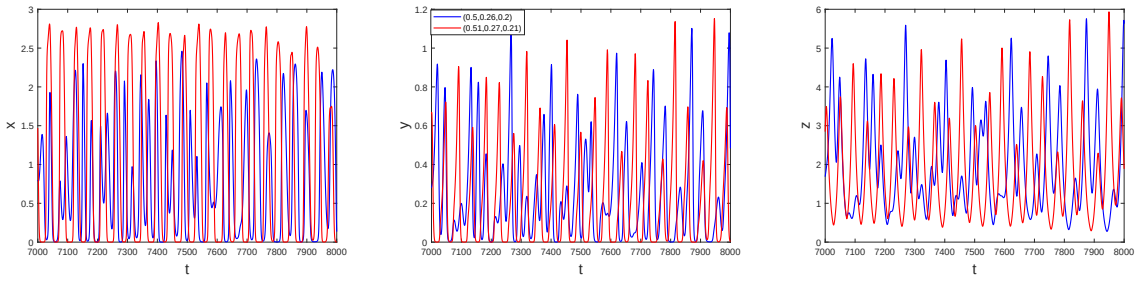

(a) (b) (c)

Fig. 6.18: The time evolution of species (a) x, (b) y, and (c) z, explaining the sensitivity towards the initial point chosen. We choose parameters from (6.32), $\tau_1 = 30$, and $\tau_2 = 57$.

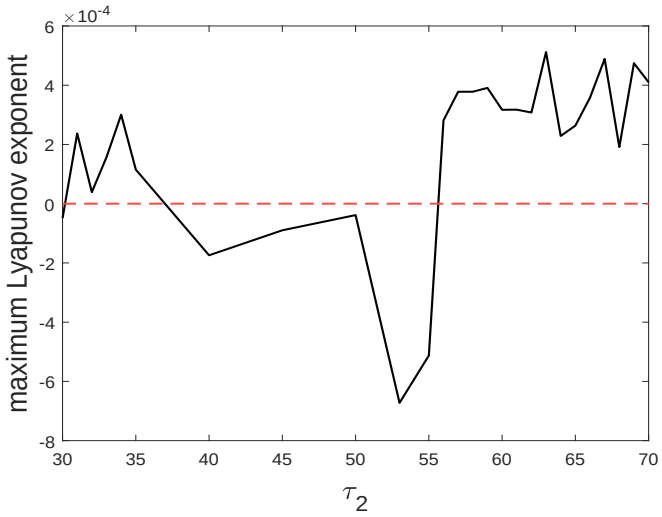

Fig. 6.19: The plot of MLE versus τ_2 when $\tau_1 = 30$, and other parameters are taken from (6.32).

6.6 Discussion and conclusion

Generally, it is an idealized fact that predator hunts and prey defend. When prey is powerful enough, it defends itself by counter-attacking feeble predator. The proposed model divides the predator class into mature (adults) and immature (juveniles). We assumed that the adult predator hunts on prey and creates fear of being killed. The fear effect has some carry-over effects on the prey population. Moreover, fear increment causes prey reproduction to decrease, and

its carry-over effect impacts the reproduction rate positively. In these life-tragic circumstances, the prey shows anti-predator behavior and kills the juvenile of the predator. These juveniles are vulnerable to predation and can neither re-attack nor reproduce. Their parents are the only source of survival. The ecological relationship between prey and predator in different stages of life has been portrayed through a set of differential equations.

In the present manuscript, we first constructed the mathematical model based on some ecological assumptions. Then we examined the well-posedness of the model by proving the positivity and boundedness of the system solutions. Next, we explored all steady-state solutions and their stability in the neighborhood. We found that the system can have at most two interior equilibrium points. The death rate of the mature predator should not exceed a threshold value for the co-existence of all species. Using the Descarte's rule of sign, we stated three theorems for the co-existence of species. Based on this, we plotted the (e, α) points associated with two, one, and zero interior equilibrium points (see Fig. 6.1).

We perceived that the existence of positive equilibrium and stability of other equilibria are independent of fear (k) and carry-over effect (c). However, the stability of interior equilibrium is tremendously affected. An increase in COE causes the populations to oscillate about their mean state. Oscillations in the system can be completely controlled when the fear level increases. Both these cases show the occurrence of super-critical Hopf-bifurcation. Moreover, we obtained a Hopf-curve in the ck-plane (see Fig. 6.7). From Fig. 6.6 (b) and Fig. 6.5(b), we can observe that the juvenile predator density decreases with a rise in fear. In contrast, it increases with the increment in the carry-over effect. While modeling these two ecological factors, we expected that the predator population would be benefited due to the fear and prey density would be boosted due to the carry-over effect. But, our findings reveal that the role reversal of prey and predator causes the fear and COE impact to get reversed. These results answer the first question from the Introduction Section.

The change in the number and stability trait of the equilibrium point encouraged us to investigate the possible bifurcations occurring in the system. We discussed the direction and stability of the Hopf-bifurcation regarding the crucial parameters. Moreover, we explored transcritical and saddle-node bifurcation for the role reversal parameter (see Fig. 6.3). Apart from these codimension-one bifurcations, we observed the Bogdanov-Takens bifurcation of codimension-two. Variations in the attack rate of predators and the counter-attack rate of prey simultaneously resulted in a Hopf curve, saddle-node curve, and a homoclinic curve in the αe-plane (see Fig. 6.10). The BT point is the splendid combination of two local (Hopf and saddle-node) and one global (homoclinic) bifurcation. These bifurcations can be closely seen in the phase portraits sketched in Fig. 6.11. This figure suggests that the attack rates (e and α) in the fixed proportion can create ecological balance. Therefore, the third question mentioned in the Introduction section has been answered.

Our system is sensitive to the initial condition as bi-stability between two attractors occurs. For a certain level of counter-attacking, species can oscillate about a positive steady-state, or predators can become extinct, depending upon the starting point. This result is concluded from the node-cycle bi-stability demonstrated in Fig. 6.2 (b). For a particular range of counter-attacking, the co-existence equilibrium becomes stable through a super-critical Hopf-bifurcation. This scenario shows the bi-stability between focus and node (see Fig. 6.2 (c)). So, the final solution can either converge to the predator-free or co-existence state; it depends on their basins. Furthermore, the predator-free equilibrium stays stable when the role reversal parameter is significant (see Fig. 6.2 (d)). In an ecological sense, too much counter-attacking can wipe out all predators. This gives the answer to the second and third objectives of our research.

When we increased the carrying capacity (by increasing r), the system was expected to become enriched. However, instead of this, instability occurred. This phenomenon is the paradox of enrichment, and we depicted it through the bifurcation diagram in Fig. 6.8. In our study, the paradox can be eliminated by adjusting the fear or attack rate of the predator. A slight increase in the fear level or decrease in the attack rate helped us to control the species' oscillations (see Fig. 6.9). It answers the fourth question raised in the Introduction section. Sajan *et al.* [21] and Sasmal and Takeuchi [25] reported a similar phenomenon regarding fear.

Considering the time delay in the model system takes it closer to reality. We incorporated a time delay due to carry-over effects τ_1 and another delay due to the fear-response τ_2 in the reproduction rate of the prey. Variation in the delay does not affect the level of any equilibrium. Our results reveal that the stability of the predator-free and extinction equilibrium is unchanged with respect to time delay, but the stability of the interior equilibrium can change tremendously. Therefore, we analyzed the local stability and Hopf-bifurcation around the positive steady-state theoretically and numerically for all the possible cases of τ_1 and τ_2. Moreover, we examined the direction and stability of Hopf-bifurcation using the center manifold theorem and normal form theory. Our numerical findings show a switching of stability multiple times with a rise in COE delay. This switching takes place due to the occurrence of a supercritical Hopf-bifurcation (see Fig. 6.12). When we examined the system dynamics concerning fear-response delay, we obtained fascinating dynamics like period-doubling and chaos. Sensitive dependence on the initial condition of the solution and plot of MLE confirms the chaotic trait of the system even when the COE delay is present or not. Moreover, when $\tau_1 = 0$ or 30, the chaos or unpredictability can be controlled for an intermediate range of τ_2. This answers our first question raised in the Introduction.

Chapter 7

Chaos in a seasonal food-chain model with migration and variable carrying capacity [1]

7.1 Introduction

Many of the prey-predator models generally focus on single or two-species interaction. However, mathematical advancements reveal that the dynamics of a three-species model can be far more complex [47, 205]. Studying the interconnection of three species to form a food chain is a popular way of understanding population dynamics ecologically and mathematically. In traditional food chains, the basal prey is the food for the middle predator, and the middle predator is the food for the top predator. Upadhyay [206] investigated the occurrence of chaos and multi-stability in a tri-trophic food-chain model.

In nature, migration is a frequently observed phenomenon. For a multitude of reasons, like habitat security, climate change, mating chances, food accessibility, shelter needs, etc., a species may migrate. Immigration and emigration are the two main types of migration that affect a particular region. In a three-species food-chain system, the intermediate predator immigrates for hunting the prey and emigrates to escape from its predator. Zooplankton performs vertical migration in a phytoplankton-zooplankton-fish system to gain the maximum benefit [50]. A broad range of tri-trophic models without migration experience chaos via a period-doubling route. Moreover, this phenomenon can be completely reversed in the presence of migration [207]. An adequate level of migration in a food chain can control the chaotic oscillations to stabilize it [208, 209]. Recently, Hossain *et al.* [51] performed an extensive numerical simulation for a simple food-chain model with middle predator migration. They observed complex non-linear dynamics such as stability switching, bi-stability, and chaos.

In population biology, carrying capacity is referred to as the maximum burden that an environment can sustain. A large piece of literature considers the carrying capacity of any species to

[1] Revised version submitted in Nonlinear Dynamics

be constant [22, 89, 112, 210]. Nevertheless, natural or species-induced environmental changes can affect the carrying capacity. Yukalov *et al.* [52] believed a population's creative or destructive activity could enrich or deplete its natural carrying capacity. They formulated carrying capacity as the function of individuals, i.e., $K(t) = A + BN(t)$, where $A > 0$ denotes the capacity for individuals $N(t)$ innately, and $B \in R$ measures the influence of activities on carrying capacity. When $B > 0$ (or < 0), the activities are constructive (or destructive). Pati and Ghosh [53] studied a prey-predator model where the carrying capacity of prey is the combination of intrinsic and prey-proportional induced carrying capacity. They determined that $B < 1$ is the necessary condition for the existence of predator-free equilibrium. Recently, Bhunia *et al.* [54] extended the work of Pati and Ghosh [53] to investigate the emergence of Turing patterns in a diffusive predator-prey model with prey harvesting and variable carrying capacity.

The majority of ecological events are modeled and studied in a constant context, which is unusual. They have a significant degree of physical variability, which causes birth rates, mortality rates, and other key population rates to change significantly over time [168]. Considering the parameters as periodic time functions makes the model more realistic because many environmental factors affecting species' survival in the ecological community are seasonally induced [211]. Zeng [59] analyzed a seasonally-forced non-autonomous food-chain model with Holling type-II functional response to establish its permanence, extinction, and global stability. Recently, Dwivedi and Kumari [49] incorporated seasonality by means of sinusoidal functions in a tri-trophic system. They observed that seasonal variations can disturb the limit cycle to make the system chaotic. Furthermore, their study highlights the phase synchronization and various bifurcations. Samanta *et al.* [212] designed a four-dimensional phytoplankton-zooplankton-fish model where zooplankton migrate between two water levels to elude their predators. They proved the periodic solution's existence and global attractivity in the non-autonomous version.

According to the authors' knowledge, no research has been done on a food-chain model with migration and variable carrying capacity, where multiple parameters can take any real value. Moreover, the authors could not find an analysis of a non-autonomous system where parameters can take a negative value. The present work attempts to fill the aforementioned gap and divides the manuscript into the following sections. Section 7.1 comprises the relevant literature survey showing the need and base to introduce a new mathematical model. Section 7.2 shows the mathematical formulation for a food-chain model. Section 7.3 discusses the well-posedness of the proposed system. Existence and stability assessment of equilibrium points are carried out in sections 7.4 and 7.5, respectively. In Section 7.6, we study the effect of seasonality in our model theoretically. Section 7.7 shows the extensive numerical simulation to verify our theoretical findings. Finally, we conclude all results with a discussion in Section 7.8.

7.2 The food chain model construction

In a food chain, let $x(t)$, $y(t)$, and $z(t)$ be the population density of the basal prey, middle predator, and top predator, respectively, at any time t. The rate of change in a population density depends on several ecological factors. In this section, we formulate the interaction of three species based on the following assumptions.

1. In the absence of y and z, x population grows logistically with the intrinsic growth rate r to achieve its carrying capacity K. Many prey activities promote resource preservation, which can improve the environment's carrying capacity. For instance, selective grazing encourages biodiversity by allowing different plant species to coexist. However, certain behaviors within the prey population could result in a reduction in the carrying capacity. For instance, in the Kaibab plateau and the bison population [213], the overgrazing and habitat degradation caused by the rising mule deer population harmed the carrying capacity. Therefore, considering the impact of species' activities on their carrying capacity is biologically more sound. Thus, we consider the variable carrying capacity of prey as $K+\beta x$, where $\beta > 0 (< 0)$ measures the constructive (destructive) impact of the activities of x on its natural carrying capacity K [52, 53, 214]. So, the logistic growth of x without y and z is given by the following differential equation.

$$\frac{dx}{dt} = rx\left(1 - \frac{x}{K+\beta x}\right).$$

2. We assume that x shows group defense against y when y consumes x. Therefore, their relationship can be presented through the simplified Holling type IV functional response: $\frac{\alpha_1 x}{a_1+x^2}$, where α_1 is the attack rate of y, and a_1 is the half-saturation constant. The population y retards by natural mortality rate d_1, and intraspecific interference rate δ_1. The prey-predator relationship of x and y is shown by the following equations.

$$\frac{dx}{dt} = rx\left(1 - \frac{x}{K+\beta x}\right) - \frac{\alpha_1 xy}{a_1+x^2}, \quad \frac{dy}{dt} = \frac{c_1\alpha_1 xy}{a_1+x^2} - d_1 y - \delta_1 y^2.$$

Table 7.1: Numeric values of parameters utilised in (7.1)

Parameters	Ecological meaning	Numerical value	Reference(s)
r	Birth rate of the prey	0.5	[33]
β	Measures the impact of activities on the carrying capacity	0.5	Assumed
K	Carrying capacity of basal prey	1.2	[215]
α_1	Predation rate of the middle predator	1	[216]
a_1	Half saturation constant when y eats x	1	[217]
c_1	Conversion efficiency of middle predator	0.9	[215]
c_2	Conversion efficiency of top predator	0.8	[193]
α_2	Predation rate of the top predator	1.8	Assumed
a_2	Half saturation constant when z eats y	1	[217]
d_1	Natural death rate of middle predator	0.3	[218]
d_2	Natural death rate of top predator	0.3	[218]
k_1	Migration rate of middle predator	0.01	Assumed
δ_1	Intraspecific interference rate among middle predators	0.001	[210]
δ_2	Intraspecific interference rate among top predators	0.001	[210]

3. When y is food for z through Holling type II functional response: $\frac{\alpha_2 y}{a_2+y}$, where α_2 is the attack rate of z and a_2 is the half-saturation constant, the model becomes three-dimensional food-chain. The loss in z is by the natural death (d_2) and intraspecific competition among them (δ_2). Thus, the tri-trophic model displaying the interaction of x, y and z is given by:

$$\begin{aligned}
\frac{dx}{dt} &= rx\left(1-\frac{x}{K+\beta x}\right)-\frac{\alpha_1 xy}{a_1+x^2},\\
\frac{dy}{dt} &= \frac{c_1\alpha_1 xy}{a_1+x^2}-\frac{\alpha_2 yz}{a_2+y}-d_1 y-\delta_1 y^2,\\
\frac{dz}{dt} &= \frac{c_2\alpha_2 yz}{a_2+y}-d_2 z-\delta_2 z^2.
\end{aligned}$$

4. To lower the predation pressure, the intermediate predator often emigrates from the system and immigrates into the system to gain the maximum food. The migration rate k_1 can be positive or negative when y immigrates or emigrates, respectively [51]. Thus, adding one more term to the y-equation finalizes our model (7.1) as

$$\begin{aligned}
\frac{dx}{dt} &= rx\left(1-\frac{x}{K+\beta x}\right)-\frac{\alpha_1 xy}{a_1+x^2} = x\phi_1(x,y,z),\\
\frac{dy}{dt} &= \frac{c_1\alpha_1 xy}{a_1+x^2}-\frac{\alpha_2 yz}{a_2+y}-d_1 y+k_1 y-\delta_1 y^2 = y\phi_2(x,y,z),\\
\frac{dz}{dt} &= \frac{c_2\alpha_2 yz}{a_2+y}-d_2 z-\delta_2 z^2 = z\phi_3(x,y,z),\\
&x(0)\geq 0,\ y(0)\geq 0\ z(0)\geq 0.
\end{aligned} \tag{7.1}$$

The ecological meaning of all the parameters with their default numeric value is listed in Table 7.1.

7.3 Well-posedness of system (7.1)

Theorem 7.3.1. *Every solution starting from a non-negative initial condition is uniformly bounded in the following region.*

$$\Omega_1 = \left\{(x,y,z):\ 0 \le x+\frac{1}{c_1}y+\frac{1}{c_1c_2}z \le \frac{(r+\nu)^2K}{4r\nu}\right\},\quad \textit{when } \beta \le 0$$

$$\Omega_2 = \left\{(x,y,z):\ 0 \le x+\frac{1}{c_1}y+\frac{1}{c_1c_2}z \le \frac{(r+\nu)x_0}{\nu}-\frac{rx_0^2}{(K+\beta x_0)\nu}\right\},\quad \textit{when } \beta > 0,$$

where ν and x_0 are defined in the proof.

Proof. To examine the boundedness of the solutions of (7.1), we take

$$W = x+\frac{1}{c_1}y+\frac{1}{c_1c_2}z.$$

We can write using system (7.1)

$$\frac{dW}{dt} = rx\left(1-\frac{x}{K+\beta x}\right)-\frac{(d_1-k_1)}{c_1}y-\frac{d_2}{c_1c_2}z-\frac{\delta_1}{c_1}y^2-\frac{\delta_2}{c_1c_2}z^2, \tag{7.2}$$

Case I: $\beta \le 0$
Since $K+\beta x \le K$, we can reduce Eq. (7.2) to the following inequality.

$$\frac{dW}{dt} \le rx\left(1-\frac{x}{K}\right)-\frac{(d_1-k_1)}{c_1}y-\frac{d_2}{c_1c_2}z.$$

Now, let $\nu > 0$ and $d_1 > k_1$, such that

$$\nu \le min\{d_2, d_1-k_1\}.$$

Therefore,

$$\frac{dW}{dt}+\nu W \le (r+\nu)x-\frac{rx^2}{K}$$

which implies

$$\frac{dW}{dt}+\nu W \le \frac{(r+\nu)^2K}{4r}.$$

Hence,

$$\limsup_{t\to\infty} W(t) \leq \frac{(r+\nu)^2 K}{4r\nu}.$$

Case II: $\beta > 0$

Eq. (7.2), can be re-written as

$$\frac{dW}{dt} + \nu W \leq (r+\nu)x - \frac{rx^2}{K+\beta x},$$

where ν is the same as discussed in Case I.

Now, we consider $f(x) = (r+\nu)x - \frac{rx^2}{K+\beta x}$.

In order to maximize the function $f(x)$, we perform derivative test.

So,

$$f'(x) = x^2 + \psi_1 x + \psi_2 = 0,$$

where $\psi_1 = \frac{2K}{\beta}$, $\psi_2 = \frac{(r+\nu)K^2}{\beta(-r+\beta(r+\nu))}$.

The above quadratic equation has a positive root under the following condition.

$$\beta < \frac{r}{r+\nu}. \tag{7.3}$$

Thus, the critical value of x is given by

$$x_0 = -\frac{K}{\beta}\left(1 - \sqrt{1 - \frac{\beta(r+\nu)}{(-r(1-\beta)+\beta\nu)}}\right) > 0.$$

Now, we evaluate the double derivative of $f(x)$ at $x = x_0$ to obtain

$$f''(x_0) = -\frac{2rK^2}{(K+\beta x_0)^3} < 0.$$

Therefore, $x = x_0$ is the point of local maximum. So, we can write

$$\frac{dW}{dt} + \nu W \leq M,$$

where

$$M = f(x_0) = (r+\nu)x_0 - \frac{rx_0^2}{K+\beta x_0}.$$

Hence,

$$\limsup_{t\to\infty} W(t) \leq \frac{M}{\nu}.$$

Therefore, all solutions of system (7.1) are bounded. □

Remark. When $\beta > 0$, the inequality (7.3) must be true for the boundedness of system (7.1).

7.4 Equilibrium points

The equilibrium points of (7.1) are its steady-state solutions. The proposed system can exhibit following equilibrium points:

(i) Population-free equilibrium $E_0(0,0,0)$, it exists trivially.

(ii) Predator-free state $E_1(x_1,0,0)$, where $x_1 = \frac{K}{1-\beta}$ is the carrying capacity, is feasible only when $\beta < 1$.

(iii) In the absence of top predator, system (7.1) acquires a planar equilibrium $E_*(x_*,y_*,0)$. Here x_* is the solution of the following five degree equation.

$$A_1x^5 + A_2x^4 + A_3x^3 + A_4x^2 + A_5x + A_6 = 0, \tag{7.4}$$

where

$$A_1 = \frac{\delta_1 r(1-\beta)}{\alpha_1} > 0,\ A_2 = -\frac{\delta_1 rK}{\alpha_1} < 0,\ A_3 = \frac{2\delta_1 ra_1(1-\beta)}{\alpha_1} - (d_1-k_1)\beta,$$

$$A_4 = -\frac{2\delta_1 ra_1K}{\alpha_1} - (d_1-k_1)K + c_1\alpha_1\beta,\ A_5 = \frac{\delta_1 ra_1^2(1-\beta)}{\alpha_1} - (d_1-k_1)a_1\beta + c_1\alpha_1K,$$

$$A_6 = -\frac{\delta_1 ra_1^2K}{\alpha_1} - (d_1-k_1)a_1K < 0.$$

As per the Descarte's rule of sign, Eq. (7.4) will have atleast one positive root. x_* obtained from Eq. (7.4) can be substituted in the following formula to obtain corresponding y_*.

$$y_* = \frac{r(a_1+x_*^2)}{\alpha_1}\left(1 - \frac{x_*}{K+\beta x_*}\right),$$

provided $x_* < x_1$.

(iv) System (7.1) can have a co-existence equilibrium $E^*(x^*,y^*,z^*)$, where x^* and y^* are determined by solving the following system.

$$r\left(1 - \frac{x}{K+\beta x}\right) - \frac{\alpha_1 y}{a_1+x^2} = 0, \tag{7.5}$$

$$\frac{c_1\alpha_1 x}{a_1+x^2}-\frac{\alpha_2}{\delta_2(a_2+y)}\left(\frac{c_2\alpha_2 y}{a_2+y}-d_2\right)-(d_1-k_1)-\delta_1 y=0. \tag{7.6}$$

The corresponding z^* can be calculated from the following expression.

$$z=\frac{1}{\delta_2}\left(\frac{c_2\alpha_2 y^*}{a_2+y^*}-d_2\right). \tag{7.7}$$

Remark. It is difficult to solve system (7.5) and (7.6) analytically, therefore we show the existence of E^* numerically.

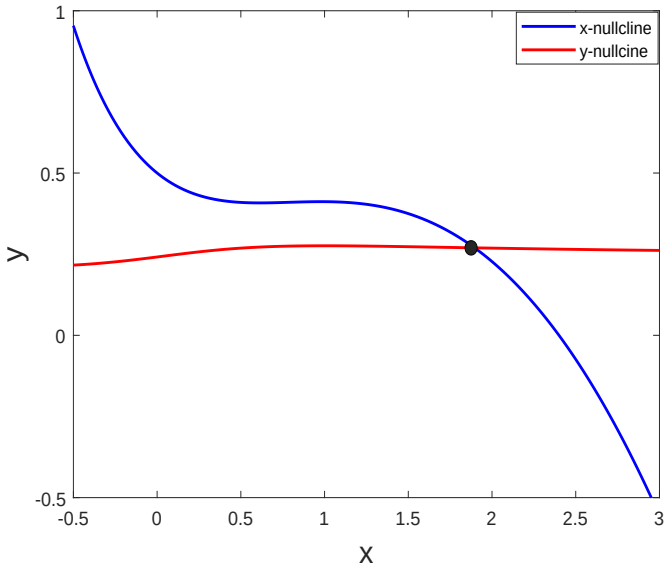

Fig. 7.1: Intersection of nullclines (7.5) and (7.6) display the existence of $x^*=1.896013$ and $y^*=0.269527$, and correspondingly we get $z^*=0.057201$ from (7.7). The parameters are taken from Table 7.1 except $\delta_2=0.1$.

7.5 Stability assessment

In this section, we examine the local stability of all the feasible equilibrium points. First, we evaluate the Jacobian matrix for system (7.1) about a steady-state, then we determine the eigenvalues associated, and the negativity of the real part of all eigenvalues confirms the stable nature of the equilibrium point.

Let V be the variational matrix evaluated at E^* such that $V=[a_{ij}]_{3\times 3}$, where

$$a_{11}=-\frac{rKx^*}{(K+\beta x^*)^2}+\frac{2\alpha_1 x^{*2}y^*}{(a_1+x^{*2})^2},\ a_{12}=-\frac{\alpha_1 x^*}{a_1+x^{*2}},\ a_{13}=0,$$

$$a_{21} = \frac{c_1\alpha_1 y^*(a_1 - x^{*2})}{(a_1 + x^{*2})^2},\ a_{22} = \frac{\alpha_2 y^* z^*}{(a_2 + y^*)^2} - \delta_1 y^*,\ a_{23} = -\frac{\alpha_2 y^*}{a_2 + y^*},$$

$$a_{31} = 0,\ a_{32} = \frac{c_2\alpha_2 a_2 z^*}{(a_2 + y^*)^2},\ a_{33} = -\delta_2 z^*.$$

The condition(s) for the local stability of all feasible equilibria are listed in Table 7.2.

Table 7.2: Equilibrium points of model (7.1) and their stability behavior.

Equilibrium points	Stability behavior
$E_0(0,0,0)$	always saddle point
$E_1(x_1,0,0)$	stable $\Leftrightarrow d_1 > k_1 + \frac{c_1\alpha_1 x_1}{a_1 + {x_1}^2}$
$E_*(x_*,y_*,0)$	stable $\Leftrightarrow d_2 > \frac{c_2\alpha_2 y_*}{a_2+y_*}$, $\Gamma_1 > 0, \Gamma_2 > 0$, where
	$\Gamma_1 = 2\delta_1 y_* + d_1 - k_1 + \frac{rKx_*}{(K+\beta x_*)^2} - \frac{2\alpha_1 x_*^2 y_*}{(a_1+x_*^2)^2} - \frac{c_1\alpha_1 x_*}{(a_1+x_*^2)}$, and
	$\Gamma_2 = (\frac{rKx_*}{(K+\beta x_*)^2} - \frac{2\alpha_1 x_*^2 y_*}{(a_1+x_*^2)^2})(2\delta_1 y_* + d_1 - k_1 - \frac{c_1\alpha_1 x_*}{(a_1+x_*^2)}) + \frac{rc_1\alpha_1 x_*(a_1 - x_*^2)}{(a_1+x_*^2)^2}(1 - \frac{x_*}{K+\beta x_*})$
$E^*(x^*,y^*,z^*)$	stable $\Leftrightarrow \Theta_1 > 0,\ \Theta_3 > 0,\ \Theta_1\Theta_2 - \Theta_3 > 0$, where
	$\Theta_1 = -a_{11} - a_{22} - a_{33}$, $\Theta_2 = a_{22}a_{33} - a_{23}a_{32} + a_{11}a_{33} + a_{11}a_{22} - a_{12}a_{21}$,
	$\Theta_3 = a_{11}(a_{22}a_{33} - a_{23}a_{32}) - a_{12}a_{21}a_{33}$

Remark.

(i) When the death rate of the middle predator exceeds a threshold, i.e.,

$$d_1 > k_1 + \frac{c_1\alpha_1 x_1}{a_1 + {x_1}^2},$$

then both predators die out, and the prey survives.

(ii) The death rate of top predators is more prominent than a critical value, i.e.,

$$d_2 > \frac{c_2\alpha_2 y_*}{a_2 + y_*}$$

is necessary for the co-existence of prey and middle predators and the extinction of top predators.

7.5.1 Hopf-bifurcation

Here we show that the system experiences Hopf-bifurcation around positive equilibrium under certain conditions.

Theorem 7.5.1. *The system exhibits limit cycle around E^* through Hopf-bifurcation at $\beta = \beta^{Hf}$ under following conditions:*

(i) $\Theta_1(\beta^{Hf}) > 0$, $\Theta_3(\beta^{Hf}) > 0$,

(ii) $\Theta_1(\beta^{Hf})\Theta_2(\beta^{Hf}) - \Theta_3(\beta^{Hf}) = 0,$

(iii) $\left(\Theta_1 \frac{d\Theta_2}{d\beta} + \Theta_2 \frac{d\Theta_1}{d\beta} - \frac{d\Theta_3}{d\beta}\right)_{\beta=\beta^{Hf}} \neq 0.$

Proof. At the Hopf-bifurcation point $\beta = \beta^{Hf}$, $\Theta_1\Theta_2 - \Theta_3 = 0$, the characteristic equation of V can be re-written as

$$(\lambda^2 + \Theta_2)(\lambda + \Theta_1) = 0.$$

This yields $\lambda_{1,2} = \pm i\sqrt{\Theta_2}$ and $\lambda_3 = -\Theta_1$, where $\Theta_1 > 0, \Theta_2 > 0$. Now, we determine the transversality condition for existence of Hopf-bifurcation. For this, we assume that $\lambda_{1,2}(\beta) = \xi_1(\beta) + i\xi_2(\beta)$ and substitute $\lambda = \xi_1 + i\xi_2$ in the characteristic equation to obtain the real and imaginary parts as follows:

$$\xi_1^3 - 3\xi_1\xi_2^2 + \Theta_1(\xi_1^2 - \xi_2^2) + \Theta_2\xi_1 + \Theta_3 = 0, \tag{7.8}$$

$$-\xi_2^3 + 3\xi_2\xi_1^2 + 2\Theta_1\xi_1\xi_2 + \Theta_2\xi_2 = 0. \tag{7.9}$$

Combining Eqs. (7.8) and (7.9), we get

$$8\xi_1^3 + 8\Theta_1\xi_1^2 + 2\xi_1(\Theta_2 + \Theta_1^2) + \Theta_1\Theta_2 - \Theta_3 = 0. \tag{7.10}$$

Now, differentiating Eq. (7.10) with respect to β, then at $\beta = \beta^{Hf}$, we obtain

$$\left.\frac{d\xi_1}{d\beta}\right|_{\beta=\beta^{Hf}} = -\frac{1}{2(\Theta_2 + \Theta_1^2)}\left[\Theta_1\frac{d\Theta_2}{d\beta} + \Theta_2\frac{d\Theta_1}{d\beta} - \frac{d\Theta_3}{d\beta}\right]_{\beta=\beta^{Hf}}.$$

Therefore, the transversality condition is

$$\left[\Theta_1\frac{d\Theta_2}{d\beta} + \Theta_2\frac{d\Theta_1}{d\beta} - \frac{d\Theta_3}{d\beta}\right]_{\beta=\beta^{Hf}} \neq 0.$$

Hence the theorem follows. □

7.5.2 Saddle-node bifurcation

Theorem 7.5.2. *System (7.1) experiences saddle-node bifurcation around interior equilibrium at $\beta = \beta^{*[sn]}$ if $\Delta \neq 0$, where Δ is defined in the proof of the theorem.*

Proof. Following the procedure of demonstrating the Sotomayor's theorem [60], we determine the eigenvectors of the Jacobian matrix V and V^T around interior equilibrium E^* at $\beta = \beta^{*[sn]}$

for zero eigenvalue, such that

$$Vp = 0,\ \ V^T q = 0,\ \text{where } p = (p_1, p_2, p_3)^T \text{ and } q = (q_1, q_2, q_3)^T.$$

So, we obtain a system of linear equations in p given by

$$a_{11}p_1 + a_{12}p_2 = 0, \tag{7.11}$$

$$a_{21}p_1 + a_{22}p_2 + a_{23}p_3 = 0, \tag{7.12}$$

and

$$p_3 = -\frac{a_{32}}{a_{33}}p_2.$$

Substituting p_3 in Eq. (7.12), we obtain

$$a_{21}p_1 + \left(a_{22} - \frac{a_{23}a_{32}}{a_{33}}\right)p_2 = 0. \tag{7.13}$$

Solving Eqs. (7.11) and (7.13), we get

$$\left[a_{11}\left(a_{22} - \frac{a_{23}a_{32}}{a_{33}}\right) - a_{12}a_{21}\right]p_1 = 0.$$

In the above equation, the coefficient of p_1 is $\frac{det(V)}{a_{33}}$, which is zero at the saddle-node bifurcation point. Therefore, p_1 can be any arbitary number, say, $p_1 = 1$. Further, simple calculation yields $p_2 = -\frac{a_{11}}{a_{12}}$ and $p_3 = \frac{a_{32}a_{11}}{a_{33}a_{12}}$.

In a similar manner done above, we calculate $q_1 = 1$, $q_2 = -\frac{a_{11}}{a_{21}}$, $q_3 = \frac{a_{11}a_{23}}{a_{21}a_{33}}$. Differentiating the right side functions of (7.1), with respect to β to obtain

$$f_\beta(\beta^{*[sn]}, E^*) = \begin{pmatrix} \frac{rx^{*3}}{(K+\beta^{*[sn]}x^*)^2} \\ 0 \\ 0 \end{pmatrix}.$$

Now

$$q^T f_\beta(\beta^{*[sn]}, E^*) = \frac{rx^{*3}}{(K+\beta^{*[sn]}x^*)^2} \neq 0.$$

Next, we evaluate $\Delta = q^T[D^2 f(\beta^{*[sn]}, E^*)](p,p)$, where

$$D^2 f = \begin{pmatrix} (a_{11})_x & (a_{11})_y & (a_{11})_z & (a_{12})_x & (a_{12})_y & (a_{12})_z & (a_{13})_x & (a_{13})_y & (a_{13})_z \\ (a_{21})_x & (a_{21})_y & (a_{21})_z & (a_{22})_x & (a_{22})_y & (a_{22})_z & (a_{23})_x & (a_{23})_y & (a_{23})_z \\ (a_{31})_x & (a_{31})_y & (a_{31})_z & (a_{32})_x & (a_{32})_y & (a_{32})_z & (a_{33})_x & (a_{33})_y & (a_{33})_z \end{pmatrix}$$

and

$$(p,p) = (p_1^2, p_1p_2, p_1p_3, p_2p_1, p_2^2, p_2p_3, p_3p_1, p_3p_2, p_3^2)^T.$$

After some calculations, we obtain

$$\Delta = (a_{11})_x + 2(a_{11})_y p_2 + q_2((a_{21})_x + 2(a_{21})_y p_2 + (a_{22})_y p_2^2 + 2(a_{22})_z p_2 p_3) + q_3((a_{32})_y p_2^2 + 2(a_{32})_z p_2 p_3 + (a_{33})_z p_3^2),$$

where $(a_{11})_x = -\frac{rK(K-\beta x^*)}{(K+\beta x^*)^3} + \frac{4\alpha_1 x^* y^*(a_1 - x^{*2})}{(a_1+x^{*2})^3}$, $(a_{11})_y = \frac{2\alpha_1 x^{*2}}{(a_1+x^{*2})^2}$, $(a_{21})_x = -\frac{2c_1\alpha_1 x^* y^*}{(a_1+x^{*2})^2} - \frac{4c_1\alpha_1 x^* y^*(a_1-x^{*2})}{(a_1+x^{*2})^3}$, $(a_{21})_y = \frac{c_1\alpha_1(a_1-x^{*2})}{(a_1+x^{*2})^2}$, $(a_{22})_y = \frac{(a_2-y^*)\alpha_2 z^*}{(a_2+y^*)^3} - \delta_1$, $(a_{22})_z = -\frac{\alpha_2 a_2}{(a_2+y^*)^2}$, $(a_{32})_y = -\frac{2c_2\alpha_2 a_2 z^*}{(a_2+y^*)^3}$, $(a_{32})_z = \frac{c_2\alpha_2 a_2}{(a_2+y^*)^2}$, and $(a_{33})_z = -\delta_2$.
Therefore, as per the Sotomayor's theorem [60], system (7.1) undergoes saddle-node bifurcation between two interior equilibrium points at $\beta = \beta^{*[sn]}$ if $\Delta \neq 0$. □

Remark. The occurrence of saddle-node bifurcation about planar steady-states can be proven under an analysis similar to Theorem 7.5.2.

7.6 Effect of seasonality

Most prey-predator models in literature take place in a deterministic and constant environment. However, the majority of biological interactions occur under very erratic settings, which causes the physical parameters related to these interactions, such as carrying capacity, birth and death rates, competition coefficients, etc., to shift dramatically. Our model becomes a non-autonomous model when environmental fluctuations are taken into account, where physical parameters fluctuate periodically for seasonal causes. Therefore, model (7.1) takes on the following form when seasonality is taken into consideration.

$$\begin{aligned}
\frac{dx(t)}{dt} &= r(t)x(t)\left(1 - \frac{x(t)}{K(t)+\beta(t)x(t)}\right) - \frac{\alpha_1(t)x(t)y(t)}{a_1(t)+x^2(t)},\\
\frac{dy(t)}{dt} &= \frac{c_1(t)\alpha_1(t)x(t)y(t)}{a_1(t)+x^2(t)} - \frac{\alpha_2(t)y(t)z(t)}{a_2(t)+y(t)} - (d_1(t)-k_1(t))y(t) - \delta_1(t)y^2(t),\\
\frac{dz(t)}{dt} &= \frac{c_2(t)\alpha_2(t)y(t)z(t)}{a_2(t)+y(t)} - d_2(t)z(t) - \delta_2(t)z^2(t),
\end{aligned} \tag{7.14}$$

To determine the upper and lower bounds of system (7.14), we will use the following result.

$$x'(t) = g(t,x)x(t)(b-x(t)),\ b \neq 0;\ x(t) = \frac{bx(0)exp(\int_0^t bg(s,x(s))ds)}{x(0)[exp(\int_0^t bg(s,x(s))ds) - 1] + b}. \tag{7.15}$$

Theorem 7.6.1. *The solutions of system (7.14) originating from R_3^+ are confined in the region $\Omega = \{(x,y,z) \in R_3^+ : m_1^\kappa < x(t) < M_1^\kappa,\ m_2^\kappa < y(t) < M_2^\kappa,\ m_3^\kappa < z(t) < M_3^\kappa,\}$, where*

$$M_1^\kappa = max\{M_1^{\kappa_1}, M_1^{\kappa_2}\},\ with\ M_1^{\kappa_1} = \frac{r^g K^g}{r^l} + \kappa_1,\ \ M_1^{\kappa_2} = \frac{\gamma^g x_0 - \frac{r^l x_0^2}{K^g + \beta^g x_0}}{\nu} + \kappa_2,$$

$$x_0 = \frac{K^g}{\beta^g}\left(\sqrt{\frac{r^l}{r^l - \gamma^g \beta^g}} - 1\right),$$

$$m_1^\kappa = min\{m_1^{\kappa_1}, m_1^{\kappa_2}\},\ with\ m_1^{\kappa_1} = r^l - \frac{r^g}{\beta^l} - \frac{\alpha_1^g M_2^\kappa}{a_1^l} - \kappa_1,\ m_1^{\kappa_2} = (r^l - \frac{\alpha_1^g M_2^\kappa}{a_1^l})\frac{K^l}{r^g} - \kappa_2,$$

$$M_2^\kappa = \frac{c_1^g \alpha_1^g M_1^\kappa}{a_1^l \delta_1^l},\ m_2^\kappa = \frac{1}{\delta_1^g}\left(\frac{c_1^l \alpha_1^l m_1^\kappa}{a_1^g + M_1^{\kappa 2}} - \frac{\alpha_2^g M_3^\kappa}{a_2^l} - (d_1^g - k_1^l)\right),$$

$$M_3^\kappa = \frac{c_2^g \alpha_2^g}{\delta_2^l} + \kappa,\ m_3^\kappa = \frac{1}{\delta_2^g}\left(\frac{c_2^l \alpha_2^l m_2^\kappa}{a_2^g + M_2^\kappa} - d_2^g\right),$$

$\kappa,\ \kappa_1,\ \kappa_2$ are sufficiently small, and the bounds of any parameter of system (7.14) such as a_1 are; $a_1^l = inf_{t\in R}\, a_1(t)$, $a_1^g = sup_{t\in R}\, a_1(t)$.

Proof. When $\beta < 0$, we can write from the first equation of the model (7.14)

$$\begin{aligned}\frac{dx(t)}{dt} &\le r(t)x(t) - \frac{r(t)x^2(t)}{K(t)} \\ &\le \frac{r^l x(t)}{K^g}\left(\frac{r^g K^g}{r^l} - x(t)\right)\end{aligned}$$

Now using (7.15), we get

$$x(t) \le \frac{M_1^{\kappa_1} x(0) exp(r^g t)}{x(0)[exp(r^g t) - 1] + M_1^{\kappa_1}} \le M_1^{\kappa_1}.$$

When $\beta > 0$, first equation of the model can be re-written as

$$\frac{dx(t)}{dt} + \nu x(t) \le (r(t) + \nu)x(t) - \frac{r(t)x^2(t)}{K(t) + \beta(t)x(t)}.$$

Let $r + \nu = \gamma$, now we have

$$\frac{dx(t)}{dt} + \nu x(t) \le \gamma^g x(t) - \frac{r^l x^2(t)}{K^g + \beta^g x(t)}.$$

Following the procedure as done in Section 3, we get

$$x(t) \leq M_1^{\kappa_2},$$

Now, we take a unique upper bound of $x(t)$ irrespective of sign of β, i.e., $M_1^{\kappa} = max\{M_1^{\kappa_1}, M_1^{\kappa_2}\}$. The second equation of the model yields

$$\begin{aligned}\frac{dy(t)}{dt} &\leq \frac{c_1^l \alpha_1^l x(t) y(t)}{a_1} - \delta_1 y^2(t), \\ &\leq \delta_1^l y(t)\left(\frac{c_1^g \alpha_1^g M_1^{\kappa}}{a_1^l \delta_1^l} - y(t)\right).\end{aligned}$$

Using (7.15), we get

$$y(t) \leq \frac{y(0) M_2^{\kappa} exp(\delta_1^l M_2^{\kappa} t)}{y(0)[exp(\delta_1^l M_2^{\kappa} t) - 1] + M_2^{\kappa}} \leq M_2^{\kappa}.$$

From the third equation of the model (7.14), we have

$$\begin{aligned}\frac{dz(t)}{dt} &\leq c_2(t)\alpha_2(t) z(t) - \delta_2(t) z^2(t), \\ &\leq \delta_2^l z(t)\left(\frac{c_2^g \alpha_2^g}{\delta_2^l} - z(t)\right).\end{aligned}$$

Now, using (7.15), we can write

$$z(t) \leq \frac{z(0) M_3^{\kappa} exp(c_2^g \alpha_2^g t)}{z(0)[exp(c_2^g \alpha_2^g t) - 1] + M_3^{\kappa}} \leq M_3^{\kappa}.$$

Next, we derive lower bounds of the solutions of system (7.14).
When $\beta < 0$, we can write from the first equation of the model (7.14)

$$\begin{aligned}\frac{dx(t)}{dt} &\geq r(t)x(t) - \frac{r(t)x(t)^2}{\beta(t)x(t)} - \frac{\alpha_1(t)x(t)y(t)}{a_1(t)}, \\ &\geq \left(r^l - \frac{r^g}{\beta^l} - \frac{\alpha_1^g M_2^{\kappa}}{a_1^l}\right)x - x^2.\end{aligned}$$

Let $\eta_1 = r^l - \frac{r^g}{\beta^l} - \frac{\alpha_1^g M_2^{\kappa}}{a_1^l} > 0$ then using (7.15), we obtain

$$x(t) \geq \frac{m_1^{\kappa_1} x(0) exp(\eta_1 t)}{x(0)[exp(\eta_1 t) - 1] + m_1^{\kappa_1}} \geq m_1^{\kappa_1}.$$

When $\beta > 0$, we have

$$\frac{dx(t)}{dt} \geq r(t)x(t) - \frac{r(t)x^2(t)}{K(t)} - \frac{\alpha_1(t)x(t)y(t)}{a_1(t)},$$
$$\geq \left(r(t) - \frac{\alpha_1(t)M_2^{\kappa}}{a_1(t)}\right)x(t) - \frac{r(t)x^2(t)}{K(t)}.$$

$$\frac{dx(t)}{dt} \geq \frac{r^g x(t)}{K^l}\left(\frac{K^l}{r^g}\left(r^l - \frac{\alpha_1^g M_2^{\kappa}}{a_1^l}\right) - x(t)\right).$$

Let $\eta_2 = r^l - \frac{\alpha_1^g M_2^{\kappa}}{a_1^l} > 0$, then

$$x(t) \geq \frac{m_1^{\kappa_2} x(0) exp(\eta_2 t)}{x(0)[exp(\eta_2 t) - 1] + m_1^{\kappa_2}} \geq m_1^{\kappa_2}.$$

Now, we take a unique lower bound of $x(t)$ irrespective of sign of β, i.e., $m_1^{\kappa} = min\{m_1^{\kappa_1}, m_1^{\kappa_2}\}$. Next, we determine the lower bound of $y(t)$, for this we have

$$\frac{dy(t)}{dt} \geq \frac{c_1\alpha_1 xy}{a_1 + x^2} - \frac{\alpha_2 yz}{a_2} - (d_1 - k_1)y - \delta_1 y^2$$
$$\geq \delta_1^g y(t)\left[\left(\frac{c_1^l \alpha_1^l m_1^{\kappa}}{a_1^g + M_1^{\kappa 2}} - \frac{\alpha_2^g M_3^{\kappa}}{a_2^l} - (d_1^g - k_1^l)\right)\frac{1}{\delta_1^g} - y(t)\right].$$

Let $\eta_3 = \frac{c_1^l \alpha_1^l m_1^{\kappa}}{a_1^g + M_1^{\kappa 2}} - \frac{\alpha_2^g M_3^{\kappa}}{a_2^l} - (d_1^g - k_1^l) > 0$ then using (7.15), we can write

$$y(t) \geq \frac{y(0) m_2^{\kappa} exp(\eta_3 t)}{y(0)[exp(\eta_3 t) - 1] + m_2^{\kappa}} \geq m_2^{\kappa}.$$

From the third equation of the model (7.14), we have

$$\frac{dz(t)}{dt} \geq \delta_2^g z(t)\left[\frac{1}{\delta_2^g}\left(\frac{c_2^l \alpha_2^l m_2^{\kappa}}{a_2^g + M_2^{\kappa}} - d_2^g\right) - z(t)\right].$$

Let $\eta_4 = \frac{c_2^l \alpha_2^l m_2^{\kappa}}{a_2^g + M_2^{\kappa}} - d_2^g > 0$ then using (7.15) yields

$$z(t) \geq \frac{z(0) m_3^{\kappa} exp(\eta_4 t)}{z(0)[exp(\eta_4 t) - 1] + m_3^{\kappa}} \geq m_3^{\kappa}.$$

Hence the theorem follows. □

Theorem 7.6.2. *System (7.14) possesses atleast one positive ω-periodic solution if the operator equation $L_3 L_4 u = 0$ has a finite number of real-valued solutions $(u_{1\zeta}, u_{2\zeta}, u_{3\zeta})$, $\zeta = 1, 2, ...n$*

such that

$$\sum_{\zeta=1}^{n} sign\ det(L_3L_4)'(u_{1\zeta},u_{2\zeta},u_{3\zeta}) \neq 0,$$

where L_3 and L_4 are defined in the proof.

Proof. Considering $x(t)=e^{u_1(t)}$, $y(t)=e^{u_2(t)}$, $z(t)=e^{u_3(t)}$, system (7.14) is transformed into the following form.

$$\begin{aligned}
\frac{du_1(t)}{dt} &= r(t)\left(1-\frac{e^{u_1(t)}}{K(t)+\beta(t)e^{u_1(t)}}\right)-\frac{\alpha_1(t)e^{u_2(t)}}{a_1(t)+e^{2u_1(t)}} = F_1(u_1,u_2,u_3),\\
\frac{du_2(t)}{dt} &= \frac{c_1(t)\alpha_1(t)e^{u_1(t)}}{a_1+e^{2u_1(t)}}-\frac{\alpha_2 e^{u_3(t)}}{a_2(t)+e^{u_2(t)}}-(d_1(t)-k_1(t))-\delta_1(t)e^{u_2(t)} = F_2(u_1,u_2,u_3),\\
\frac{du_3(t)}{dt} &= \frac{c_2(t)\alpha_2(t)e^{u_2(t)}}{a_2(t)+e^{u_2(t)}}-d_2(t)-\delta_2(t)e^{u_3(t)} = F_3(u_1,u_2,u_3).
\end{aligned} \tag{7.16}$$

If the transformed system (7.16) has a ω-periodic solution $(u_1(t),u_2(t),u_3(t))$ then the proposed non-autonomous system (7.14) will also have a ω-periodic solution $(e^{u_1(t)},e^{u_2(t)},e^{u_3(t)})$.

For implementation of the continuation theorem [72], we define two Banach Spaces P and Q such that

$$P=Q=\{(u_1,u_2,u_3)\in C(R,R^3)|\ u_j(t+\omega)=u_j(t),\ j=1,2,3\},$$

provided with the norm

$$\|(u_1,u_2,u_3)\| = \sum_{j=1}^{3}\max_{t\in[0,\omega]}|u_j(t)|.$$

Let

$$L_1u(t)=u'(t),\ L_2u(t)=L_3u(t)=\frac{1}{\omega}\int_0^{\omega}u(t)dt,\ \text{and}\ L_4u(t)=F(t),$$

where $u(t)=(u_1(t),u_2(t),u_3(t))^T$ and $F(t)=(F_1(t),F_2(t),F_3(t))^T$.
It is easy to note that system (7.16) is equivalent to the equation $L_1u=L_4u$. In order to prove the existence of ω-periodic solution of (7.16), we need to verify all conditions of Lemma 3.2 mentioned in [210].
It is simple to examine that

$$\text{Ker}(L_1)=\{(u_1,u_2,u_3)\in P|\ (u_1,u_2,u_3)=(c_1,c_2,c_3)\in R^3\},$$

$$\text{Im}(L_1)=\{(u_1,u_2,u_3)\in P|\ \int_0^{\omega}u_j(t)dt=0,\ j=1,2,3\},$$

and the quotient space $\frac{P}{\mathrm{Im}L_1}$ is isomorphic to $\mathrm{Ker}L_1$ then $\mathrm{codim}\,\mathrm{Im}L_1 = \dim \mathrm{Ker}L_1 = 3$. Hence, L_1 is a Fredholm mapping of index three. The operators L_2 and L_3 are such that $\mathrm{Im}L_2 = \mathrm{Ker}L_1$, $\mathrm{Im}L_1 = \mathrm{Ker}L_3 = \mathrm{Im}(I - L_3)$. An inverse map $L_{1_{L_2}}^{-1} : \mathrm{Im}L_1 \to \mathrm{Dom}L_1 \cap \mathrm{Ker}L_2$ exists, which is given by

$$L_{1_{L_2}}^{-1}\begin{pmatrix} u_1 \\ u_2 \\ u_3 \end{pmatrix} = \begin{pmatrix} \int_0^t u_1(s)ds - \frac{1}{\omega}\int_0^\omega \int_0^t u_1(s)dsdt \\ \int_0^t u_2(s)ds - \frac{1}{\omega}\int_0^\omega \int_0^t u_2(s)dsdt \\ \int_0^t u_3(s)ds - \frac{1}{\omega}\int_0^\omega \int_0^t u_3(s)dsdt \end{pmatrix}.$$

Since L_3L_4 and $L_{1_{L_2}}^{-1}(I - L_3)L_4$ are continuous, we are able to confirm that L_4 is L_1-compact on any closed bounded set in $\bar{\Omega}^*$ [210].
From the previous theorem, we have

$$m_1^\kappa < x(t) < M_1^\kappa,\ m_2^\kappa < y(t) < M_2^\kappa,\ m_3^\kappa < z(t) < M_3^\kappa,$$

then for the system $L_1u = \rho L_4u$, where $0 < \rho < 1$, we can write

$$\max_{t\in[0,\omega]} |u_1(t)| \le max\{|ln(m_1^\kappa)|, |ln(M_1^\kappa)|\} = D_1,$$

$$\max_{t\in[0,\omega]} |u_2(t)| \le max\{|ln(m_2^\kappa)|, |ln(M_2^\kappa)|\} = D_2,$$

$$\max_{t\in[0,\omega]} |u_3(t)| \le max\{|ln(m_3^\kappa)|, |ln(M_3^\kappa)|\} = D_3.$$

Let $\Omega^* = \{(u_1,u_2,u_3)^T \in P|\ \|(u_1,u_2,u_3)\| < D\}$ and $D = D_1 + D_2 + D_3 + D_4$, where $D_4 > 0$ is adequately large such that each solution of $L_1u = \rho L_4u$, given by

$$\begin{pmatrix} \frac{1}{\omega}\int_0^\omega [r(1 - \frac{e^{u_1}}{K+\beta e^{u_1}}) - \frac{\alpha_1 e^{u_2}}{a_1+e^{2u_1}}]dt \\ \frac{1}{\omega}\int_0^\omega [\frac{c_1\alpha_1 e^{u_1}}{a_1+e^{2u_1}} - \frac{\alpha_2 e^{u_3}}{a_2+e^{u_2}} - (d_1 - k_1) - \delta_1 e^{u_2}]dt \\ \frac{1}{\omega}\int_0^\omega [\frac{c_2\alpha_2 e^{u_2}}{a_2+e^{u_2}} - d_2 - \delta_2 e^{u_3}]dt \end{pmatrix} = 0 \tag{7.17}$$

satisfies $\|(u_1,u_2,u_3)\| < D$, which implies $u \notin \partial\Omega^*$. This verifies the first condition of Lemma 3.2 [210].
For the demonstration of second condition of Lemma, we consider $(u_1,u_2,u_3) \in \partial\Omega^* \cap \mathrm{Ker}L_1 = \partial\Omega^* \cap R^3$ with $\|(u_1,u_2,u_3)\| = D$, then

$$L_3L_4u = \begin{pmatrix} \frac{1}{\omega}\int_0^\omega [r(1 - \frac{e^{u_1}}{K+\beta e^{u_1}}) - \frac{\alpha_1 e^{u_2}}{a_1+e^{2u_1}}]dt \\ \frac{1}{\omega}\int_0^\omega [\frac{c_1\alpha_1 e^{u_1}}{a_1+e^{2u_1}} - \frac{\alpha_2 e^{u_3}}{a_2+e^{u_2}} - (d_1 - k_1) - \delta_1 e^{u_2}]dt \\ \frac{1}{\omega}\int_0^\omega [\frac{c_2\alpha_2 e^{u_2}}{a_2+e^{u_2}} - d_2 - \delta_2 e^{u_3}]dt \end{pmatrix} \neq 0. \tag{7.18}$$

If the matrix in (7.18) becomes zero, then u is the solution of (7.17) where $u \notin \partial\Omega^*$, which is the contradiction of our assumption. Therefore, the second condition of Lemma 3.2 is fulfilled. Now, we define a homomorphism

$$H:\ \mathrm{Im}L_3 \to \mathrm{Ker}L_1,\ (u_1,u_2,u_3)^T \to (u_1,u_2,u_3)^T,$$

then

$$\deg(HL_3L_4, \partial\Omega^* \cap \mathrm{Ker}L_1, 0) = \deg(L_3L_4, \partial\Omega^* \cap \mathrm{Ker}L_1, 0).$$

We further assume that $L_3L_4u = 0$ has a finite number of real-valued solutions $(u_{1\zeta}, u_{2\zeta}, u_{3\zeta})$, $\zeta = 1,2,...n$ such that

$$\sum_{\zeta=1}^{n} \mathrm{sign}\ \det(L_3L_4)'(u_{1\zeta}, u_{2\zeta}, u_{3\zeta}) \neq 0. \tag{7.19}$$

Thus, taking the assumption stated in (7.19), we can derive from the Brouwer's degree theory [66] that

$$\deg(HL_3L_4, \partial\Omega^* \cap \mathrm{Ker}L_1, 0) \neq 0.$$

Hence, all conditions of Lemma 3.2 stated in [210] are satisfied, and $L_1u = L_4u$ possesses atleast one solution in $\mathrm{Dom}L_1 \cap \bar{\Omega}^*$. Furthermore, we reach to the conclusion that there exists atleast one ω-periodic solution $(u_1(t), u_2(t), u_3(t))$ of system (7.16). Equivalently, we can confirm the existence of atleast one ω-periodic solution $(e^{u_1(t)}, e^{u_2(t)}, e^{u_3(t)})$ of system (7.14). □

Theorem 7.6.3. *The positive $\omega-$ periodic solution (x_1, y_1, z_1) is globally asymptotically stable if $J_i > 0,\ i = 1,2,3$, where J_i is defined in the proof.*

Proof. Let (x_1, y_1, z_1) and (x_2, y_2, z_2) be two distinct $w-$ periodic solutions. Now we define

$$V_1 = |lnx_1(t) - lnx_2(t)|,\ V_2 = |lny_1(t) - lny_2(t)|,\ V_3 = |lnz_1(t) - lnz_2(t)|.$$

We calculate the Dini's derivative of $V_i,\ i = 1,2,3$ along system (7.14) to get

$$\begin{aligned} D^+V_1(t) &= sgn(lnx_1(t) - lnx_2(t))\left[\frac{\dot{x_1}}{x_1} - \frac{\dot{x_2}}{x_2}\right] \\ &= sgn(x_1 - x_2)\left[-\frac{rK}{(K+\beta x_1)(K+\beta x_2)}(x_1 - x_2) - \frac{\alpha_1}{a_1 + x_2^2}(y_1 - y_2) + \frac{\alpha_1 y_1}{(a_1 + x_1^2)(a_1 + x_2^2)}(x_1^2 - x_2^2)\right] \\ &\leq \left[\frac{\alpha_1 y_1 (x_1 + x_2)}{(a_1 + x_1^2)(a_1 + x_2^2)} - \frac{rK}{(K+\beta x_1)(K+\beta x_2)}\right]|x_1 - x_2| + \frac{\alpha_1}{a_1 + x_2^2}|y_1 - y_2|. \end{aligned}$$

In the similar manner we obtain

$$D^+V_2(t) \leq \frac{c_1\alpha_1(a_1 - x_1x_2)}{(a_1 + x_1^2)(a_1 + x_2^2)}|x_1 - x_2| + \left[\frac{\alpha_2 z_1}{(a_2 + y_1)(a_2 + y_2)} - \delta_1\right]|y_1 - y_2| + \frac{\alpha_2}{(a_2 + y_2)}|z_1 - z_2|,$$

$$D^+V_3(t) \leq \frac{c_2\alpha_2 a_2}{(a_2+y_1)(a_2+y_2)}|y_1-y_2| - \delta_2|z_1-z_2|.$$

Combining all the above inequalities for $V = V_1+V_2+V_3$, we get

$$\begin{aligned} D^+V(t) &\leq \left[\frac{\alpha_1(y_1(x_1+x_2)+c_1(a_1-x_1x_2))}{(a_1+x_1^2)(a_1+x_2^2)} - \frac{rK}{(K+\beta x_1)(K+\beta x_2)}\right]|x_1-x_2| + \left[\frac{\alpha_1}{a_1+x_2^2}\right. \\ &+ \left.\frac{\alpha_2(z_1+c_2a_2)}{(a_2+y_1)(a_2+y_2)} - \delta_1\right]|y_1-y_2| + \left[\frac{\alpha_2}{(a_2+y_2)} - \delta_2\right]|z_1-z_2| \\ &\leq \left[\frac{\alpha_1(2M_1^\kappa M_2^\kappa + c_1(a_1-m_1^{\kappa 2}))}{(a_1+m_1^{\kappa 2})^2} - \frac{rK}{(K+\beta M_1^\kappa)^2}\right]|x_1-x_2| + \left[\frac{\alpha_1}{a_1+m_1^{\kappa 2}}\right. \\ &+ \left.\frac{\alpha_2(M_3^\kappa+c_2a_2)}{(a_2+m_2^\kappa)^2} - \delta_1\right]|y_1-y_2| + \left[\frac{\alpha_2}{(a_2+m_2^\kappa)} - \delta_2\right]|z_1-z_2|. \end{aligned}$$

This yields

$$D^+V(t) \leq -J_1|x_1-x_2| - J_2|y_1-y_2| - J_3|z_1-z_2|, \tag{7.20}$$

where

$$J_1 = \frac{rK}{(K+\beta M_1^\kappa)^2} - \frac{\alpha_1(2M_1^\kappa M_2^\kappa + c_1(a_1-m_1^{\kappa 2}))}{(a_1+m_1^{\kappa 2})^2},$$

$$J_2 = \delta_1 - \frac{\alpha_1}{a_1+m_1^{\kappa 2}} - \frac{\alpha_2(M_3^\kappa+c_2a_2)}{(a_2+m_2^\kappa)^2},$$

$$J_3 = \delta_2 - \frac{\alpha_2}{(a_2+m_2^\kappa)}.$$

When all J_1, J_2 and J_3 are positive then we can say that $V(t)$ is a non-increasing function on $[0,\infty)$, integrating (7.20), we obtain

$$V(t) + J_1\int_0^t |x_1-x_2|ds + J_2\int_0^t |y_1-y_2|ds + J_3\int_0^t |z_1-z_2|ds < \infty \tag{7.21}$$

Using Lemma 3.1 stated in [210], we conclude that

$$\lim_{t\to\infty}|x_1-x_2| = 0,\ \lim_{t\to\infty}|y_1-y_2| = 0,\ \lim_{t\to\infty}|z_1-z_2| = 0.$$

Therefore, the positive solution of $\omega-$ period of the non-autonomous system (7.14) is globally asymptotically stable. □

7.7 Numerical Simulation

In this section, we can visualize all the dynamics of the seasonal and non-seasonal models for a certain set of parameters using MATLAB R2021a. Numerical simulations can witness

the existence and stability of equilibrium points studied theoretically. Furthermore, we explore various bifurcations like Hopf, saddle-node, transcritical, and homoclinic for the crucial factors. The non-linearity in three-dimensional models has a high chance of opening the door to chaos.

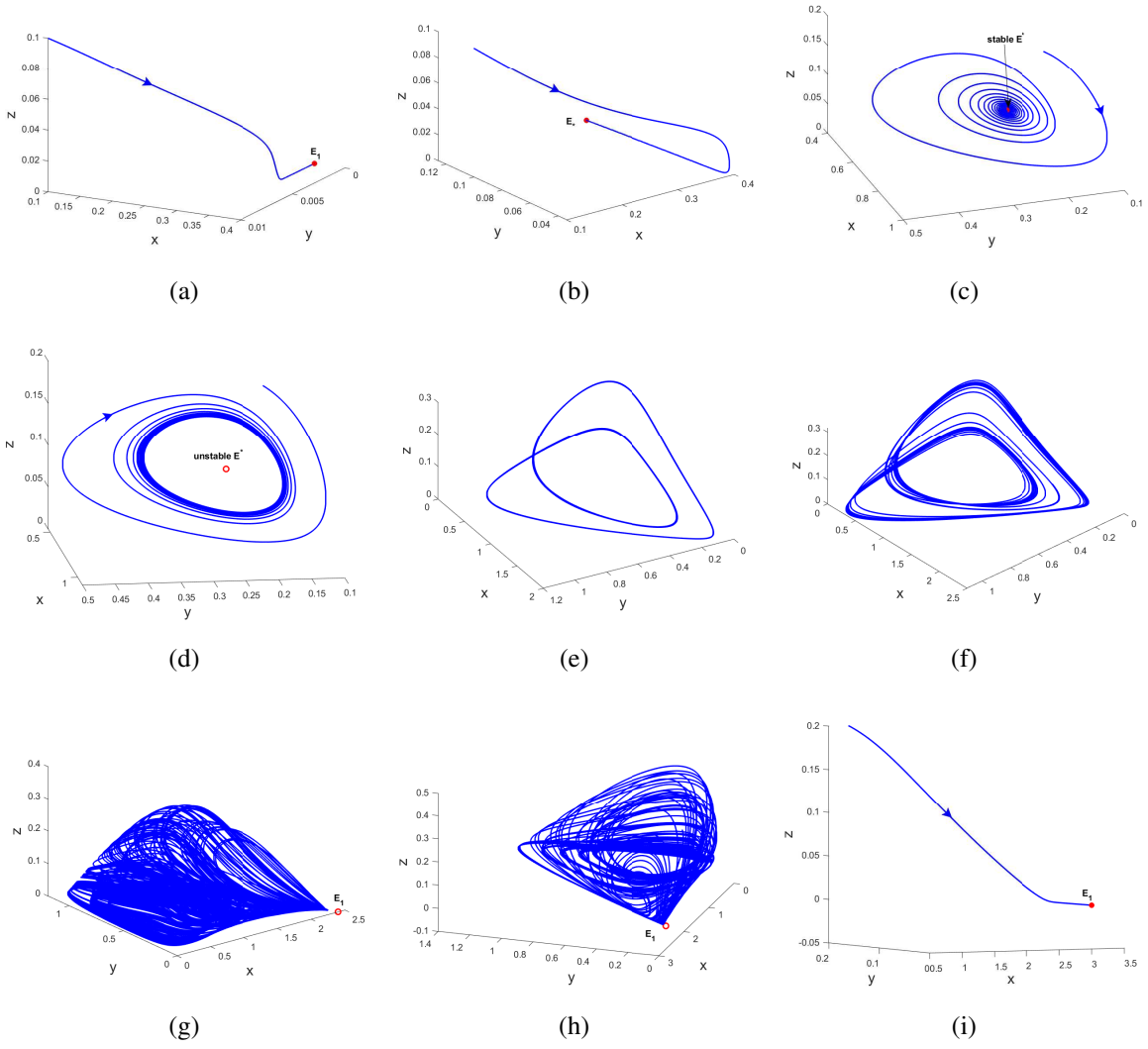

Fig. 7.2: Phase portraits showing different dynamics of system (7.1) with regard to β at (a) $\beta = -2.4$, (b) $\beta = -2$, (c) $\beta = -0.05$, (d) $\beta = 0.05$, (e) $\beta = 0.42$, (f) $\beta = 0.46$, (g) $\beta = 0.5$, (h) $\beta = 0.55916$, (i)$\beta = 0.6$. Here the parameters are same as in Table 7.1.

When populations' activities alter the natural carrying capacity, it can also alter the system's dynamics. For an increasing value of β, we plot a series of phase portraits showing significant changes in the dynamics (see Fig. 7.2). At $\beta = -2.4$ (Fig. 7.2(a)), only the predator-free equilibrium E_1 exists and is stable. No other attractor is present at this stage. With an increment in β, at $\beta = -2$ (Fig. 7.2(b)), the planar equilibrium E_* comes into existence, and E_1 transfers its stability to E_* through a transcritical bifurcation. With a further rise in β, the z population

takes a positive number via transcritical bifurcation between planar and interior states, and the co-existence equilibrium E^* exists as a stable focus at $\beta = -0.05$ (Fig. 7.2(c)). This E^* leaves its stability through a supercritical Hopf-bifurcation, and consequently, a stable limit cycle arises surrounding repeller E^* at $\beta = 0.05$ (Fig. 7.2(d)). Further, solutions of system (1) oscillate between two maximum and two minimum values for $\beta = 0.42$ (Fig. 7.2(e)), which is the period-doubling phenomenon. With a slight rise in β, the solution becomes higher-periodic at $\beta = 0.46$ (Fig. 7.2(f)) and eventually becomes chaotic at $\beta = 0.5$ (Fig. 7.2(g)). This chaotic attractor forms a homoclinic connection with saddle E_1 at $\beta = 0.55916$ (Fig. 7.2(h)), and finally, the cyclic loop breaks and E_1 becomes stable through homoclinic bifurcation at $\beta = 0.6$ (Fig. 7.2(i)).

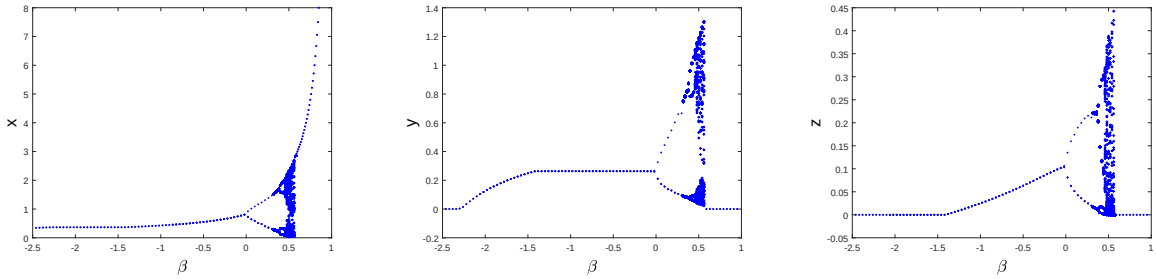

(a) (b) (c)

Fig. 7.3: Bifurcation diagram of all species displaying the emergence of chaos with respect to β.

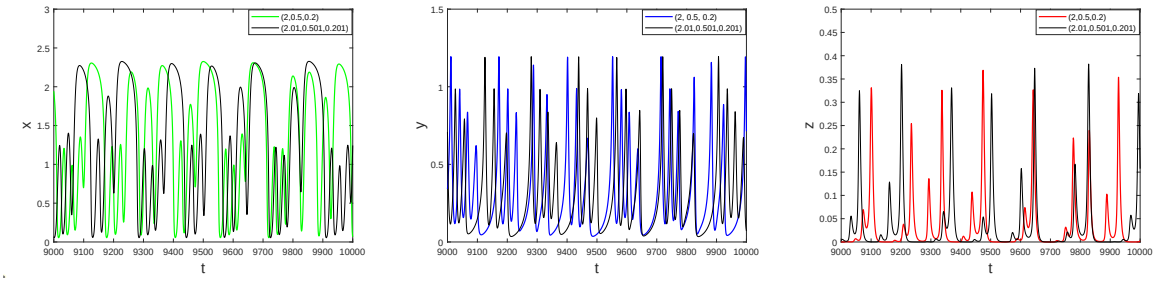

(a) (b) (c)

Fig. 7.4: Sensitive dependence of solutions $x,\ y,\ z$ on the initial condition when solution is perturbed by $(0.01, 0.001, 0.001)$ for the parameters corresponding to Fig. 7.2 (g).

All the aforementioned dynamical properties can be combinedly presented through a bifurcation diagram in Fig. 7.3. This diagram helps us observe the change in population numbers and their oscillations with respect to β. The rise in β enhances the carrying capacity of prey, but this does not enrich our system. In fact, expanding carrying capacity destabilizes the system

and generates chaotic solution. Therefore, our model exhibits the phenomenon of paradox of enrichment.

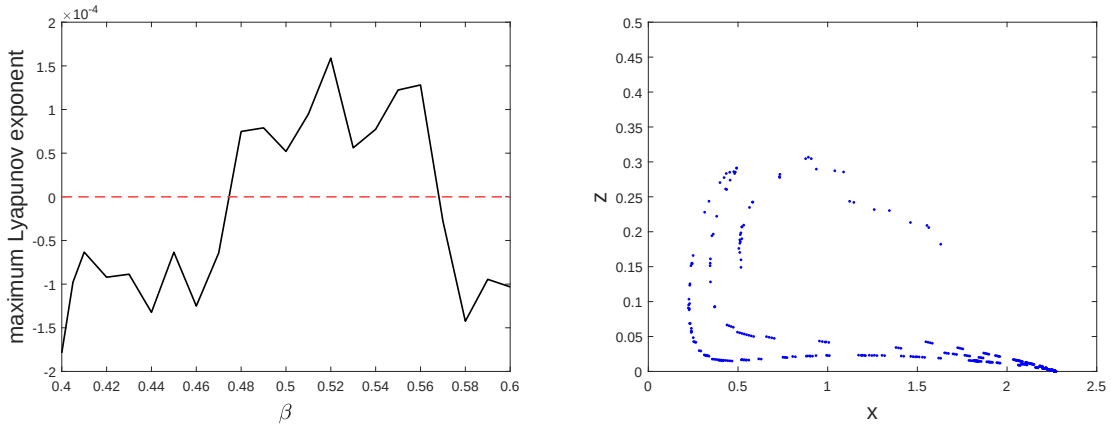

(a) (b)

Fig. 7.5: (a) The positive nature of the Maximum Lyapunov exponent shows the chaotic behavior with respect to β, and (b) Randomness in the Poincare map for $y = 0.1$ at $\beta = 0.5$ also verifies chaos. The parameter set is same as Table 7.1.

For the investigation of chaos at $\beta = 0.5$, we perform a time-series analysis for two solutions starting from very near but different initial conditions. Over time, we notice that solutions initiating from a very little perturbation are showing significant deviation. We plot these two series with different colors to observe the difference in the final solution (see Fig. 7.4). This abrupt behavior explains the chaotic trait of the system. Furthermore, to confirm chaos, we plot the maximum Lyapunov exponent with respect to β. From Fig. 7.5(a), we observe a specific range of β in which the MLE takes the positive value. Hence, the occurrence of chaos is confirmed. At $y = 0.1$, we plot the Poincare map with many scattered points in xz-plane (see Fig. 7.5(b)). The randomness of these points ensures the chaotic nature of system (7.1).

Middle predator migration from or into the system can affect the interacting species' population density and food chain dynamics. Thus, it is crucial to examine the dynamics of system (7.1) regarding migration. For the parameters from Table 7.1, the system is chaotic in the absence of migration. When intermediate predators immigrate, the chaos can be suppressed via a period-halving path to the limit cycle for an acceptable level of immigration (see Fig. 7.6(a)).

When intermediate predator emigrates, there are chances of food scarcity for the top predator. Consequently, inappropriate emigration can cause elimination of middle and top predator. We can observe from Fig. 7.6(b), system is chaotic in the absence of migration. With an increase in emigration, the chaotic attractor gradually connects the saddle predator-free equilibrium, and finally, after a threshold of k_1, E_1 becomes stable.

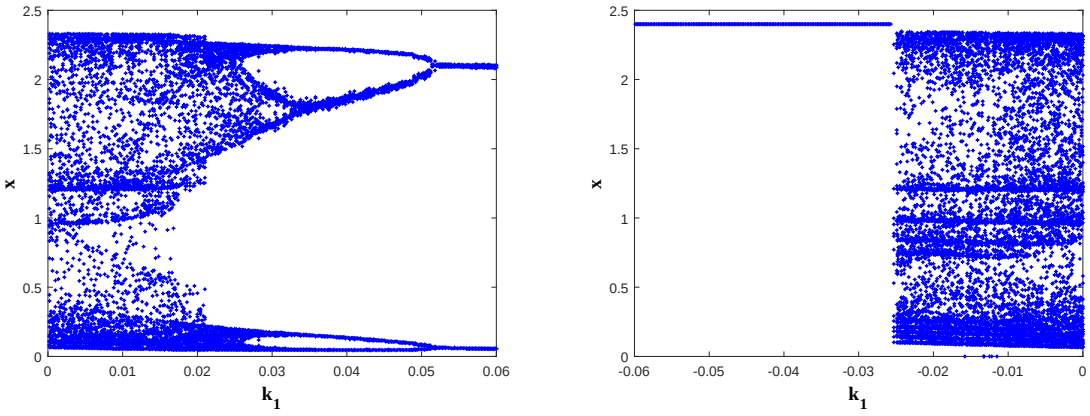

(a) (b)

Fig. 7.6: Bifurcation digram illustrating x-density with respect to the migration rate of middle predator k_1. (a) Reduction of chaos to a stable limit cycle by the route of period-halving due to immigration. (b) Emigration can control chaos by eradicating y and z population density. Rest of the parameters are kept unchanged.

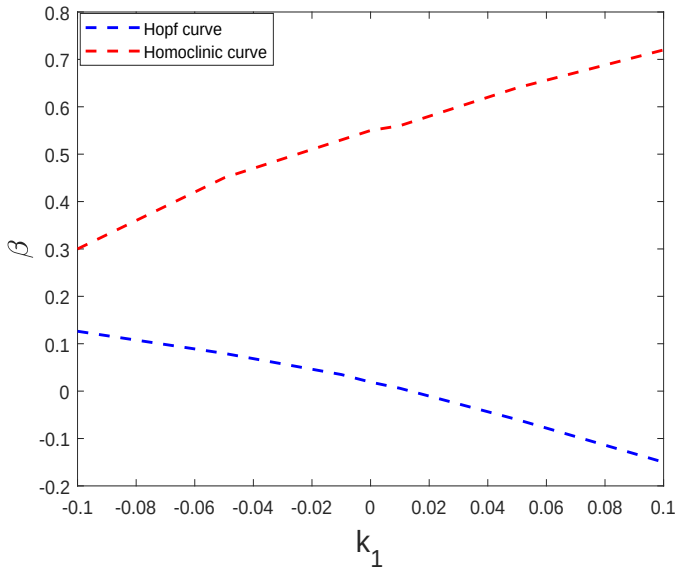

Fig. 7.7: Hopf-bifurcation and homoclinic bifurcation curves in $k_1\beta$-plane.

Our model has two very influential parameters β and k_1. Varying them simultaneously can be of significant consequence. For $k_1 \in [-0.1, 0.1]$, we obtain two critical values of β at which the system experiences Hopf-bifurcation and homoclinic bifurcation, respectively (see Fig. 7.7). The blue and red curves in Fig. 7.7 divide the $k_1\beta$-plane into three regions. Below the blue curve, the interior equilibrium is stable, and it loses stability through a supercritical Hopf-bifurcation when it crosses the blue curve. Therefore, in between the blue and red curves,

the solution is oscillatory, and a stable cycle persists. The cycle connects the saddle axial equilibrium at the red curve by forming a homoclinic loop. The homoclinic loop disappears in the region above the red-colored curve, and the axial point is stable.

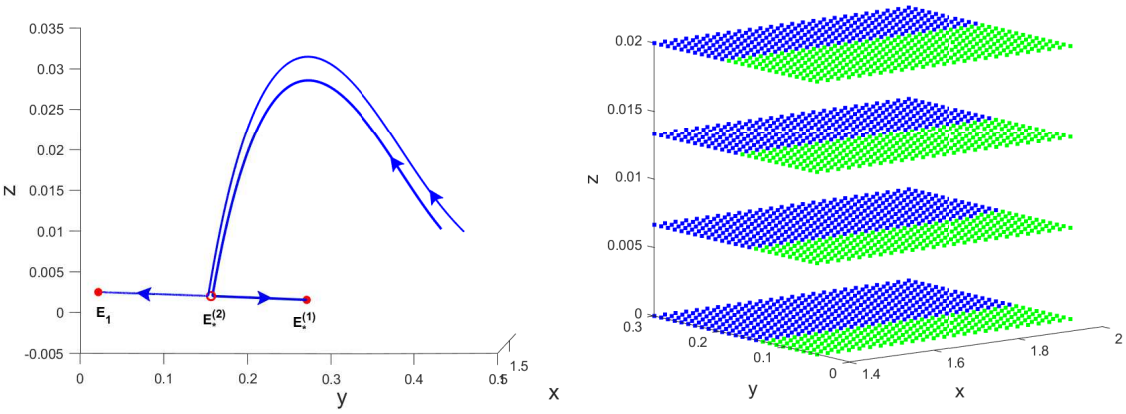

(a) (b)

Fig. 7.8: System (7.1) achieves bi-stability between E_1 and E_* for $\beta = 0.32$, $a_1 = 2.4$. Rest of the parameters are same as in Table 7.1. (a) Phaseportrait showing co-existence of two planar $E_*^{(1)}$, $E_*^{(2)}$, and an axial equilibrium point E_1. Trajectories starting from very close two different points converge to E_1 and $E_*^{(1)}$, simultaneously. (b) The solution starting from green and blue region will eventually approach towards attractors E_1 and $E_*^{(1)}$, respectively.

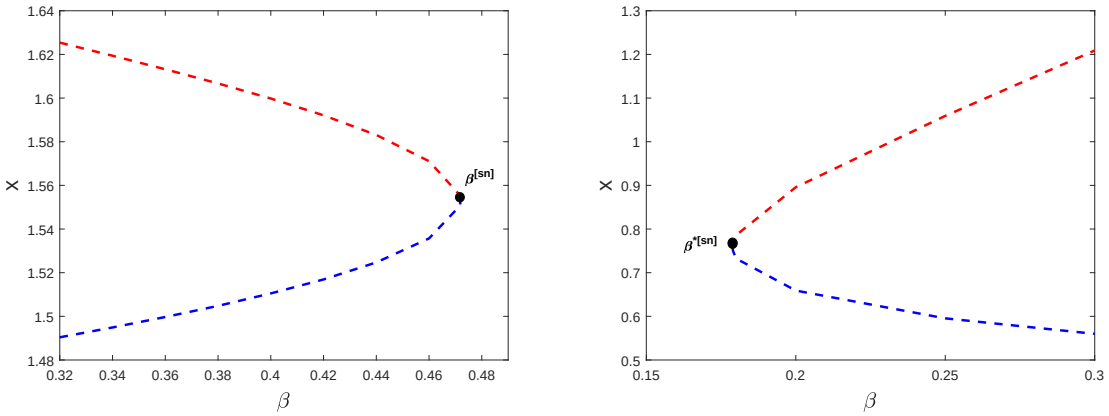

(a) (b)

Fig. 7.9: (a) Two planar equilibrium points approach towards each other with increase in β, and eventually annihilate at $\beta = \beta^{[sn]} = 0.471932$ through saddle-node bifurcation. Here all parameters are taken from Table 7.1 except $a_1 = 2.4$. (b) System (7.1) experiences saddle-node bifurcation of two interior equilibrium points with decrease in β at $\beta = \beta^{*[sn]} = 0.17875$. Here $a_1 = 0.4$, $a_2 = 0.8$, and rest of the parameters are taken from Table 7.1.

In non-linear systems, multi-stability is an intriguing property in which more than one attractor is present at the same time for the same parameter set. For $a_1 = 2.4$ and $\beta = 0.32$, system (7.1) has two planar steady-states $E_*^{(1)}(1.4914, 0.2561, 0)$ and $E_*^{(2)}(1.6254, 0.1387, 0)$, and one axial state $E_1(1.7647, 0, 0)$. According to Table 7.2, stability conditions for $E_*^{(1)}$ and E_1 are fulfilled for the chosen set, and both are stable nodes. Therefore, the phenomenon of bi-stability arises between $E_*^{(1)}$ and E_1. Figure 7.8(a) demonstrates solutions starting from two different but nearby points converging towards one planar $E_*^{(1)}$ and one axial E_1 steady-state. These co-stable attractors have different basins of attraction for the same parameter set. Fig. 7.8(b) displays the green-colored region corresponding to the axial equilibrium E_1, and the blue-colored region is the basin for planar state $E_*^{(1)}$.

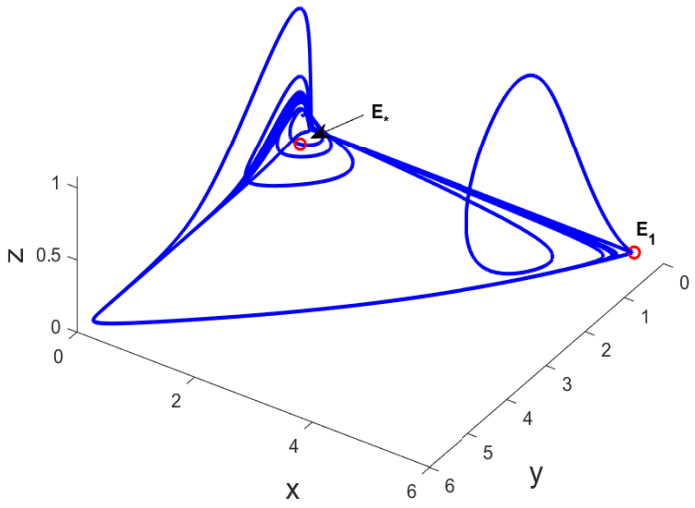

Fig. 7.10: Shilnikov-like connection of saddle-focus E_* and saddle E_1. Here $r = 0.58$, $K = 2.2$, $d_2 = 0.4$, $c_2 = 0.9$, $k_1 = 0.2$, $a_1 = 0.7$, $a_2 = 1.2$, $\beta = 0.6$, and other parameters are taken from Table 7.1.

When two equilibriums approach each other and eventually annihilate with respect to the change in parameter, the saddle-node bifurcation happens. After this phenomenon, the equilibriums mentioned above do not exist. For $a_1 = 0.4$, $a_2 = 0.8$, and $\beta = 0.17875$, the co-existence state $E^*(0.7561, 0.2107, 0.2302)$ exists, and the determinant of the Jacobian matrix at E^* is zero. Moreover, we calculate $\Delta = -0.41591$, which is non-zero. Hence, as per Theorem 7.5.2, the system exhibits saddle-node bifurcation about interior equilibrium. In a similar fashion, saddle-node bifurcation of two planar equilibrium points can be explained. We can visualize the saddle-node bifurcation of two planar and two interior steady-states from Fig. 7.9(a) and 7.9(b), respectively. The change in the number of steady-states with respect to β demonstrates the saddle-node bifurcation.

For a slightly different set of parametrs: $r = 0.58,\ K = 2.2,\ d_2 = 0.4,\ c_2 = 0.9,\ k_1 = 0.2,\ a_1 = 0.7,\ a_2 = 1.2,\ \beta = 0.6$, we have a saddle-focus $E_*(0.078, 0.3952, 0)$ with eigenvalues $-0.0052 \pm 0.2348i,\ 0.0013$, and a saddle-node $E_1(5.5, 0, 0)$ with eigenvalues $-0.232, 0.06, -0.4$. The stable manifold of E_* is of dimension two, and the unstable one is of one dimension. The limit cycle emerged around E_* is eventually repelled, and it connects the saddle-node E_1 to form a Shilnikov-like connection (see Fig. 7.10). Furthermore, the existence of a Shilnikov-like connection promotes chaotic dynamics of the system [219].

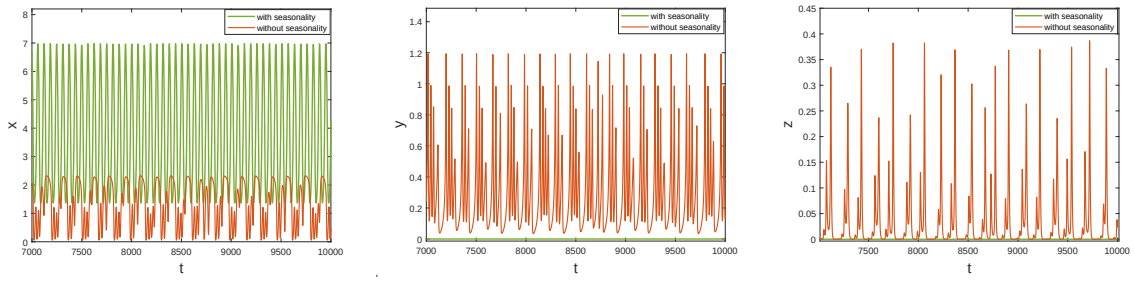

(a) (b) (c)

Fig. 7.11: The time series solution of seasonal and non-seasonal models starting from $(2, 0.3, 0.05)$ for parameter values given in Table 7.1. The non-seasonal system has a chaotic solution but including seasonality eliminates chaos and solution converges to the predator-free equilibrium E_1 for $\beta(t) = \beta + \beta_0 sin(\omega t)$ and $r(t) = r + r_0 cos(\omega t)$, where $\omega = 0.1$, $\beta_0 = 0.4$ and $r_0 = 0.4$.

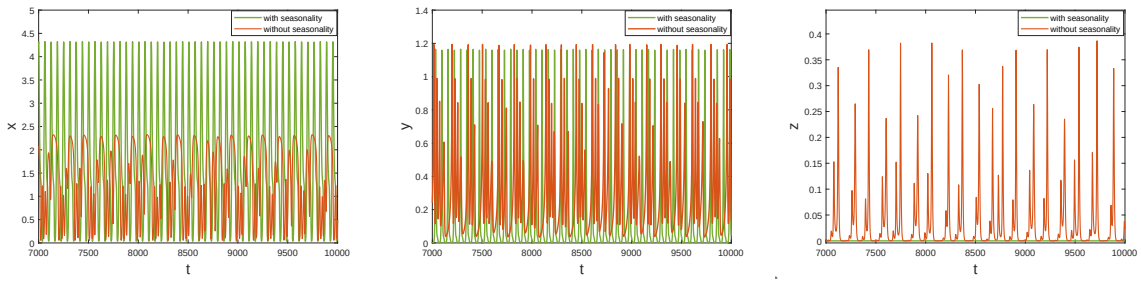

(a) (b) (c)

Fig. 7.12: The time series solution of seasonal and non-seasonal models starting from $(2, 0.3, 0.05)$ for parameter values given in Table 7.1. The non-seasonal system has a chaotic solution but including seasonality eliminates chaos and solution converges to the planar equilibrium E_1 periodically for $\beta(t) = \beta + \beta_0 sin(\omega t)$ and $d_1(t) = d_1 + d_{10} sin(\omega t)$, where $\omega = 0.1$, $\beta_0 = 0.4$ and $d_{10} = 0.2$.

Now, we investigate the non-autonomous system's dynamics with the help of numerical simulation. According to various ecological and environmental aspects, realistic scenarios allow the seasonal model parameters for periodic fluctuations. We consider β, d_1 parameters in a sinusoidal form, and r in cosinusoidal form such that $\beta(t) = \beta + \beta_0 sin(\omega t)$, $d_1(t) = d_1 + d_{10} sin(\omega t)$, and $r(t) = r + r_0 cos(\omega t)$, where β_0, d_{10}, and r_0 are the intensity of seasonality, their default value is set zero unless mentioned. The rest of the parameters are considered as time independent.

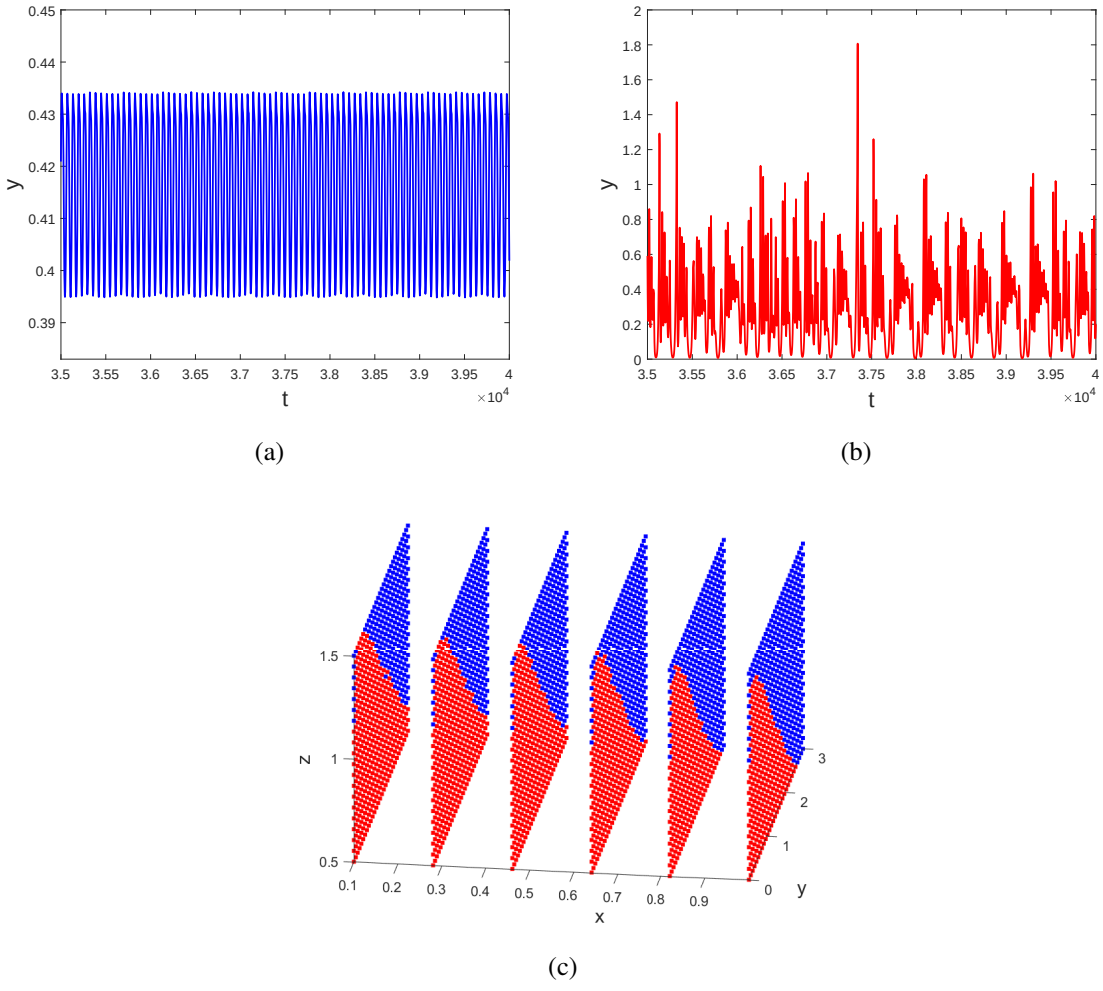

Fig. 7.13: System (7.14) achieves bi-stability between (a) periodic attractor (blue) and (b) chaotic attractor (red) when started from two different initial conditions $(2,1,2)$ and $(0.1,0.1,0.1)$, respectively. (c) The blue and red regions are the basins of attraction for periodic and chaotic attractors, respectively. The parameters set is taken from Table 7.1 with seasonality in β such that $\beta(t) = \beta + \beta_0 sin(\omega t)$, where $\beta_0 = 0.44$, $\omega = 0.1$.

For the chosen parameters set from Table 7.1, we have seen that the autonomous system is chaotic. The chaotic trait vanishes from sight upon introducing seasonality, and the solution

initiated from the same point can converge to two different solutions. We consider seasonally forced intensity in β and r as $\beta_0 = 0.4$, $r_0 = 0.4$, and observe that the solution of the seasonal model goes to the predator-free state E_1 in a periodic manner (see Fig. 7.11). However, the seasonal model's solution converges to the planar equilibrium E_* periodically when seasonality is taken for β and d_1 as $\beta_0 = 0.4$ and $d_{10} = 0.2$ (see Fig. 7.12). Furthermore, system (7.14) achieves bi-stability between a chaotic and a periodic attractor for a slightly large value of β_0. Figures 7.13(a) and 7.13(b) demonstrate the existence of a periodic and chaotic solution for the same set of parameters with $\beta_0 = 0.44$. Figure 7.13(c) represents the two sets of initial values for which the solution eventually goes to either periodic or chaotic attractor for the same parameters, simultaneously.

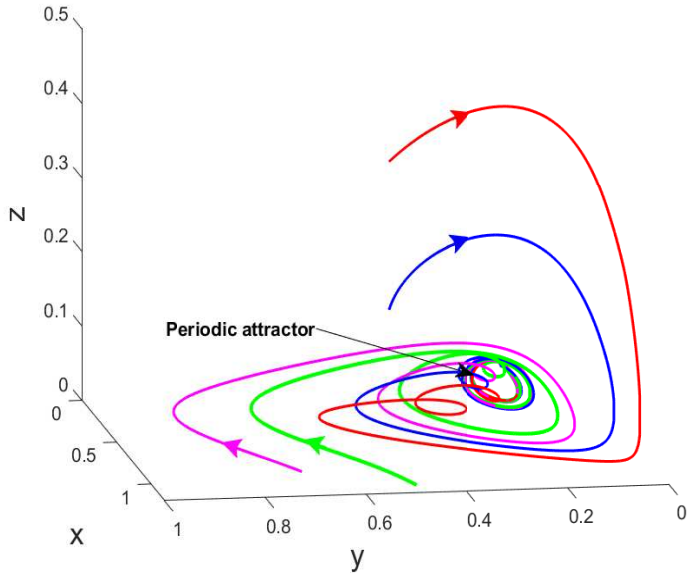

Fig. 7.14: Global stability of the periodic solution of the non-autonomous system (7.14) due to seasonality in d_1 such that $d_1(t) = d_1 + d_{1_0} sin(\omega t)$, with $d_{1_0} = 0.03$, $\omega = 0.1$, $\beta = -0.2$, and other parameters are taken from Table 7.1.

The locally asymptotic stable interior equilibrium exhibited in the autonomous model (7.1) for $\beta = -0.2$ changes to globally attractive periodic solutions when the mortality rate of middle predator is influenced by seasonality with intensity $d_{10} = 0.03$ (see Fig. 7.14). In Fig. 7.14, the non-autonomous system's solutions from different initial conditions eventually converge to the periodic attractor. Furthermore, the bi-stability trait in the autonomous system between planar E_* and axial E_1 equilibrium points switches to the global stability of E_1 when β is considered seasonal with intensity $\beta_0 = 0.2$. The other parameters are taken from Table 7.1 except $\beta = 0.32$ and $a_1 = 2.4$. Fig. 7.15 depicts the globally attractive behavior of time series solution with respect to different initial conditions.

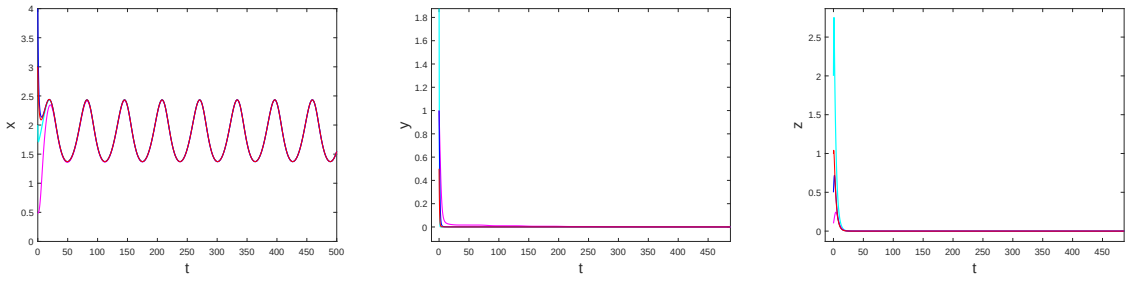

(a) (b) (c)

Fig. 7.15: System (7.14)'s periodic solution is globally stable aboutE_1 for $\beta = 0.32$ $a_1 = 2.4$, $\beta_0 = 0.2$, $\omega = 0.1$ for initial values: $(2,2,2)$, $(0.5,1,0.1)$, $(4,1,0.5)$, and $(3,0.5,1)$. The corresponding non-seasonal model is bi-stable between an axial and a planar equilibrium (see Fig. 7.8(a)).

7.8 Discussion and conclusion

The present article investigates the dynamics of a food-chain model showing the interaction between basal prey x, intermediate predator y, and top predator z. We presumed that prey has a non-constant carrying capacity $K + \beta x$, where β measures the influence of the population's activity on the carrying capacity. We further assumed that the intermediate predator plays wisely and migrates with the rate k_1 from or into the system for maximum benefit. These two real-valued parameters, β and k_1, are crucial and offer intricate dynamics. Furthermore, we explored the impact of seasonality on the autonomous system.

Firstly, we performed the formal analysis to ensure the boundedness of formulated system (7.1), which is a prerequisite for further analysis. Next, we examined feasible steady-state's existence, stability, and possible bifurcations. Furthermore, the system's persistence, existence, and global stability of its periodic solution are investigated for the non-autonomous system. In the numerical simulation, we mainly focused on the impact of the activity measure of population on its carrying capacity, migration, and seasonality. According to Yukolov *et al.* [214], populations' damaging actions on their carrying capacity or the interacting population cause extreme occurrences and finite-time extinctions. Our results reveal that the destructive action of species can alter the system dynamics through transcritical bifurcation twice. When the level of destruction increases, one or more species can become extinct. The bifurcation diagram against β depicts the stability of the co-existence state for less destructive action. However, as β declines, the top predator first becomes extinct, followed by the extinction of the middle predator. Furthermore, constructive action by the population on its carrying capacity can promote instability and induce chaos in the system through the period-doubling route. This phenomenon is

popularly known as the paradox of enrichment. We performed time-series sensitivity concerning the initial condition for chaos detection and sketched the maximum Lyapunov exponent and a Poincare map for confirmation. For the significantly immense value of β, the chaotic attractor expands and connects the prey-only saddle state E_1, eventually leading to the stability of E_1 through the homoclinic bifurcation. Therefore, the population's extremely constructive and destructive activities can cause the basal prey to survive and eliminate both predators.

The pressure of being killed triggers the emigration of middle predators from the food-chain, and their greed for hunting prey provokes them to immigrate into the system. In our model, the increment in immigration rate controls chaos through the period-halving route. Therefore, immigration can be seen as a preventive measure for chaotic dynamics. Some research articles [207, 209, 220] witnessed a similar result of suppression of chaos in the presence of immigration of middle predators in a food-chain. Thus, species migration can critically alter the dynamics of a food-chain system. We also examined the impact of emigration on the chaotic system. The emigration beyond the limit can cause the eradication of both predator densities. This is likely due to the specialist nature of top predators. A study by Hossain *et al.* [51] also reveals species extinction at high migration rates. They mainly analyzed their model through numerical simulation to demonstrate bi-stability and chaos in a tri-trophic model. However, they did not theoretically study the system to explain its boundedness and occurrence of bifurcations. Our study attempts to fill this gap, and we are able to obtain some theoretical results. Furthermore, due to the criticality of β and k_1, we varied them simultaneously for the bi-parametric study. For each k_1, we obtained two critical values of β at which the system undergoes Hopf and homoclinic bifurcations, plotting Hopf and homoclinic curves in $k_1\beta$-plane.

The rich features of our non-linear system include bi-stability, Shilnikov-like connection, and different kind of bifurcations. We considered periodicity in model parameters to incorporate seasonality to make the model more realistic. The results of autonomous and non-autonomous systems are recognizably comparable. Bi-stability between E_1 and E_* in a no-seasonal model shifts to the globally stable periodic solution about E_1 in the presence of seasonality in β. Considering β as seasonal also promotes bi-stability between a chaotic and a periodic attractor when the non-seasonal model has a chaotic attractor only. Furthermore, instead of the solution converging to the chaotic attractor (as in an autonomous system), the extinction of one or more species is possible when seasonality is taken for the intrinsic growth rate of prey or the death rate of the middle predator along with β.

Conclusions and future directions

Conclusions

In this thesis, we focused on the mathematical formulation and analysis of the model representing prey-predator interactions. Several ecological and epidemic factors significantly affect the dynamics of the system. Therefore, we examined each proposed model theoretically and numerically with respect to the crucial parameters. The well-posedness of every model has been thoroughly investigated to ensure that the populations cannot go negative or unbounded in the future. Following this, we determined the feasible equilibrium points and their stability behavior. Then, we explored possible local and global bifurcations occurring in the system. Many of our non-linear systems exhibited rich dynamical properties like multi-stability and chaos. Through extensive numerical simulation, we presented system dynamics by drawing numerous time-series plots, phase portraits, and basins of attraction.

Chapter 2 includes a modified Leslie-Gower prey-predator model with fear, group defense, hunting cooperation, and fear-response delay. We obtained transcritical, saddle-node, and Hopf-bifurcations for fear and cooperation strength parameters in the non-delayed system. Apart from this, the phenomenon of bi-stability occurred between two co-existence steady-states. Moreover, the system with delay experiences stability switching multiple times due to supercritical Hopf-bifurcation.

In Chapter 3, a modified Leslie-Gower prey-predator model with fear, refuge, additional food, gestation, and fear-response delay has been proposed and analyzed. The inclusion of these many ecological factors makes the system complex and offer intricate dynamics. We determined the conditions for the persistence and extinction of both species. Apart from local bifurcations, we observed a global bifurcation, homoclinic bifurcation, in which the limit cycle connects the prey-free equilibrium. Prey refuge in limit can benefit both species; otherwise, predators might be extinct. However, additional food provided to the predator can enrich their density and promote co-existence. Moreover, supplementary food above a threshold can eliminate prey species. We observed the impact of delay on the bi-stability between interior and axial equilibriums. The delayed system undergoes subcritical Hopf-bifurcation several times, which yields an unstable limit cycle.

In Chapter 4, we considered an infectious disease among prey that divides the prey population into two compartments: susceptible and infected. Assuming susceptible prey to be healthy, they perform group defense against predation. Unlike them, infected ones are easy to

catch. Therefore, we formulated a three-dimensional eco-epidemic model where the predators can switch to additional food. Our theoretical and numerical results revealed that the adequate arrangement of supplementary food can eradicate the disease among prey. Moreover, a minor adjustment in additional food parameter led to more fascinating system dynamics, like heteroclinic bifurcation and multi-stability.

When a herd of susceptible (healthy) prey exhibits a defensive strategy, their herd shape can alter the predator's attack rate. Additionally, they can even kill their predators. Chapter 5 presents the aforementioned prey-predator interaction with a discrete delay. We performed a detailed analysis of the uniqueness and positivity of solutions. The attack rate of predator and prey, disease transmission rate and time delay are the crucial factors governing the system dynamics. In this chapter, we witnessed the occurrence of chaos through the period-doubling route. The maximum Lyapunov exponent was sketched to confirm the chaotic phenomenon. Time delay causes the shifting of the Hopf-bifurcation curve in a significant manner. We also conducted a sensitivity analysis to check the influence of parameters on basic reproduction numbers associated with the epidemic and ecological subsystems.

Chapter 6 is dedicated to a stage-structured prey-predator model incorporating fear and its carry-over effects (COE) on prey birth rate. We assumed that the adult predator kills prey and prey counter-attacks on the juvenile predator (vulnerable). This loop continues, and the process turns into the role reversal of prey and predator. The mathematical model explaining these ecological aspects is formulated using ordinary differential equations. We observed that the predation rate of predator and prey plays a crucial role in maintaining ecological balance. Simultaneous variation in both these rates causes the system to undergo Bogdanov-Takens bifurcation. This bifurcation point is the point where the Hopf, saddle-node, and homoclinic curves meet. We observed the paradox of enrichment, which can be ruled out by increasing the fear level. The system attains bi-stability of node-focus and node-cycle type. Furthermore, we analyzed our model with respect to the fear-response delay and COE delay. For an intermediate delay range, the system achieves switching of stability several times and the emergence of chaotic phenomenon.

In Chapter 7, we studied three species food-chain model where the middle predator migrates from or into the system for its optimum benefit. We assumed that the carrying capacity of prey is non-constant. The constructive or destructive activities of species can enrich or deplete their carrying capacity. Therefore, we replaced the natural carrying capacity with a combination of natural carrying capacity and a function of its population density. We investigated the proposed system concerning two crucial real-valued parameters: β (measuring the impact of activities on carrying capacity) and k_1 (migration rate). The proposed system exhibits the enrichment paradox when β is increased. In fact, the chaotic solution arises for sufficiently large β. Variation in β generates several bifurcations like Hopf, saddle-node, homoclinic, and two times

transcritical bifurcation. However, variation in k_1 is proven to be a chaos control strategy. We plotted the Poincare map to show the existence of chaos. Next, we examined the system in the presence of seasonality. The non-autonomous system exhibits more intriguing dynamics than the non-seasonal model. We proved the persistence, existence, and global stability of the periodic solution. Our numerical results demonstrate the bi-stability between chaotic and periodic attractors. We also thoroughly compared the findings of both the autonomous and non-autonomous systems.

Future directions

This thesis focuses on the dynamical study of ecological and eco-epidemic models representing prey-predator relationships with several environmental factors. The following are possible future goals for our work.

- In this thesis, we worked on temporal models and would like to extend our work in a spatial-temporal direction to study diffusion and delay-diffusion models using partial differential equations.
- We investigated either two or three-species interactions in this thesis. It would be more captivating to investigate the dynamics of four or more populations' interactions.
- Working on eco-epidemic models has developed our immense interest in infectious disease modeling. In this thesis, we considered general disease in prey only. However, we can study a particular disease spread among interacting populations. Moreover, we can fit the model with real-life data for more accurate outcomes to predict disease outbreaks and control strategies.

Bibliography

[1] T. R. Malthus, *An Essay On The Principle Of Population, As It Affects The Future Imporvement Of Society, With Remarks On The Speculations Of Mr. Godwin, M. Condorcet, And Other Writers*. The Lawbook Exchange, Ltd., 1798.

[2] P.-F. Verhulst, “Notice sur la loi que la population suit dans son accroissement”, *Correspondence mathematique et physique*, vol. 10, pp. 113–129, 1838.

[3] A. J. Lotka, *Elements of Physical Biology*. Williams & Wilkins, 1925.

[4] V. Volterra, *Variazioni e fluttuazioni del numero d’individui in specie animali conviventi*. Societá anonima tipografica" Leonardo da Vinci", 1927.

[5] P. H. Leslie, “Some further notes on the use of matrices in population mathematics”, *Biometrika*, vol. 35, pp. 213–245, 1948.

[6] P. H. Leslie and J. C. Gower, “The properties of a stochastic model for the predator-prey type of interaction between two species”, *Biometrika*, vol. 47, pp. 219–234, 1960.

[7] M. Aziz-Alaoui and M. D. Okiye, “Boundedness and global stability for a predator-prey model with modified Leslie-Gower and Holling-type II schemes”, *Applied Mathematics Letters*, vol. 16, pp. 1069–1075, 2003.

[8] C. S. Holling, “Some characteristics of simple types of predation and parasitism”, *The Canadian Entomologist*, vol. 91, pp. 385–398, 1959.

[9] Y. Zhu and K. Wang, “Existence and global attractivity of positive periodic solutions for a predator–prey model with modified Leslie–Gower Holling-type II schemes”, *Journal of Mathematical Analysis and Applications*, vol. 384, pp. 400–408, 2011.

[10] Z. Zhang, R. K. Upadhyay, and J. Datta, “Bifurcation analysis of a modified Leslie–Gower model with Holling type-IV functional response and nonlinear prey harvesting”, *Advances in Difference Equations*, vol. 2018, pp. 1–21, 2018.

[11] M. Onana, B. Mewoli, and J. J. Tewa, “Hopf bifurcation analysis in a delayed Leslie–Gower predator–prey model incorporating additional food for predators, refuge and threshold harvesting of preys”, *Nonlinear Dynamics*, vol. 100, pp. 3007–3028, 2020.

[12] F. Rihan and C Rajivganthi, "Dynamics of fractional-order delay differential model of prey-predator system with Holling-type III and infection among predators", *Chaos, Solitons & Fractals*, vol. 141, p. 110 365, 2020.

[13] J. C. Woodson, D. Macintosh, M. Fleshner, and D. M. Diamond, "Emotion-induced amnesia in rats: working memory-specific impairment, corticosterone-memory correlation, and fear versus arousal effects on memory", *Learning & Memory*, vol. 10, pp. 326–336, 2003.

[14] W. Cresswell, "Predation in bird populations", *Journal of Ornithology*, vol. 152, pp. 251–263, 2011.

[15] S. Creel and D. Christianson, "Relationships between direct predation and risk effects", *Trends in Ecology & Evolution*, vol. 23, pp. 194–201, 2008.

[16] S. L. Lima, "Predators and the breeding bird: Behavioral and reproductive flexibility under the risk of predation", *Biological Reviews*, vol. 84, pp. 485–513, 2009.

[17] X. Wang, L. Zanette, and X. Zou, "Modelling the fear effect in predator-prey interactions", *Journal of Mathematical Biology*, vol. 73, pp. 1179–1204, 2016.

[18] M. J. Sheriff, C. J. Krebs, and R. Boonstra, "The sensitive hare: Sublethal effects of predator stress on reproduction in snowshoe hares", *Journal of Animal Ecology*, vol. 78, pp. 1249–1258, 2009.

[19] L. Y. Zanette, A. F. White, M. C. Allen, and M. Clinchy, "Perceived predation risk reduces the number of offspring songbirds produce per year", *Science*, vol. 334, pp. 1398–1401, 2011.

[20] S. Pal, N. Pal, S. Samanta, and J. Chattopadhyay, "Effect of hunting cooperation and fear in a predator-prey model", *Ecological Complexity*, vol. 39, p. 100 770, 2019.

[21] Sajan, B. Dubey, and S. K. Sasmal, "Chaotic dynamics of a plankton-fish system with fear and its carry over effects in the presence of a discrete delay", *Chaos, Solitons & Fractals*, vol. 160, p. 112 245, 2022.

[22] S. Pal, A. Gupta, A. K. Misra, and B. Dubey, "Chaotic dynamics of a stage-structured prey-predator system with hunting cooperation and fear in presence of two discrete delays", *Journal of Biological Systems*, vol. 31, pp. 611–642, 2023.

[23] D. Sahoo and G. Samanta, "Oscillatory and transient dynamics of a slow–fast predator–prey system with fear and its carry-over effect", *Nonlinear Analysis: Real World Applications*, vol. 73, p. 103 888, 2023.

[24] D. R. Norris and C. M. Taylor, "Predicting the consequences of carry-over effects for migratory populations", *Biology Letters*, vol. 2, pp. 148–151, 2006.

[25] S. K. Sasmal and Y. Takeuchi, "Modeling the Allee effects induced by cost of predation fear and its carry-over effects", *Journal of Mathematical Analysis and Applications*, vol. 505, p. 125 485, 2022.

[26] S. Mondal and G. Samanta, "A comparison study of predator–prey system in deterministic and stochastic environments influenced by fear and its carry-over effects", *The European Physical Journal Plus*, vol. 137, p. 70, 2022.

[27] H. Zhang, Y. Cai, S. Fu, and W. Wang, "Impact of the fear effect in a prey-predator model incorporating a prey refuge", *Applied Mathematics and Computation*, vol. 356, pp. 328–337, 2019.

[28] H. Kruuk, *The Spotted Hyena: A Study of Predation and Cocial Behavior*. 1972.

[29] V. Ajraldi, M. Pittavino, and E. Venturino, "Modeling herd behavior in population systems", *Nonlinear Analysis: Real World Applications*, vol. 12, pp. 2319–2338, 2011.

[30] E. Venturino and S. Petrovskii, "Spatiotemporal behavior of a prey–predator system with a group defense for prey", *Ecological Complexity*, vol. 14, pp. 37–47, 2013.

[31] C. Xu, S. Yuan, and T. Zhang, "Global dynamics of a predator–prey model with defense mechanism for prey", *Applied Mathematics Letters*, vol. 62, pp. 42–48, 2016.

[32] I. M. Bulai and E. Venturino, "Shape effects on herd behavior in ecological interacting population models", *Mathematics and Computers in Simulation*, vol. 141, pp. 40–55, 2017.

[33] S. Djilali, C. Cattani, and L. N. Guin, "Delayed predator–prey model with prey social behavior", *The European Physical Journal Plus*, vol. 136, pp. 1–20, 2021.

[34] J. Li, X. Liu, and C. Wei, "The impact of role reversal on the dynamics of predator-prey model with stage structure", *Applied Mathematical Modelling*, vol. 104, pp. 339–357, 2022.

[35] H. I. Freedman and G. S. Wolkowicz, "Predator-prey systems with group defence: The paradox of enrichment revisited", *Bulletin of Mathematical Biology*, vol. 48, pp. 493–508, 1986.

[36] A. Kumar and B. Dubey, "Stability and bifurcation of a prey-predator system with additional food and two discrete delays", *Computer Modeling in Engineering & Sciences*, vol. 126, 2021.

[37] M. W. Hayward, J. Adendorff, J. O'Brien, A. Sholto-Douglas, C. Bissett, L. C. Moolman, P. Bean, A. Fogarty, D. Howarth, R. Slater, and G. I. Kerley, "Practical considerations for the reintroduction of large, terrestrial, mammalian predators based on reintroductions to South Africa's Eastern Cape Province", *The Open Conservation Biology Journal*, vol. 1, pp. 1–11, 2007.

[38] S. Mondal, A. Maiti, and G. Samanta, "Effects of fear and additional food in a delayed predator-prey model", *Biophysical Reviews and Letters*, vol. 13, pp. 157–177, 2018.

[39] A. Das and G. Samanta, "A prey-predator model with refuge for prey and additional food for predator in a fluctuating environment", *Physica A: Statistical Mechanics and its Applications*, vol. 538, p. 122 844, 2020.

[40] B. Sahoo, "Disease control through provision of alternative food to predator: A model based study", *International Journal of Dynamics and Control*, vol. 4, pp. 239–253, 2016.

[41] W. O. Kermack and A. G. McKendrick, "A contribution to the mathematical theory of epidemics", *Proceedings of the Royal Society of London. Series A, Containing Papers of a Mathematical and Physical Character*, vol. 115, pp. 700–721, 1927.

[42] J.-J. Wang, J.-Z. Zhang, and Z. Jin, "Analysis of an SIR model with bilinear incidence rate", *Nonlinear Analysis: Real World Applications*, vol. 11, pp. 2390–2402, 2010.

[43] B. Dubey, P. Dubey, and U. S. Dubey, "Dynamics of an SIR model with nonlinear incidence and treatment rate", *Applications and Applied Mathematics: An International Journal (AAM)*, vol. 10, p. 5, 2015.

[44] R. M. Anderson and R. M. May, "The invasion, persistence and spread of infectious diseases within animal and plant communities", *Philosophical Transactions of the Royal Society of London. B, Biological Sciences*, vol. 314, pp. 533–570, 1986.

[45] M. Haque and D. Greenhalgh, "When a predator avoids infected prey: A model-based theoretical study", *Mathematical Medicine and Biology: A Journal of the IMA*, vol. 27, pp. 75–94, 2010.

[46] M. Banerjee, B. W. Kooi, and E. Venturino, "An ecoepidemic model with prey herd behavior and predator feeding saturation response on both healthy and diseased prey", *Mathematical Modelling of Natural Phenomena*, vol. 12, pp. 133–161, 2017.

[47] A. Hastings and T. Powell, "Chaos in a three-species food chain", *Ecology*, vol. 72, pp. 896–903, 1991.

[48] R. K. Upadhyay and S. N. Raw, "Complex dynamics of a three species food-chain model with Holling type IV functional response", *Nonlinear Analysis Modelling and Control*, vol. 16, pp. 553–374, 2011.

[49] S. Dwivedi and N. Kumari, "Effectiveness of phase synchronization in chaotic food chain model with refugia and Allee effects during seasonal fluctuations", *Chaos: An Interdisciplinary Journal of Nonlinear Science*, vol. 33, p. 063 117, 2023.

[50] M. Z. Gliwicz, "Predation and the evolution of vertical migration in zooplankton", *Nature*, vol. 320, pp. 746–748, 1986.

[51] M. Hossain, R. Kumbhakar, N. Pal, and J. Kurths, "Structure of parameter space of a three-species food chain model with immigration and emigration", *Nonlinear Dynamics*, vol. 111, pp. 1–18, 2023.

[52] V. I. Yukalov, E. Yukalova, and D. Sornette, "Punctuated evolution due to delayed carrying capacity", *Physica D: Nonlinear Phenomena*, vol. 238, pp. 1752–1767, 2009.

[53] N. Pati and B. Ghosh, "Delayed carrying capacity induced subcritical and supercritical hopf bifurcations in a predator–prey system", *Mathematics and Computers in Simulation*, vol. 195, pp. 171–196, 2022.

[54] B. Bhunia, S. Ghorai, T. K. Kar, S. Biswas, L. T. Bhutia, and P. Debnath, "A study of a spatiotemporal delayed predator–prey model with prey harvesting: Constant and periodic diffusion", *Chaos, Solitons & Fractals*, vol. 175, p. 113 967, 2023.

[55] Y. Kuang, *Delay Differential Equations: With Applications in Population Dynamics*. Academic press, 1993.

[56] K. Gopalsamy, *Stability and Oscillations in Delay Differential Equations of Population Dynamics*. Springer Science & Business Media, 1992.

[57] D. Bai, J. Yu, M. Fan, and Y. Kang, "Dynamics for a non-autonomous predator-prey system with generalist predator", *Journal of Mathematical Analysis and Applications*, vol. 485, p. 123 820, 2020.

[58] B. Mondal, S. Roy, U. Ghosh, and P. K. Tiwari, "A systematic study of autonomous and nonautonomous predator–prey models for the combined effects of fear, refuge, cooperation and harvesting", *The European Physical Journal Plus*, vol. 137, p. 724, 2022.

[59] Z. Zeng, "Dynamics of a non-autonomous ratio-dependent food chain model", *Applied Mathematics and Computation*, vol. 215, pp. 1274–1287, 2009.

[60] L. Perko, *Differential Equations and Dynamical Systems*. Springer Science & Business Media, 2013.

[61] C. S. Holling, “The components of predation as revealed by a study of small-mammal predation of the european pine sawfly”, *The Canadian Entomologist*, vol. 91, pp. 293–320, 1959.

[62] C. S. Holling, “The functional response of invertebrate predators to prey density”, *The Memoirs of the Entomological Society of Canada*, vol. 98, pp. 5–86, 1966.

[63] J. F. Andrews, “A mathematical model for the continuous culture of microorganisms utilizing inhibitory substrates”, *Biotechnology and Bioengineering*, vol. 10, pp. 707–723, 1968.

[64] J. R. Beddington, “Mutual interference between parasites or predators and its effect on searching efficiency”, *The Journal of Animal Ecology*, pp. 331–340, 1975.

[65] P. H. Crowley and E. K. Martin, “Functional responses and interference within and between year classes of a dragonfly population”, *Journal of the North American Benthological Society*, vol. 8, pp. 211–221, 1989.

[66] C. Bandle and W. Reichel, “Solutions of quasilinear second-order elliptic boundary value problems via degree theory”, *Stationary Partial Differential Equations, in: Handb. Differ. Equ*, vol. 1, pp. 1–70, 2004.

[67] J. Muscat, *Functional analysis: An Introduction to Metric Spaces, Hilbert Spaces, and Banach Algebras*. Springer, 2014.

[68] S. Ahmad and M. R. M. Rao, *Theory of Ordinary Differential Equations: With Applications of Biology and Engineering*. Affiliated East-West Private Lmt., 1999.

[69] Y. A. Kuznetsov, I. A. Kuznetsov, and Y Kuznetsov, *Elements of Applied Bifurcation Theory*. Springer, 1998.

[70] O. Diekmann, J. Heesterbeek, and M. G. Roberts, “The construction of next-generation matrices for compartmental epidemic models”, *Journal of the Royal Society Interface*, vol. 7, pp. 873–885, 2010.

[71] N. Chitnis, J. M. Hyman, and J. M. Cushing, “Determining important parameters in the spread of malaria through the sensitivity analysis of a mathematical model”, *Bulletin of Mathematical Biology*, vol. 70, pp. 1272–1296, 2008.

[72] R. E. Gaines and J. L. Mawhin, *Coincidence Degree and Nonlinear Differential Equations*. Springer, 2006.

[73] M. Clinchy, M. J. Sheriff, and L. Y. Zanette, “Predator-induced stress and the ecology of fear”, *Functional Ecology*, vol. 27, pp. 56–65, 2013.

[74] M. J. Sheriff, S. D. Peacor, D. Hawlena, and M. Thaker, "Non-consumptive predator effects on prey population size: A dearth of evidence", *Journal of Animal Ecology*, vol. 89, pp. 1302–1316, 2020.

[75] P. K. Tiwari, M. Verma, S. Pal, Y. Kang, and A. K. Misra, "A delay nonautonomous predator–prey model for the effects of fear, refuge and hunting cooperation", *Journal of Biological Systems*, vol. 29, pp. 927–969, 2021.

[76] S. K. Sasmal, "Population dynamics with multiple Allee effects induced by fear factors - A mathematical study on prey-predator interactions", *Applied Mathematical Modelling*, vol. 64, pp. 1–14, 2018.

[77] B. Dubey, S. Sajan, and A. Kumar, "Stability switching and chaos in a multiple delayed prey-predator model with fear effect and anti-predator behavior", *Mathematics and Computers in Simulation*, vol. 188, pp. 164–192, 2021.

[78] J. E. Orpwood, A. E. Magurran, J. D. Armstrong, and S. W. Griffiths, "Minnows and the selfish herd: Effects of predation risk on shoaling behaviour are dependent on habitat complexity", *Animal Behaviour*, vol. 76, pp. 143–152, 2008.

[79] Z. Shang and Y. Qiao, "Bifurcation analysis of a Leslie-type predator–prey system with simplified Holling type IV functional response and strong Allee effect on prey", *Nonlinear Analysis: Real World Applications*, vol. 64, p. 103 453, 2022.

[80] A. Gupta and B. Dubey, "Bifurcations and multi-stability in an eco-epidemic model with additional food", *The European Physical Journal Plus*, vol. 137, pp. 1–20, 2022.

[81] P Mishra, S. Raw, and B Tiwari, "Study of a Leslie–Gower predator-prey model with prey defense and mutual interference of predators", *Chaos, Solitons & Fractals*, vol. 120, pp. 1–16, 2019.

[82] H. Freedman and G. Wolkowicz, "Predator-prey systems with group defence: The paradox of enrichment revisited", *Bulletin of Mathematical Biology*, vol. 48, pp. 493–508, 1986.

[83] M. T. Alves and F. M. Hilker, "Hunting cooperation and Allee effects in predators", *Journal of Theoretical Biology*, vol. 419, pp. 13–22, 2017.

[84] S. Saha and G. Samanta, "A prey-predator system with disease in prey and cooperative hunting strategy in predator", *Journal of Physics A: Mathematical and Theoretical*, vol. 53, p. 485 601, 2020.

[85] A. Nindjin and M. Aziz-Alaoui, "Persistence and global stability in a delayed Leslie–Gower type three species food chain", *Journal of Mathematical Analysis and Applications*, vol. 340, pp. 340–357, 2008.

[86] F. Chen, L. Chen, and X. Xie, "On a Leslie–Gower predator–prey model incorporating a prey refuge", *Nonlinear Analysis: Real World Applications*, vol. 10, pp. 2905–2908, 2009.

[87] S Ruan, "On nonlinear dynamics of predator-prey models with discrete delay", *Mathematical Modelling of Natural Phenomena*, vol. 4, pp. 140–188, 2009.

[88] P. Panday, S. Samanta, N. Pal, and J. Chattopadhyay, "Delay induced multiple stability switch and chaos in a predator–prey model with fear effect", *Mathematics and Computers in Simulation*, vol. 172, pp. 134–158, 2020.

[89] A. Gupta and B. Dubey, "Role reversal in a stage-structured prey–predator model with fear, delay, and carry-over effects", *Chaos: An Interdisciplinary Journal of Nonlinear Science*, vol. 33, 2023.

[90] A. Nindjin, M. Aziz-Alaoui, and M Cadivel, "Analysis of a predator–prey model with modified Leslie–Gower and Holling-type II schemes with time delay", *Nonlinear Analysis: Real World Applications*, vol. 7, pp. 1104–1118, 2006.

[91] L. Berec, "Impacts of foraging facilitation among predators on predator-prey dynamics", *Bulletin of Mathematical Biology*, vol. 72, pp. 94–121, 2010.

[92] G. T. Skalski and J. F. Gilliam, "Functional responses with predator interference: Viable alternatives to the Holling type II model", *Ecology*, vol. 82, pp. 3083–3092, 2001.

[93] M. Falconi, Y. Vera-Damian, and C. Vidal, "Predator interference in a Leslie–Gower intraguild predation model", *Nonlinear Analysis: Real World Applications*, vol. 51, p. 102 974, 2020.

[94] M. Aziz-Alaoui, "Study of a Leslie-Gower-type tritrophic population model", *Chaos, Solitons & Fractals*, vol. 14, pp. 1275–1293, 2002.

[95] A. Korobeinikov, "A Lyapunov function for Leslie-Gower predator-prey models", *Applied Mathematics Letters*, vol. 14, pp. 697–699, 2001.

[96] C. Ji, D. Jiang, and N. Shi, "Analysis of a predator-prey model with modified Leslie-Gower and Holling-type II schemes with stochastic perturbation", *Journal of Mathematical Analysis and Applications*, vol. 359, pp. 482–498, 2009.

[97] P. Aguirre, E. González-Olivares, and E. Sáez, "Three limit cycles in a Leslie-Gower predator-prey model with additive Allee effect", *SIAM Journal on Applied Mathematics*, vol. 69, pp. 1244–1262, 2009.

[98] F. Chen, L. Chen, and X. Xie, "On a Leslie-Gower predator-prey model incorporating a prey refuge", *Nonlinear Analysis: Real World Applications*, vol. 10, pp. 2905–2908, 2009.

[99] A. J. Wirsing and W. J. Ripple, "A comparison of shark and wolf research reveals similar behavioral responses by prey", *Frontiers in Ecology and the Environment*, vol. 9, pp. 335–341, 2011.

[100] S. Samaddar, M. Dhar, and P. Bhattacharya, "Effect of fear on prey–predator dynamics: Exploring the role of prey refuge and additional food", *Chaos: An Interdisciplinary Journal of Nonlinear Science*, vol. 30, p. 063 129, 2020.

[101] M. Sen, P. Srinivasu, and M. Banerjee, "Global dynamics of an additional food provided predator-prey system with constant harvest in predators", *Applied Mathematics and Computation*, vol. 250, pp. 193–211, 2015.

[102] R. P. Kaur, A. Sharma, and A. K. Sharma, "The impact of additional food on plankton dynamics in the absence and presence of toxicity", *Biosystems*, vol. 202, p. 104 359, 2021.

[103] M. van Baalen, V. Křivan, P. C. van Rijn, and M. W. Sabelis, "Alternative food, switching predators, and the persistence of predator-prey systems", *The American Naturalist*, vol. 157, pp. 512–524, 2001.

[104] R. D. Holt, "Predation, apparent competition, and the structure of prey communities", *Theoretical Population Biology*, vol. 12, pp. 197–229, 1977.

[105] R. Holt and J. Lawton, "The ecological consequences of shared natural enemies", *Annual Review of Ecology and Systematics*, vol. 25, pp. 495–520, 1994.

[106] P. C. J. van Rijn, Y. M. van Houten, and M. W. Sabelis, "How plants benefit from providing food to predators even when it is also edible to herbivores", *Ecology*, vol. 83, pp. 2664–2679, 2002.

[107] J. T. Wootton, "The nature and consequences of indirect effects in ecological communities", *Annual Review of Ecology and Systematics*, vol. 25, pp. 443–466, 1994.

[108] J. D. Harwood and J. J. Obrycki, "The role of alternative prey in sustaining predator populations", in *Proceedings of the Second International Symposium Biology Control of Arthropods*, Citeseer, vol. 2, 2005, pp. 453–462.

[109] P. Srinivasu, B. Prasad, and M Venkatesulu, "Biological control through provision of additional food to predators: A theoretical study", *Theoretical Population Biology*, vol. 72, pp. 111–120, 2007.

[110] J. Ghosh, B. Sahoo, and S. Poria, "Prey-predator dynamics with prey refuge providing additional food to predator", *Chaos, Solitons & Fractals*, vol. 96, pp. 110–119, 2017.

[111] B. Prasad, M. Banerjee, and P. Srinivasu, "Dynamics of additional food provided predator-prey system with mutually interfering predators", *Mathematical Biosciences*, vol. 246, pp. 176–190, 2013.

[112] T. K. Kar, "Stability analysis of a prey–predator model incorporating a prey refuge", *Communications in Nonlinear Science and Numerical Simulation*, vol. 10, pp. 681–691, 2005.

[113] Y. Huang, F. Chen, and L. Zhong, "Stability analysis of a prey–predator model with Holling type III response function incorporating a prey refuge", *Applied Mathematics and Computation*, vol. 182, pp. 672–683, 2006.

[114] H. Yu, M. Zhao, and R. P. Agarwal, "Stability and dynamics analysis of time delayed eutrophication ecological model based upon the Zeya reservoir", *Mathematics and Computers in Simulation*, vol. 97, pp. 53–67, 2014.

[115] C. Dai, M. Zhao, H. Yu, and Y. Wang, "Delay-induced instability in a nutrient-phytoplankton system with flow", *Physical Review E*, vol. 91, p. 032 929, 2015.

[116] D. Adak, N. Bairagi, and R. Hakl, "Chaos in delay-induced Leslie–Gower prey–predator–parasite model and its control through prey harvesting", *Nonlinear Analysis: Real World Applications*, vol. 51, p. 102 998, 2020.

[117] H. J. Alsakaji, S. Kundu, and F. A. Rihan, "Delay differential model of one-predator two-prey system with Monod-Haldane and Holling type II functional responses", *Applied Mathematics and Computation*, vol. 397, p. 125 919, 2021.

[118] R. Yang, Y. Ma, and C. Zhang, "Time delay induced Hopf bifurcation in a diffusive predator–prey model with prey toxicity", *Advances in Difference Equations*, vol. 2021, pp. 1–17, 2021.

[119] H. Hu and L. Huang, "Stability and Hopf bifurcation in a delayed predator–prey system with stage structure for prey", *Nonlinear Analysis: Real World Applications*, vol. 11, pp. 2757–2769, 2010.

[120] S. Liu, E. Beretta, and D. Breda, "Predator–prey model of Beddington–DeAngelis type with maturation and gestation delays", *Nonlinear Analysis: Real World Applications*, vol. 11, pp. 4072–4091, 2010.

[121] M Bandyopadhyay and S. Banerjee, "A stage-structured prey–predator model with discrete time delay", *Applied Mathematics and Computation*, vol. 182, pp. 1385–1398, 2006.

[122] A. Kumar and B. Dubey, "Modeling the effect of fear in a prey–predator system with prey refuge and gestation delay", *International Journal of Bifurcation and Chaos*, vol. 29, p. 1 950 195, 2019.

[123] J. P. Tripathi, S. Abbas, and M. Thakur, "A density dependent delayed predator-prey model with Beddington-DeAngelis type function response incorporating a prey refuge", *Communications in Nonlinear Science and Numerical Simulation*, vol. 22, pp. 427–450, 2015.

[124] B. D. Hassard, N. D. Kazarinoff, and Y.-H. Wan, *Theory and Applications of Hopf Bifurcation*. CUP Archive, 1981.

[125] Y. Song and J. Wei, "Bifurcation analysis for Chen's system with delayed feedback and its application to control of chaos", *Chaos, Solitons & Fractals*, vol. 22, pp. 75–91, 2004.

[126] S. H. Strogatz, *Nonlinear Dynamics and Chaos: With Applications to Physics, Biology, Chemistry, and Engineering*. CRC Press, 2018.

[127] P. Panday, N. Pal, S. Samanta, and J. Chattopadhyay, "Stability and bifurcation analysis of a three-species food chain model with fear", *International Journal of Bifurcation and Chaos*, vol. 28, p. 1 850 009, 2018.

[128] S. Mishra and R. Upadhyay, "Exploring the cascading effect of fear on the foraging activities of prey in a three species agroecosystem", *The European Physical Jounal Plus*, vol. 136, pp. 1–36, 2021.

[129] M. Jiang, Y. Shen, J. Jian, and X. Liao, "Stability, bifurcation and a new chaos in the logistic differential equation with delay", *Physics Letters A*, vol. 350, pp. 221–227, 2006.

[130] Y. Kang, S. K. Sasmal, A. R. Bhowmick, and J. Chattopadhyay, "Dynamics of a predator-prey system with prey subject to Allee effects and disease", *Mathematical Biosciences & Engineering*, vol. 11, pp. 877–918, 2014.

[131] J. Chattopadhyay and O. Arino, "A predator-prey model with disease in the prey", *Nonlinear Analysis*, vol. 36, pp. 747–766, 1999.

[132] D. Greenhalgh and M. Haque, "A predator–prey model with disease in the prey species only", *Mathematical Methods in the Applied Sciences*, vol. 30, pp. 911–929, 2007.

[133] S. Kant and V. Kumar, "Stability analysis of predator–prey system with migrating prey and disease infection in both species", *Applied Mathematical Modelling*, vol. 42, pp. 509–539, 2017.

[134] M. Banerjee and S. Banerjee, "Turing instabilities and spatio-temporal chaos in ratio-dependent Holling–Tanner model", *Mathematical Biosciences*, vol. 236, pp. 64–76, 2012.

[135] P. Paul, T. Kar, and E. Das, "Reactivity in prey–predator models at equilibrium under selective harvesting efforts", *The European Physical Jounal Plus*, vol. 136, p. 510, 2021.

[136] H. Verma, K. Antwi-Fordjour, M. Hossain, N. Pal, R. Parshad, and P. Mathur, "A "Double" fear effect in a tri-trophic food chain model", *The European Physical Jounal Plus*, vol. 136, p. 905, 2021.

[137] D. Mukherjee, "Hopf bifurcation in an eco-epidemic model", *Applied Mathematics and Computation*, vol. 217, pp. 2118–2124, 2010.

[138] K. Hadeler and H. Freedman, "Predator-prey populations with parasitic infection", *Journal of Mathematical Biology*, vol. 27, pp. 609–631, 1989.

[139] S. Biswas, S. Samanta, and J. Chattopadhyay, "Cannibalistic predator–prey model with disease in predator—a delay model", *International Journal of Bifurcation and Chaos*, vol. 25, p. 1 550 130, 2015.

[140] A. Majumder, D. Adak, and N. Bairagi, "Persistence and extinction of species in a disease-induced ecological system under environmental stochasticity", *Physical Review E*, vol. 103, p. 032 412, 2021.

[141] D. O. Joly and F. Messier, "The distribution of Echinococcus granulosus in moose: Evidence for parasite-induced vulnerability to predation by wolves?", *Oecologia*, vol. 140, pp. 586–590, 2004.

[142] D. C. Behringer and M. J. Butler, "Disease avoidance influences shelter use and predation in Caribbean spiny lobster", *Behavioral Ecology and Sociobiology*, vol. 64, pp. 747–755, 2010.

[143] S. A. Temple, "Do predators always capture substandard individuals disproportionately from prey populations?", *Ecology*, vol. 68, pp. 669–674, 1987.

[144] C. R. Alma, D. R. Gillespie, B. D. Roitberg, and M. S. Goettel, "Threat of infection and threat-avoidance behavior in the predator Dicyphus hesperus feeding on whitefly nymphs infected with an entomopathogen", *Journal of Insect Behavior*, vol. 23, pp. 90–99, 2010.

[145] A. Yamauchi and N. Yamamura, "Effects of defense evolution and diet choice on population dynamics in a one-predator–two-prey system", *Ecology*, vol. 86, pp. 2513–2524, 2005.

[146] A. M. Bate and F. M. Hilker, "Disease in group-defending prey can benefit predators", *Theoretical Ecology*, vol. 7, pp. 87–100, 2014.

[147] G. Gimmelli, B. W. Kooi, and E. Venturino, "Ecoepidemic models with prey group defense and feeding saturation", *Ecological Complexity*, vol. 22, pp. 50–58, 2015.

[148] S. Samanta, A. K. Mandal, K. Kundu, and J Chattopadhyay, "Control of disease in prey population by supplying alternative food to predator", *Journal of Biological Systems*, vol. 22, pp. 677–690, 2014.

[149] B. Sahoo and S. Poria, "Effects of additional food in a susceptible-exposed-infected prey–predator model", *Modeling Earth Systems and Environment*, vol. 2, pp. 1–17, 2016.

[150] S. Haldar, A. Khatua, K. Das, and T. Kar, "Modeling and analysis of a predator–prey type eco-epidemic system with time delay", *Modeling Earth Systems and Environment*, vol. 7, pp. 1753–1768, 2020.

[151] U. Feudel, "Complex dynamics in multistable systems", *International Journal of Bifurcation and Chaos*, vol. 18, pp. 1607–1626, 2008.

[152] A. N. Pisarchik and U. Feudel, "Control of multistability", *Physics Reports*, vol. 540, pp. 167–218, 2014.

[153] N. Knowlton, "Multiple "stable" states and the conservation of marine ecosystems", *Progress in Oceanography*, vol. 60, pp. 387–396, 2004.

[154] S. He, S. Banerjee, and K. Sun, "Complex dynamics and multiple coexisting attractors in a fractional-order microscopic chemical system", *The European Physical Journal Special Topics*, vol. 228, pp. 195–207, 2019.

[155] B. Dubey, A. Patra, P. Srivastava, and U. S. Dubey, "Modeling and analysis of an SEIR model with different types of nonlinear treatment rates", *Journal of Biological Systems*, vol. 21, p. 1 350 023, 2013.

[156] A. K. Misra, R. K. Rai, P. K. Tiwari, and M. Martcheva, "Delay in budget allocation for vaccination and awareness induces chaos in an infectious disease model", *Journal of Biological Dynamics*, vol. 15, pp. 395–429, 2021.

[157] A. A. S. Bentout S. Djilali, "Bifurcation analysis of an age-structured prey–predator model with infection developed in prey", *Mathematical Methods in the Applied Sciences*, vol. 45, pp. 1189–1208, 2022.

[158] K. D. Lafferty and A. K. Morris, "Altered behavior of parasitized killifish increases susceptibility to predation by bird final hosts", *Ecology*, vol. 77, pp. 1390–1397, 1996.

[159] H. W. Hethcote, "The mathematics of infectious diseases", *SIAM review*, vol. 42, pp. 599–653, 2000.

[160] Q. Zheng, V. Pandey, J. Shen, Y. Xu, and L. Guan, "Pattern dynamics in the epidemic model with diffusion network", *Europhysics Letters*, vol. 137, p. 42 002, 2022.

[161] V. Capasso and G. Serio, "A generalization of the Kermack-McKendrick deterministic epidemic model", *Mathematical Biosciences*, vol. 42, pp. 43–61, 1978.

[162] L. Han, Z. Ma, and H. W. Hethcote, "Four predator prey models with infectious diseases", *Mathematical and Computer Modelling*, vol. 34, pp. 849–858, 2001.

[163] M. Haque, J. Zhen, and E. Venturino, "An ecoepidemiological predator-prey model with standard disease incidence", *Mathematical Methods in the Applied Sciences*, vol. 32, pp. 875–898, 2009.

[164] H. W. Hethcote, W. Wang, L. Han, and Z. Ma, "A predator–prey model with infected prey", *Theoretical Population Biology*, vol. 66, pp. 259–268, 2004.

[165] Sajan and B. Dubey, "Chaos control in a multiple delayed phytoplankton–zooplankton model with group defense and predator's interference", *Chaos: An Interdisciplinary Journal of Nonlinear Science*, vol. 31, p. 083 101, 2021.

[166] A. A. Shaikh, H. Das, and N. Ali, "Complex dynamics of an eco-epidemic system with disease in prey species", *International Journal of Bifurcation and Chaos*, vol. 31, p. 2 150 046, 2021.

[167] A. K. Alzahrani, A. S. Alshomrani, N. Pal, and S. Samanta, "Study of an eco-epidemiological model with Z-type control", *Chaos, Solitons & Fractals*, vol. 113, pp. 197–208, 2018.

[168] P. K. Tiwari, S. Roy, A. K. Misra, and R. K. Upadhyay, "Effect of seasonality on a nutrient-plankton system with toxicity in the presence of refuge and additional food", *The European Physical Journal Plus*, vol. 137, pp. 1–24, Mar. 2022.

[169] A. Eilersen, M. H. Jensen, and K. Sneppen, "Chaos in disease outbreaks among prey", *Scientific Reports*, vol. 10, pp. 1–7, 2020.

[170] S. Djilali, "Effect of herd shape in a diffusive predator-prey model with time delay", *Journal of Applied Analysis & Computation*, vol. 9, pp. 638–654, 2019.

[171] G. Gimmelli, B. W. Kooi, and E. Venturino, "Ecoepidemic models with prey group defense and feeding saturation", *Ecological Complexity*, vol. 22, pp. 50–58, 2015.

[172] S. Saha and G. Samanta, "Analysis of a predator–prey model with herd behavior and disease in prey incorporating prey refuge", *International Journal of Biomathematics*, vol. 12, p. 1 950 007, 2019.

[173] W. Yang, "Bifurcation and dynamics in double-delayed chua circuits with periodic perturbation", *Chinese Physics B*, vol. 31, p. 020 201, 2022.

[174] S.-X. Wu and X. Meng, "Dynamics of a delayed predator-prey system with fear effect, herd behavior and disease in the susceptible prey", *AIMS Mathematics*, vol. 6, pp. 3654–3685, 2021.

[175] S. Djilali, "Impact of prey herd shape on the predator-prey interaction", *Chaos, Solitons & Fractals*, vol. 120, pp. 139–148, 2019.

[176] Y. Choh, M. Ignacio, M. W. Sabelis, and A. Janssen, "Predator-prey role reversals, juvenile experience and adult antipredator behaviour", *Scientific Reports*, vol. 2, pp. 1–6, 2012.

[177] S. Saha and G. Samanta, "Impact of fear in a prey-predator system with herd behaviour", *Computational and Mathematical Biophysics*, vol. 9, pp. 175–197, 2021.

[178] D. Mukherjee, "Dynamics of an eco-epidemic model with stage structure for predator", *Journal of Mathematical Modeling*, vol. 4, pp. 103–115, 2016.

[179] A. Gupta, A. Kumar, and B. Dubey, "Complex dynamics of Leslie–Gower prey–predator model with fear, refuge and additional food under multiple delays", *International Journal of Biomathematics*, vol. 15, p. 2 250 060, 2022.

[180] T. Zheng, L. Zhang, Y. Luo, X. Zhou, H.-L. Li, and Z. Teng, "Stability and Hopf bifurcation of a stage-structured cannibalism model with two delays", *International Journal of Bifurcation and Chaos*, vol. 31, p. 2 150 242, 2021.

[181] C. Jana, A. P. Maiti, and D. K. Maiti, "Complex dynamical behavior of a ratio-dependent eco-epidemic model with Holling type-II incidence rate in the presence of two delays", *Communications in Nonlinear Science and Numerical Simulation*, vol. 110, p. 106 380, 2022.

[182] S Olaniyi, O. Obabiyi, K. Okosun, A. Oladipo, and S. Adewale, "Mathematical modelling and optimal cost-effective control of COVID-19 transmission dynamics", *The European Physical Journal Plus*, vol. 135, p. 938, 2020.

[183] F. Souna, A. Lakmeche, and S. Djilali, "The effect of the defensive strategy taken by the prey on predator–prey interaction", *Journal of Applied Mathematics and Computing*, vol. 64, pp. 665–690, 2020.

[184] G. Bardon and F. Barraquand, "Effects of stage structure on coexistence: Mixed benefits", *Bulletin of Mathematical Biology*, vol. 85, p. 33, 2023.

[185] P. Georgescu and Y.-H. Hsieh, "Global dynamics of a predator-prey model with stage structure for the predator", *SIAM Journal on Applied Mathematics*, vol. 67, pp. 1379–1395, 2007.

[186] H. Freedman and J. Wu, "Persistence and global asymptotic stability of single species dispersal models with stage structure", *Quarterly of Applied Mathematics*, vol. 49, pp. 351–371, 1991.

[187] S. A. Gourley and Y. Kuang, "A stage structured predator-prey model and its dependence on maturation delay and death rate", *Journal of Mathematical Biology*, vol. 49, pp. 188–200, 2004.

[188] W. Wang, G Mulone, F Salemi, and V Salone, "Permanence and stability of a stage-structured predator–prey model", *Journal of Mathematical Analysis and Applications*, vol. 262, pp. 499–528, 2001.

[189] T. K. Kar and S. Jana, "Stability and bifurcation analysis of a stage structured predator prey model with time delay", *Applied Mathematics and Computation*, vol. 219, pp. 3779–3792, 2012.

[190] N. Dorn, G. Mittelbach, and W. Kellogg, "More than predator and prey: A review of interactions between fish and crayfish", *Vie et Milieu/Life & Environment*, vol. 49, pp. 229–237, 1999.

[191] R John Power and R. Shem Compion, "Lion predation on elephants in the Savuti, Chobe national park, Botswana", *African Zoology*, vol. 44, pp. 36–44, 2009.

[192] A. Janssen, E. Willemse, and T. Van Der Hammen, "Poor host plant quality causes omnivore to consume predator eggs", *Journal of Animal Ecology*, vol. 72, pp. 478–483, 2003.

[193] R. Kaushik and S. Banerjee, "Predator-prey system: Prey's counter-attack on juvenile predators shows opposite side of the same ecological coin", *Applied Mathematics and Computation*, vol. 388, p. 125 530, 2021.

[194] S. Mondal, G. Samanta, and M. De la Sen, "A comparison study of predator–prey model in deterministic and stochastic environments with the impacts of fear and habitat complexity", *Bulletin of Mathematical Biology*, vol. 84, p. 115, 2022.

[195] K. D. Prasad and S. K. Sasmal, "Dynamics of anti-predator behavior and effect of fear on prey–predator model", *Journal of Biological Systems*, vol. 30, pp. 887–912, 2022.

[196] C. Wang, S. Yuan, and H. Wang, "Spatiotemporal patterns of a diffusive prey-predator model with spatial memory and pregnancy period in an intimidatory environment", *Journal of Mathematical Biology*, vol. 84, p. 12, 2022.

[197] S. Mishra and R. K. Upadhyay, "Spatial pattern formation and delay induced destabilization in predator–prey model with fear effect", *Mathematical Methods in the Applied Sciences*, vol. 45, pp. 6801–6823, 2022.

[198] C. M. O'Connor, D. R. Norris, G. T. Crossin, and S. J. Cooke, "Biological carryover effects: Linking common concepts and mechanisms in ecology and evolution", *Ecosphere*, vol. 5, pp. 1–11, 2014.

[199] R. Yafia, F. El Adnani, and H. T. Alaoui, "Limit cycle and numerical similations for small and large delays in a predator–prey model with modified Leslie–Gower and Holling-type II schemes", *Nonlinear Analysis: Real World Applications*, vol. 9, pp. 2055–2067, 2008.

[200] R. Yafia, M. Aziz-Alaoui, H. Merdan, and J.-J. Tewa, "Bifurcation and stability in a delayed predator–prey model with mixed functional responses", *International Journal of Bifurcation and Chaos*, vol. 25, p. 1 540 014, 2015.

[201] P. Georgescu, Y.-H. Hsieh, and H. Zhang, "A lyapunov functional for a stage-structured predator–prey model with nonlinear predation rate", *Nonlinear Analysis: Real World Applications*, vol. 11, pp. 3653–3665, 2010.

[202] J. Roy, S. Dey, and M. Banerjee, "Maturation delay induced stability enhancement and shift of bifurcation thresholds in a predator–prey model with generalist predator", *Mathematics and Computers in Simulation*, vol. 211, pp. 368–393, 2023.

[203] A. Misra and J. Maurya, "Modeling the importance of temporary hospital beds on the dynamics of emerged infectious disease", *Chaos: An Interdisciplinary Journal of Nonlinear Science*, vol. 31, p. 103 125, 2021.

[204] A. Gupta and B. Dubey, "Bifurcation and chaos in a delayed eco-epidemic model induced by prey configuration", *Chaos, Solitons & Fractals*, vol. 165, p. 112 785, 2022.

[205] A. Klebanoff and A. Hastings, "Chaos in three species food chains", *Journal of Mathematical Biology*, vol. 32, pp. 427–451, 1994.

[206] R. K. Upadhyay, "Multiple attractors and crisis route to chaos in a model food-chain", *Chaos, Solitons & Fractals*, vol. 16, pp. 737–747, 2003.

[207] L. Stone and D. Hart, "Effects of immigration on the dynamics of simple population models", *Theoretical Population Biology*, vol. 55, pp. 227–234, 1999.

[208] T. Chowdhury, S. Chakraborty, and J Chattopadhyay, "Migratory effect of middle predator in a tri-trophic food chain model", *Mathematical Methods in the Applied Sciences*, vol. 33, pp. 1699–1711, 2010.

[209] N. Pal, S. Samanta, and S. Rana, "The impact of constant immigration on a tri-trophic food chain model", *International Journal of Applied and Computational Mathematics*, vol. 3, pp. 3615–3644, 2017.

[210] Sajan, K. K. Choudhary, and B. Dubey, "A non-autonomous approach to study the impact of environmental toxins on nutrient-plankton system", *Applied Mathematics and Computation*, vol. 458, p. 128 236, 2023.

[211] S. Samanta, P. K. Tiwari, A. K. Alzahrani, and A. S. Alshomrani, "Chaos in a nonautonomous eco-epidemiological model with delay", *Applied Mathematical Modelling*, vol. 79, pp. 865–880, 2020.

[212] S. Samanta, M. Alquran, and J. Chattopadhyay, "Existence and global stability of positive periodic solution of tri-trophic food chain with middle predator migratory in nature", *Applied Mathematical Modelling*, vol. 39, pp. 4285–4299, 2015.

[213] E. Reimondo, T. Sisk, and T. Thiemer, "Effects of introduced bison on wetlands of the Kaibab Plateau, Arizona", in *The Colorado Plateau VI: Science and Management at the Landscape Scale. University of Arizona Press, Tucson, Arizona*, 2015, pp. 120–135.

[214] V. I. Yukalov, E. Yukalova, and D. Sornette, "Extreme events in population dynamics with functional carrying capacity", *The European Physical Journal Special Topics*, vol. 205, pp. 313–354, 2012.

[215] S. Khajanchi, "Dynamic behavior of a Beddington–DeAngelis type stage structured predator–prey model", *Applied Mathematics and Computation*, vol. 244, pp. 344–360, 2014.

[216] A. Ojha and N. K. Thakur, "Complex dynamics induced by multiple gestation delays in a Leslie–Gower-type system with competitive interference", *Mathematical Methods in the Applied Sciences*, vol. 46, 17725–17759, 2023.

[217] N. K. Thakur and A. Ojha, "Complex plankton dynamics induced by adaptation and defense", *Modeling Earth Systems and Environment*, vol. 6, pp. 907–916, 2020.

[218] P. Panday, N. Pal, S. Samanta, P. Tryjanowski, and J. Chattopadhyay, "Dynamics of a stage-structured predator-prey model: Cost and benefit of fear-induced group defense", *Journal of Theoretical Biology*, vol. 528, p. 110 846, 2021.

[219] M. Itik and S. P. Banks, "Chaos in a three-dimensional cancer model", *International Journal of Bifurcation and Chaos*, vol. 20, pp. 71–79, 2010.

[220] K. L. Drury, J. D. Suter, J. B. Rendall, A. M. Kramer, and J. M. Drake, "Immigration can destabilize tri-trophic interactions: Implications for conservation of top predators", *Theoretical Ecology*, vol. 8, pp. 285–296, 2015.

List of Publications

Published

1. **Ashvini Gupta** and Balram Dubey. Bifurcations and multi-stability in an eco-epidemic model with additional food, The European Physical Journal Plus, 137:118, (2022).
   (Impact Factor **3.4**, Indexed in **SCI**, Q2)
   https://doi.org/10.1140/epjp/s13360-022-02340-3

2. **Ashvini Gupta**, Ankit Kumar and Balram Dubey. Complex dynamics of Leslie-Gower prey-predator model with fear, refuge and additional food under multiple delays, International Journal of Biomathematics, 15:2250060, (2022).
   (Impact Factor **2.2**, Indexed in **SCIE**, Q2)
   https://doi.org/10.1142/S1793524522500607

3. **Ashvini Gupta** and Balram Dubey. Bifurcation analysis of a Leslie-Gower prey-predator model with fear and cooperative hunting, In: Banerjee, S., Saha, A. (eds) Nonlinear Dynamics and Applications. Springer Proceedings in Complexity, 1069–1080, (2022).
   (Indexed in **Scopus**)
   https://doi.org/10.1007/978-3-030-99792-2_90

4. **Ashvini Gupta** and Balram Dubey. Bifurcation and chaos in a delayed eco-epidemic model induced by prey configuration, Chaos, Solitons & Fractals, 165:112785, (2022).
   (Impact Factor **9.922**, Indexed in **SCI**, Q1)
   https://doi.org/10.1016/j.chaos.2022.112785

5. Soumitra Pal, **Ashvini Gupta**, A.K. Misra and Balram Dubey. Chaotic dynamics of a stage-structured prey-predator system with hunting cooperation and fear in presence of two discrete delays, Journal of Biological Systems, 31:611-642, (2023).
   (Impact Factor **1.6**, Indexed in **SCIE**, Q2)
   https://doi.org/10.1142/S0218339023500213

6. Arjun Kumar, **Ashvini Gupta**, Uma S. Dubey and Balram Dubey. Stability and bifurcation analysis of an infectious disease model with different optimal control strategies, Mathematics and Computers in Simulation, 213: 78-114, (2023).
   (Impact Factor **4.6**, Indexed in **SCI**, Q1)
   https://doi.org/10.1016/j.matcom.2023.05.024

7. **Ashvini Gupta** and Balram Dubey. Role reversal in a stage-structured prey–predator model with fear, delay, and carry-over effects, Chaos: An Interdisciplinary Journal of Nonlinear Science, 33:093114, (2023).
   (Impact Factor **3.741**, Indexed in **SCI**, Q1)
   https://doi.org/10.1063/5.0160222

8. Soumitra Pal, **Ashvini Gupta**, A.K. Misra and Balram Dubey. Complex dynamics of a predator-prey system with fear and memory in the presence of two discrete delays, The European Physical Journal Plus, 138:984, (2023).
   (Impact Factor **3.4**, Indexed in **SCI**, Q2)
   https://doi.org/10.1140/epjp/s13360-023-04614-w

Communicated

1. **Ashvini Gupta**, Sajan and Balram Dubey. Chaos in a seasonal food-chain model with migration and variable carrying capacity. (Revised version submitted in Nonlinear Dynamics)

Workshops and Conferences

1. The 15th Conference on Dynamical Systems Applied to Biology and Natural Sciences, DSABNS-2024, hosted by the NOVA SCHOOL OF SCIENCE AND TECHNOLOGY|NOVA FCT in Portugal, (06-09 February 2024).

2. National Webinar on the topic Period-Doubling Route to Chaos-A brief introduction, organized by Department of Mathematics, Gargi College, University of Delhi, under the aegis of IQAC, India, (16 October 2023).

3. A Five-Day Online FDP on Mathematical Modeling in Biological Systems organized by Vellore Institute of Technology Chennai, India, (19-23 June 2023).

4. Workshop on Fundamentals of Mathematical Biology organized by Indian Institute of Information Technology Allahabad, India, (11-12 May 2023).

5. International Conference on Advances in Biomathematics organized by Amity University Lucknow, India, (21-23 July 2022).

6. International Conference on Nonlinear Dynamics and Applications organized by Sikkim Manipal Institute of Technology, Sikkim, India, (9-11 March 2022).

7. Workshop on Teaching-Learning Workshop for Next Generation Academicians organized by TLC BITS Pilani, Pilani Campus, India (27 November 2021).

8. Workshop on Bio-Mathematics (WoBM-2020) organized by Indian Institute of Technology Patna, India, (8-11 December 2020).

9. International Webinar on Some Applications of Mathematics to Analyze and Solve Problems of Real Life organized by Department of Mathematics, Bharati College, University of Delhi, India, (29 May 2020).

10. National Webinar on Role of Mathematics in COVID-19: Existing literature, Outcomes, and Challenges in various direction organized by Atma Ram Sanatan Dharma College, University of Delhi, India, (14 May 2020).

Brief Biography of the Supervisor

Prof. Balram Dubey is a Professor and Former Head of the Department of Mathematics at Birla Institute of Technology & Science, Pilani, Pilani Campus, India. He earned his Bachelor's Degree (B.Sc. Hons) with the first merit rank from Bhagalpur University, Bhagalpur, India, in 1988. He received his Master's degree in 1990 and Ph.D. in 1994 from the Department of Mathematics, Indian Institute of Technology Kanpur. Kanpur, India. He was a Research Associate at IIT Kanpur from 1994-1995, and later, he joined IIT Kanpur as visiting faculty during 2000-2002. He was awarded the "Best Teaching Award" for tutorship in MATH1102 in 2001 at IIT Kanpur. Prof. Dubey served as Lecturer and Senior Lecturer in the Department of Mathematics at Tezpur University, India, from 1995 to 2000. There, he guided two Ph.D. students. In 2002, he joined the Department of Mathematics, Birla Institute of Technology & Science, Pilani, Pilani Campus, as an Assistant Professor. He was promoted to Associate Professor in August 2010 and Professor in February 2013. His research interests are Mathematical Biology, Mathematical Ecology, Ecotoxicology, Soil Erosion and Conservation, Epidemiology, Mathematical Immunology, and Applications of ODEs & PDEs in Real-world Problems. As a result of his research accomplishments, he has published more than 100 research articles in national and international journals of repute. He also authorizes "Introductory Linear Algebra," Asian Books, Pvt. Ltd. 2007. He has successfully guided six Ph.D. students.

Brief Biography of the Candidate

Ashvini Gupta, a Senior Research Fellow at the Department of Mathematics, BITS Pilani, Pilani Campus, joined the institute in January 2020. Her research focuses on mathematical biology, which involves formulating and analyzing population dynamics models. She has attended various workshops/webinars and presented her work at several conferences. Ashvini received financial support under SERB's International Travel Grant to participate in the 15th Conference on Dynamical Systems Applied to Biology and Natural Sciences, DSABNS-2024, in Portugal in February 2024. She was awarded under the theme "Her Research, Our Future Empowering Women in Research," a G20 Initiative by Springer Nature and the Ministry of Education, Government of India, in September 2023. Ashvini's research is funded by the UGC, New Delhi, India.

Ashvini qualified for CSIR-UGC NET JRF in December 2019. She holds a M.Sc. in Mathematics and Computing from IIT(ISM) Dhanbad (2017-2019). She qualified for IIT JAM in 2016 and 2017. Before that, she completed her B.Sc. from the Janki Devi Bajaj College, Kota, Rajasthan (2013-2016).